



**Development and Evaluation of Phase Change Material-Enhanced Earthbag
Buildings for Thermally Comfortable and Sustainable Temporary Housing in
Nigeria: Numerical and Experimental Approach**

Mahmoud Murtala Farouq

B. Eng Civil, MEng Construction management

Supervisors

Dr Pharham A. Mirzaei

Dr. Carlos Jimenez Bescos

Prof. Dr. Saffa Riffat

Department of Architecture and Built Environment

University of Nottingham

This thesis is submitted for the degree of

Doctor of Philosophy

May, 2023

ABSTRACT

Many developing countries face an increasing demand for affordable and sustainable housing, particularly for refugees and displaced communities that require temporary housing. However, there is a lack of research on the thermal comfort of such housing, which poses risks to vulnerable occupants, especially children. Existing studies on the thermal performance of shelters have predominantly focused on cold environments, neglecting hot climates, leaving this area of research underdeveloped. Earthbag buildings are promising options because of their low cost, sustainability, and ease of construction. However, indoor thermal comfort is often inadequate. This research aims to address this issue by developing and integrating phase change materials (PCM) into earthbag building to create a more comfortable living environment. The study began by fabricating earthbag blocks containing varying amounts of paraffin wax encapsulated in expanded perlite and graphite which was formed as PCM composite, to investigate the microstructural properties of the embedded PCM composite in soil, followed by testing the block thermal characteristics. Subsequently, an experimental analysis was conducted to understand the thermal properties of a wall embedded with optimum earthbag blocks. Two PCMs, namely A31 paraffin wax and Inertek26 powder microencapsulated, were incorporated into reduced-scale earthbag walls to create two distinct wall types: Wall-2_WA31 (a wall with A31 paraffin wax), and Wall-3_WInk26 (a wall with microencapsulated inertek26 powder). The performances of these PCM-integrated earthbag walls and Wall-1_baseline (a wall without PCM), were then monitored in an environmental chamber. To complement the experimental findings, a numerical model was developed using the EnergyPlus numerical simulation engine, employing the conduction finite difference (CondFD) approach and validated with experimental data. Through parametric analysis, the study identified the most effective PCM and the PCM supporting materials. Finally, a case study was presented, demonstrating the successful implementation of the optimum PCM-integrated earthbag walls (PCM-E wall) in a temporary housing unit in Maiduguri, Nigeria. This case study aimed to investigate the practical application and effectiveness of PCM-E wall in achieving optimal thermal comfort of temporary housing.

The study revealed that the PCM and PCM composites exhibited favourable thermal stability, based on the Differential Scanning Calorimetry (DSC) and Thermogravimetric Analysis (TGA) tests. The Scanning Electron Microscope (SEM) results suggest that the PCM was evenly dispersed within the pores of the expanded perlite (EP) material at a 50% EP to PCM weight ratio. Moreover, the thermal performance results of the PCM-integrated earthbag blocks demonstrate that integrating PCM into earthbag block significantly moderates inner surface block wall temperatures by 1.2 to 4.1°C compared to the reference block. The integration of PCM into earthbag walls demonstrated remarkable improvements in thermal performance. Notably, the thermal conductivity of the earthbag walls significantly decreased with PCM incorporation, with Wall-3_WInk26 having achieved the lowest thermal conductivity at 0.43 W/mK . PCM-enhanced walls exhibited stable inner wall temperatures, with maximum reductions of 2.4°C compared to the baseline, and a substantial reduction in heat flux by up to 63.76%. The time lag in reaching the peak inner wall temperature increased by 3-5 hours, enhancing thermal comfort. The study identified an optimal PCM transition temperature of 31°C. Furthermore, PCM integration outperformed insulation alone, and increasing PCM and insulation layer thickness optimized thermal performance. A numerical model validated these findings, supporting the conclusion that PCMs enhanced thermal mass, reduced temperature fluctuations, and improved energy efficiency in earthbag construction. When combined with night ventilation strategies, PCM walls eliminated the need for air conditioning and maintained indoor temperatures within the comfort range of 23-32°C. In the long term, PCM-enhanced earthbag walls demonstrated significant thermal comfort improvements, with 94% comfort hours over the summer period. This research offered a promising solution for affordable, energy-efficient housing in hot climates using local earthen materials and passive cooling techniques.

ACKNOWLEDGEMENT

In the name of Allah, the Most Gracious, the Most Merciful. All praise is due to Allah, the Lord of the world, who has enabled me to complete my PhD thesis. Without His grace and guidance, this accomplishment would not have been possible.

I want to sincerely thank my supervisor, Dr. Parham A. Mirzaei, for all of his help and support during my research. His priceless advice and criticism were quite helpful in helping me to develop my work. I also thank Dr Carlos Jimenez-Bescos and my Co-supervisor, Prof. Saffa Riffat, for their thoughtful assistance. I owe a debt of gratitude to Engineering's faculty and staff, who have supported me throughout my academic career and given me a wonderful academic environment.

I am grateful to have had amazing people in my life, including friends and colleagues from inside and outside the institution, who have provided support, inspiration, and assistance throughout the years. Their kindness and generosity have helped me navigate the challenges of the PhD program.

I am thankful for the love and support I have received from my family, especially my parents, as I have pursued my academic goals. Their support and inspiration have been what have propelled my accomplishment. Special thanks to my wife and her parents for their unwavering support, love, and encouragement throughout this journey. My wife's patience, understanding, and sacrifices have been invaluable to me, and I am forever grateful for her presence in my life.

I am immensely grateful to Allah for blessing me with the gift of a beautiful newborn baby towards the end of my PhD journey. This bundle of joy has brought immense happiness and motivation to my life, and I thank Allah for this precious blessing.

Finally, I want to express my sincere gratitude to the Petroleum Technology Development Fund (PTDF) for providing me with a scholarship for the duration of my studies. In addition to allowing me to continue my PhD, this grant has given me priceless chances to advance my academic and scientific abilities.

TABLE OF CONTENTS

ABSTRACT	
ACKNOWLEDGEMENT	
TABLE OF CONTENTS	i
LIST OF FIGURES	v
LIST OF TABLES	viii
LIST OF EQUATIONS	ix
ABBREVIATIONS	x
NOMENCLATURE	xii
Chapter 1. Introduction	1
1.1 Background	1
1.2 Aim and objectives.....	5
1.3 Research knowledge contribution	5
1.4 Research scope and limitations	6
1.5 Research design methodology.....	7
1.6 Thesis structure.....	9
Chapter 2. Literature Review	11
2.1 Thermal comfort of earth building	11
2.1.1 Trend and history of earth building	11
2.1.2 Sustainability and thermal performance of Natural earth and its building.....	13
2.2 History and sustainability of earthbag building	16
2.2.1 Earthbag construction techniques.....	18
2.2.2 Soil type for earthbag building.....	23
2.2.3 The structural integrity of earthbag.....	24
2.2.4 Thermal Performance of Earthbag	25
2.3 Phase change material as thermal energy storage.....	30
2.4 PCMs categories.....	30
2.4.1 Organic PCMs.....	32
2.4.2 Inorganic PCM.....	33
2.4.3 Eutectic PCM	35
2.5 PCM selection criteria	36
2.6 Characterization and Thermal Analysis Methods of PCM	37
2.6.1 Differential Scanning Calorimetry (DSC)	37
2.6.2 Thermogravimetric analysis (TGA).....	38

2.6.3 Scanning Electron Microscopic analysis (SEM)	40
2.6.4 Thermal conductivity	41
2.7 Application of PCM in building.....	46
2.7.1 Application of PCM in the block.....	46
2.7.2 Application of PCM in the walls	48
2.8 PCM in vernacular building	50
2.9 Phase change materials in Nigeria and their application	51
2.9.1 SelectedPCMs for the region of experiment in Nigeria (Kano state).....	52
2.10 PCM modelling and simulation	53
2.10.1 The developed mathematical model used for simulation purposes based on the literature	54
Chapter 3. Development of PCM-Integrated Earthbag Block.....	60
3.1 Development and thermal characteristics of PCM-integrated earthbag block.....	60
3.1.1 Selection of materials	60
3.1.2 Fabrication and properties of PCM/EP/EG	62
3.1.1 Earthbag block	64
3.1.1 Properties of PCM and PCM composite and earthbag materials	65
3.1.2 Thermal property	66
3.1.3 Thermal stability analysis.....	67
3.1.1 Thermal conductivity	68
3.1.1 Prototype development and thermal performance analysis of earthbag block	70
3.2 Result	72
3.2.1 Thermal stability of PCM composite and PCM composite in soil	72
3.2.2 Surface morphology of EP, PEP, and PEPG and PEPGS using SEM	74
3.2.3 DSC Analysis of PCM, PCM/EP, PCM/EP/EG composite sample	77
3.2.4 Thermal degradation of PCM and PCM composites.....	78
3.2.5 Thermal conductivity of PEPS and PEPGS	81
3.2.6 Surface temperature reduction	82
3.3 Summary	85
Chapter 4. Development and Thermal Performance of PCM-Integrated Earthbag Wall.....	86
4.1 Experimental and Numerical Study on the Performance of Earthbag-wall Incorporated with Phase Change Materials	86
4.1.1 Experimental Study of PCM-intergrated earthbag wall.....	87
4.1.1 Wall thermal performance testing.....	90
4.1.2 Location and Climate	97
4.1.3 Model validation metrics	98

4.2 Description of the Case Study PCM-integrated earthbag wall	99
4.2.1 Climate	99
4.2.2 Modelling geometry and parameters	99
4.3 Result	104
4.3.1 Thermal conductivity of earthbag walls.....	104
4.3.2 Wall surface temperatures	106
4.3.3 Time lag (TL) and Decrement factor	108
4.3.4 Heat flux	110
4.3.5 Reduction in heat gain	111
4.4 Validation of numerical model.....	113
4.5 Parametric analysis	116
4.5.1 The effect of PCM transition temperature	116
4.5.2 Comparison between wall with pure PCM, PCM composite and expanded perlite insulation.....	118
4.5.3 Effect of optimum PCM/insulation thickness on earthbag wall surface temperature.....	120
4.6 Summary	122
Chapter 5. Numerical Investigation of PCM-Integrated Earthbag Wall in Temporary Housing	123
5.1 Determination of thermal performance of PCM-integrated earthbag walls in temporary housing.....	123
5.1.1 Thermal comfort analysis.....	124
5.2 Description of the case study.....	125
5.2.1 Numerical modelling and Methodology	125
5.3 Result	129
5.3.1 Inner surface temperature reduction	129
5.3.2 Effect of night ventilation on Inner surface temperature reduction	130
5.3.3 Heat flux through the walls.....	131
5.3.4 Peak indoor temperature reduction	133
5.3.5 Effect of night ventilation on peak indoor temperatures reductions.....	135
5.3.6 Effect of ventilation on indoor air temperature for summer period	136
5.4 Summary	138
Chapter 6. Discussion and Conclusion	140
6.1 Summary of the research study	140
6.2 Conclusions	141
6.2.1 Development and thermal characteristics of PCM-integrated earthbag block....	141

6.2.2 Experimental and Numerical Study on the Performance of Earthbag-wall Incorporated with Phase Change Materials	143
6.2.3 Determination of thermal performance of PCM-integrated earthbag walls in temporary housing.....	145
6.3 Future work.....	147
Appendix A.....	148
Publications.....	149
Bibliography	149

LIST OF FIGURES

Figure 1-1 Schematic design methodology flow chart	8
Figure 2-1 Alhambra Palace in Spain made from mud [49].....	11
Figure 2-2 The proportion of households living in dwellings with earth floors and earth walls [56]	13
Figure 2-3 Earthbag barrier during Russo-Japanese War 1904-1905 [78]	16
Figure 2-4 Green retaining wall made with earthbags [79]	17
Figure 2-5 Architect Nader Khalili during earthbag building demonstration [80]	18
Figure 2-6 Barbed wire layered between bags filled with earth	19
Figure 2-7 Rubble Trench Foundation [86].....	20
Figure 2-8 Earthbag house with dome roof [97]	22
Figure 2-9 (a) thatched roofs and (b) pitched roofs on earthbag buildings [99]	23
Figure 2-10 Interior simulated and monitored temperature, exterior temperature, solar radiation and radiation through the glazed surface, during the equinox [112] .	26
Figure 2-11 Construction of the residential area with Earthbag buildings (left), and Earthbag model (right) [98]	27
Figure 2-12 Annual Hours of discomfort and annual degree days of discomfort for earthbag base case and earthbag with solar protection [98].	28
Figure 2-13 Phase change material categories [126]	31
Figure 2-14 The melting enthalpy and melting temperature for the different groups of phase change materials [127].....	31
Figure 2-15 Eutectic PCM[149]	36
Figure 2-16 Phase change material selection criteria[155].....	37
Figure. 2-17 Pans used and balance relative weighting method of the TGA (a) available pans (b) balance system [164].....	39
Figure 2-18 The SEM images of EP and CM/EPPCM.....	41
Figure 2-19 Thermal conductivity of SSOPCCs with different contents of BN[184]....	42
Figure 2-20 (a) The guarded hot plates system and (b) sketch of the cross-section of system [188].....	44
Figure 2-21 Photographs of the tested walls: (a) the composite-PCMs wall; (b) the common wall [189]	45
Figure 2-22 Schematic diagram and the experimental set-up of the concrete blocks, with construction layers and the test chamber [211]	47
Figure 2-23 Tested bricks under hot Iraqi climate weather [214].....	48
Figure 2-24 The multilayer wall (a) dynamic wall simulator in the laboratory test and (b) schematic diagram showing the wall assembly [225].....	50
Figure 2-25 Physical illustrations of enthalpy form of the energy equation and boundary conditions [242].....	55
Figure 2-26 Control volume for heat conduction in EnergyPlus [246].....	57
Figure 3-1 Encapsulation process of Phase Change Material.....	63
Figure 3-2 Testing samples of earthbag block.....	65
Figure 3-3 Heat flow meter apparatus [266].....	68

Figure 3-4 Testing samples for thermal conductivity test: (a) raw sample and (b) sample enclosed in Polystyrene bag.....	69
Figure 3-5 Earthbag block arrangement outdoors	72
Figure 3-6 Comparison of leakage performance of (a) PEP(b) PEPG(c) PEPS and (d) PEPGS sample specimen	73
Figure 3-7 Earthbag block thermal cycling process	74
Figure 3-8 The SEM micrographs of (a) EP, (b) EG, (c) PEP x250, (d) PEP (x2k), (d) PEP x1k, (e) PEP (x 2k), (f) PEPG x 2k, and (g) PEPGS x 2k	76
Figure 3-9 DSC curves of PCM and PCM composites	78
Figure 3-10 TGA curves of PCM and PCM composite.....	80
Figure 3-11 Thermal conductivity of PEPS and PEPGS	82
Figure 3-12 Surface temperature of earthbag block without PCM and earthbag block with PCM.....	84
Figure 4-1 Flowchart of development of the earthbag-PCM model.....	87
Figure 4-2 Earthbag block mould.....	89
Figure 4-3 Earthbag block preparation.....	89
Figure 4-4(a) Test walls prototype in climatic chamber and (b) prototype's picture .	91
Figure 4-5 Air speed in a typical summer day in Kano state	94
Figure 4-6 Outdoor temperature variation for a typical summer months of Kano state	98
Figure 4-7 Developed SketchUp model geometry	100
Figure 4-8 Conversion process of PCM composites to layers.....	102
Figure 4-9 Phase transition temperature for A31, A28, Inertek26, and Inertek23 PCM	103
Figure 4-10 Enthalpy temperature curves of Inertek26, 23 and A31, 28 PCM	104
Figure 4-11 Inner and outer surface temperatures of earthbag walls at steady state	105
Figure 4-12 Inner surface temperatures of Wall-1 (baseline), Wall-2 (WA31) and Wall-3 (WInk26)	107
Figure 4-13 Outer surface temperatures of Wall-1 (baseline), Wall-2 (WA31) and Wall-3 (WInk26)	108
Figure 4-14 Time lags of Wall-2 (WA31) and Wall-3 (WInk26).....	109
Figure 4-15 Decrement factor of Wall-2 (WA31) and Wall-3 (WInk26)	110
Figure 4-16 Heat flux in the Wall-1 (baseline), Wall-2 (WA31) and Wall-3 (WInk26)	111
Figure 4-17 Heat transfer reduction comparison between the Wall-1 (baseline), Wall-2 (WA31) and Wall-3 (WInk26)	113
Figure 4-18 Temperature profile of Wall-1 (baseline), Wall-2 (WA31) and Wall-3 (WInk26).....	115
Figure 4-19 Various configurations for parametric analysis.....	116
Figure 4-20 Inner surface temperature for PCM A31, A28, Inertek26, and Inertek23	117
Figure 4-21 Comparison between wall with pure PCM, PCM composite and expanded perlite insulation	119

Figure 4-22 Percentage heat flux reduction	120
Figure 4-23 Effect of optimum PCM/insulation thickness on earthbag wall surface temperature.....	121
Figure 5-1 A tent constructed for IDP shelter in Maiduguri (selected case study) ...	125
Figure 5-2 PCM-E wall arrangement on earthbag building model.....	127
Figure 5-3 Sketchup 3D Earthbag Building Model.....	128
Figure 5-4 Inner surface temperature profile.....	130
Figure 5-5 Earthbag wall Inner surface temperature (a) without ventilation (0ACH) (b) with Ventilation (5ACH)	131
Figure 5-6 Heat flux densities through the walls profile	132
Figure 5-7 Earthbag indoor air temperature profile.....	134
Figure 5-8 Effect of night ventilation on peak indoor temperatures reductions	136
Figure 5-9 Overall summer temperature points over mean outdoor temperature for Earthbag building	137
Figure 5-10 Annual Hours of discomfort earthbag base-wall, E-wall, EN-wall, and ENW-wall.....	138

LIST OF TABLES

Table 2-1 Advantages and disadvantages of Organic PCMs.....	32
Table 2-2 Organic paraffin use as PCM.....	33
Table 2-3 Advantages and disadvantages of inorganic PCMs	34
Table 2-4 Inorganic PCM.....	34
Table 2-5 Summary of research conducted with PCM in vernacular building	51
Table 2-6 PCMs used in hot climate	52
Table 3-1 A31 paraffin technical data for PCM with a melting point of 31 °C	61
Table 3-2 Physical properties of expanded perlite.....	62
Table 3-3 PCM, expanded perlite and graphite proportions.....	63
Table 3-4 Sample specimen for earthbag block production	65
Table 3-5 PCM and PCM composite sample specimen	67
Table 3-6 Sample compositions for a thermal conductivity test.....	70
Table 3-7 The changes in thermal properties of the form-stable PCM composite after the addition of EG	78
Table 3-8 Measured thermal conductivities of the samples.....	81
Table 4-1 Technical data for the thermos-physical characteristic Inertek26.....	88
Table 4-2 Numerical model materials properties.....	101
Table 4-3 Average heat flux reduction between reference, WA31, and WInk26 earthbag walls.....	111
Table 4-4 Discrepancies between numerical and experimental results	115
Table 4-5 Validation metrics	115
Table 4-6 Inner surface temperature reduction of PCM A31, A28, Inertek26, and Inertek23	118
Table 5-1 Input parameters for earthbag model geometry	128
Table 5-2 Indoor Temperature reduction for different PCM-E orientation	134

LIST OF EQUATIONS

Eqn 2.1	54
Eqn 2.2	56
Eqn 2.3	57
Eqn 2.4	57
Eqn 2.5	57
Eqn 2.6	58
Eqn 2.7	59
Eqn 2.8	59
Eqn 3.1	67
Eqn 3.2	69
Eqn 4.1	92
Eqn 4.2	93
Eqn 4.3	93
Eqn 4.4	93
Eqn 4.5	93
Eqn 4.6	93
Eqn 4.7	94
Eqn 4.8	95
Eqn 4.9	95
Eqn 4.10	95
Eqn 4.11	95
Eqn 4.12	96
Eqn 4.13	96
Eqn 4.14	96
Eqn 4.15	98
Eqn 4.16	98
Eqn 4.17	99
Eqn 4.18	99
Eqn A6.1	148

ABBREVIATIONS

EG	Expanded graphite
EP	Expanded perlite
PCM	Phase change materials
PEP	PCM/EP composite
PEPG	PCM/EP/EG composite
PEPS	PCM/EP composite mixed with soil
PEPGS	PCM/EP/EG composite mixed with soil
PCM-E Block	PCM-integrated earthbag block
PCM-E wall	PCM-integrated earthbag wall
S	Soil
Wall-1 (baseline)	Reference wall
Wall-2 (WA31)	Wall with PCM composite
Wall-3 (WInk26)	Wall with microencapsulated PCM
UNHCR	United Nations High Commissioner for Refugees
IDP	Internally Displaced Person
TES	Thermal energy storage
DSC	Differential scanning calorimetry
TGA	Thermogravimetric analysis
SEM	Scanning electron microscopic
EHS/EP	Eutectic hydrated salt/expanded perlite
SSOPCC	Shape-stable organic phase change composite
BN	Boron nitride
EPOP	Paraffin/hydrophobic expanded perlite
GNP	Graphene nanoplatelets
MPCM	Microencapsulated phase change materials
SSPCM	Shape-stabilized phase change material
HVAC	Heating, ventilation, and air conditioning
CEBs	Compacted earth blocks
PCT	Phase change temperature
LHS	Latent heat storage
IDF	Input Data File Editor
CTF	Conduction Transfer Functions
CondFD	Conduction Finite Difference
EPS	Expanded Polystyrene Insulation
XPS	Extruded polystyrene insulation

cPCM

capric acid-myristyl (CM) alcohol/expanded
perlite composite

PCM-CLSC

PCM-concrete thermal storage blocks

NOMENCLATURE

Symbol	Term	Unit
A	Surface area	m^2
C_p	Specific heat	J/kg.K
d	Thickness	m
F_o	Fourier number	
FB	Fractional bias	
$FAC2$	Fraction of predictions within a factor of two	
f	Decrement factor	
h_c	Convective heat transfer coefficient	
H	Enthalpy	J/g
H_{PCM}	Measured latent heat of PCM	J/g
H_T	Theoretical latent heat	J/g
k	Thermal conductivity	$W/(m.k)$
$NMSE$	Normalized mean square error	
Q	Heat flow	Wh/m^2
q	Heat flux	W/m^2
r	Correlation coefficient	
T	Temperature	$^{\circ}C$
T_b	Temperature of the inner wall surface	$^{\circ}C$
T_i	Temperature of the indoor air	$^{\circ}C$
TL	Time lag	hour
V_w	Air speed	m/s
W_{PCM}	Weight percentage of PCM	%
ΔT	Temperature difference	$^{\circ}C$
ρ	Density	kg/m^3

Chapter 1. Introduction

1.1 Background

Temporary housing and its challenges have been a global concern for many years. The forced displacement of people due to natural disasters, conflicts, and poverty has resulted in millions of people living in temporary housing [1]. Most live in harsh climates, including extreme heat or cold temperatures [2]. This has led to poor indoor living conditions in these houses and has negative impacts on their inhabitants' physical and mental health [3]. Despite being temporary solutions to rapid displacement, these housings are often used for more than the intended timeframe [4], leading to the development of new housing designs that can ensure thermal comfort while fulfilling social needs [5]. The UNHCR (United Nations High Commissioner for Refugees) is currently interested in protecting over 71 million people, of whom nearly 20 million are refugees and 39 million are internally displaced [6].

A major challenge for these housing systems is thermal comfort. Most current temporary housing designs lack thermal mass and do not respond to the extreme thermal conditions to which inhabitants are usually exposed [7]. This has made it difficult to ensure the physical and mental health of users while enhancing energy efficiency. Traditional solutions to achieve thermal comfort in buildings require a constant supply of electricity to households for cooling or heating purposes, particularly in regions with hot or cold weather [8]. However, the living conditions of IDPs (Internally Displaced Persons) in displacement camps are often characterized by overcrowding and inadequate access to basic amenities such as water, sanitation, health care, and most notably, electricity [9][10]. This lack of access to electricity affects the living conditions of IDPs, leading to increased morbidity and mortality owing to harsh climatic conditions [11],[12]. Using bioclimatic design techniques with highly efficient active systems is essential to significantly reduce the cooling energy demand in buildings, reduce dependency on grid electricity supply, and improve energy security [13].

Energy is an essential component of sustainable development, and the use of fossil fuels to generate energy is the most common method used globally [14]. However, it is evidence that energy availability and efficient use are crucial for humanity's well-being, as they significantly impact the quality of life, social security, welfare, and steady economic growth and development [15]. Conversely, the environmental problems associated with fossil fuels, such as greenhouse gas emissions, global warming, air pollution, climate change, oil spills, and acidic rain, have highlighted the need for sustainable energy systems [16],[17].

The building sector is a major energy consumer, accounting for 30-40% of the total global primary resources [18]. In developing countries such as Nigeria, where extremely high temperatures and intense solar radiation are common, the challenge of energy consumption in buildings is intensified, driving the need for more energy use within buildings. As a result, the scarcity of fossil fuels due to high demand and their negative impact on the environment have led to global efforts to explore alternative energy sources and reduce energy consumption [14],[19].

Renewable energy sources have been identified as the most convenient alternative energy source to dwindle the power-generating capabilities imposed by rising energy demand [20]. However, renewable energy sources such as wind and solar power are intermittent, leading to an increased demand for energy storage [21] and the use of sustainable materials as an essential component of future energy-saving systems that use variable renewables. The building sector is particularly affected by this demand for energy storage, as buildings consume 40% of global energy [22].

Various measures, such as utilising sustainable materials and incorporating energy storage materials, can be employed to decrease the energy demand of buildings. Sustainable materials that are locally abundant, recyclable, regeneratable, and have low embodied energy are known to be effective in reducing the impact of carbon on the environment and human health, and increasing thermal comfort [23],[24],[25]. Earth is an example of a sustainable source for building materials that can be found in different climates and regions as a locally available and eco-friendly [26][27][28]. However, its economic viability depends on the construction technique, labour costs, stabilizing procedure, durability, and repair requirements [29]. In less developed

countries, earth buildings can be economical because of cheap labour and availability of raw materials [30] [28].

One of the traditional earthen buildings with the advantages mentioned above can be attributed to earthbag buildings, which, according to Geiger and Zemskova [31], is an inexpensive, sustainable, and straightforward method for building structures. Earthbag buildings can be built with any type of soil with little or no stabilization process [32]. In such housing, the need to transport building materials from other places is not a barrier, as most of the materials are available in the place of construction. Therefore, such buildings could be a solution for internally displaced people and those in need of temporary buildings. Nevertheless, the thermal comfort of earthbag buildings is in question, as researchers have pointed out that earthbag buildings are thermally unstable [33], [34], whereas one of the primary objectives of designers and building engineers is thermal comfort [12].

To enhance the thermal comfort of buildings, phase change material (PCM) have been employed as energy storage technology in building envelopes [35][36][37][38][39]. Phase change materials (PCMs) can provide passive heating and cooling in buildings through their high latent heat capacity. PCMs absorb heat during the day through melting and release the heat at night through solidification, reducing temperature fluctuations and peak loads in buildings [40]. This thermal mass effect can reduce HVAC system size, energy consumption, and costs [41]. PCMs are reported to achieve cooling energy savings from 10-17% in brick buildings and up to 2.1 kWh/m² reduction in annual cooling load [40],[42]. PCM wallboards and plasters can also moderate indoor air temperatures by 0.3-0.7°C and reduce up to 7% of summer discomfort hours[43],[44]. PCM panels in walls and roofs are found to decrease annual energy consumption in residential buildings by 10-15% [44]. PCM incorporation thus enhances building energy efficiency and indoor thermal comfort. However, despite its widespread use as a thermal storage medium, the use of PCM for thermal comfort satisfaction in vernacular buildings has not received much attention compared to conventional buildings.

Pakand and Toufigh, [45] proposed that incorporating thermal energy storage (TES) materials, such as PCM, can improve the thermal performance of traditional rammed

earth walls. Therefore, incorporating PCM into earthbag buildings can solve their thermal instability of earthbag buildings. However, earthbag buildings do not support insulation materials, making the use of PCM a viable solution for producing a thermally comfortable earthbag building.

Nevertheless, PCM pose a challenge, particularly those that undergo phase shifts at room temperature, which is the case for most PCMs used in buildings. The solution is to trap PCM in an appropriate matrix, such as expanded perlite, because organic PCMs tend to flow or exude onto the surface of the matrices during the phase change process, leading to a greasy and discoloured surface and a gradual deterioration of the PCM's heat storage capabilities [46].

Despite the urgent need to host many refugees within a short notice, there is a lack of research on the thermal comfort of temporary housing. Moreover, among the limited studies that have focused on the thermal performance of shelters, there has been a greater emphasis on cold environments compared to hot climate environments [47], resulting in an underdeveloped area of research that poses potential risks for vulnerable occupants, particularly children. Therefore, this research proposes strategies for improving thermal comfort in temporary housing by assessing the thermal performance of earthbag-integrated PCM (PCM-E wall). Hence, this study aims to address the research gap in the thermal performance of temporary housing by developing sustainable and affordable housing designs that ensure thermal comfort while fulfilling social needs, particularly in areas with hot and dry climates. The goal is to provide sustainable solutions that can be replicated in other areas with hot and dry climates, thereby benefiting vulnerable populations worldwide.

1.2 Aim and objectives

The study aims to develop and evaluate PCM-integrated earthbag buildings for temporary housing in hot and dry climates. Housing sustainability will be achieved by integrating PCMs into the earthbag technique, which could help produce non-mechanical buildings for building thermal comfort. Therefore, the objectives of this project are:

1. To provide a general overview of an earthbag building technique along with a passive design strategy, with an emphasis on summarizing existing research on the thermal performance of earthbag buildings.
2. To conduct a comprehensive literature review on phase change with a focus on PCM in vernacular buildings and to select a promising PCM candidate suitable for applying PCM in earthbag buildings in hot climate regions.
3. To develop and investigate the thermal properties of a PCM-integrated earthbag block for use in temporary buildings.
4. To conduct an experimental and numerical study to investigate the performance of earthbag-wall integrated with phase change material.
5. To conduct a numerical investigation to evaluate the thermal performance of temporary IDP housing, specifically IDP houses in Nigeria, by incorporating optimum PCM-integrated earthbag walls (PCM-E).

1.3 Research knowledge contribution

This study aims to contribute to the knowledge gap regarding the thermal performance of temporary housing in hot and dry climates by developing sustainable and affordable housing designs that ensure thermal comfort and fulfil social needs. Based on a comprehensive literature review, it is evident that although natural earth building materials have been extensively investigated, little attention has been given to incorporating modern commercial technologies, such as energy storage materials, specifically PCM, into earth building practices. Moreover, few studies have assessed the thermal behaviour of earth buildings and the thermal characteristics of earthen materials. Therefore, this study proposes a novel and sustainable earthbag building incorporating PCM for hot and dry climates to overcome the identified limitations.

Additionally, there is a lack of research on the thermal comfort of temporary housing, especially in hot climates, which pose potential risks to vulnerable occupants, particularly children. Hence, this research also aims to assess the thermal performance of earthbags integrating PCM to propose strategies for improving the thermal comfort in temporary housing. This research contributes to the field of sustainable building practices and provides insights for future research on integrating energy storage materials into earth building practices to reduce energy consumption and carbon emissions.

1.4 Research scope and limitations

The research scope is limited to the analysis of earthbag building thermal performance in Kano state climate conditions, despite the distribution of IDPs in every state of Nigeria, with the highest number in the North-East region. Therefore, there are certain limitation of this research listed as follows:

1. The research did not consider the heterogeneous characteristics of soil in different states of Nigeria as only the soil available in Kano state was studied.
2. The lack of equipment in Nigerian laboratories led to the use of soil from the United Kingdom, which underwent modifications to approximate the soil characteristics of Kano state.
3. The analysis was limited to a single earthbag room without considering the entire house analysis.
4. Cost-benefit analysis of PCM integration in the earthbag building was not conducted.
5. The research findings can only be applied to hot and dry climate states in Nigeria as Nigeria has different vegetation zones and temperature regimes due to its proximity to the equator and Sahara Desert, resulting in different comfort requirements.

1.5 Research design methodology

The methodology employed in this research followed a systematic approach, encompassing literature reviews, experimental studies, and numerical investigations. This approach is undertaken to fulfil the research objective of developing PCM-integrated earthbag buildings for temporary housing. The primary focus is on enhancing housing sustainability through the integration of PCMs within the earthbag construction technique. This integration has the potential to create non-mechanical buildings for building thermal comfort. The methodology was carefully designed to ensure that all the necessary steps were taken to effectively achieve the research objectives. The methodology employed in this research consists of the five main steps outlined below, and the schematic design methodology flow chart is presented in [Figure 1-1](#).

Step 1: A thorough literature review related to earthen buildings and their thermal performance was conducted. This review helped to gain a deep understanding of the advantages and disadvantages of earthbag buildings in terms of thermal comfort, as well as the potential for incorporating this building concept into temporary housing.

Step 2: The second step involves an in-depth literature review of PCM in buildings. This review focused on incorporating PCM in vernacular buildings and aimed to identify the most suitable types of PCM for integration into earthbag buildings to achieve the research aim.

Step 3: This step is centred on the development and study of the thermal characteristics of integrated PCM earthbag blocks. This involved the selection of suitable soil compositions through preliminary tests and the fabrication of PCM composites for integration into the earthbag blocks. The characterization of the PCM composite, such as DSC, TGA, SEM, thermal conductivity, and oozing circle tests, in addition to the thermal performance of the integrated PCM earthbag blocks, were studied in detail under real weather conditions.

Step 4: The fourth step involved the development of PCM-E wall using the optimum block identified in the previous step. This included material and preparation, conducting experiments in an environmental chamber to measure thermal

performance, validating experimental data obtained using the numerical model developed in EnergyPlus 8.7© of a 1-zone building temporary housing, and conducting a parametric analysis to determine the optimal quantity of PCM to be used.

Step 5: In the final step, a numerical investigation was conducted using EnergyPlus 8.7© to evaluate the thermal performance of temporary IDP housings in Nigeria as a case study, incorporating the optimum PCM-E walls identified in step four. This step included a parametric study of PCM-E walls in temporary IDP housing, considering PCM-E wall configurations for thermal comfort determination.

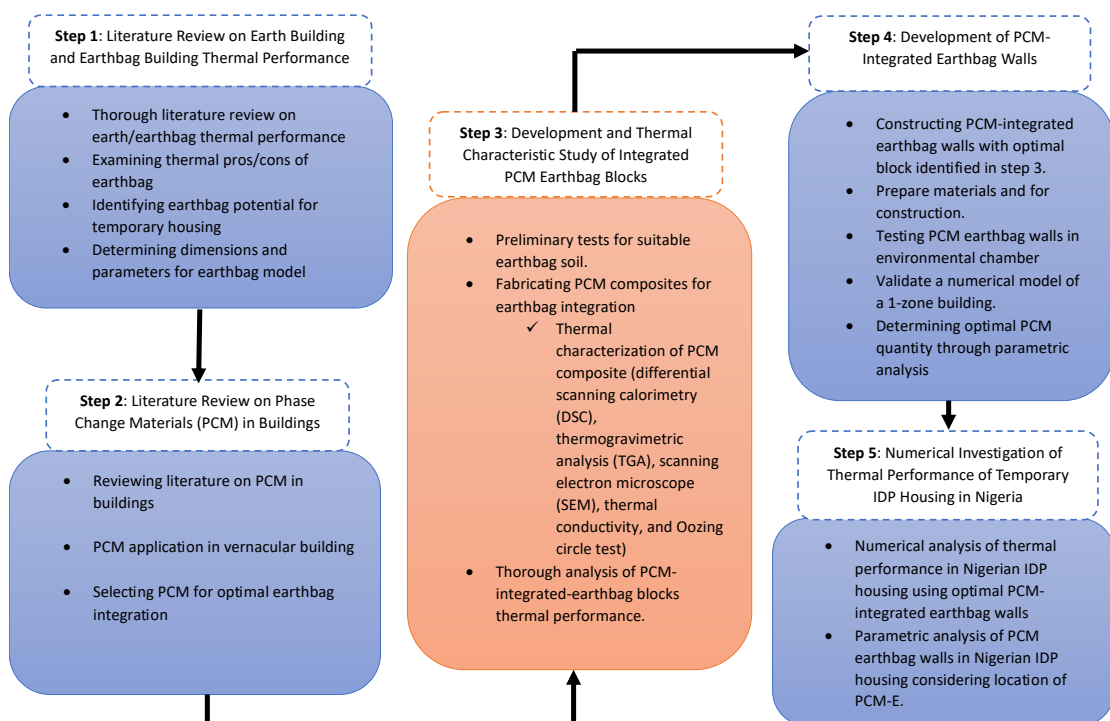


Figure 1-1 Schematic design methodology flow chart

1.6 Thesis structure

This thesis is divided into eight sections.

Chapter 1: This chapter comprises an introduction that gives an overview of the internally displaced person housing situation in the world and Nigeria. The benefits of PCM in earth buildings for thermal comfort are briefly highlighted. There is also a concise explanation for the energy crisis in Nigeria. The aims and objectives, research knowledge contribution, and research structure are also provided.

Chapter 2: A comprehensive review of earth and earthbag building thermal performance and the history of earthbag building evolution was conducted. This is related to Objective 1. An overview of earthbag soil type, classification, and soil selection criteria is presented in this chapter.

Chapter 3: Thermal energy storage in a building is discussed in this section. A comprehensive review of PCMs includes their classification, characteristics, advantages and disadvantages, and selection criteria are discussed. In addition, the applications of PCM in vernacular buildings and Nigeria were reviewed. This is connected to Objectives 1 and 2.

Chapter 4: This chapter outlines the methodology used in the research, including the material preparation specifics and development of the tested model. In addition, this chapter covers the approach used for the model simulation and validation design. All of these elements were connected to the overall objectives of the study.

Chapter 5: The development and thermal characteristics of PCM-E blocks are investigated in this chapter. This involves conducting an experimental study to understand the microstructural properties of embedded PCM composites in soil. Differential scanning calorimetry (DSC), thermogravimetric analysis (TGA), scanning electron microscopy (SEM), thermal conductivity, and oozing circle tests were employed over the developed blocks to measure their thermal characteristics. Finally, this section investigates and presents the block thermal performance under a hot climate. This is connected to Objectives 2, 3, and 4.

Chapter 6: presents an experimentally validated numerical model that was employed to determine the performance of the PCM-E wall. Parametric analysis was conducted to determine the suitable quantity of PCM required for the PCM-E walls. This is connected to Objectives 4 and 5.

Chapter 7: This chapter focuses on the numerical investigation of the thermal performance of PCM-E wall in selected temporary IDP housing (taken as a case study) in Nigeria. This chapter includes a parametric study that considers the effects of PCM-E wall orientation on the performance thermal performance of temporary IDP housing. This is related to Objective 6.

Chapter 8: The final chapter of this thesis presents the conclusions and recommendations drawn from the research conducted in the previous chapters and suggestions for future work.

Chapter 2. Literature Review

“Earth turns to gold in the hands of the wise” -Rumi

12th-century Persian poet and mystic

2.1 Thermal comfort of earth building

2.1.1 Trend and history of earth building

In an earth building, a significant percentage of the framework or fabric is constructed of graded soil (also known as earth) generated using one or more processes, such as rammed earth or compressed earth blocks [48]. Earth was used as a building material in all ancient cultures, not only for homes but also for religious structures [49]. However, earthen building techniques have been practiced for over 9000 years. In Russian Turkestan, mudbrick (adobe) houses dating from 8000 to 6000 BC have been found. Assyrian rammed earth foundations from around 5000 BC have been discovered [49]. The Great Wall of China, some of which was built with rammed earth over 2,000 years ago, and the Alhambra Palace in Spain, as seen in Figure 2-1, constructed in the 10th century, are other historical examples of earth construction [50]. Raw earth buildings can be found in different climates, from arid zones to tropical and temperate latitudes [49].



Figure 2-1 Alhambra Palace in Spain made from mud [51].

For thousands of years, humans have used various forms of unprocessed earth to build their homes. However, due to the widespread use of concrete and steel after the Second World War, raw earth was abandoned in industrialized nations. Similarly, in Nigeria, the remnants of earthen structures are viewed as historical reminders in traditional city centres. These old earth structures, associated with the Natives, are gradually replaced by illustrious sons and daughters of these families with more contemporary constructions [52]. This trend has recently reversed, as interest in earth buildings among architects, engineers, and policymakers has increased because of its ecological advantages [53]. It is estimated that more than a third of the world's population lives in natural earth houses [54], [55], with a higher concentration in developing countries [56]. In India, there are estimated to be as many as 80 million dwellings made with Earth, and in China, the number of people living in earthen homes is estimated to be 100 million [57]. In Nigeria, there is a lack of tentative data on the number of people living in earth buildings. However, a study by Marsh and Kulshreshtha [58] shows that many people live in dwellings with earth floors and earth walls in Nigeria as indicated in the [Figure 2-2](#).

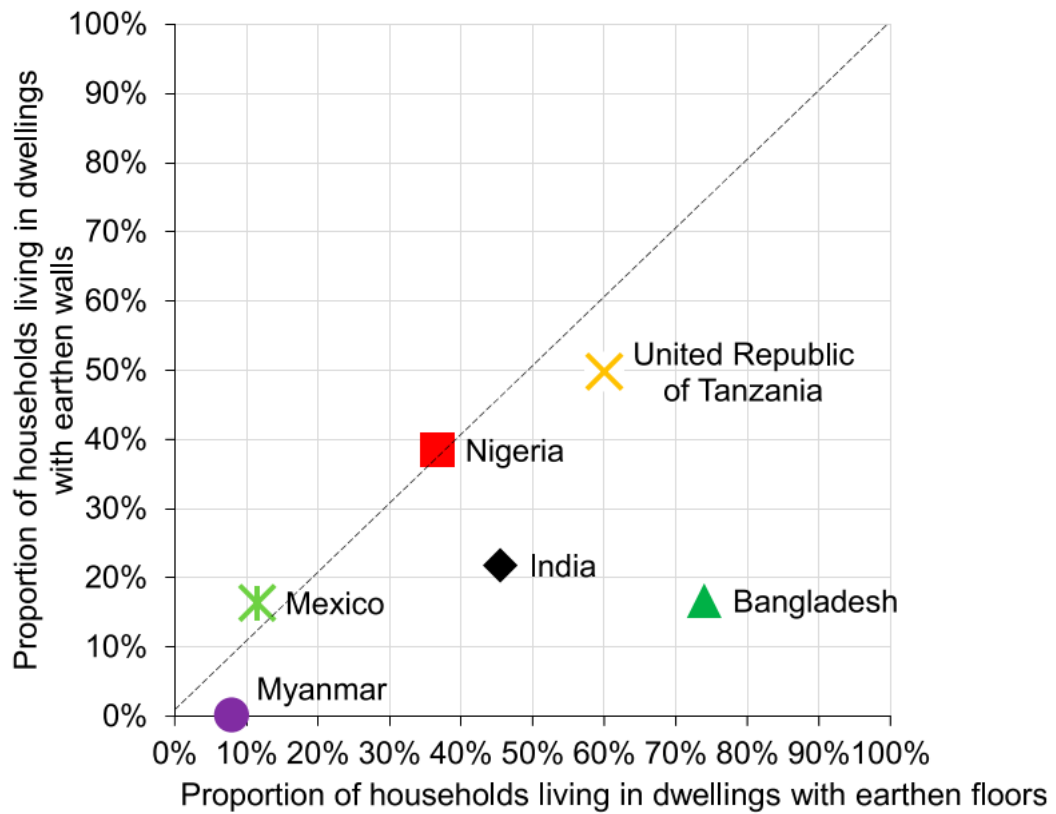


Figure 2-2 The proportion of households living in dwellings with earth floors and earth walls [58]

2.1.2 Sustainability and thermal performance of Natural earth and its building

The use of earth as a construction material is becoming more popular because it has good physical characteristics for ecological design and satisfies all the strength and serviceability requirements for thermal transmittance. This development is also due to the current concerns for sustainable development that have emerged due to serious environmental issues, including climate change and resource depletion, and the accelerating rate of technological advancement in the building industry [59]. Most earth buildings are sustainable and their building materials are reusable, making them less expensive [54]. Earth is categorised as a green building material because it can be found in various climates, from deserts to tropical regions in different temperate regions, while it is available locally, economically attractive, and environmentally friendly [9-11].

Most earth buildings are located in hot and dry climates, representing a suitable cooling performance [60]. Nonetheless, this cannot be taken as an ultimate fact in

many developed countries because the economics of earth buildings are influenced by various factors such as construction techniques, labour costs, stabilising procedures, durability, and repair requirements [29]. Inversely, this technology can be an economical option in less-developed countries because of the cheap labour and availability of raw earth materials [59][28].

Nevertheless, making earth buildings comfortable does not require sophisticated technology compared with conventional buildings, where high-energy consumption technologies are used to provide comfortable spaces in buildings. In this respect, extensive research has demonstrated that raw earthen materials are preferable to green technologies. For example, Reddy et al. [61] conducted a study in 2016 that examined rammed earth as material with low-embodied energy. The researchers concluded that the cement-stabilized rammed earth (CSRE) case-study building exhibited a low embodied energy of $1.15 \text{ GJ}/\text{m}^2$. In comparison, conventional burnt clay brick load-bearing masonry buildings and reinforced concrete framed structure buildings had embodied energies ranging from 3 to 4 GJ/m^2 and 4–10 GJ/m^2 , respectively. Another effective technique adopted for earth construction is cob building. Hamard et al. [62] studied the sustainability of cob buildings based on the construction process. This study revealed that cob buildings have many environmental (low energy use and low carbon emissions), social, and health benefits. Khaksar et al. [63] studied the Bhutanese vernacular wattle, and daub houses sustainability assessment. They found that wattle and daub houses are more sustainable than the dominant structural forms in Bhutan. Similar studies on earth building sustainability can be found in many other works in the literature, such as earth bricks [17- 21] and adobe [22-23].

Numerous works in literature show that earthen buildings are suitable for achieving thermal comfort [68][69][70][71][72]. Adegun and Adeyi [26] summarised the advantages of earthen buildings from other African research regarding thermal conductivity, resistivity, diffusivity, indoor and outdoor temperature, and cooling and heating loads. The results indicate that earthen materials can reduce annual cooling and heating loads by reducing hourly heat gain, which increases the total annual hours within a comfort zone. Desogus et al. [73] studied the thermal behaviour of a two-story earth building without HVAC (Heating, ventilation, and air conditioning) system

throughout the measurement period. The findings demonstrate that the lower floor offers comfortable conditions, whereas the bedroom on the upper floor shows overheating issues. Palme et al. [74] investigated the thermal performance of four buildings made from different materials (i.e., earth, concrete, and wood). This investigation was conducted using simulations and monitoring studies. The results showed that adobe and rammed earth buildings performed better than wood and concrete in terms of thermal decrement, thermal lag, insulation properties, and solar radiation gain. Another intriguing investigation of earth buildings was conducted by Cheikhi et al. [75]. In this study, the energy efficiency of rammed earth buildings compared to that of concrete structures and masonry envelopes was determined using DesignBuilder simulation software. The simulation results revealed that rammed earth is a sustainable, energy-efficient, and environmentally friendly building material. However, caution must be taken because if heating requirements are considerably reduced in winter, it causes an increase in the air-conditioning load in summer. Other studies have focused on Nigeria's climate. Nwalusi et al. [76] examine the thermal comfort of Igbo traditional residential buildings using the experimental research method. The study revealed that the average temperature sensation felt by the building occupants ranged from cool to slightly warm. This study suggests including high-level window apertures in future building designs to produce ventilation through the stack effect and wind. Ogunrin [77] researched traditional buildings compared to modern buildings and showed that the traditional house envelope promotes thermal comfort in contrast to the modern house envelope. Nevertheless, few studies have been conducted on traditional housing comfort in Nigeria's hot and dry climates.

2.2 History and sustainability of earthbag building

Earthbag construction can be categorized among the earth construction techniques, which are also older but only used during military operations for protection against bullets and grenades (Figure 2-3), fluid control, and retaining walls (Figure 2-4). Earthbag buildings can be built in different shapes with desired aesthetic requirements. Nevertheless, the investigation into using natural building materials such as sand and gravel as a house was started by Gernot Minke of the Research Laboratory for an experimental building in Kassel, Germany, in 1976 [78]. In the 1980s, the idea of building permanent structures using bags filled with earthen materials (see Figure 2-5) was first promoted [31]. Since then, these techniques have continued to grow, especially in developing countries with high housing deficits. Canadell et al. [79] highlighted that the interest in earthbag dome construction (also known as sandbag, superadobe, or superblock construction) is increasing as global consciousness develops to achieve the planet's equilibrium for sustainable living.



Figure 2-3 Earthbag barrier during Russo-Japanese War 1904-1905 [80]



Figure 2-4 Green retaining wall made with earthbags [81]

Earthbag technology is an inexpensive, sustainable, and straightforward method for building structures [31]. Earthbags do not deplete scarce local resources, as wood or brick buildings do. Most of the materials used for earthbag buildings can be supplied from local and natural subsoil. Thus, earthbag buildings have a minimal carbon footprint.



Figure 2-5 Architect Nader Khalili during earthbag building demonstration [82]

2.2.1 Earthbag construction techniques

Soil is a widely accessible resource that can be utilised for various earthen construction techniques and is readily available at little to no cost [83]. Earthbag buildings use raw earth to construct walls and roofs for dome structures. However, the assessment of soil for earth buildings is crucial because not all soils are suitable for building construction. Therefore, the soil type generally suitable for earthbag buildings is discussed based on the literature. However, there is still no code for earthbag buildings despite the growing awareness of this type of structure, especially among developing countries for emergency structures. The earthbag construction technique of the walls is based on stacked bags filled with soil with a barbed wire layered between them, as depicted in Figure 2-6 [84]. Construction techniques are based on empirical or semi-empirical rules [85]. However, these techniques require careful planning, as Geiger [86] mentioned.

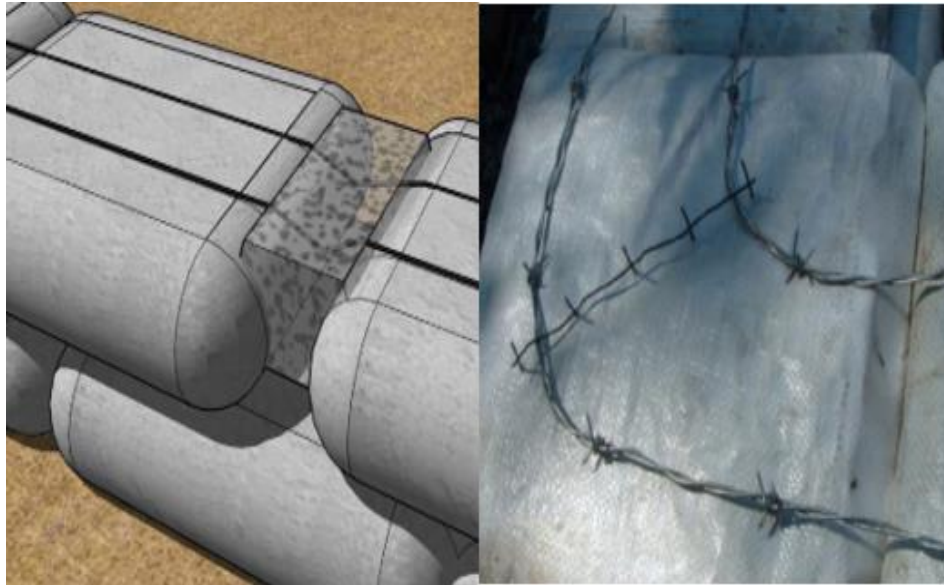


Figure 2-6 Barbed wire layered between bags filled with earth

2.2.1.1 Foundation

Earthbag buildings can use many traditional foundation types, but a rubble trench foundation is generally preferable [31]. This is because rubble trench footing is the easiest and cheapest footing foundation [85], and it takes only 10% to 15% of the total building cost; usually, a foundation depth of 3 to 4 ft is sufficient [87]. Trench foundation is an old historical technique that employs loose stone or rubble to improve drainage and reduce the need for concrete. This strategy has been used for centuries, but was first popularised by Wright [88],[86]. The trench foundation strategy involves filling a foundation with stones or bricks, which can support a wall 50-60 *cm* wide. To protect the wall from moisture rising from the ground or precipitation sprinkling when it hits the ground, the foundation must be sufficiently tall, as shown in Figure 2-7 [89]. Another advantage is that the foundation wall can resist swelling damage when built on swelling clay, and is better than reinforced concrete because it can flex [90].

According to Hart[91], loose materials can also fill the foundations of earthbags. He added that all these loose materials have unique qualities, most of which can be categorised as insulation. Perlite, vermiculite, lightweight volcanic stone (such as scoria or pumice), and rice hulls are insulating filler materials. Nevertheless, the

preferred material is scoria, which is unaffected by moisture and tends to assume a solid shape that is not readily deformed after it is tamped into place. Under compression, scoria, pumice, and perlite were sufficiently stable to withstand heavy weights. Vermiculite and rice hulls should only be used as fillers in other weight-bearing structures, such as post and beam or wood frame systems, because they compress significantly when subjected to a load. Few studies have been conducted on earthbag foundations in earthbag research. Daigle[92] investigated the strength of crushed granite with a nominal diameter of 12.7 mm, screened all fine particles. Crushed granite was selected for testing due to its increasing popularity as a fill material for earthbag foundations. The strength determined from the results shows that, compared with other conventional building buildings, an earthbag filled with crushed granite has a higher strength. However, an investigation by Daigle et al.[93] showed that gravel-filled earthbag specimens fail at lower loads compared to soil-filled specimens because of abrasion at the bag–bag interface, leading to loss of fill. Therefore, gravel-filled earthbags may not be more suitable for earthbag walls than soil-filled earthbags.

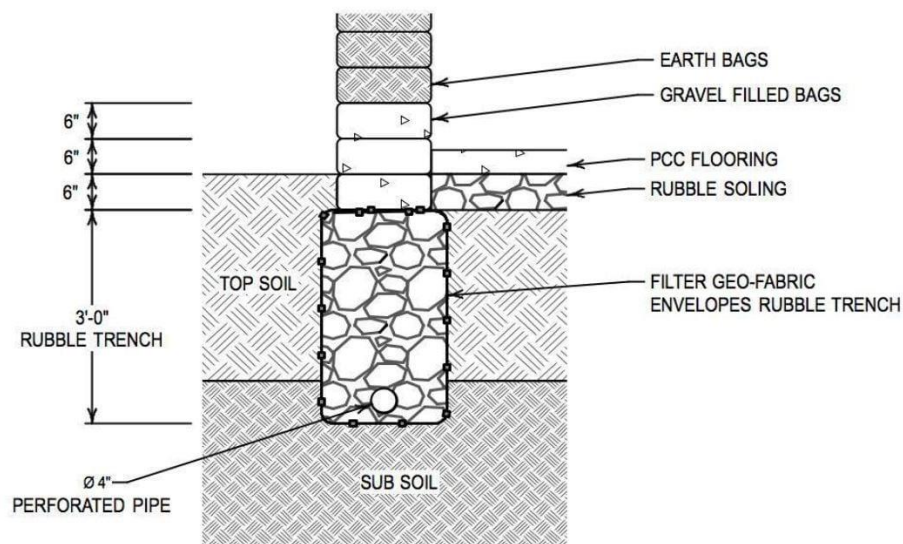


Figure 2-7 Rubble Trench Foundation [88]

2.2.1.2 Wall construction

The earthbag wall system was designed to cooperate with compression forces to preserve its structural integrity [94]. Earthbag walls can be built using locally available materials [95]. Earthbag wall-building techniques involve filling soil in a polypropylene bag and closing each bag with a metal wire, thread, or heavy-duty stapler [85]. Each bag should be tamped as a soil fill to avoid deterioration in this significant compression area. The filled bags were then laid on a trench foundation made from gravel fills. Each bag layer was tamped to attain the desired compressive strength [56]. Every course needs to be tamped before being keyed with a four-point barbed wire or thorny plant branches, which will provide friction to stop the bags from shifting over time. The bags can either be strongly buttressed or fastened to the bags if no barbed wire is available [96]. The thickness of the earthbag wall depends on the size of the available bag and the number of building stories. According to Hart[91], for single story earthbag buildings, the most typical earthbag construction bags are around 18 inches (45 *cm*) wide. Once filled and tamped, these bags create a wall approximately 14 in (36 *cm*) wide. Design flexibility exists for most single-story buildings because the rule of 1:8 dictates that an earthbag wall created with these bags should not be taller than approximately 9 feet (2.7 *m*) [97]. K. Hunter and D. Kiffmeyer[98] added that for a two story building, the first floor should be built with even larger bags. Similarly, with 15-inch (37.5 *cm*) wide earthbag walls, ten feet (3 *m*) tall would be significant.

2.2.1.3 Roofing

The most common roofing type for earthbag buildings is corbelled earthbag domes, as shown in Figure 2-8. The concept of corbelled earthbag domes has been around for centuries, with evidence of such domes found in ancient civilisations, such as the Incas and Mesopotamians. Corbelled earthbag domes are constructed from layers of earthbags filled with soil or other materials, such as rice husks, arranged in an arch-like form. The bags were then tamped and compacted, and the dome was finished with a layer of mortar or plaster [96]. Because the bags are filled with local materials, such as soil, corbelled earthbag domes can be constructed relatively inexpensively,

and their energy efficiency makes them suitable for regions with extreme climates [56].

Despite the potential of corbelled earthbag domes, some challenges are associated with building methods. Domes are labour intensive and require considerable skill for proper construction. The domes are self-supporting and require no additional structural support, making them an ideal choice for remote areas where access to building supplies may be limited [98].



Figure 2-8 Earthbag house with dome roof [99]

The bags must be tamped with and compacted thoroughly to ensure that the structure is stable and strong enough to withstand extreme weather conditions [34]. Several other types of roofs can be used in earthbags, such as thatched and pitched roofs (see Figure 2-9). A pitched roof was made by placing two earthbag walls in an A-frame shape and then covering them with a layer of plastic, tar paper, or metal sheeting. This type of roofing is simple to construct and provides an effective method to shed rain and snow. It is also relatively inexpensive and does not require additional support structures or materials [96]. However, mono-pitched roofs are unsuitable for climates

with high winds, as they may not withstand the force of the winds [96]. Another type of roofing suitable for earthbag buildings is a thatched roof, consisting of a layer of vegetation such as grass, straw, or reeds laid over the earthbag walls. Thatched roofs are more energy-efficient than truss roofs and provide better insulation. However, thatched roofs require regular maintenance and are susceptible to damage under extreme weather conditions. Therefore, this study focused on pitched roofs with relatively low slopes in the final simulation and project demonstration [100].



Figure 2-9 (a) thatched roofs and (b) pitched roofs on earthbag buildings [101]

2.2.2 Soil type for earthbag building

Soil is the main material used in earthbag construction and is easily accessible and often free. Sandy clay soil with optimal water content is recommended for filling earthbags. This soil combines sandy and cohesive soils that can be compacted and dried to form earthen bricks [102]. Most soils do not require hardening additives such as cement, asphalt, or lime [94]. Compared with other earthen building methods, a wider range of soils can be used with earthbags [103]. The soil used for roads, called road bases, is often suitable for earthbag construction [104]. The amount of clay in the soil is crucial because it acts as a binding agent [93]. Bags filled with soil containing a 30% clay component are characterised by low expansion when exposed to moisture,

such as kaolinite [105]. The bag's most robust and stable soil fill contains many particle sizes, from sand to clay, and most subsoils are sufficient as fill and can be found on or near construction sites. It is possible to modify the soil by adding sand or clay if needed. The most common mix is approximately 25-30% clay soil and 70-75% sandy soil, although precise ratios are difficult to address [85].

Testing may be necessary to determine if the site-based soil is suitable for earthbag wall buildings, and the amount of clay or sand needed to be added [85]. Soils containing excessive amounts of clay can be utilized, but they pose additional difficulties during excavation and bag filling [96]. These types of soils require careful maintenance of dryness to ensure manageability because they tend to slump when excessively wet [103]. A 5 to 30% clay content in the soil with a balance made up of fine to coarse sand and gravel is generally acceptable for earthbag wall building [106]. A field test is necessary to determine whether soils with a clay content of over 30% are suitable for wall building [98].

2.2.3 The structural integrity of earthbag

The application of this particular type of earthen building is limited in comparison to other earthen structures, such as adobe, earth bricks, and conventional building structures. This limitation arises from the uncertainty surrounding its structural integrity. However, due to this constraint, many types of research have been conducted in different regions to understand its structural behaviour [78], [107], [108], [109] and found it stronger than the aforementioned types of buildings and their capacity to be used as building alternatives around the world for low-income earners and refugees [110] [111], [112]. Many researchers have proven that the earthbag structure is even more durable and reliable than the conventional structure of cement and concrete and other earthen structures such as adobe and earth bricks. According to Canadell et al. [79], earthbag buildings are so strong that they can resist driving a speeding vehicle into the wall, detonating grenades, or shooting them with a machine gun; only minor damage can be observed. Similarly, Geiger[85] said that people are discovering that, besides the earthbag being sustainable, it is safe, quiet, durable, non-toxic, rodent-proof, and resistant to bullets, floods, and fires. Stouter

[113] stated that the advantage of earthbag techniques over other earthen building techniques is that a wide range of soil types can be built with earthbags. Bags from plaster, grains, or cement are available worldwide, and mesh tubes are used for vegetable packaging. Because the bags or tubes are light, they can be easily transported to buildings in remote areas. This construction technique is best used in rural areas with limited resources. It can also help provide a permanent or temporary building for people displaced from their homes because of war or insecurity. Earthbag construction can offer many benefits to those in need of affordable housing.

2.2.4 Thermal Performance of Earthbag

Rincón et al.[114] conducted a study to compare the hygrothermal behaviour of an earthbag dwelling in Mediterranean continental climate with a numerical model using EnergyPlus v8.8. This study examined various ventilation and controlled indoor temperature scenarios. The results showed that the natural materials used in the earthbag construction provided suitable insulation with reductions of 90% in interior thermal amplitude during summer and 88% in winter compared to exterior temperatures. The temperature behaviour for the scenarios analysed demonstrated a close correspondence between the experimental data and simulation results, as shown in Figure 2-10. The position of glazed openings was crucial in direct solar gains, contributing to temperature increases of 1.31 °C in winter and 1.37 °C in the equinox. Night ventilation during the summer performed well as a passive system, and passive solar gains resulted in a reduction in heating energy consumption by 2.3% in winter and 8.9% in the equinox. However, the study concluded that a heating system would still be necessary for winter to achieve thermal comfort levels in earthbag buildings.

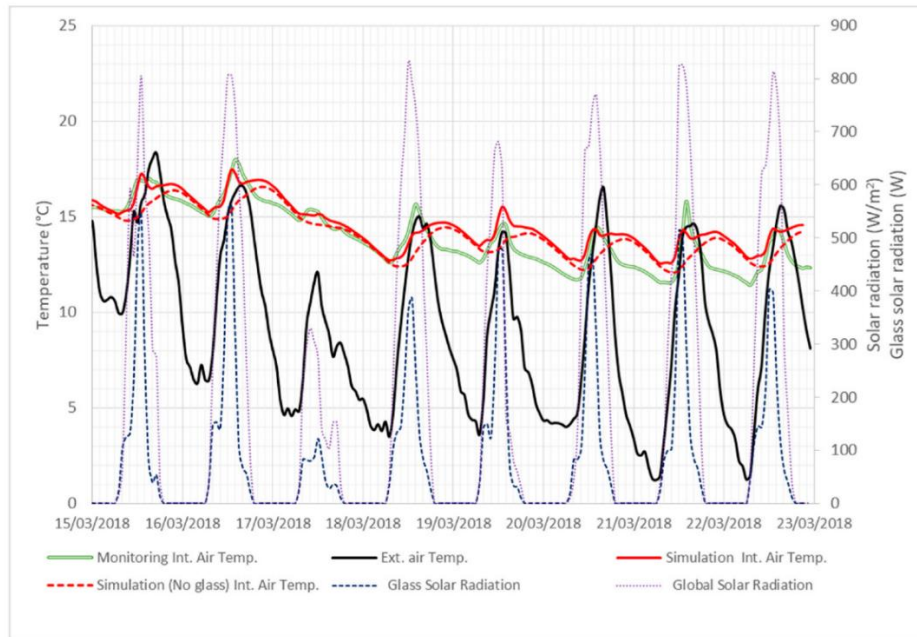


Figure 2-10 Interior simulated and monitored temperature, exterior temperature, solar radiation and radiation through the glazed surface, during the equinox [114]

Castell et al.[33] investigated an earthbag building in dry tropical climate of Burkina Faso to achieve thermal comfort using radiative cooling . This study simulates the cooling requirements of a Training Medical Center in Ouagadougou as shown in Figure 2-11 and compares them to the energy production of a Radiative Cooling (RC) system. The results showed that the RC system could cover a significant portion of the building's cooling needs, with a coverage of approximately 35% for an installed RC of $10m^2$ and an inlet water temperature of 25 °C. However, the technology could not fully cover the cooling demands during the most demanding months, indicating the need for further research to investigate the interaction between RC and HVAC distribution systems. Another study by Rincón, et al.[100] examined a low-cost alternative technique using earthbags for earthen construction in semi-hot climates. These bags were filled with local soil and natural materials and covered with a plaster finish. Researchers compared the thermal performance of earthbag dwellings with traditional Adobe constructions in Burkina Faso. The results showed that earthbag dwellings had better insulation performance and lower thermal transmittance than traditional Adobe constructions.

Further data analysis showed that combining night ventilation and solar roof protection in a high-inertia earthbag building almost eliminated thermal discomfort during the year. Only 209 h did not meet adaptive comfort and 3.1°C-days of discomfort. On the other hand, the same combination of passive measures in the traditional Burkinabe dwelling improved thermal comfort, but it was not as effective in providing comfort for more than 3000 h and 200 degree-days of annual discomfort, as demonstrated in [Figure 2-12](#).

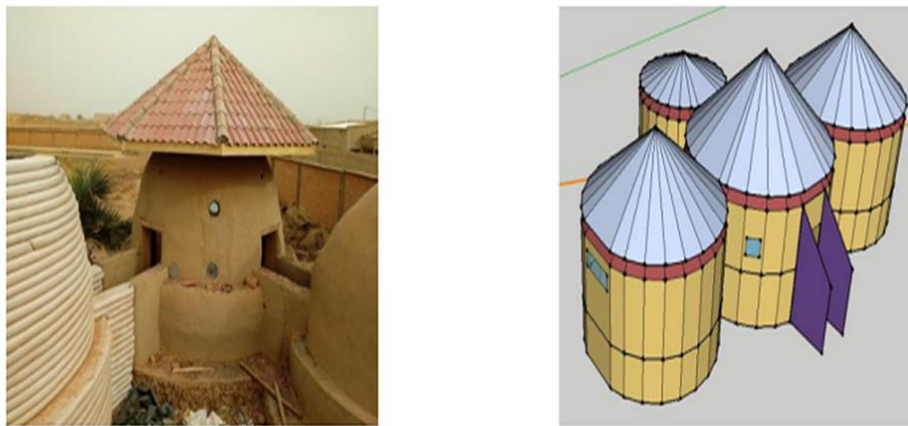


Figure 2-11 Construction of the residential area with Earthbag buildings (left), and Earthbag model (right) [100]

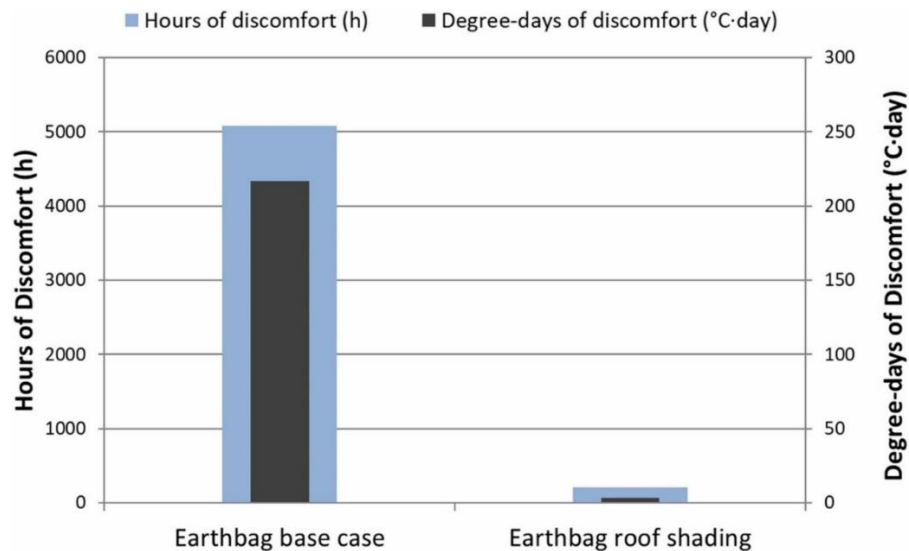


Figure 2-12 Annual Hours of discomfort and annual degree days of discomfort for earthbag base case and earthbag with solar protection [100].

Zhao et al.[115] studied the ventilation, lighting, and insulation of a prototype of the Superadobe (known as earthbag building) system. They found that mud, which is a natural material, has good thermal inertia. The small openings in the superadobe structure reduce the likelihood of heat bridging, resulting in good maintenance integrity. The dome roof design also increases the heat-radiating area and allows skylights to save on artificial lighting. The use of white plaster on the interior walls of the house creates a diffuse reflection of light. Additionally, thick walls provide shade for the windows, reducing solar radiation. All of these factors contribute to the good physical properties of the Superadobe system.

According to Kamal and Rahman[116], earthbag buildings provide a good thermal mass, but are not great insulators. The compacted earth has an R-value of approximately R-1/ft, meaning that a standard earthbag wall would provide no more than an R-2 insulation value comparable to a dual-pane glass window. To improve the insulating properties of earthbag walls, materials that create air pockets, such as volcanic rock, rice hulls, perlite, and vermiculite, can be added, although there are both positive and negative aspects of this procedure. Additionally, Desideri et al.[105] noted that earthbags generally have high thermal inertia but low insulation effectiveness. To address this issue, straw layers can be added to increase the wall

structure (70-80 *cm*). Although traditional insulation materials have been used in thick or multiple layers to achieve greater thermal resistance, this leads to heavier load bearing and can complicate the building details [93].

Furthermore, conventional insulation materials (such as Expanded Polystyrene Insulation (EPS), extruded polystyrene insulation (XPS), Foam etc.) are unsuitable for traditional building façades [117], because conventional insulation materials, can create a barrier that traps moisture within the walls. This can lead to issues such as mold growth, rot, and deterioration of the building's structural integrity. Therefore, to address the need for innovative techniques to improve the insulating properties of earthbag walls, this research proposes incorporating PCMs as part of passive design strategies. According to current research, this technique has the potential to increase insulation while maintaining a high thermal mass, which aligns with the improvement in insulation without adding weight or complexity to the construction process. Local PCMs such as beeswax and paraffin wax can also contribute to the sustainability and affordability of earthbag construction. Using locally available materials like beeswax reduces transportation costs and emissions associated with importing commercial PCMs. Beeswax can be sustainably harvested as a byproduct of apiculture operations. Paraffin wax can be produced from local crude oil refining or recycled from waste products. Utilizing these local PCM resources supports local industry while providing an affordable thermal mass option. Incorporating low-cost and easily accessible local PCMs into earthbag construction enhances sustainability and affordability. Therefore, investigating the optimal design and placement of PCMs in building envelopes could lead to a more energy-efficient and comfortable living space.

2.3 Phase change material as thermal energy storage

The use of PCM for thermal energy storage has been extensively studied in recent years. Eddhahak-Ouni et al. [118] investigated Portland cement concrete modified with organic microencapsulated PCMs and found that the addition of PCMs improved the heat storage capacity of PCM-concrete. Huang et al. [119] used palmitic acid-stearic acid eutectics mixes as PCMs for thermal energy storage in composites and found that adding expanded graphite significantly improved the heat storage and release rates. Zhang et al. [120] determined the heat storage capacity of gypsum and bricks impregnated with PCM and found that wallboards impregnated with esters and mixture of esters have a greater capacity to store heat overall because of the latent heat of fusion. Qunli et al. [121] constructed a cooling ceiling with PCM and found that the energy storage capacity of the ceiling with PCM was higher than that without PCM. Peippo et al. [122] developed a lightweight passive solar house integrated with PCM in a plaster board and found that approximately 15% of the energy cost could be saved. Ramakrishnan et al. [123] studied the synthesis and properties of PCM composite-integrated aerated/foamed geopolymer concrete for enhancing the thermal storage capacity and found that the incorporation of 15% and 30% PCM composite decreased the test room peak indoor temperature by 1.85°C and 3.76°C, respectively, while the thermal storage capacity was increased by 105% and 181%.

2.4 PCMs categories

In general, PCM are categorized as Organic, Inorganic and Eutectic materials [124], [125], [46], [126],[127]. The PCM categories are shown in Figure 2-13. Among the PCM materials, paraffin and hydrated salts are the most frequently used in construction applications. Each method was applied within a specific temperature range. Figure 2-14 demonstrates that various paraffin and salt hydrate types have melting temperatures within the range of human comfort, making them ideal for use in buildings. Therefore, this research will primarily concentrate on solid-liquid PCMs because they are widely available in the market.

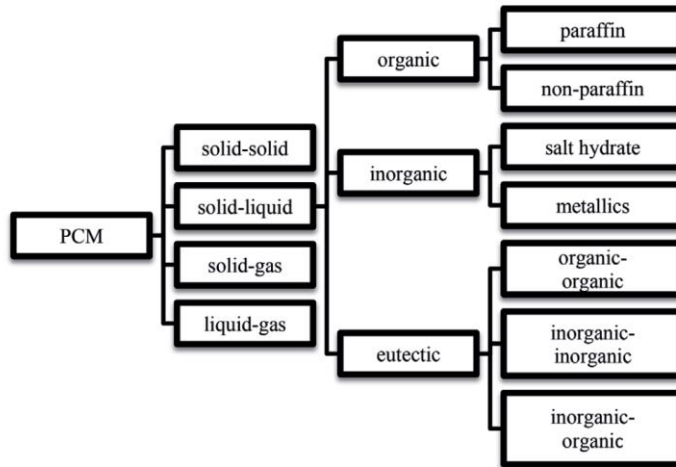


Figure 2-13 Phase change material categories [128]

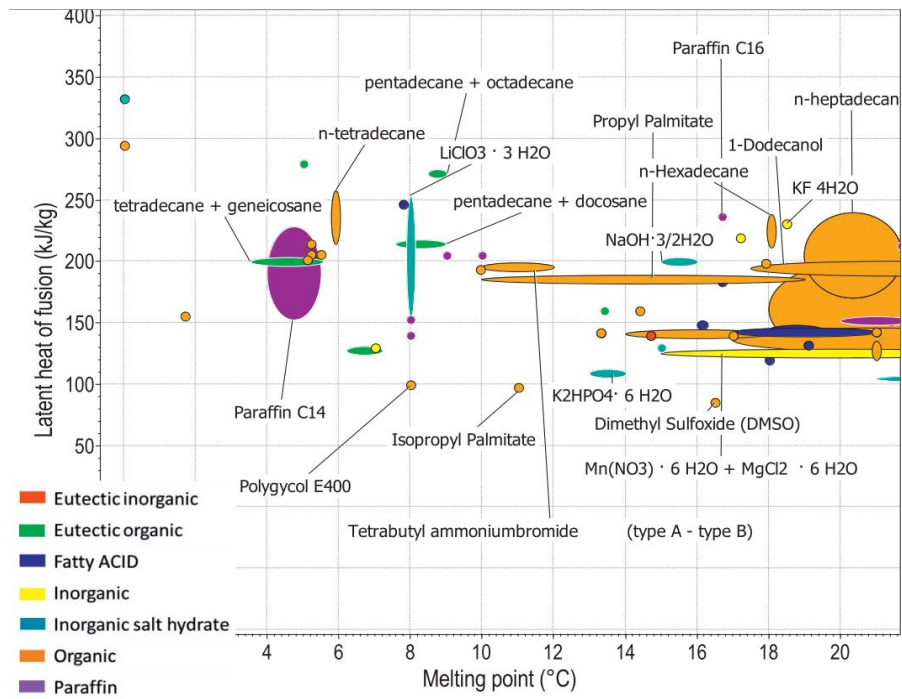


Figure 2-14 The melting enthalpy and melting temperature for the different groups of phase change materials [129]

2.4.1 Organic PCMs

Generally, organic PCMs, like paraffin wax, are made of straight n-alkane chains $CH_3 - CH_2 - CH_3$ [130]. The melting temperature increased as the number of C atoms in the C_nH_{2n+2} structure increased [131]. However, a significant amount of latent heat is released during the crystallisation of the (CH_3) -chain. With increasing chain length, the melting point and latent heat of fusion increase. Paraffin is non-corrosive and safe. Below 500°C, they were chemically inert and stable. When melting, they exhibit less volume change (~ 10 %) and have little vapour pressure. Typically, paraffin has extremely large freezing-melting cycles. Additionally, the beneficial aspects of paraffin include its high latent heat, self-nucleating tendency, and commercial availability at low cost. These characteristics make them the most promising candidates for energy-storage systems [132]. One disadvantage of paraffin is its low thermal conductivity. However, this advantage can be overcome by either transferring heat through an intermediary mass or by combining PCM with materials with higher thermal conductivities [133] [134] [135] [136]. Table 2-1 highlights the advantages and disadvantages of the organic paraffin PCMs. Examples of the organic PCMs are listed in Table 2-2.

Table 2-1 Advantages and disadvantages of Organic PCMs

Advantage	Disadvantage
Non-toxicity and not corrosive	Low thermal conductivity (0.2 W/m/K)
Better thermal properties	Flammability and low thermal conductivity
Long-term thermal reliability under the application of several heating-cooling cycles	Non-compatible with plastic containers
Large latent heat	
Low cost	
Negligible supercooling and segregation	
Chemical stability	
Self-nucleating behaviour	
Paraffins have high specific heat than salt hydrates	
Compatible with construction materials	
Recyclable	

*[124],[137],[138]

Table 2-2 Organic paraffin use as PCM

PCM	Melting point (°C)	Heat of fusion (kJ/kg)	Thermal conductivity (W/m.k)	Density (kg/m ³)
Dodecane	-9.6	216	2.21 (liquid)	-
Triethylene glycol	-7	247	-	-
Paraffin C14	5.5	228	-	-
n-Tetradecane	6	230	-	-
Polyglycerol E400	8	99.6	0.187	1125
Paraffin C15–C16	8	153	-	-
n-Pentadecane	10	-	-	770
Isopropyl palmitate	11	95-100	-	-
Isopropyl stearate	14-18	140-142	-	-
Propyl palmitate	16-19	186	-	-
n-Heptadecane	19	240	0.21	760
Paraffin C16–C18	20-22	152	-	-
Polyglycol E600	22	127.2	0.19	1126 (liquid, 25oC) 1232 (solid, 4°C)
Paraffin C13–C24	22-24	189	0.21 (liquid)	0.76(liquid) 0.90 (solid)
Octadecyl thioglycolate	26	184	-	-
Vinyl stearate	27-29	122	-	-
Paraffin C18	28	244	0.148	0.774
n-Octadecane	28-28.1	250–247.7	0.148	779
capric acid	27.9–30.2	142.7	0.1 (solid) 0.2 (liquid)	752 (solid) and 815 (liquid)
	28–33	63	0.15	750(solid)
Paraffin C19	32	222	-	-
Paraffin C20	36.7	246	-	-

*[124], [139],[140]

2.4.2 Inorganic PCM

Inorganic PCMs, such as salt hydrates and metals, are non-carbon molecules [141]. Metallics have extremely high melting temperatures and are unsuitable for building-envelope applications. Salt hydrate is a frequently used inorganic PCM. They comprise a mixture of salts and water with a phase change temperature (PCT) range of 15–80°C [142]. They have double the latent heat storage ability per unit volume compared with organic materials. They can be used in applications ranging from building energy conservation to textiles, solar water heat recovery, and cold chain logistics [141]. However, salt hydrates lack the stability of other PCMs because some salt hydrates fail to recrystallize entirely, which can create complications and inconsistencies in the

thermal, cooling, and heating cycles [142]. However, they are superior to other materials because they possess ideal properties for use as TES materials [143]. The advantages and disadvantages of inorganic PCMs are listed in Table 2-3. Table 2-4 shows some of the available inorganic PCMs.

Table 2-3 Advantages and disadvantages of inorganic PCMs

Advantage	Disadvantage
High volumetric latent heat storage (Almost double that of organic materials)	Undergo supercooling during freezing.
High latent heat of fusion	Undergo phase segregation during the transition.
High thermal conductivity	Corrosive to most metals
Cheaper and readily available	Irritant
Compatible with plastic containers	Have high vapour pressure (Induce water loss and cause a progressive change in thermal behaviour during the thermal cycling process)
Sharp phase change	May show long term degradation by oxidization, hydrolysis, thermal decomposition, and other reactions
Low environmental impact	Exhibit variable chemical stability
Having recycling potential	High volume change

*[124],[144]

Table 2-4 Inorganic PCM

PCM	Melting point	Heat of fusion (kJ /kg)
Ammonium chloride sodium sulfate decahydrate NH₄Cl.Na₂SO₄.10H₂O	11	163
CaCl₂.6H₂O	24	140
Iron(III) bromide hexahydrate FeBr₃.6H₂O	27	105
Potassium iron alum dodecahydrate KFe(SO₄)₂.12H₂O	33	173
Calcium bromide hexahydrate CaBr₂.6H₂O	34	138
Na₂P₂O₇.10H₂O	70	184
Ba(OH₂).8H₂O	78	266
(NH₄)Al(SO₄)₂.H₂O	95	269

*[145][146]

2.4.3 Eutectic PCM

Eutectic PCM comprise at least two components with a minimum melting temperature and can be either organic, inorganic, or a combination of both [147]. By combining two or more commercially available PCM, a eutectic mixture can be created that melts and freezes at similar temperatures, thereby avoiding the need for two separate phase transitions [148]. The ratio of components in the eutectic PCM can be adjusted to achieve the desired PCT and latent heat [149]. Eutectic PCM possess the combined properties of both organic and inorganic PCMs, and an example of a type of eutectic PCM is the EO-PCM (Eutectic organic PCM), which is a mixture of two or more organic PCM that function as a single candidate and coherently change phase [150]. Eutectic mixtures of fatty acids have lower melting points than individual PCMs but exhibit excellent properties, such as individual O-PCM (organic PCM), making them a suitable choice for thermal energy storage applications [150]. However, eutectic PCMs are more expensive than organic and inorganic PCMs. However, many eutectics can be customized to achieve almost any desired melting point for TES systems [150]. However, many eutectics can be customized to achieve almost any desired melting point for TES systems [151]. Some examples of eutectic PCM were given pictorially by Hayat et al. [151], as shown in Figure 2-15.

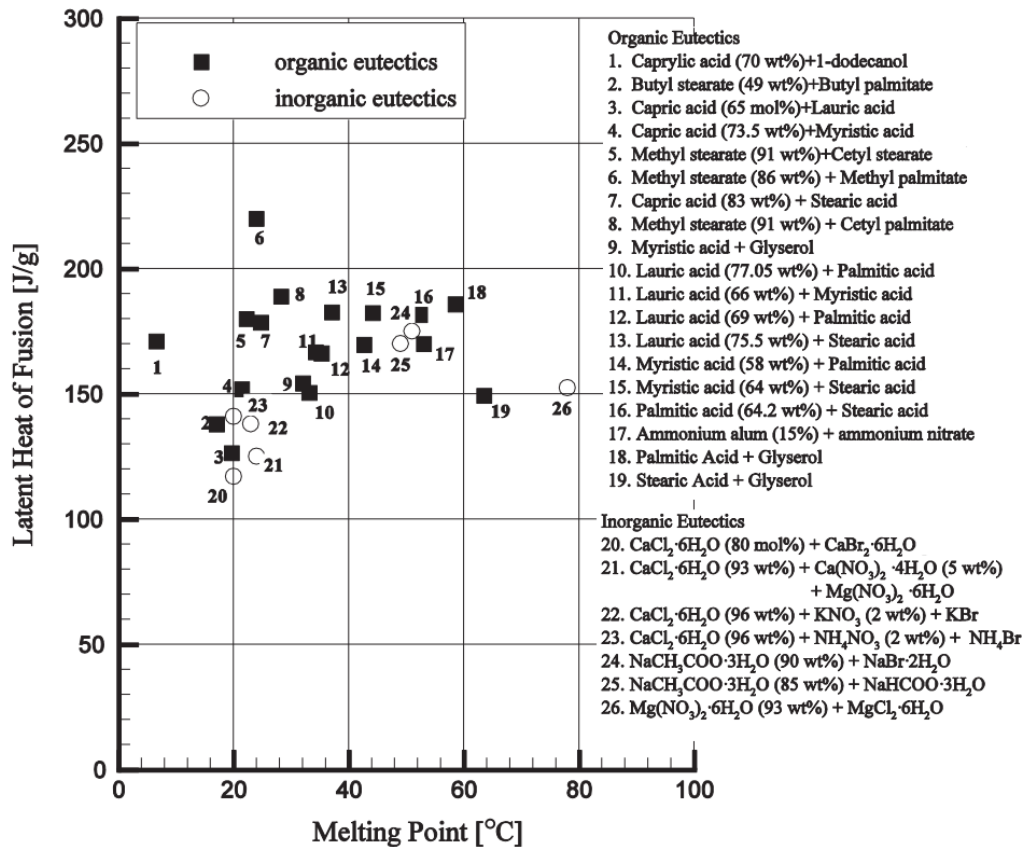


Figure 2-15 Eutectic PCM[151]

2.5 PCM selection criteria

The selection of an appropriate PCM is essential for the design and development of building [152]. However, it is worth noting that no single PCM possesses all the desirable properties. Therefore, the selection process requires careful examination of the thermophysical, kinetic, chemical, economic, and environmental properties of the candidates [124], [153]. One of the critical factors to be considered when selecting a suitable PCM is the melting temperature range. For building applications, it is recommended to select a PCM with a melting temperature range of 15–30 °C or 20–32 °C, which is within the range of thermal comfort [154]. Additionally, the selected PCM should possess important thermal, physical, chemical, and kinetic properties, be economically feasible, non-toxic, non-corrosive, and not decompose during the phase change [139], [155]. The selection criteria for PCMs also depend on their cost, availability, safety, and adaptability, which are crucial for the end-use application of PCM [149]. Properties such as latent heat of fusion, melting/freezing temperature,

thermal conductivity, specific heat capacity, energy density, supercooling, and corrosion resistance must be considered when selecting a suitable PCM [156]. Figure 2-16 provides details of the selection criteria presented by Tyagi et al. [157].

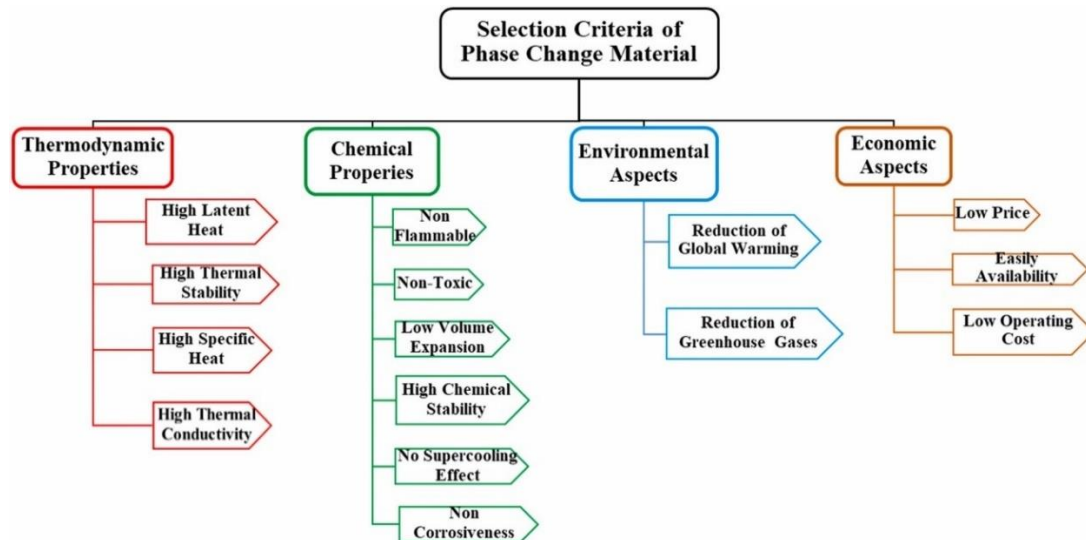


Figure 2-16 Phase change material selection criteria [157]

2.6 Characterization and Thermal Analysis Methods of PCM

2.6.1 Differential Scanning Calorimetry (DSC)

The most common method used for the thermal analysis of PCMs is DSC. It measures the melting enthalpy, freezing enthalpy, peak temperature, melting point, freezing point, and specific heat capacity [158]. The DSC method can be used to characterize the PCM composites used in building applications [159], [160],[119],[161]. Karaipekli & Sari [162] prepared a novel form-stable PCM by impregnating a eutectic mixture of capric acid (CA) and myristic acid (MA) into expanded perlite (EP). The melting and freezing temperatures and latent heat of the form-stable composite PCM were measured using DSC analysis at heating and cooling rates of $5\text{ }^{\circ}\text{C min}^{-1}$ for $10\text{--}50\text{ }^{\circ}\text{C}$ in a nitrogen atmosphere. The melting and freezing temperatures latent heats were found to be 22.61 and $21.18\text{ }^{\circ}\text{C}$, 154.83 and 156.42 J/g for CA–MA eutectic mixture, and 21.70 and $20.70\text{ }^{\circ}\text{C}$, 85.40 and 89.75 J/g for CA–MA/EP composite. The thermal cycling test of the form-stable composite PCM indicated good thermal reliability in

terms of changes in the thermal properties after 5000 thermal cycles. The melting point, thermal capacity, and latent heat of beeswax/graphene as a PCM were examined by Amin et al. [163] and evaluated using DSC. Jiesheng et al. [164] prepared a form-stable PCM consisting of paraffin and expanded perlite (PA/EP). The DSC method was used at a heating rate of 5 °C/min from 0 to 100°C. The DSC results indicate that the melting point and latent heat of the PA/EP form-stable PCM (53.6°C, 105.58 J/g) are lower than those of paraffin (56.6°C, 148.3 J/g). Therefore, in this study, the studies mentioned earlier were used to determine the melting and freezing temperatures and latent heat of the PCM used. The main reason for using DSC is its simplicity, rapidity, and economical sample requirement [165]. A conventional measurement method using DSC, as specified in the ASTM E793 Standard, was also followed.

2.6.2 Thermogravimetric analysis (TGA)

A TGA is used to measure the weight changes of a sample as it undergoes chemical and physical changes due to heat over time and temperature. It can be used to determine the elements in a sample from room temperature to 1200°C and to examine its thermal stability [166]. The device employed platinum pans, as shown in Figure. 2-17 were used to hold the sample, and an infrared oven lined with graphite to provide an accurate thermal response [167]. It is an essential parameter for assessing the potential of new materials in the construction industry, with no danger of thermal degradation [168].

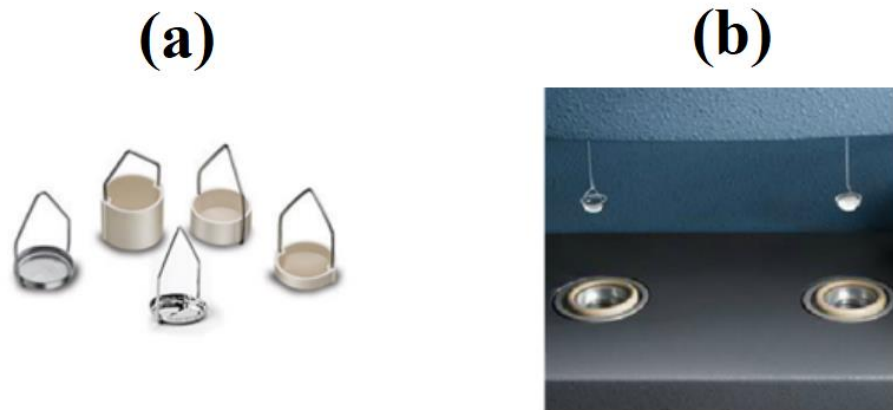


Figure. 2-17 Pans used and balance relative weighting method of the TGA (a) available pans (b) balance system [167]

Research has been conducted to analyse the performance of shape-stabilized PCM's using TGA [169],[170],[171],[172],[173]. Sun et al.[174] successfully developed formed stable PCM of paraffin/expanded perlite and expanded graphite. Thermal stability was measured by thermogravimetric analysis (TGA, TGA/ SDTA851e) under a nitrogen atmosphere at a heating rate of 10 °C/min from 25 °C to 600 °C. The results showed that the form-stable PCMs exhibited good thermal stability during their operating temperature range. Yao et al.[175] fabricated paraffin/hydrophobic expanded perlite composite PCM. Thermogravimetric analysis (TGA) tests showed that the fabricated PCM composite exhibited good thermal stability. Another study was conducted by Dixit et al.[176], in which a PCM composite was prepared by impregnating propyl palmitate in expanded perlite (EP, as a support matrix), and its thermal buffering performance was tested in building applications. The thermal stability of the PCM and its composite samples was evaluated using TGA. The results demonstrated that the EP-55 composite exhibited good thermal stability and reliability. This study used an approach similar to that used in previous studies to determine the thermal stability of the composite PCM.

2.6.3 Scanning Electron Microscopic analysis (SEM)

The microstructure of a novel capric acid-myristyl (CM) alcohol/expanded perlite composite PCM (CPCM) was analysed by C. Liu et al.[177] using SEM analysis. As shown in Figure 2-18a, b, and c EP has a highly porous structure, which provides space for PCM adsorption. The EP pores decreased with increasing mass fraction of CM, as shown in Figure 2-18 d to o. SEM tests showed the effective combination of EP and CM, with CM existing in the pores and on the surface of EP through adsorption and entrapment. Liu et al. [178] prepared a paraffin/red-mud composite with four different compositions 40:60, 45:55, 50:50, and 55:45. The SEM results showed that the composite had good thermal stability. Ramakrishnan et al.[135] observed the morphology and microstructure of paraffin/hydrophobic expanded perlite (EPOP) form-stable PCM seeded with graphene nanoplatelets (GNP) as a heat transfer promoter. The SEM findings demonstrated that some of the GNP particles were submerged in paraffin residing in the pores of EPO, which increased the rate of heat transfer to the paraffin. Gurmen[179] fabricated form-stable composite PCM for latent heat storage by impregnating paraffin wax into the EP pores. SEM images showed that paraffin was uniformly dispersed in the pores and on the EP surface.

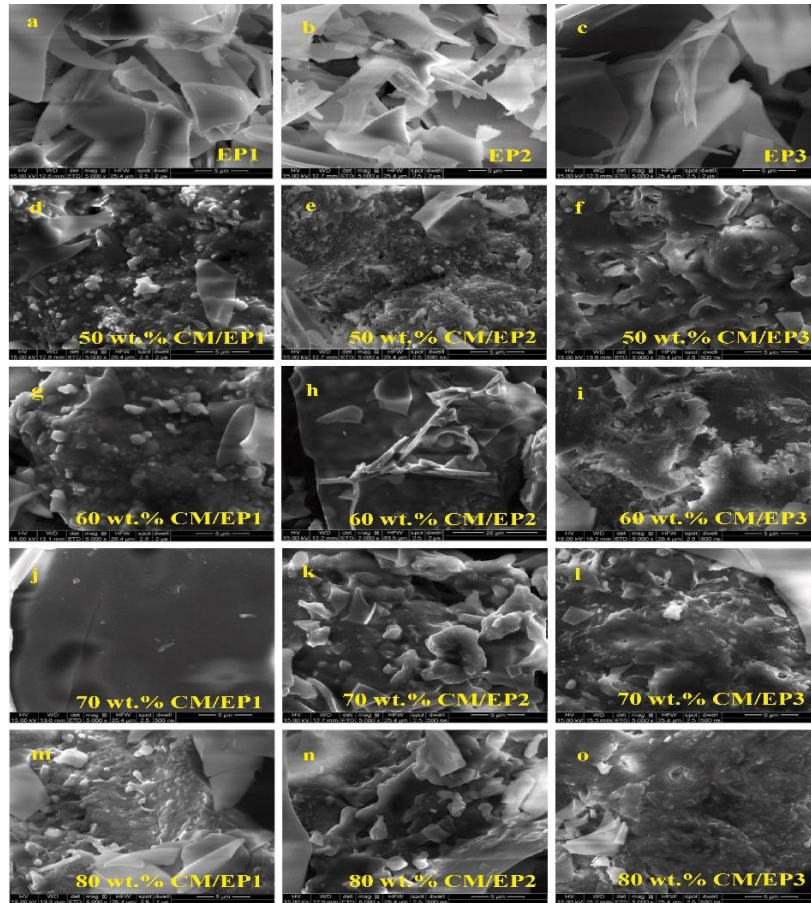


Figure 2-18 The SEM images of EP and CM/EPPCM

2.6.4 Thermal conductivity

2.6.4.1 Thermal conductivity measurement of PCM composites and composites with conductivity enhancers

Thermal conductivity (k value) is a material property that demonstrates its heat conduction capability [180]. The amount of heat transferred based on the thermal conductivity is of great importance for thermal energy storage systems. The low thermal conductivity of the PCM causes the heat transfer rates to be slow, which means that the storage and release of heat during the heating and cooling processes would be reduced. This leads to more energy to maintain the desired temperature [181]. Evidence shows that PCMs have low thermal conductivity [182] and are bound to leak when used directly in building materials [183]. To this end, many researchers have proposed using porous materials to encapsulate PCM. However, most of these porous materials have low thermal conductivity, so encapsulating PCMs in porous

materials does not enhance the thermal conductivity of the composite, which could result in better thermal performance. Rao et al., 2018 [184] prepared a eutectic hydrated salt/expanded perlite (EHS/EP) composite for thermal energy storage. The thermal conductivities of the composites were measured at different percentages of EHS and EP. It was shown that 70% EHS/EP2 had a higher thermal conductivity than EP2, likely due to the pores in EP2 being filled with hydrated salts. However, the difference was not obvious when compared with the thermal conductivity of the pure material.

The lack of efficient heat transfer during the charging and discharging processes of form-stable PCM is an additional problem that prevents their widespread use [185], [186]. The most frequently used methods to increase the heat-transfer efficiency of PCM composites are additives with high thermal conductivities. Huang et al. [187] developed a novel bio-based shape-stable organic phase change composite (SSOPCC) with boron nitride (BN) as a thermal conductivity enhancer. The thermal conductivity of the composites increased from 0.407 to 0.596 W/mK when BN sheets at different percentages were incorporated into the SSOPCCs, as shown in Figure 2-19.

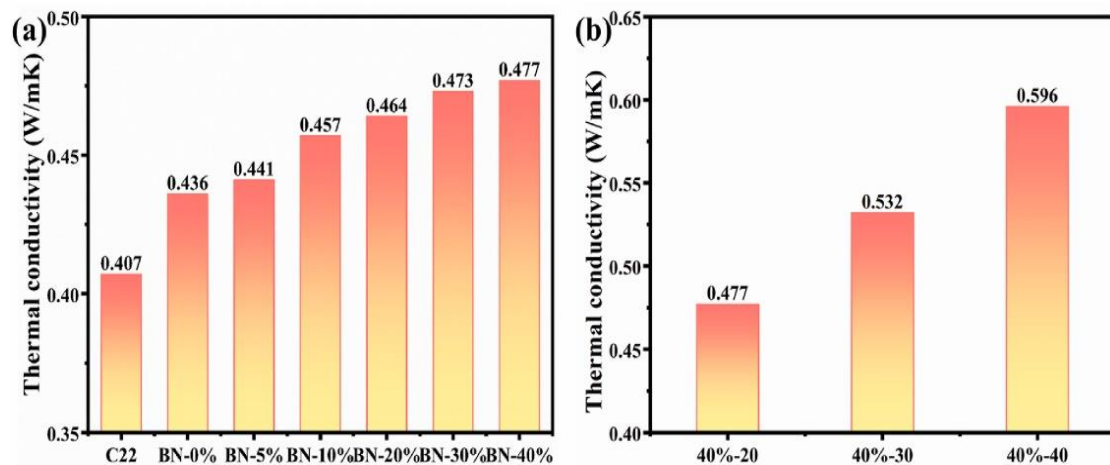


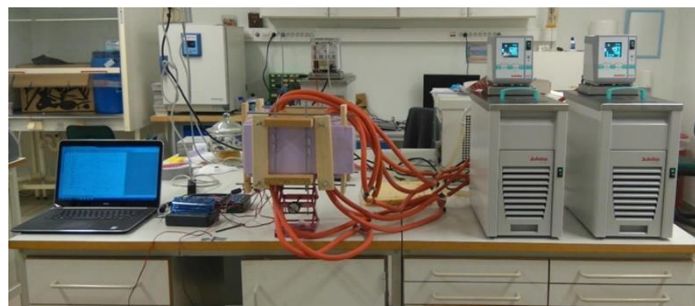
Figure 2-19 Thermal conductivity of SSOPCCs with different contents of BN [187]

Sun et al.[174] found that by incorporating 5 wt% of graphite into a form-stable paraffin/expanded perlite composite, its thermal conductivity could be increased by 192% compared to a pure paraffin/expanded perlite composite. Ramakrishnan et al.[135] developed a paraffin/hydrophobic expanded perlite (EPOP) form-stable PCM seeded with graphene nanoplatelets (GNP) as a heat transfer promoter. The authors claimed that GNP particles are partly submerged in the paraffin present in the pores of EPO, which significantly enhances the thermal characteristics of the composite PCM and heat exchange capacities. Compared to EPOP, the addition of 0.5 wt% GNP increased the thermal conductivity by as much as 49%.

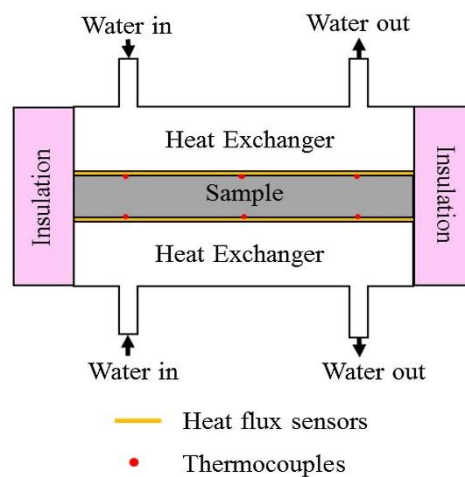
2.6.4.2 Thermal conductivity of sample materials with PCM composites

The thermal conductivity of bulk solid materials can be determined using transient and steady-state experimental approaches [188]. Various steady and transient approaches can be used to evaluate the thermal conductivity of a material. The thermal conductivity may vary depending on the method used [180]. However, the focus of this study was on the steady-state method. The main steady-state methods include guarded hot plates, axial flow, pipes, and heat flow meters [189]. Hakim et al.[190] investigated the thermal characteristics of building materials integrated with PCM material, namely, beeswax, using the guarded hot plate method. Cao et al.[191] developed a guarded hot plate system (see Figure 2-20) to analyse the thermal properties of cement and geopolymer concrete infused with microencapsulated PCMs for use in passive building applications. The disadvantage of this method is that it's mainly adopted dynamic method and also the significant sample mass that contains high volume of PCM makes it difficult to prevent the hysteresis phenomenon from occurring. The path followed during heating might be different from the path followed during cooling, even if the temperature trajectory is the same [192]. The axial flow method [193], [194] and pipe method [195] have also been studied to measure the thermal conductivity of PCM in building materials. However, heat flow meters are highly accurate and easy to use, and their quick result function makes them popular among industry professionals [196]. Heat flow meters have been used in many studies to measure the thermal conductivities of PCM composites in building materials [197],[198]. Sukontasukkul et al. [199] studied the thermal conductivity of lightweight

concrete containing high contents of PCM. The results show that the HFM apparatus can be used to measure the thermal conductivity of PCM composites in building materials. Ahmad et al. [200] also investigate the thermal conductivity of graphite polymer asphalt concrete using a heat flow meter apparatus. Another study by Sukontasukkul et al. [201] measured the thermal conductivity of concrete containing PCM aggregates at different stages. A heat flow meter apparatus was assembled at King Mongkut University of Technology, North Bangkok. The setup consisted of two hot plates with two heat flux sensors and eight K-type thermocouples. Given the similarities in materials and equipment, this study focuses on Alssaad et al. [202]. It was found that their study used local materials, such as straw and mud, and a heat flow meter for measuring thermal conductivity, which is particularly interesting and relevant to the current research.



(a)



(b)

Figure 2-20 (a) The guarded hot plates system and (b) sketch of the cross-section of system [191]

2.6.4.3 Thermal conductivity measurement of wall prototype with PCM or PCM composites

To determine the thermal conductivity of building envelopes such as walls, a prototype of a wall or the entire building wall was studied in a climate chamber Ye et al.[203], Ramakrishnan et al.[204]. Khalifa [205] developed a new wall panel to improve the thermal performance of existing and new domestic buildings in the UK by investigating the thermal conductivity of Micronal Phase Change Material (MPCM) in a controlled environment chamber. They found that the best thermal conductivity was obtained using a mixture of 20% PCM, 75% gypsum, and 5% silica with a honeycomb. Wang et al. [206] evaluated the thermal behaviour of a wall made with a PCM called cPCM. The control and PCM walls were tested in a climate-control chamber, as shown in Figure 2-21. The study found a linear relationship between the effective thermal conductivity and the wall temperature; however, when the temperature increased from 15 °C to 30 °C, the thermal conductivity decreased because the PCM underwent a phase change. In another study, Guardia et al. [207] investigated the thermal conductivity of brick wall enclosures with PCM cement-lime mortars under different climatic conditions. The temperature and heat flux on both sides of the mortar layer were monitored during heating and cooling cycles in a climatic chamber. The results show that adding PCM to the mortars decreased the mechanical properties and thermal conductivity in the solid state, while increasing it in the liquid state.

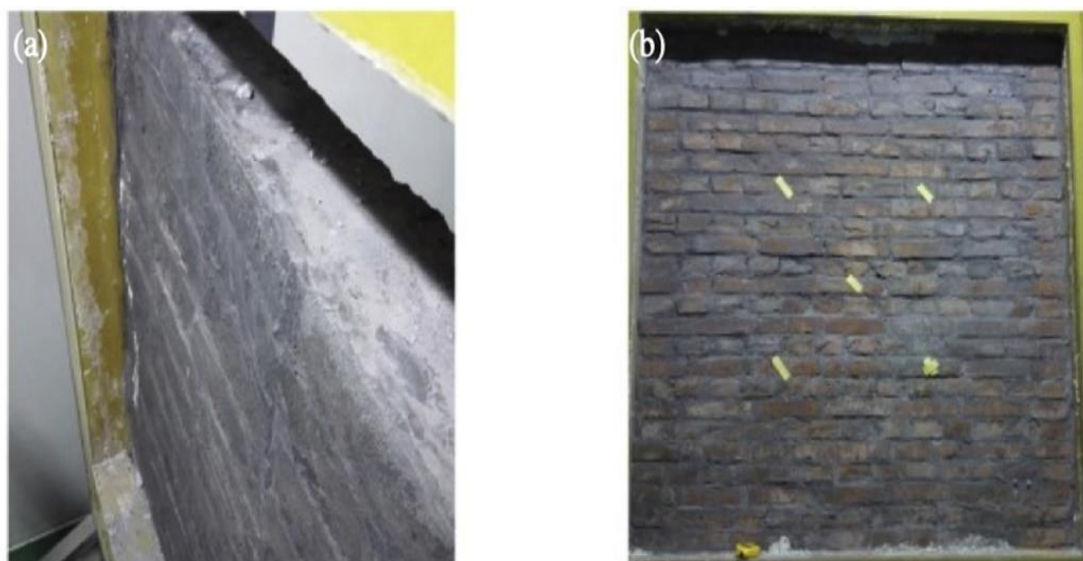


Figure 2-21 Photographs of the tested walls: (a) the composite-PCMs wall; (b) the common wall [192]

2.7 Application of PCM in building

In recent years, the use of PCM in buildings has attracted increasing attention as a technique to improve energy efficiency [208], reduce peak energy demand [41], and improve occupant comfort [209]. It is possible to reduce the requirement for heating and cooling systems, energy consumption, and greenhouse gas emissions by introducing PCMs into the building envelope [208]. This technique can be employed in various building envelopes, including walls, roofs, floors, and their unit components such as blocks. Furthermore, PCMs can be installed in new and existing buildings, making them a versatile solution for improving the thermal performance of buildings.

2.7.1 Application of PCM in the block

It has been demonstrated that using PCMs in blocks enhances the thermal characteristics of the building envelope by minimising heat transfer through the wall. PCMs can be included in blocks in various ways, such as encapsulating them within the blocks [210] and/or impregnating them in the block material [211]. Studies have investigated the thermal properties of PCM-enhanced blocks and shown that they can significantly reduce the peak temperatures within buildings, resulting in lower energy consumption for cooling. For example, Hasan et al.[212] investigated the performance of a PCM contained in an insulated concrete block under extremely hot weather conditions in the UAE. To replicate an indoor space, an insulated chamber was constructed beneath the PCM-containing block (Figure 2-22). The effect of PCM installation on indoor heat gain was investigated in two different locations. Compared to concrete blocks without PCM, those with PCM performed better, and those with PCM and insulation layers adjacent to the inside performed better than those with PCM and insulation layers adjacent to the outdoors. This study proposed the use of mechanical ventilation in hot regions to improve PCM regeneration for optimal performance. Azmi and Khalid[213] studied the thermal analysis of cement bricks encapsulated with PCM under ambient weather conditions. The results showed that PCM encapsulation in building bricks is an effective practice for the passive thermal control of buildings and reduces temperature fluctuations. Similarly, Qu et al.[214] developed a new phase change in foam concrete to compensate for building energy consumption. Fumed silica was used to absorb paraffin for the formation of composite

PCM formation. The proposed phase change foam concrete blocks have low thermal conductivity and strong heat storage capacity, indicating a promising way to improve the economic feasibility of renewable energy systems.

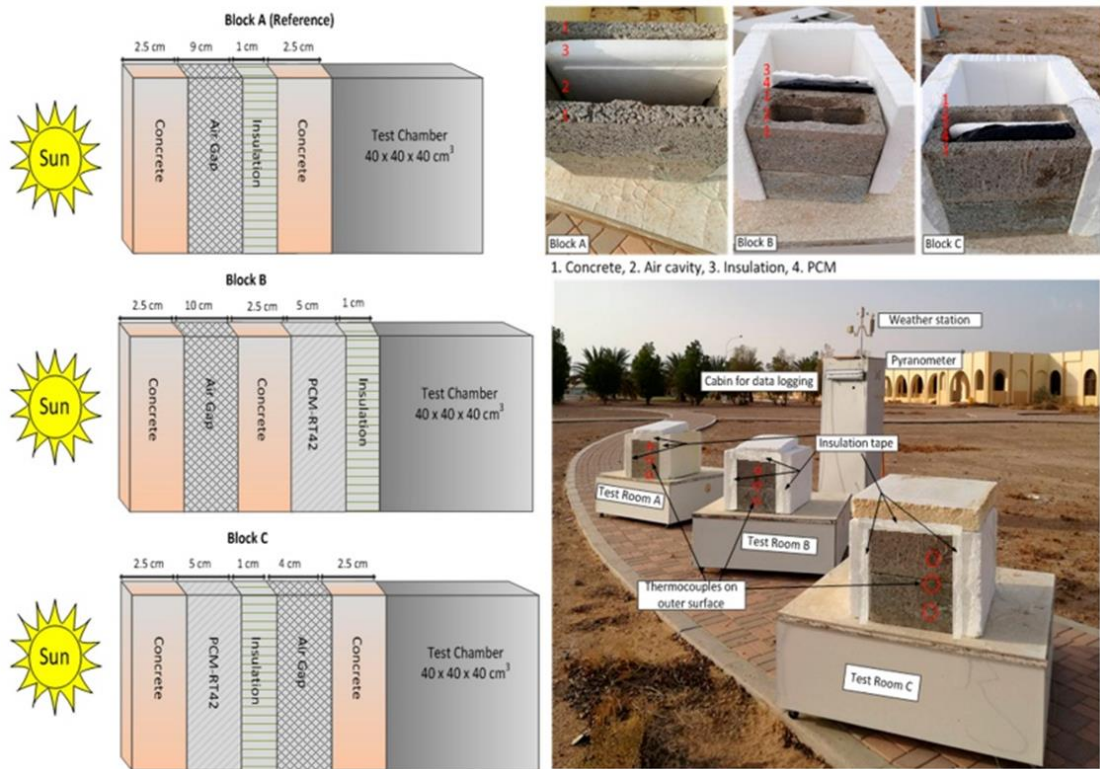


Figure 2-22 Schematic diagram and the experimental set-up of the concrete blocks, with construction layers and the test chamber [213]

In addition, Shen et al. [215] prepared PCM-CLSC aggregate and PCM-concrete thermal storage blocks with varied PCM weight percentages to improve the heat storage capacity of PCM-concrete blocks. The results of the experiments revealed that the average specific heat capacity of the PCM-concrete thermal storage blocks improved by 12.54% (2 wt% PCM), 31.60% (4 wt% PCM), and 41.23% (6 wt% PCM), respectively. Al-Yasiri & Szabó [216] focused on investigating the thermal performance of PCM incorporated with concrete bricks under hot climatic conditions. Three different PCM capsule arrangements were considered, as shown in Figure 2-23, and the results showed that the thermal performance of concrete bricks can be significantly improved using PCM, even under maximum outdoor temperatures. Three different PCM capsule arrangements were considered, and the results showed that the thermal performance of concrete bricks can be significantly improved using PCM, even under maximum outdoor temperatures.

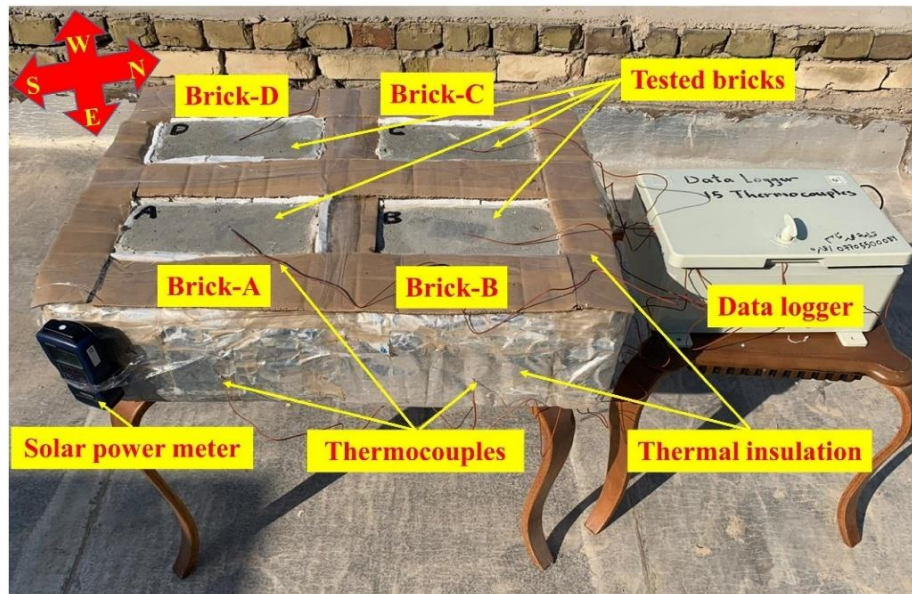


Figure 2-23 Tested bricks under hot Iraqi climate weather [216].

2.7.2 Application of PCM in the walls

The use of PCM in building walls has gained significant attention owing to their ability to integrate into various wall layers and building materials [217]. PCMs can be placed between the external and internal layers of multi-layer walls [218] or integrated into concrete [219] and gypsum panels as microencapsulated phase change materials (MPCM) [220]. Experimental and numerical studies have shown promising potential for integrating PCMs into walls to reduce energy consumption. For example, Vicente & Silva [221] experimentally and numerically investigated the use of PCM macrocapsules in hollow clay brick masonry walls. They reported that PCM reduced the thermal amplitude or fluctuation in temperature by up to 80% and enhanced the capacity of the walls to store heat. Gounni & El Alami [222] conducted an experimental study on a reduced-scale cavity incorporating PCM into its vertical walls. They found that PCM reduced the maximum temperature by 10% and delayed the time at which the maximum temperature was reached. Other researchers have used PCM as an additional layer on the wall. Lee et al. [223] developed an EnergyPlus-based algorithm to predict heat transfer through building walls integrated with PCMs. The developed model was experimentally validated and found to accurately predict the total heat-transfer reduction produced by the PCM. Wang et al. [224] Using parametric analysis,

model a south-facing wall with a PCM layer inside under hot summer climates. In comparison to a wall without PCM, they revealed that the PCM wall reduced the heat flow by up to 34.9% after optimization. Li et al. [225] investigated the thermal performance of conventional walls of buildings in Isfahan, Iran, by incorporating thirteen different PCM. The results indicated that the performance of the PCM-based wall was strongly influenced by the thermal conductivity, phase-change enthalpy, and melting temperature of the PCM. The study revealed that a PCM can efficiently reduce heat transfer to the interior space when it has a lower thermal conductivity, has a higher latent heat of phase change, and its phase-change temperature is closer to room temperature.

A PCM can be incorporated into a wall as a shape-stabilized PCM. For example, Zhu et al. [226] studied the thermal performance of a building integrated with double-layer shape-stabilized phase change material (SSPCM) wallboards under real weather conditions. The results showed that the PCM room could prevent overheating in summer and undercooling in winter compared with the reference room. Moreover, the performance of PCMs in wall investigations has been studied under different climatic conditions. Li et al. [227] used COMSOL Multiphysics® software to conduct a numerical analysis on multilayer wall (see Figure 2-24) to investigate the impact of crucial design parameters such as PCM layer placement, thickness and stress conditions on selecting PCM melting points. The results showed that choosing the appropriate PCM melting point based on these design criteria lowered the interior temperature oscillation, resulting in lower HVAC system energy usage. Salihi et al. [228] investigated PCM-enhanced building walls in a semi-arid region. This study considered the PCM phase-change temperature range, thicknesses, location, and configurations, as well as the effect of mechanical ventilation on the PCM wall performance. According to the findings, the PCM walls increased the indoor comfort while lowering the cooling and heating loads and temperature swings.

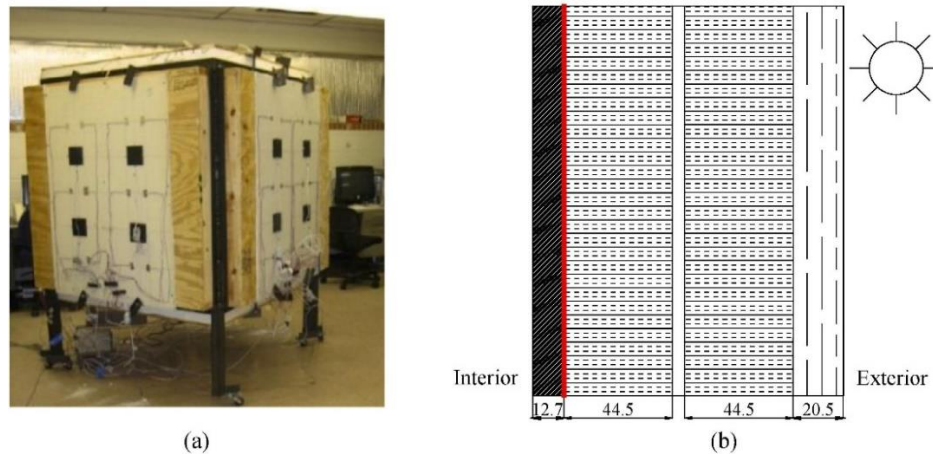


Figure 2-24 The multilayer wall (a) dynamic wall simulator in the laboratory test and (b) schematic diagram showing the wall assembly [227]

2.8 PCM in vernacular building

The use of PCM in natural building materials such as compacted earth blocks (CEBs), rammed earth, cobs, and straw has gained attention in recent years. Research has shown that incorporating PCM into these materials can enhance thermal performance. Sandra et al. [229] found that incorporating 25% PCM and 10% Portland cement in CEBs resulted in satisfactory physical, mechanical, and durability characteristics. Similarly, Serrano et al. [230] optimized the formulation of stabilized rammed earth with 10% PCM, resulting in a 9.3% increase in heat capacity and a 23.5% decrease in thermal conductivity. M'hamdi et al. [231] found that using PCM was more efficient for cooling in the arid climate and heating in the sub-arid and Mediterranean climates, with the rammed earth envelope showing a maximum energy reduction of 10.7%. Gounni & Louahlia [232] demonstrated that integrating PCM in a cob house reduced the annual temperature oscillation and heating loads compared to conventional building materials. The study conducted by Toufigh and Samadianfard [233] showed that using PCM in rammed earth helped control temperature variations. Ben Zaid et al. [234] in their study reported that incorporating PCM into a clay-straw wall can reduce the surface temperature by up to 3 °C and decrease the peak heat flux by 31.95%. Placing the PCM next to the heat source significantly reduces the surface temperature by 1°C compared placing on the outer wall layer, and the PCM-integrated wall stores an average of 14.17 W/m^3 of the inlet heat flux, indicating that adding

PCM to a vernacular building can enhance thermal performance. Other studies related to PCM in vernacular buildings are summarized in [Table 2-5](#).

Table 2-5 Summary of research conducted with PCM in vernacular building

S/n	Building type	PCM type	Findings on thermal behaviour	Ref.
1	Rammed Earth	commercial encapsulated PCM as a stabilizer	micro- PCM enhanced thermal properties of RE	[45]
2	Rammed Earth	commercial encapsulated PCM as a stabilizer	micro- PCM reduced the thermal conductivity of rammed earth from 0.95 to 0.85 W/K.m	[235]
3	Rammed Earth	Encapsulated Micronal®PCM	The overall energy efficiency performance was simulated to be well above the maximum five-star greenhouse standard of the Australian Building Greenhouse Rating Scheme.	[236]

2.9 Phase change materials in Nigeria and their application

Several studies have been conducted to assess the benefits of using PCM in buildings. PCMs absorb and store energy, changing from a solid to liquid state as the temperature increases. Owing to increasing research on PCM in buildings, there are numerous commercially available PCMs worldwide. However, the type of PCM used in a building depends on the temperature, humidity, and air velocity in the region where the building is located. According to Xu et al. [192], the operating principle of PCMs involves changing their status according to the temperature of the environment. Conversely, they can release previously stored energy when the temperature decreases, changing from a liquid to a solid state. Batagarawa [237] investigated the use of a PCM to reduce the cooling load in 15 Nigerian office buildings through simulation analysis using DesignBuilder V3 and EnergyPlus V6 and V7. The results showed that significant energy savings can be achieved by optimizing passive and climate-sensitive design aspects. However, the use of PCM may not entirely eliminate mechanical cooling. However, there has been limited research on PCM in buildings in

Nigeria. A field study is needed to further explore its potential in the arid regions of Nigeria.

2.9.1 Selected PCMs for the region of experiment in Nigeria (Kano state)

To ensure that the PCM charges and discharges daily, its Phase Change Temperature must lie within the maximum and minimum temperature of the location; otherwise, the PCM does not behave as a latent heat storage (LHS) material [238]. A PCM with a transition temperature higher than the average temperature reduces the temperature peaks and should also be above the average indoor temperature. In this case, the PCM prevents the temperature from increasing or decreasing above a specified mark. In hot climates, such as Nigeria, a PCM with a higher transition temperature option is preferable to reduce high temperatures [237]. Sovetova et al. [239] conducted research on hot desert countries (United Arab Emirates, Algeria, Egypt, Pakistan, India, Saudi Arabia and Mauritania) to determine the thermal and energy efficiency performance of PCM integrated residential building by simulation using EnergyPlus. The results showed that PCM with higher melting points performed better. Other studies considered in selecting PCMs phase transition temperatures are tabulated in Table 2-6.

Table 2-6 PCMs used in hot climate

S/N	Country	Climate	PCM type	PCM melting point (°C)	Ref.
1	India	Hot and dry climate	HS30 and HS29	32.1 and 31	[240]
2	Arizona	Hot Arid Climate	BioPCM	23	[241]
3	Iraqi	hot climate	Paraffin wax	19 - 44	[242]
4	-	Hot and dry climate	SP29	29	[243]

2.10 PCM modelling and simulation

EnergyPlus is a unified simulation software that concurrently solves all the three parts of the building, system, and plants. The software comprises a series of program modules that work together to measure the energy needed to heat and cool a building using various energy sources and systems [237]. The energy simulation building model was generated using the EnergyPlus Input Data File Editor (IDF). The Energy Plus model provides all the parameters required to conduct an energy simulation over a year. Within Energy Plus, there are many algorithms in building systems for measuring and simulating heat transfer and storage [244]. It applies the guidelines of the "ASHRAE heat balance system" for heating and cooling load calculations, which are based on balancing all the energy flows into a thermal zone. This involves solving a series of energy balance equations for the outside and the inside surface and indoor air for each building feature (wall, roof, etc.) [245]. The conductive transfer function (CTF) approach is one of the most common methods for predicting transient heat transfer in whole-building energy simulation programs. Stephenson and Mitalas (1967) developed the CTF method using inverse Laplace transforms and Z-transforms to estimate transient heat transfer through building walls [246]. The surface constructions in EnergyPlus are traditionally simulated as layers with one-dimensional heat transfer that move through the layers using Conduction Transfer Functions (CTF) to simulate heat transfer. These are the coefficients of the time series, which define the transient conduction process using an algebraic equation [247]. Similarly, Ozdenefe & Dewsbury [245] added that conduction through building elements (walls and roofs) is formulated by conduction transfer functions (CTF), which relate the conductive heat fluxes with current and past surface temperatures and past heat fluxes. This method has both advantages and disadvantages, as discussed below.

Advantages of the CTF method

- CTF solution has the advantage of utilizing single and relatively simple linear equations with constant coefficients [248]
- The coefficients involved in these linear equations are evaluated only once for each type of construction [245]

The disadvantage of the CTF method

- It is not possible to simulate temperature-dependent thermal properties [248]
- Advanced materials such as PCMs, which have variable heat-storing capacity depending on temperature, cannot be modelled by the CTF [245]

2.10.1 The developed mathematical model used for simulation purposes based on the literature

A finite-difference algorithm is included in Energy Plus to address the challenge of the CTF method, allowing the modelling of materials with variable thermal properties. This algorithm uses the enthalpy method, which considers all PCM enthalpies during simulation [245]. Nevertheless, the enthalpy (total internal energy) equation is used to model engineering systems that require a change of state, such as melting/freezing, which is a reliable approach to modelling energy conservation. A possible reason for this is that the overall impact of the phase change can be modelled with a well-defined temperature–enthalpy relationship without knowing the exact location of the PCM region. This makes numerical solutions reasonably simple because there is no need to monitor the continually moving phase change area across the discrete numerical grid [249]. The benefit of the enthalpy approach is that a single energy equation is correct in both the phases. Thus, there is no need to separate the liquid and solid phases. Therefore, every numerical scheme, such as the finite-differential or finite-element approaches, can be readily implemented for the solution. Furthermore, the enthalpy method can handle phase-change problems, where the phase change occurs over an extended temperature range and not at a single phase-change temperature [131]. The enthalpy formulation equation for the model is given by Eqn 2.1 [250].

$$\rho \frac{\partial H(T)}{\partial t} = \nabla(k\nabla T) \quad \text{Eqn 2.1}$$

Where ρ , k , and H were the PCM's density, thermal conductivity, and enthalpy, respectively.

Heat transfer is typically viewed as one-dimensional across building elements (walls, roofs, etc.) in building simulation. Let us find a solidification of a liquid that is initially at a uniform temperature of T_0 that is higher than the melting temperature with boundaries of $0 \leq x \leq B$. If, for times $t > 0$, the boundary temperature at $x=0$ is kept at f , which is lower than the melting temperature and if it is assumed that there is no temperature gradient at the boundary $x = B$, then Eqn 2.1 and the related boundary conditions become as Eqn 2.2. This physical illustration is given in Figure 2-25 [245].

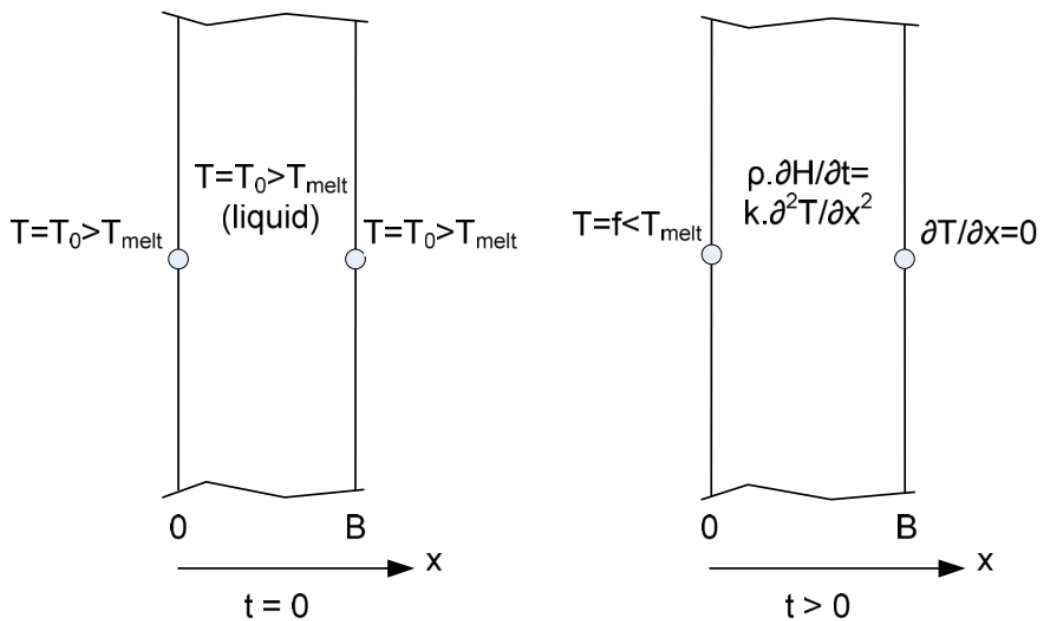


Figure 2-25 Physical illustrations of enthalpy form of the energy equation and boundary conditions [244]

Eqn 2.2 gives the enthalpy formulation of this phase-change problem [251].

$$\rho \frac{\partial H(T)}{\partial t} = k \frac{\partial^2 T}{\partial x^2} \quad \text{Eqn 2.2}$$

$$\rho \frac{\partial H(T)}{\partial t} = k \frac{\partial^2 T}{\partial x^2} \quad \text{in } 0 < x < B \quad t > 0$$

$$T(x = 0, t > 0) = f$$

$$\frac{\partial T}{\partial x} = 0$$

$$T(t = 0) = T_0 \quad H(t = 0) = H_0 \quad \text{for } 0 \leq x \leq B$$

Therefore, Eqn 2.2 allows the use of the implicit finite difference approximation for the region $0 < x < B$ [245]. However, the EnergyPlus CondFD model for implicit finite difference approximation uses two solution schemes for the simulation, which depend on the user's choice based on the Adams–Moulton solution approach: (a) a semi-implicit second-order in time Crank Nicholson Second-Order and (b) a Fully Implicit First-Order in time Fully Implicit First-Order [252], but the fully implicit scheme is more stable than the Crank–Nicholson scheme over time [244]. Therefore, as suggested by Özdenefe et al. [244] fully implicit first-order scheme is employed in this study, as many researchers have used it and fully recommended its application [131], [248], [252], [253].

However, because of the implicit solution of the equation set, it is more efficient to set a time step shorter than those used for the CTF solution algorithm [254], as the default time step of the CTF solution algorithm in EnergyPlus is 10 min (600 s) [246]. Moreover, the Conduction Finite Difference (CondFD) model is more advantageous because it allows the modeller to carry out simulations with time steps as short as 1 min and enables the prediction of interior temperatures of the building fabric and simulation of advanced technologies such as PCM. Zastawna-Rumin et al. [254] cited that Tabares-Velasco recommended a simulation time step of fewer than three minutes for a more accurate prediction of the behaviour of PCM. Hence, a 2 min time step was considered in this study.

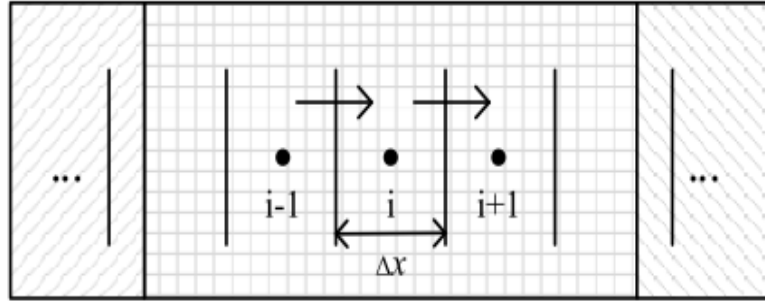


Figure 2-26 Control volume for heat conduction in EnergyPlus [248]

Seong and Lim [248] reported that the CTF solution algorithm does not simulate temperature-dependent thermal properties. Hence, the solution for this can be generated using the CondFD algorithm in EnergyPlus, as shown in Figure 2-26. By assuming steady-state conditions, heat conduction from control volume "i - 1" to control volume "i" that can be calculated by Fourier's equation. The control volume for heat conduction in the EnergyPlus diagram, which describes the fully implicit scheme used in EnergyPlus inside a homogeneous material to calculate the correct enthalpy, is given by Eqn 2.3 to Eqn 2.5 [255].

$$C_p \rho \Delta X \frac{(T_i^{j+1} - T_i^j)}{\Delta t} = k_W \frac{(T_{i+1}^{j+1} - T_i^{j+1})}{\Delta X} + k_E \frac{(T_{i-1}^{j+1} - T_i^{j+1})}{\Delta X} \quad \text{Eqn 2.3}$$

Where,

$$k_W = \frac{(k_{i+1}^{j+1} + k_i^{j+1})}{2} \quad \text{Eqn 2.4}$$

$$k_E = \frac{(k_{i-1}^{j+1} + k_i^{j+1})}{2} \quad \text{Eqn 2.5}$$

Where,

$k_i = k(T_i^{i+1})$ If thermal conductivity is viable

T = Temperature

i = Node being modelled

i + 1 = Adjacent node to the interior of the construction

i - 1 = Adjacent node to the exterior of the construction

j + 1 = New time step

j = Previous time step

Δt = Finite difference layer thickness

C_p = Specific heat of the material

ρ = Density of material

In the CondFD algorithm, all elements are automatically divided or discretised using [Eqn 2.6](#), which depends on the space discretization constant (c), thermal diffusivity of the material (α), and time step. Users can leave the default space discretisation value of 3 (equivalent to a Fourier number (F_0) of 1/3) or input other values [\[255\]](#).

$$\Delta x = \sqrt{c \cdot \alpha \cdot \Delta t} = \sqrt{\frac{\alpha \cdot \Delta t}{F_0}} \quad \text{Eqn 2.6}$$

For the PCM algorithm, the CondFD method is coupled with an enthalpy-temperature function ([Eqn 2.7](#)) that the user inputs to account for enthalpy changes during phase change. The enthalpy-temperature function develops an equivalent specific heat at each time step ([Eqn 2.8](#)). The resulting model is a modified version of the enthalpy method [\[255\]](#).

$$h = h(T) \quad \text{Eqn 2.7}$$

where h = enthalpy

$$C_p^*(T) = \frac{h_i^j - h_i^{j-1}}{T_i^j - T_i^{j-1}} \quad \text{Eqn 2.8}$$

2.11 Summary of the literature review gap

- Earth buildings like rammed earth and earthbags have been used for thousands of years and offer sustainability benefits. However, there is limited research on their thermal performance and integration with phase change materials (PCMs) in hot, arid climates like Nigeria.
- PCMs can improve building insulation and thermal mass when integrated into walls and other building envelopes. But optimal design and placement of PCMs for earth buildings needs further study.
- Local, low-cost PCMs like paraffin wax could provide an affordable thermal mass solution for earthbag construction in developing countries like Nigeria. But investigation is needed into suitable local PCMs.
- Simulation tools like EnergyPlus allow modelling of PCMs using enthalpy methods. But experimental validation is important to confirm modelling accuracy for specific PCMs and earth building designs.
- Prior work studied PCMs in concrete, brick and other conventional walls. But field testing of PCM integration strategies tailored to earthbag construction is lacking.

In summary, the key research gaps are:

- Thermal performance testing of earthbags in hot climates
- Investigation of optimal local PCM selection for earthbags
- Experimental analysis of PCM placement and configurations for earthbags
- Validation of PCM-earthbag building simulations against field data

Chapter 3. Development of PCM-Integrated Earthbag Block

In this chapter, the development of a PCM -integrated earthbag block and the thermal performance of the block under real weather conditions are discussed. The PCM composite was developed incorporated into the block. Prior to the incorporation of the PCM composite, the composited leakage test (Oozing circle test) was conducted. Thermal characterisation tests such as differential scanning calorimetry, thermogravimetric analysis, and scanning electron microscope were conducted to determine the thermal stability and comfortability of the composite. Moreover, thermal conductivity test of the composite was also done to determine the optimum PCM composite that can transfer less heat. The developed block was then subjected to real weather conditions in the Kano region.

3.1 Development and thermal characteristics of PCM-integrated earthbag block

3.1.1 Selection of materials

3.1.1.1 Soil

Earthbag buildings are typically constructed using available materials in the construction region [91]. Earthbag buildings can be built with any soil, although some soils need to be more stabilised than others [256]. Nigeria was selected for this study to simulate a hot and dry climate. A preliminary test using jar test was then conducted to determine the soil composition to choose the best soil for fabricating the earthbag. As a general guideline, an earthbag block with 30% clay and 70% well-graded sand is suitable for building high-strength structures [98].

3.1.1.2 Phase change material

Commercially available PCM was purchased from PCM Product LTD, the United Kingdom (label A31), and its properties are listed in Table 3-1. The purpose of the PCM selection is mainly to achieve (a) a practical operational temperature range of melting according to the changes in indoor temperatures and (b) economically affordable, non-toxic, and non-corrosive materials. The best PCM options for hot regions are those with melting points below the upper limit of the comfort zone. Thus, the material melts during the day and absorbs extra thermal energy to maintain

comfortable indoor temperatures. Otherwise, the PCM may not solidify to absorb heat the next day, thereby reducing its effectiveness and increasing the demand for active cooling [257]. The comfort zone of the Kano state, the region for the experiment as determined by Ali et al.[258], was 23 °C to 32 °C. Thus, the PCM selected with a PCT of 31 °C was found to be below the upper limit of the Kano comfort zone. Other considerations for the selection were also based on the recommendation given by Batagarawa [44] and studies on PCM carried out in a similar Nigerian climate as related to hot and dry climate regions in the world [45],[46].

Table 3-1 A31 paraffin technical data for PCM with a melting point of 31 °C

Product	A31
Melting area	27 to 33 °C peak 31 °C
Heat storage capacity (± 7.5%)	182 kJ/kg
Specific heat capacity	2.22 kJ/kg. K
Density (solid)	0.86 kg/l
Heat conductivity	0.2 <i>W(m.k)</i>
Max. operation temperature	200°C

3.1.1.3 Expanded perlite

Expanded perlite was used as a supporting material with particle sizes ranging between 2.38–4.78 mm (mesh #8), provided by Hobben International Ltd., United Kingdom. It was used to absorb and retain the PCMs in its pores. A similar practice was conducted and used by many other researchers [160],[259], and it was proved that this technique can prevent PCM leakage (see Section 2.6.3). The EP properties are presented in Table 3-2.

Table 3-2 Physical properties of expanded perlite

Physical properties of perlite	
pH (mud of water)	6.5-8
Density	32-400 kg/m ³
Specific gravity	2.2-2.4
Softening point	871-1093 °C
Melting point	1260-1343 °C
Specific heat	387 kJ/kg. K
Thermal conductivity at 24°C	0.04-0.06 W(m. k)
% Retention of water	35-50

3.1.2 Fabrication and properties of PCM/EP/EG

The porous expanded perlite and graphite materials were used as carriers to hold the PCM via a direct impregnation method. This allowed the PCM to be evenly dispersed throughout the pores within the expanded perlite and graphite structures. First, the expanded perlite was dried in an oven at 110°C for 1 hour to remove any moisture present within its porous structure. Removing this moisture was an important step to ensure the pores were clear for the PCM to infiltrate into. The PCM with mass fraction of 60% ,50%, and 40% was combined and mixed with variable amounts of the dried expanded perlite at 40% ,50%, 60% as tabulated in [Table 3-3](#). The quantity of perlite used was determined as a percentage weight relative to the amount of PCM. This allowed different perlite-PCM ratios to be tested. In addition to the perlite and PCM, 10 wt% of expanded graphite was added to each sample. The expanded graphite was incorporated to improve the overall thermal conductivity of the composite. The perlite-PCM-graphite mixtures were kept in an oven at 50°C for 3 hours to allow the melted PCM to fully permeate into the pores of the perlite and graphite. The samples

were then cooled at room temperature for 2 hours to solidify the PCM within the carrier structures. These different compositions were tested, as explained in Section 3.1.1, to determine the optimal perlite-to-PCM ratio that would allow for complete accommodation of the PCM into the porous structures. A schematic diagram of this PCM encapsulation process is provided in [Figure 3-1](#).

Table 3-3 PCM, expanded perlite and graphite proportions

S/N	PCM(%)	EP (%)_	EG (g)	PCM composite (g)
1	60	40	10	491
2	50	50	10	976
3	40	60	10	1459

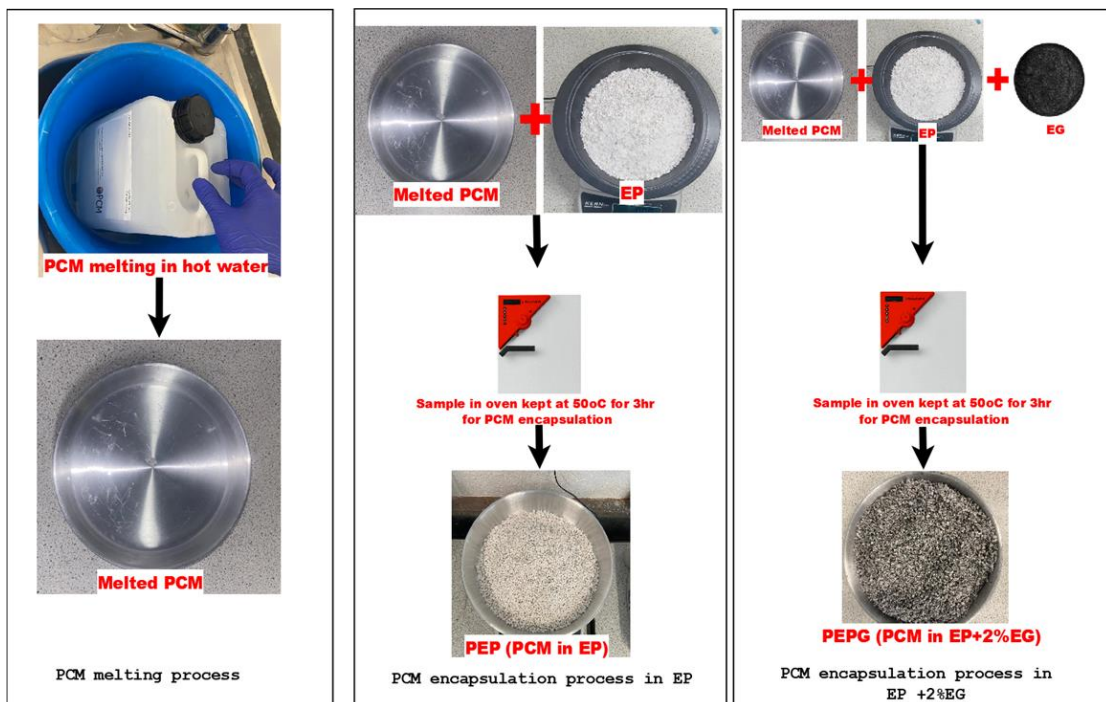


Figure 3-1 Encapsulation process of Phase Change Material

3.1.1 Earthbag block

The sample of the earthbag block comprised soil, water, phase change materials, expanded perlite, and expanded graphite to enhance the thermal conductivity of the PCM.

3.1.1.1 Earthbag block materials preparation

The materials used to prepare the earthbag block were soil, water, PCM, expanded perlite, and graphite. An optimal combination of 30% clay and 70% well-graded soil sand has been suggested [256]. However, there is no tentative code for the fabrication of earthbag buildings. Hence, a similar combination was followed to the suggested values, but with some modifications. According to Wang et al., 2016 [260], two methods are primarily used when integrating PCM in mortar: (1) adding PCM with a different composition in the mortar and (2) replacing a certain amount of sand in the mixture, that is, the replacement method. Therefore, in this study, a PCM composite was added by replacing a certain amount of the soil. The PCM composite of 1, 2, and 3 cm of the PCM layer was calculated to be 2.2%, 4.3%, and 6.5% of the total block mixture composition, respectively. The total block mass was found to be 17.8Kg. The composite was then mixed with soil and water to achieve 10% moisture [261]. To analyse the thermal performance of the earthbag, four different Block A specimens were formed, including Block A (considered the reference specimen) and Blocks B, C, and D, as depicted in Figure 3-2. The blocks have dimension of 400mm × 250mm × 100mm with total weight of 17.8Kg. Table 3-4 presents the block specimens containing the PCM composite.

Table 3-4 Sample specimen for earthbag block production

Earthbag block	PCM composite (g)	70% Sand (g)	30% Clay (g)	10% Moisture (L)
A	0	11214	4806	1.78
B	392	10967	4700	1.74
C	766	10734	4600	1.70
D	1157	10495	4498	1.65



Figure 3-2 Testing samples of earthbag block

3.1.1 Properties of PCM and PCM composite and earthbag materials

3.1.1.1 Leakage test

The PCM composite was tested to determine the stabilities of the PEP and PEPG compositions. The method proposed by Ma et al. [262] was employed and successfully used by Xu and Li [263]. The PCM composite was inserted on a circular filter paper with a diameter of 150 mm, dried in an oven, and kept for 3 h at 50 °C to ensure that

the PCM melted completely and entered the pores of the supporting materials. The filter paper was removed from the oven and inspected to determine whether there was any sign of liquid.

3.1.1.2 Scanning electron microscope analysis

In this study, a scanning electron microscope (SEM, Tescan VegaA3) at 8.0 kV accelerating voltage was used to examine the morphological characteristics and microstructure of PCM, PCM composite, and PCM composite with earth. The morphological characteristics determine the material's shape, size, and structure.

3.1.2 Thermal property

The selected PCM with PCT of 29 °C to 33 °C was analysed using differential scanning calorimetry and thermogravimetric analysis to assess its thermal stability. The primary reason for characterising PCM composite materials is to understand and evaluate their thermal properties and performance in various applications. Characterization of these composites involves analysing their thermal behaviour, stability, phase change characteristics, and overall effectiveness in heat storage and transfer. This information is essential for determining the suitability of the composite material for thermal energy storage.

3.1.2.1 Latent heat and transition temperature

DSC analysis was used to acquire data on time, temperature, and heat absorbed and released during the transition from the solid to the liquid phases. A single DSC test, which entails the controlled cooling or heating of small samples of a substance, can yield qualitative data aim to find the exact temperature of a PCM and its composite component and quantitative data about the phase transition, including the transition temperature, enthalpy, and specific heat [264]. The procedure reported by Sang et al. [265] was utilised to determine the PCT, latent heat, and specific heat of PCM, PEP, and PEPG. 5-10 mg of PCM, PEP, and PEPG samples were tested under a nitrogen atmosphere at a heating temperature range of 10°C to 45°C, and then, for the cooling temperature, the range was decreased from 45°C to 10°C. A heating and cooling rate between 0.5°C/min and 2°C/min have been recommended to avoid modelling and measuring errors in the building applications [264]. Thus, in the current study, the

PCMs was tested at a ramp rate of 2°C/min. Based on these measurements, the melting and freezing points (phase transition temperatures) were determined. The integration of curves can obtain the specific and latent heat capacities of the materials. The theoretical latent heat (H_T) of PCM composite in phase change processes for the comparison with experimental latent heat can be calculated using Eqn 3.1 [161]:

$$H_T = H_{PCM} \times W_{PCM}\% \quad \text{Eqn 3.1}$$

where H_T is the theoretical latent heat, H_{PCM} is the measured latent heat of PCM, and W_{PCM} is the weight percentage of PCM.

3.1.3 Thermal stability analysis

The TGA instrument explains the temperature range at which the PCM is applicable [266]. The thermal stability of PCM, PEP, and PEPG, as presented in Table 3-5, was investigated using a thermogravimetric analyser (Pyris 1 TGA, Perkin–Elmer). TGA measurement was performed within the temperature range of 25°C to 800°C with a sample of approximately 30–50 mg at a heating rate of 10°C min⁻¹. Nitrogen was used as purge gas at a flow rate of 20 ml min⁻¹.

Table 3-5 PCM and PCM composite sample specimen

S/N	PCM (g)	PEP composite (50% EP)	PEPG composite (50% EP +10g EG)	PCM
1	345	Sample A	Sample B	-
2	688	Sample C	Sample D	-
3	1032	Sample E	Sample F	-
4		-	-	Sample G

3.1.1 Thermal conductivity

To measure a sample's thermal conductivity, a heat flow meter apparatus is used as shown in Figure 3-3. The hot plate is heated to a predetermined temperature and the cold plate is kept at a lower temperature [267]. The available commercial thermal heat flow meter (HFM-100 Heat Flow Meter) was used to measure different samples of PCM composite in soil (PEPS and PEPGS) for earthbag block preparation.

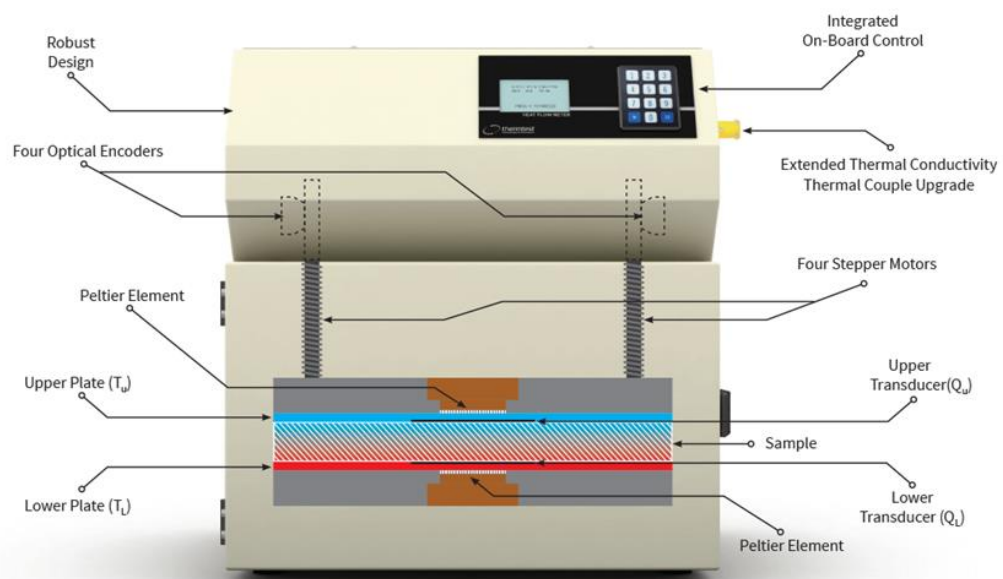


Figure 3-3 Heat flow meter apparatus [268]

The thermal conductivity measurement of PEPS and PEPGS samples combined with soil, as seen in Table 3-6, was performed on 250 mm × 250 mm × 50 mm square samples (see Figure 3-4) before and after drying in an environmental chamber at 25°C and 65% relative humidity. The benefit of drying is to make sure that the moisture content would not be a factor in influencing the thermal conductivity [269]. The thermal conductivity of the PEPS and PEPGS samples was determined at temperatures below and above the melting range of PCM (MPCM) as 10–38°C used. The sample was inserted between the top and bottom plates, with one heat flux sensor separating each plate from it. The sensors were carefully mounted in grooves such that they were flush with the surface that was in touch with the sample [270]. The thermal

conductivity was determined when the heat flux became a constant value. Thermal conductivity was measured two times for each sample at a temperature difference between hot and cold plate falls within 10–38°C. The thermal conductivity of the sample was then calculated based on the Fourier's law (Eqn 3.2):

$$k = \frac{Q \times d}{A \times \Delta T} \quad \text{Eqn 3.2}$$

where k is the sample thermal conductivity, d is the thickness of the sample, Q is the quantity of heat that flows through the sample, A is the sample surface area, and ΔT is the difference in temperature between the top and bottom plates.

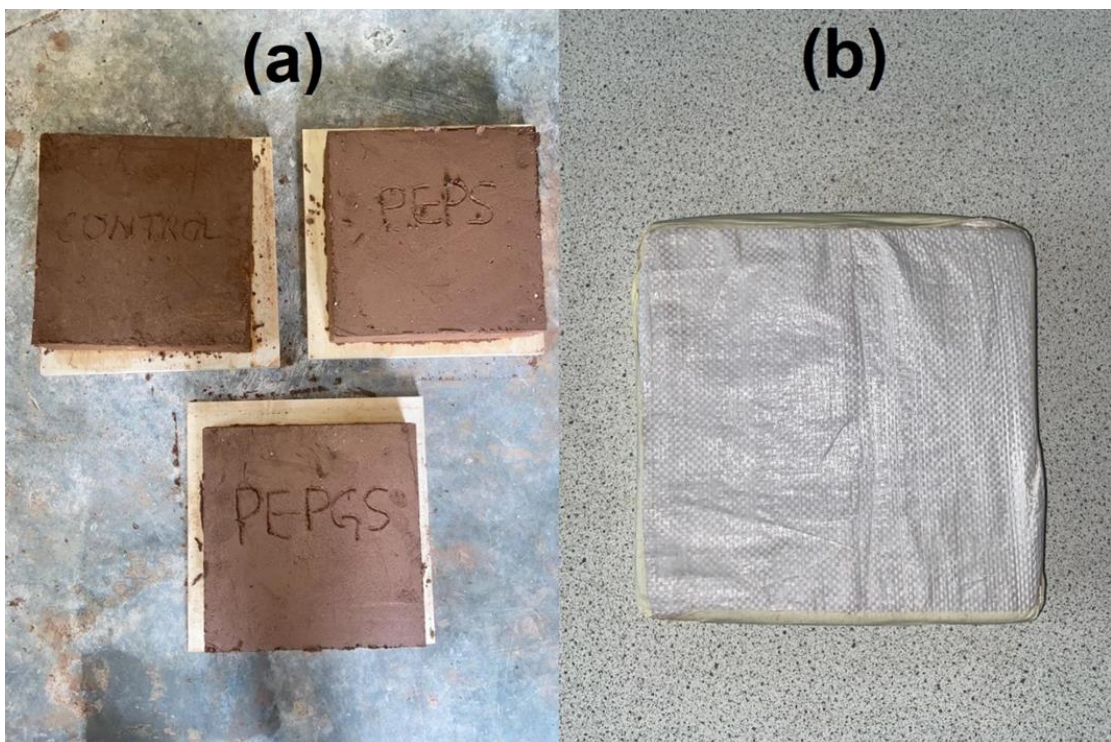


Figure 3-4 Testing samples for thermal conductivity test: (a) raw sample and (b) sample enclosed in Polystyrene bag

Table 3-6 Sample compositions for a thermal conductivity test

	PCM (g)	EP (g)	EG (g)
Reference sample	-	-	-
0.01 PEP	220	110	-
PEPG	220	110	10
0.02 PEP	440	220	-
PEPG	440	220	10
0.03 PEP	660	330	-
PEPG	660	330	10

3.1.1 Prototype development and thermal performance analysis of earthbag block

The primary purpose of this experiment is to investigate how the inclusion of different quantities of PCM within earthbag block affects their thermal behaviour. The experiment is motivated by the desire to improve the energy efficiency of earthbag buildings, making them more comfortable for occupants and potentially reducing the need for external heating or cooling systems. Studying the thermal performance of a single block of a wall before analysing the whole wall is crucial because by focusing on individual blocks, the analysis can address the issue of homogeneity within supposedly uniform walls. It uncovers variations that can arise from manufacturing processes, material composition, and other factors. Consequently, this process refines predictions for the overall wall's performance. It is also allowing for a detailed examination of specific heat transfer mechanisms, particularly conduction. Moreover, Single block studies also play a pivotal role in model validation. They offer a controlled setting for fine-tuning predictive models against empirical data before applying them to complex wall structures. Therefore, this experiment compares the thermal performance of four earthbag blocks, comprising of one without PCM (block A) and the other three blocks (block B, block C, and block D), containing various quantities of PCM composite as shown in [Table 3-5](#). The dimension of each block was 300 mm × 250 mm × 100 mm, and the blocks were fully insulated at the lateral sides to

act as adiabatic walls. Behind the blocks, a scaled-down test chamber with dimensions of 100 mm × 250 mm × 100 mm was built to represent an indoor space of an earthbag building as shown in [Figure 3-5 \(a\) and \(b\)](#). To provide an adiabatic boundary condition, the test chambers were made of a 150 mm thick polystyrene sheet at top, bottom, and lateral sides placed toward the North-South direction. Each chamber side was bonded with wood glue to minimise the heat loss. Since the total mass of polystyrene and wood glue was so small compared to the mass of earthbag blocks, their thermal energy storage capacity was neglected. For temperature monitoring k-type thermocouples with an accuracy of 0.05 °C were positioned at the inner and outer surfaces of the test blocks. All temperature sensors were connected to an automatic data acquisition system (data logger) with a data recording frequency of 10 minutes. Moreover, a mobile weather station was mounted near the testing site to measure the dry-bulb temperature and wind speed. Details arrangement of each prototype is shown in [Figure 3-5](#).

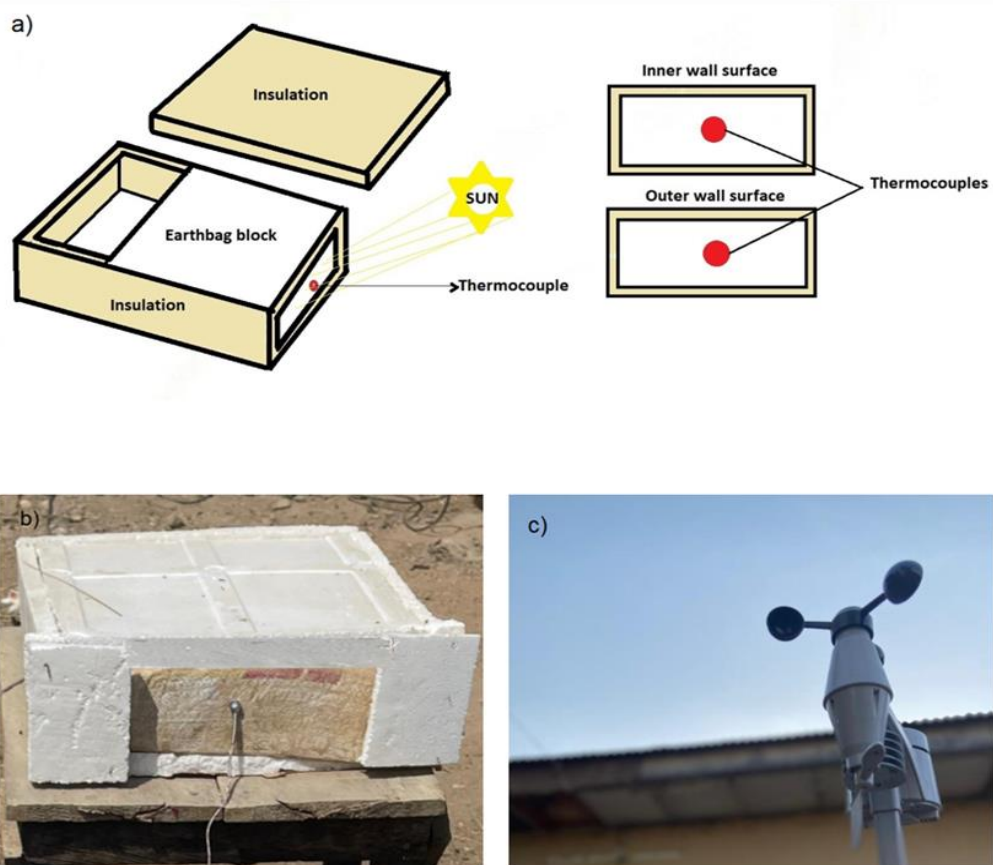


Figure 3-5 Earthbag block arrangement outdoors

3.2 Result

3.2.1 Thermal stability of PCM composite and PCM composite in soil

The thermal stability of PCM composite (PEP and PEPG) is tested with different percentages of EP and fixed percentages of EG as tabulated in [Table 3-5](#). From the results, paraffin leakage is observed with a decrease in an oozing circle diameter as the EP percentage is increased, which is in line with the result reported by Li et al. [271]. When EP reached 50% by the weight of the PCM, equivalent to 52% in the volume, the leakage was seen to be relatively small, as indicated by the oozing circle diameter. Though, when 10% fixed EG is added, no sign of paraffin is noted, as depicted in [Figure 3-6](#). The PEPG is found to be relatively stable, whereas the PEP is not. However, the stability of the PCM composite in the earthbag material mixture (PEPS and PEPGS) is also tested. From [Figure 3-6](#), it is noted that there is no sign of

leakage of PCM in all the samples with PEPG composite. While that of the PEP composite in soil, a small amount of leakage is observed, which is relatively smaller than the PEP composite alone. Hence, this test shows that earthen material can act as a supporting material to prevent leakage of PCM from the sample. The thermal reliability of the PEPS and PEPGS earthbag block sample is evaluated by subjecting the samples to 300 thermal cycles of melting and freezing and then observing whether leakage occurs on the sample surfaces. The samples are kept in an oven at a temperature above PCM melting point for 60min and then removed to cold down at the room temperature. The test is repeated while the leakage is observed after each cycle. The blocks sample before and after a thermal cycling are shown in [Figure 3-7](#). After 83 thermal cycling, the PCM appears on the surface of the PEPS sample, while PEPGS do not show any change up to 300 cycles. Hence, from the result, it can be concluded that the earthbag block combined with the PCM composite is thermally stable after being subjected to the thermal cycling.

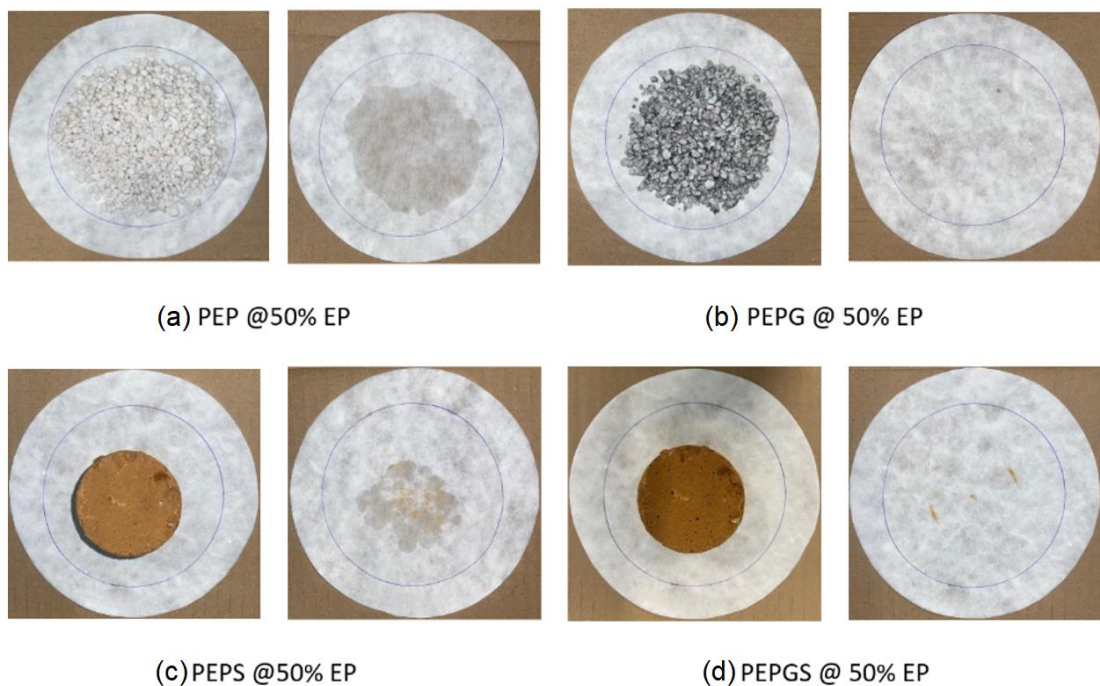


Figure 3-6 Comparison of leakage performance of (a) PEP(b) PEPG(c) PEPS and (d) PEPGS sample specimen



Figure 3-7 Earthbag block thermal cycling process

3.2.2 Surface morphology of EP, PEP, and PEPG and PEPGS using SEM

Scanning electron microscopy (SEM) was utilized to analyse the microstructure and surface morphology of expanded perlite (EP), expanded graphite (EG), PCM-expanded perlite composite (PEP), PCM-expanded perlite-graphite composite (PEPG), and PCM-expanded perlite-graphite-soil composite (PEPGS). SEM imaging was performed at different magnifications of 250X, 500X, 1000X, and 2000X to visualize the pore structure of EP and EG and examine the distribution and impregnation of the PCM within these porous supporting materials. [Figure 3-8a](#) shows the highly porous structure of EP, with varied pore sizes up to 70 μm . This indicates EP can serve as an effective supporting material to accommodate PCM within its pore network. [Figure 3-8b](#) reveals the worm-like folded structure of EG, which imparts a high specific surface area to enhance thermal conductivity. Comparing [Figure 3-8c](#) and [Figure 3-8d](#) for PEP shows more refinement of the pore structure at higher 2000X magnification versus 500X. The PCM appears uniformly distributed across the EP, filling pores and gaps and smoothing the uneven EP surface. The addition of EG in PEPG ([Figure 3-8e](#) and [Figure 3-8f](#)) covers the PEP surface and reduces visible porosity, as the PCM has already occupied the EP pores. This demonstrates EG acting as a thermal conductivity enhancer. Finally, [Figure 3-8g](#) indicates strong bonding between the PEPG composite

and earthbag soil in the PEPGS sample. Minimal observable pores suggest effective PCM impregnation.

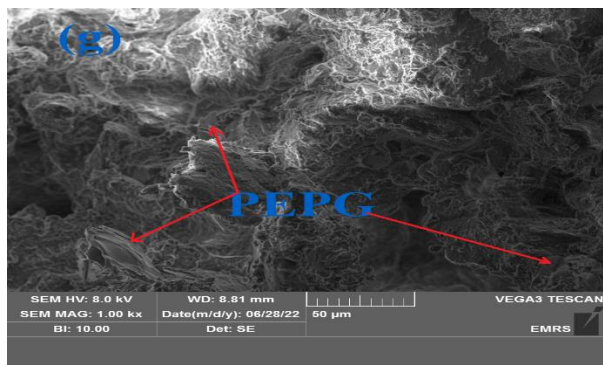
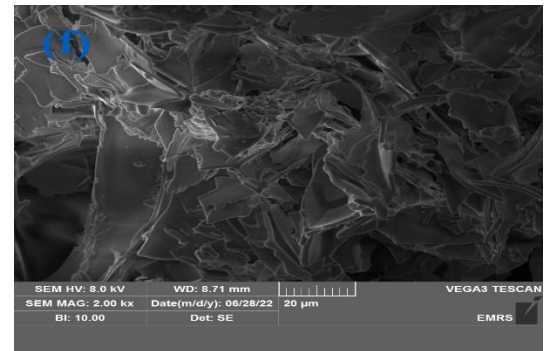
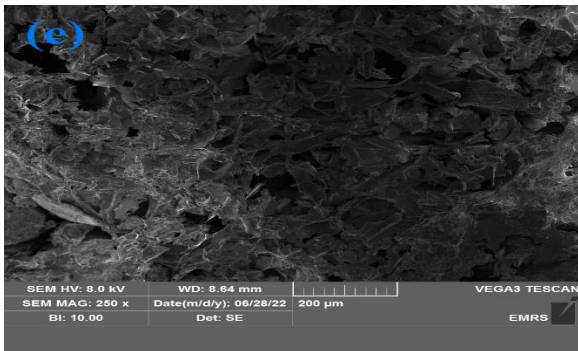
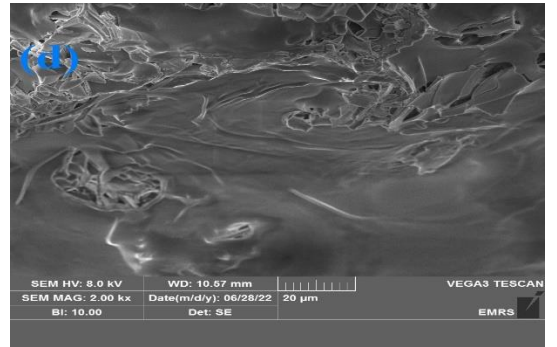
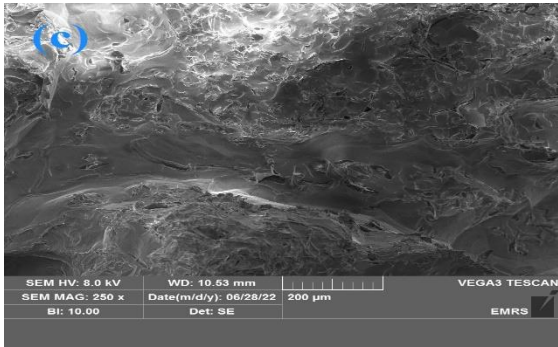
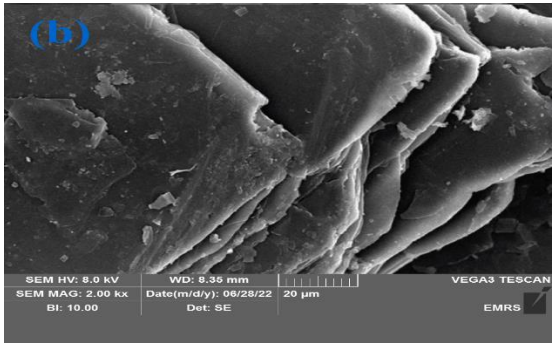
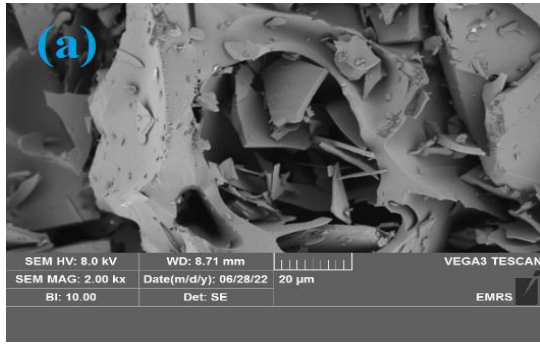


Figure 3-8 The SEM micrographs of (a) EP, (b) EG, (c) PEP x250, (d) PEP (x2k), (d) PEP x1k, (e) PEP (x 2k), (f) PEPGS x 2k, and (g) PEPGS x 2k

3.2.3 DSC Analysis of PCM, PCM/EP, PCM/EP/EG composite sample

The thermal properties of the PCM (sample G), the PCM composite with EG only (sample B, D, and F), as labelled in [Table 3-4](#), are investigated using DSC. [Figure 3-9](#) shows the heat flow rate variation against the temperature for the PCM and PCM composites. From [Figure 3-9](#), it is evident that the curves are drawn to overlap each other with a slight deviation. The overlap indicates that the PCM is well impregnated in the pores of expanded perlite. Additionally, [Table 3-7](#) summarises the latent heat values and phase change peak temperatures for the PCM and PCM composite phase transitions. The enthalpy of samples B, D, F, and G (the PCM) is 83.1 J/g, 83.7 J/g, 84.9 J/g, and 147.0 J/g, respectively. The (H_T) theoretical latent heat of the composite is found to be 70.84 J/g, while as shown in [Table 3-7](#), the enthalpies of the composites found from the experiment are within the range of 83-85 J/g. The H_T is relatively close to H_E and implies that paraffin is well impregnated into EP pores. The effect of adding EG can be observed from the onset temperature found in [Table 3-7](#). The onset temperature, i.e., melting temperature from the PCM manufacturer, is 27°C, while the absorbed melting temperature of the composites is found to be within 24-24.5°C. The temperature difference is due to the increased thermal conductivity of the composites with EG, showing that heat is absorbed quicker than the case without EG.

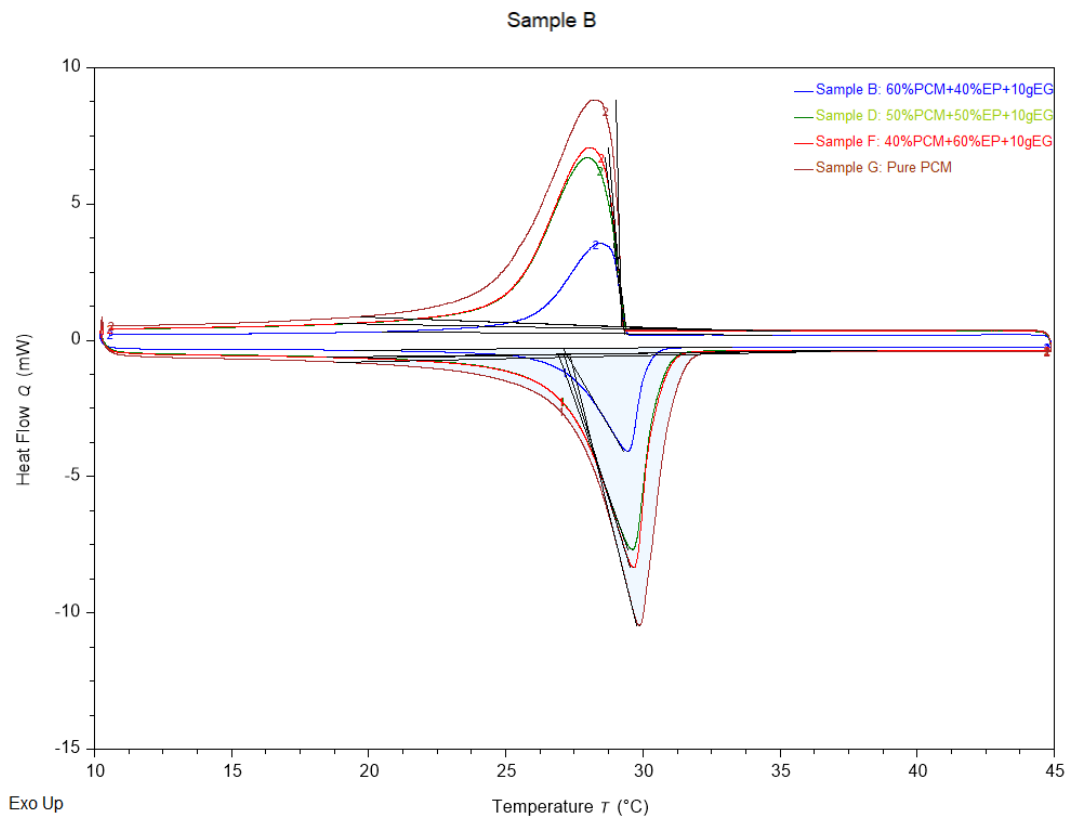


Figure 3-9 DSC curves of PCM and PCM composites

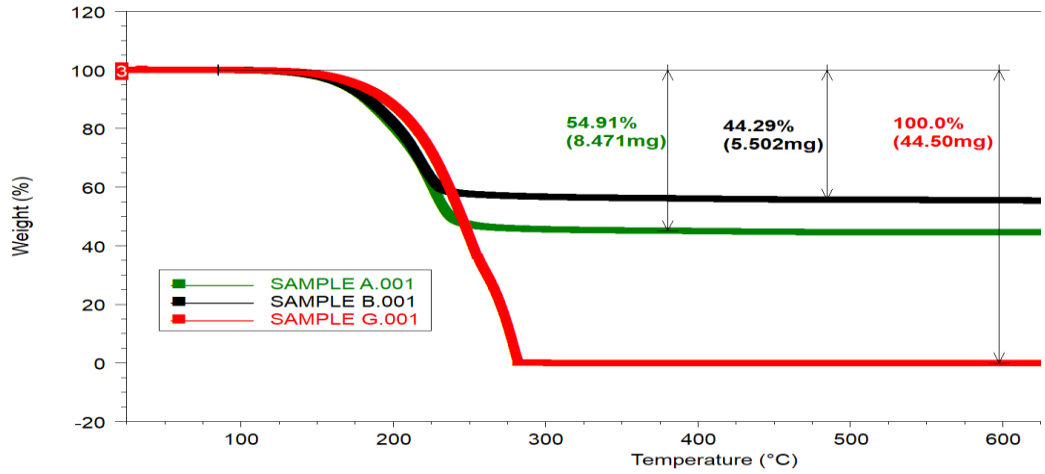
Table 3-7 The changes in thermal properties of the form-stable PCM composite after the addition of EG

Specimen	Onset temp (°C)	Peak temp (°C)	End set temp (°C)	Enthalpy (J/g)
B (60%PCM+40%EP+10gEG)	24.1	28.5	29.4	83.1
D (50%PCM+50%EP+10gEG)	24.5	28.0	29.4	83.7
F (40%PCM+60%EP+10gEG)	24.4	28.1	29.3	84.9
G (100% PCM)	26.2	28.2	29.2	147.0

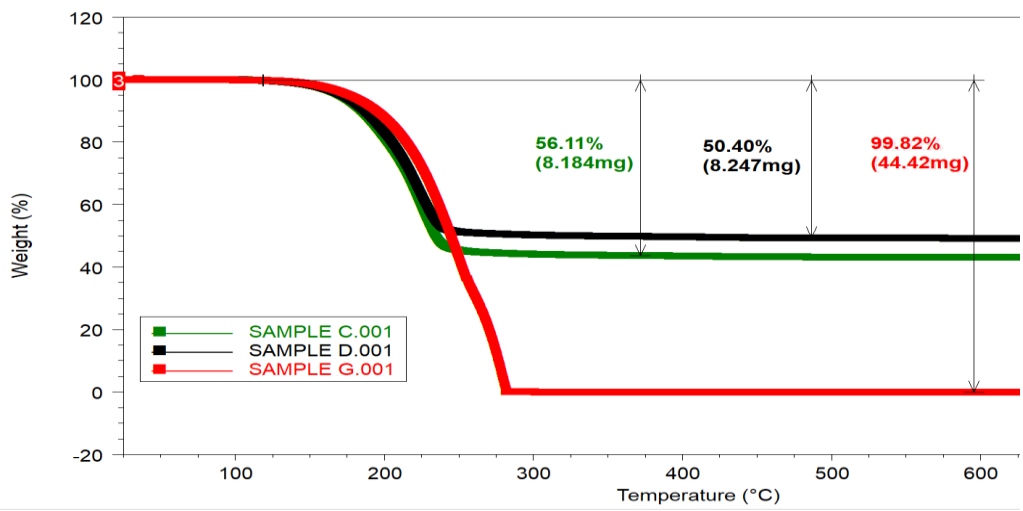
3.2.4 Thermal degradation of PCM and PCM composites

Thermogravimetric analysis is useful in understanding the thermal degradation of a material. Therefore, analysing the thermal resistance of the PCM composite is one of the key thermal properties that need to be considered. This study investigates the thermal degradation of PCM and PCM composites (see Table 3-5). Figure 3-10 a, b, and c display the TG curves of PCM and PCM composites obtained from the thermal degradation analysis. It can be seen from the graphs that the sample weights remain

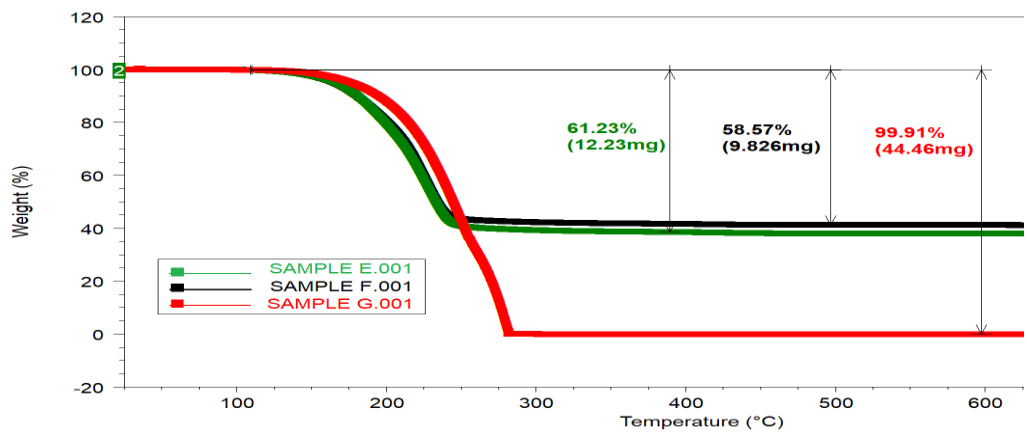
constant up to the point where the temperature reaches around 180 °C, which is nearly close to the maximum operating temperature of A31 as given in [Table 3-1](#). Then, the weight starts decreasing at a temperature of about 240°C. The weights of samples A to F and G (PCM) remain constant, indicating that all the paraffin in the composites has dissipated. The PCM (sample G) shows one-step thermal degradation from 180 °C to 240 °C in all curves a, b, and c, while the PCM embedded in a supporting material of EP and EG (samples A to F) is degraded in at least two steps. The alkali oxide in both EP and EG samples A to F elements begins to decompose if the composite's heating process is carried out for the second or third steps [\[273\]](#). The weight loss percentage for sample G (PCM) is nearly 100%. The weight losses for samples A, B, C, D, E, and F are 54.91%, 44.29%, 56.11%, 50.40%, 61.23%, and 58.57%, respectively. The weight loss for the composite, especially when EG is added, shows less weight loss compared to the composite with EP only, which shows that samples B, D, and F are thermally stable compared to other samples. The result agrees with the leakage test conducted and the result found in [\[273\]](#).



(a)



(b)



(c)

Figure 3-10 TGA curves of PCM and PCM composite

3.2.5 Thermal conductivity of PEPS and PEPGS

The experimental work results of thermal conductivities are shown in Table 3-8 and graphically presented in Figure 3-11. It is evident from the results (Table 3-8) that the thermal conductivity of the reference block is higher than that of PEPS and PEGS. This is the fact because of the presence of phase change material and expanded perlite, which decreases the thermal conductivity of the samples. It is apparent that the PCM exhibits a low thermal conductivity [274], making the rate of the heat storage/release of the organic PCM low [275]. For this reason, the expanded perlite is introduced to the sample to increase the conductivity. The graph shows that the higher the quantity of PEP, the lower the thermal conductivity. However, as expanded graphite is added, the thermal conductivity increases. Despite the addition of EG, the thermal conductivity of PEPG at 6.4% PCM cannot reach the value of the reference block.

Moreover, the thermal conductivity found for all the samples, including the reference one, is within the range of result reported in the literature [70- 73]. Based on the result, the sample with EG exhibits a better thermal performance compared to the one with only PCM and EP. Therefore, the PEPGS sample is taken as the optimum combination for further analysis.

Table 3-8 Measured thermal conductivities of the samples

Specimen	percentage of PCM and EG	Thermal conductivity values ($W m^{-1}. K^{-1}$)
Reference	0% PCM	1.43
Sample A	2.2% PCM	1.21
Sample B	2.2% PCM+EG	1.33
Sample C	4.3%PCM	1.02
Sample D	4.3% PCM+EG	1.19
Sample E	6.5%PCM	0.89
Sample F	6.5% PCM+EG	1.09

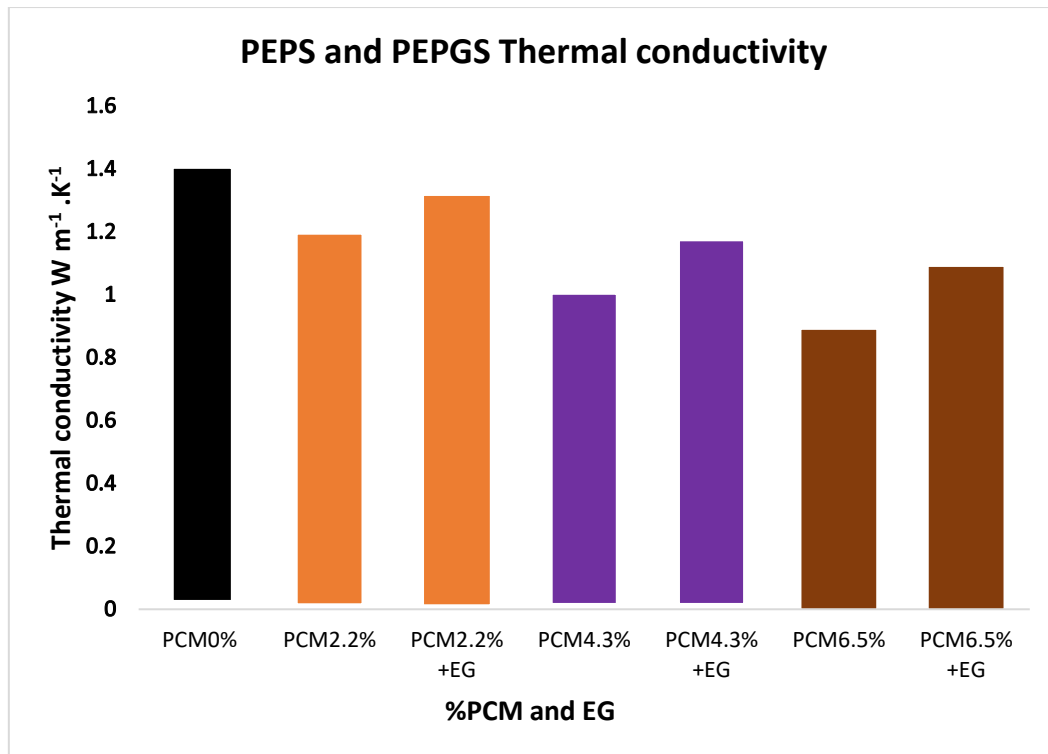


Figure 3-11 Thermal conductivity of PEPS and PEPGS

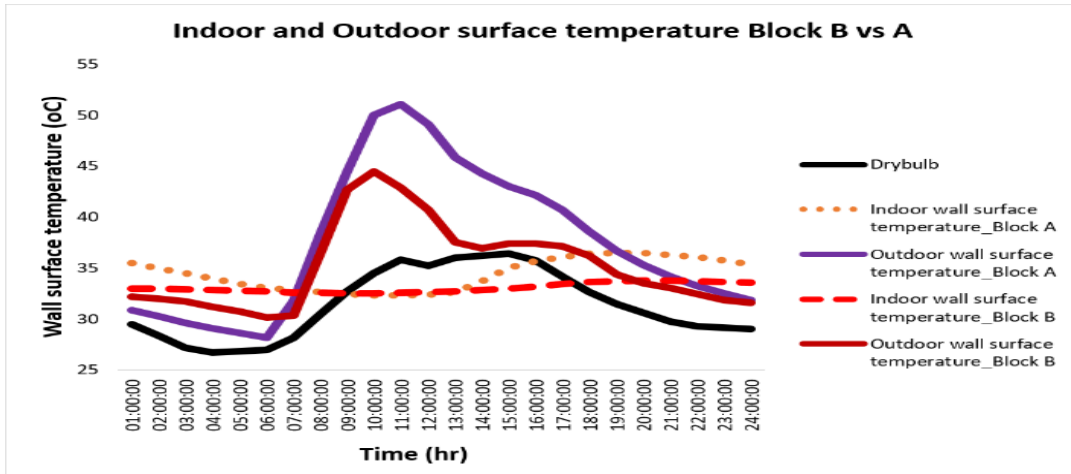
3.2.6 Surface temperature reduction

The indoor and outdoor surface temperature profiles of the experimental blocks as a function of time during the experiment days are shown in [Figure 3-12 a, b, and c](#), respectively. The ambient temperature, as shown in [Figure 3-12 a, b, and c](#), starts at 29°C, which is below the melting point of the PCM and continues to decrease during the night up to 28°C around 08:00. From 08:00, the ambient temperature increases afterwards above the melting point of PCM with a stable gradient to the peak value of 36.4°C at 15:00. The ambient temperature then drops to 30.6°C at 20:00, which is below the melting point of PCM. Berardi and Soudian [276] mentioned that one of the major issues with PCMs is the inability to fully solidify at night due to high surface temperatures that do not reach the freezing point. When PCMs do not discharge the stored energy at night, they lose their ability to reduce heat gain in the cell in the next heat storage cycle because they remain melted. Hence, a close look at the pattern of rising and dropping in [Figure 3-12 a, b, and c](#) shows that during the day, the ambient temperature stays above the melting temperature of PCM for about 12hrs, which

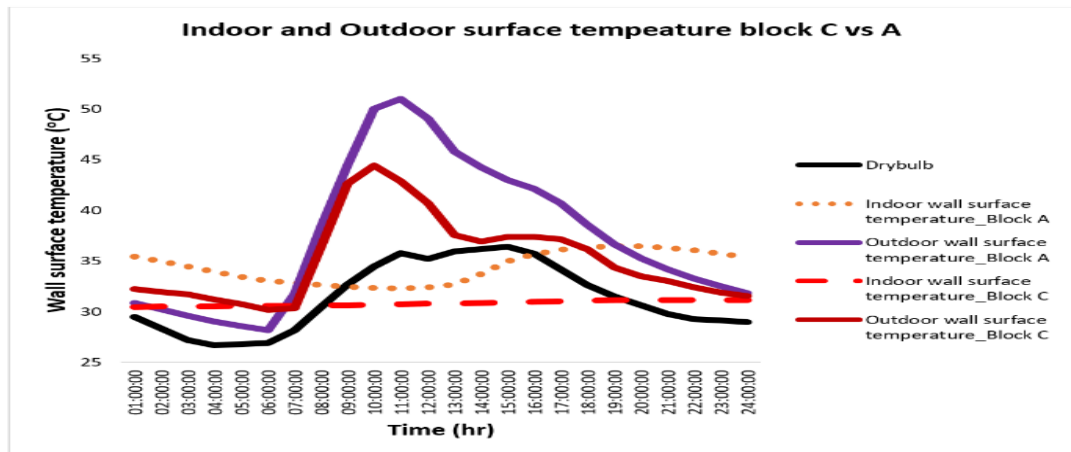
gives the PCM ample time to melt and charge. While at the night-time, for another 12hrs, the ambient temperature is below the PCM's melting point, giving enough time for the PCM to discharge the heat.

The importance of PCM integration in the earthbag block has been demonstrated in this study through experimental analysis, in which the indoor and outdoor surface temperature reduction of Blocks B, C, and D indicate the substantial effect of the PCM in an earthbag block. From [Figure 3-12 a, b, and c](#), the indoor surface temperatures of all the blocks with the PCM start at an approximate temperature of about 30°C. In contrast, the block without PCM (block A) shows a different temperature level of about 35.5°C. However, as the day continues, all the blocks with and without PCM show a temperature decrease, but the blocks with PCM show a higher temperature reduction. The cooling effect caused by the PCM contained in Blocks B, C, and D can be attributed to the observed decrease in the surface temperatures. The average temperature drops generated by Block B, Block C, and Block D compared to the reference Block A are found to be 1.2°C, 3.3°C, and 4.1°C, respectively. The temperature reduces as the quantity of the PCM is increased; it is indicated that the higher the PCM content, the more energy is stored within the earthbag block.

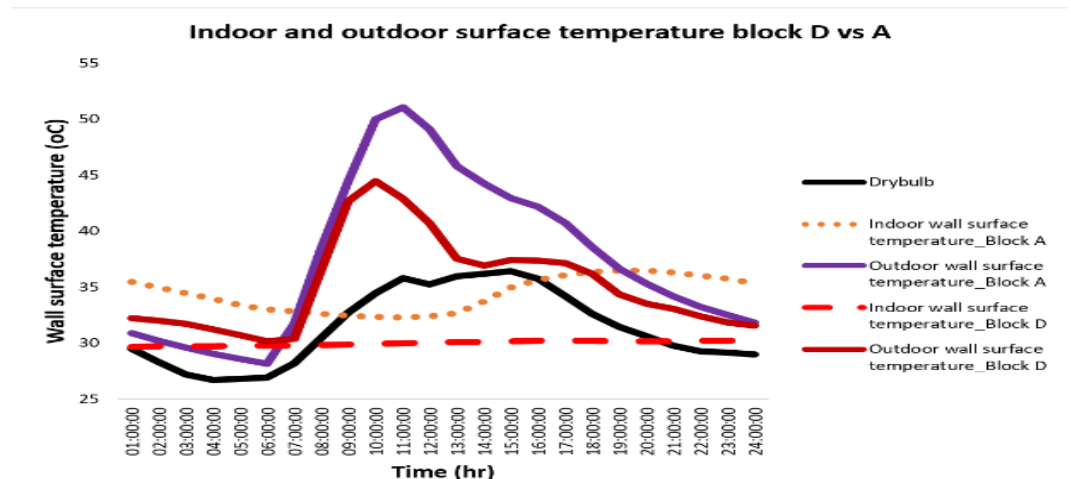
The time lag, a significant factor to consider when analysing the influence of PCM in the earthbag block, has also been investigated. Thus, for all blocks, excluding the reference block, the time lag that helps to delay the time at which indoor surface temperature reaches its peak was highlighted. The reference block reaches its peak at 36.5°C at 19:00, while Block B, C, and D reach their peak indoor surface temperatures of 33.7°C, 31.1°C and 30.2°C at 22:00, 23:00, and 23:30, respectively. Thus, the time duration for the temperature of the earthbag block with PCM in different proportions are reduced by 3hrs for Block B, 4hrs for Block C, and 4.5hrs for Block D. The above result analysis clearly shows the benefit of integrating PCM in an earthbag block.



(a)



(b)



(c)

Figure 3-12 Surface temperature of earthbag block without PCM and earthbag block with PCM

3.3 Summary

The main findings in this chapter are:

- Four different earthbag blocks were tested: Block A (reference, no PCM), Block B (2.2% PCM + EG), Block C (4.3% PCM + EG), and Block D (6.5% PCM + EG). Blocks B, C and D contained varying amounts of a PCM-expanded perlite-expanded graphite (PEPG) composite.
- Leakage testing showed the PEPG composite was stable and did not leak PCM, while the PCM-expanded perlite (PEP) composite without graphite did leak slightly.
- SEM imaging confirmed the PCM was well distributed in the pores of the expanded perlite and graphite.
- DSC testing indicated the PCM successfully impregnated into the carriers, with measured latent heats close to theoretical values. Addition of graphite increased heat absorption rate.
- TGA results showed the composites were thermally stable up to $\sim 180^{\circ}\text{C}$. The PEPG composites showed less weight loss versus PEP, indicating higher stability.
- Thermal conductivity decreased with increasing PCM content but improved with the addition of graphite.
- During outdoor testing, the surface temperature reduction and time lag increased with higher PCM content in Blocks B, C and D compared to the reference Block A.
- The maximum indoor surface temperature reductions achieved were 1.2°C , 3.3°C and 4.1°C for Blocks B, C and D, respectively, versus Block A.
- Time lags of 3-4.5 hrs were observed for Blocks B, C and D to reach peak temperature versus Block A, showing the thermal regulation effect of the PCM.

Chapter 4. Development and Thermal Performance Evaluation of PCM-Integrated Earthbag Wall

In this study, an experimental and numerical investigation was conducted to evaluate the performance of earthbag walls incorporated with PCMs. The study consisted of four main steps, including materials and preparation, thermal performance tests, validation of a numerical model, and parametric analysis to determine the suitable quantity of PCM composite required. The model is developed to resemble the experimental setup to validate the experiment. The description of the experiment is elaborated in [Section 4.1.1](#).

4.1 Experimental and Numerical Study on the Performance of Earthbag-wall Incorporated with Phase Change Materials

The overall work on PCM-E wall development, and thermal performance test consisted of four main steps as shown in [Figure 4-1](#). The first step was the materials and preparation of the earthbag walls. This step involved selecting and preparing the materials that were used in constructing the earthbag wall. The second step was the experiment conducted on the earthbag wall in an environmental chamber that measured the thermal performance of the walls. Therefore, the performance of the wall was monitored within a 1-zone scaled building. The third step was validating the experimental result using developed numerical model of a 1-zone building. Finally, a parametric analysis was conducted to determine the suitable quantity of the PCM required for the PCM-E walls to achieve a better thermal comfort in their indoor environments.



Figure 4-1 Flowchart of development of the earthbag-PCM model

4.1.1 Experimental Study of PCM-intergrated earthbag wall

4.1.1.1 Material and preparation of earthbag block for test wall

For this study, two of PCMs, including A31 paraffin wax and Inertek26 powdered, were used as the thermal energy storage materials in an earthbag wall. The A31 paraffin wax was formed into a PCM composite (PEPG) (see Section 3.1.2). The Inertek26 PCM was already microencapsulated and thus did not require a supporting material, so it was directly incorporated into the wall. However, previous experiments on earthbag wall considered only A31 PCM. Hence, to further verify the benefits of PCM in hot and dry climate such as Nigeria, Inertek26 powdered PCM was also introduced, which is within the comfort zone of Kano state (23°C and 32°C) [258]. The thermophysical properties of Inertek26 powdered PCM presented in Table 4-1, while for A31 paraffin wax was presented already in Table 3-1.

Table 4-1 Technical data for the thermos-physical characteristic Inertek26

Product	Inertek 26
Melting range	26°C to 28°C
Heat storage capacity ($\pm 7.5\%$)	215 kJ/kg
Specific heat capacity	-
Density (solid)	-
Heat conductivity	0.20 W(m.K)
Max. operation temperature	-

4.1.1.2 Preparation of earthbag block

Twenty-four earthbag blocks were fabricated to construct the PCM-Etest wall. The wooden frame for the earthbag block fabrication with the dimension of 400mm x 250mm x 100mm (see [Figure 4-2](#)) was prepared to enclose the mixture. 30% clay to 70% well-graded soil is the suggested as an optimal combination for making an earthbag block as reported [\[256\]](#). The optimum soil was found based on a preliminary test conducted using simple Jar test which was found to be 27% clay and 71% sand with 2% silt. To prevent air gaps that can reduce the block strength, the mixture was carefully pressed into the frame. The soil and the microencapsulated PCM (inertek26) and PCM composited (PEPG) (refer to [Table 3-4](#)) were mixed with 2.2% PCM content (see [Section 4.2.3.1](#)). Water was added to the mixture up to the point where 10% moisture was achieved [\[261\]](#). With special attention paid to the PCM microencapsulation, the mixture has been thoroughly blended in a concrete mixer to achieve homogeneity. Additionally, while pouring the mixture into the block mould, several tamping was made to ensure that the mixture in the bag was fully compacted. It was essential for consolidation that the tamping be moderate to avoid damaging the encapsulated PCM. Sixteen blocks were formed with PCM, including eight with PCM composite (PEPG), and the other eight with microencapsulated PCM. The remaining eight out of 24 blocks were made without PCM, referred to the reference blocks. [Figure 4-3](#) displays the graphical criteria for preparing the mixes and the block development.



Figure 4-2 Earthbag block mould

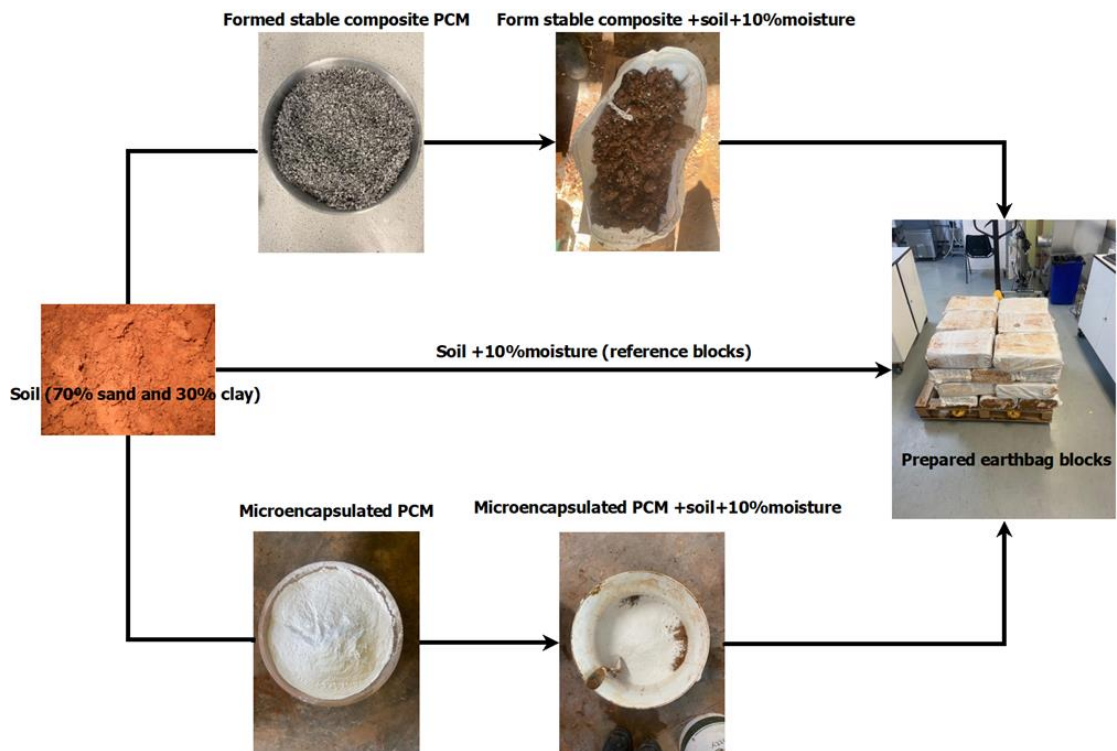


Figure 4-3 Earthbag block preparation

4.1.1 Wall thermal performance testing

Three identical wall prototypes were built to assess PCM's behaviour in an earthbag-building model. Wall-1 (baseline) was constructed without PCM, whereas Wall-2 (WA31) and Wall-3 (WInk26) were built with PCM Composite (PEPG) and Inertek26 (powdered), respectively. The prototype wall [Figure 4-4](#) was placed inside a controlled climatic chamber. [Figure 4-4 b](#) is the schematic layout of thermocouples and heat flux at outer and inner surface of PCM-E test wall. The test wall was arranged with the upper portion constructed as a PCM wall, and the lower portion as a non-PCM wall. The test wall was placed 600mm away from the climate chamber door. A wooden barrier and an expanded polystyrene board were used to separate the two walls and create an indoor space for testing (Room 1 and Room 2 as shown in [Figure 4-4a](#)). The climatic chamber was programmed to simulate summer climatic conditions in Kano, Nigeria (see [Section 4.1.2](#)) to replicate the real condition of the wall if tested outdoor. The climate chamber was divided into two-part, one part set as outdoor temperature and the other part as indoor space. Additionally, ten k-type thermocouples of 0.5 °C accuracy were installed on the test wall, including five on the inner surface and five on the outer surface (refer to [Figure 4-4b](#)). Moreover, two heat flux sensors with uncertainty of calibration of $\pm 3\%$ ($k=2$) were mounted on the wall to measure heat flow rates. The relative humidity was set to 50% throughout experiments. A thermocouple was placed in each indoor space created to measure the indoor temperature (refer to [Figure 4-4c](#)). All sensors were connected to an automatic data acquisition system (DT80 DataTaker Data Logger) with a data recording frequency of 10 minutes. The data logger has voltage measurement accuracy of 0.1%. According to the experimental procedure, both the hot and cold chambers had initially kept at a temperature of 20 °C, to make sure the PCM stays in its solid form. The hot side was set with Kano state profile temperature of three days. The experiment began once the hot chamber started to warm up from the initial temperature to the first profile set temperature 32 °C, causing a variable thermal boundary condition on the hot side of the PCM sample. The experiment was carried out for three days to observe variations in the behaviour of the PCM-E wall in a typical summertime as set in the climate chamber.

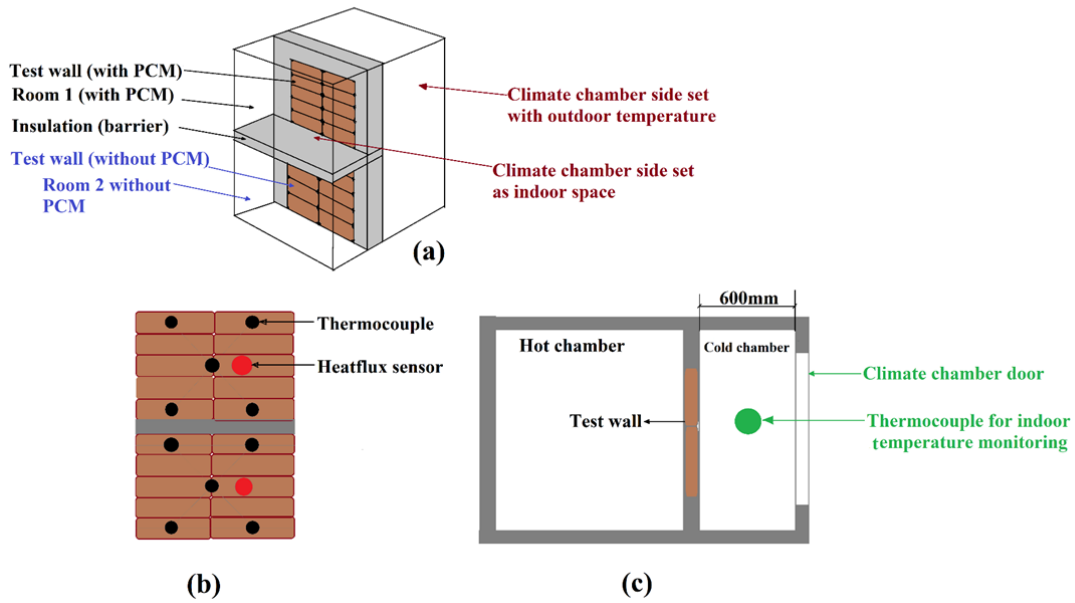


Figure 4-4(a) Test walls prototype in climatic chamber and (b) prototype's picture

4.1.1.1 Uncertainty analysis

To determine the accuracy of the experiment on thermal performance of earthbag wall, an Uncertainty analysis is needed. In this study, focus was made on the measurements of inner wall surface temperature and heat flow through the wall. Therefore, the uncertainties were derived from the random measurement of error of the K-type thermocouples and the heat flux sensors. For the thermocouples, the accuracy was $\pm 0.5^{\circ}\text{C}$, which means that the actual temperature could be within $\pm 0.5^{\circ}\text{C}$ of the measured value. For the heat flux sensor, the calibration uncertainty was $\pm 3\%$ ($k=2$) as from the manufacturer's data sheet, which means there is a 95% chance that the actual heat flux is within $\pm 3\%$ of the measured value. Then, the uncertainty of the K-type thermocouples is $\pm 0.3^{\circ}\text{C}$ with an average temperature of 36.1°C and the uncertainty of the heat flux sensors is $\pm 0.68 \text{ W}/\text{m}^2$ with an average heat flux of $24.6 \text{ W}/\text{m}^2$. Thus, to calculate the percentage uncertainty of the measurement, we can divide the total uncertainty by the measured value and multiply it by 100%. Therefore, the percentage uncertainty of the K-type thermocouple was found to be 0.8%, and the percentage uncertainty of the heat flux sensor was 2.8%. Now that we have the individual uncertainties, we can calculate the combined uncertainty using the root

sum of squares (RSS) method as reported by Tokuç et al. [277] using Eqn 4.1:

$$\omega_R = \left[\left(\frac{\partial R}{\partial x_1} \omega_1 \right)^2 + \left(\frac{\partial R}{\partial x_2} \omega_2 \right)^2 + \dots + \left(\frac{\partial R}{\partial x_n} \omega_n \right)^2 \right]^{1/2} \quad \text{Eqn 4.1}$$

where, ω_R is the total uncertainty in the result, R is the calculated result based on the uncertainties of the independent variables $x_1, x_2, x_3, \dots, x_n$, and $\omega_1, \omega_2, \dots, \omega_n$ are percentage uncertainty.

Hence, the resulting total uncertainty of the experiment is found to be 2.9%. The result indicates that after accounting for all these potential sources of uncertainty, it was determined that the total uncertainty associated with the measurements of earthbag wall thermal performance was calculated to be 2.9%. This means that the reported thermal performance values of earthbag wall have an associated margin of error of 2.9%, which reflects the confidence level of the study have in the accuracy of the measurements.

4.1.1.2 Thermal conductivity determination of test walls

To evaluate the thermal conductivity, an experiment was conducted using a controlled thermal chamber to determine the heat transfer through the walls. The method employed for the experiment was the Calibrated hot-box method, as outlined in the British Standard (BS 874-3.2, 1990). The aim was to establish a temperature difference between the two sides of the wall by situating a heat source (on the hot side of the chamber) on one side and allowing heat to transfer through the wall layer to the other side (cold side of the chamber) (refer to Figure 4-4a). The temperature of both wall surfaces was monitored in a steady state condition. The temperature range chosen for the experiment was between 10 °C to 70 °C, which falls within the melting and solidification range of the selected PCMs. The data collected from the data logger through the heat flux sensors at the steady state condition were used to calculate the thermal conductivity of the walls. The heat flux sensitivity was $64.6 \mu V / W \cdot m^2$, where the heat flux (q) (Eqn 4.2) was estimated by dividing the voltage by the sensor's sensitivity [278]:

$$q = \frac{\text{voltage} \times 1000}{64.6} \quad \text{Eqn 4.2}$$

Also, k (Eqn 4.3) as the thermal conductivity (W/mK) is determined as follows:

$$k = \frac{Ql}{A \times \Delta T} \quad \text{Eqn 4.3}$$

where A is the area of the wall (m^2), ΔT is the temperature difference between the wall surfaces ($^{\circ}C$), and l is the wall thickness (m).

4.1.1.3 Heat transfer from surfaces

Convective heat transfer is used to calculate the amount of heat transfer between the inner surface of the wall and the indoor air. This temperature difference typically has a low value, so the radiative heat exchanges between them can be neglected. Thus, the convective heat exchange (Eqn 4.4) can be calculated as follows:

$$q = h_c A (T_b - T_i) \quad \text{Eqn 4.4}$$

where q is the rate of heat transfer from the inner surface to the interior environment, h_c is the convective heat transfer coefficient, T_b is the temperature of the inner surface, and T_i is the temperature of the indoor air. h_c can be adapted from the below Eqn 4.5 and Eqn 4.6 by applying either a linear or a power regression [212]:

$$h_c = 3.3v_w + 6.5 \quad \text{Eqn 4.5}$$

$$h_c = 9.5v_w^{0.48} \quad \text{Eqn 4.6}$$

where v_w is the air speed (see Figure 4-5).

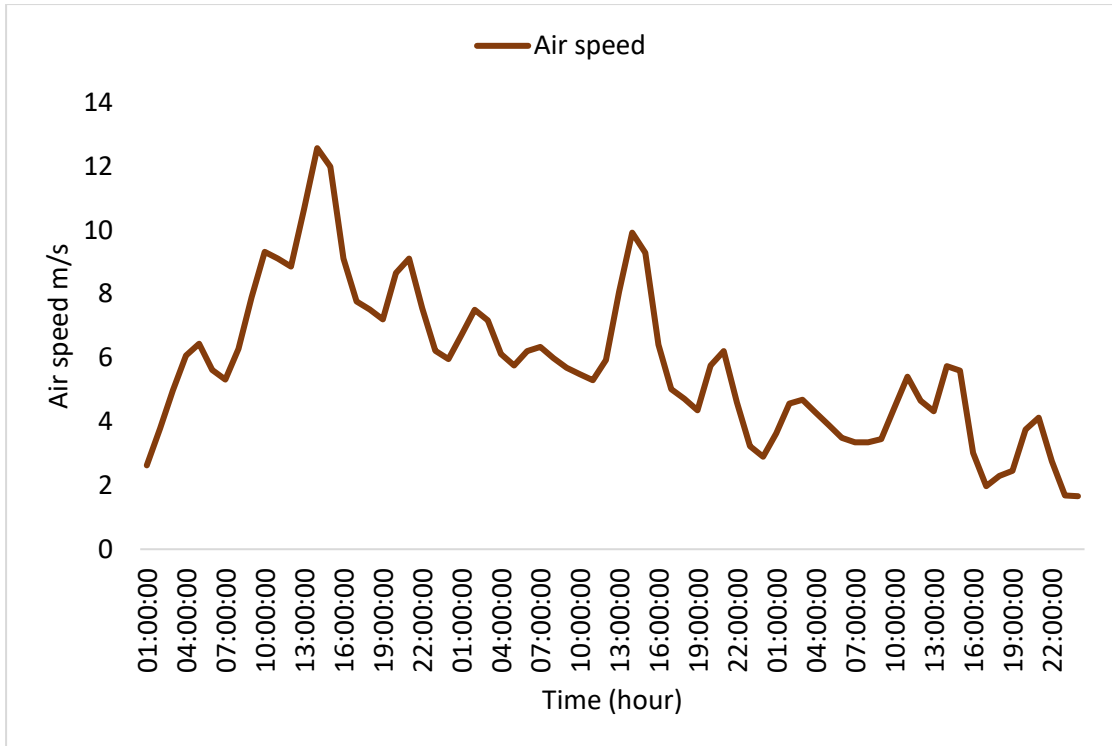


Figure 4-5 Air speed in a typical summer day in Kano state

4.1.1.4 Time lag and decrement factor

Time lag (TL) is the time when peak load is shifted to off-load. It can, therefore, be calculated as the difference between the time at the maximum inner surface temperature ($T_{i,max}$) and the time at maximum average outer surface temperature ($T_{o,max}$) ([Error! Reference source not found.](#)) [279]:

$$TL = \tau T_{i,max} - \tau T_{o,max} \quad \text{Eqn 4.7}$$

where $\tau T_{i,max}$ and $\tau T_{o,max}$ are the times at the maximum inner and outer surface temperatures of the wall, respectively. The decrement factor (f) represented the ratio of the peak heat transfer out of the external surface of the element per unit degree of external temperature swing to the steady state heat transfer through the element per unit degree of temperature difference between the internal and external environmental temperatures [280]. The decrement factor (Eqn 4.8) can be calculated as below [281]:

$$f = \frac{T_{in\ max} - T_{in\ min}}{T_{out\ max} - T_{out\ min}} \quad \text{Eqn 4.8}$$

Where $T_{in\ max}$ and $T_{in\ min}$ are respectively the maximum and minimum inner surface temperature of the wall (°C). Likewise, $T_{out\ max}$ and $T_{out\ min}$ are respectively the maximum and minimum outer surface temperature of the wall (°C).

4.1.1.5 PCM modelling

A finite difference approach is included in EnergyPlus (EnergyPlus CondFD) to model materials with variable thermal properties using the enthalpy method [282]. As suggested by Özdenefe et al.[244], a fully implicit first-order scheme was employed in this study as the solution scheme. The solution scheme was used to validate the established experimental PCM-E wall presented in Section 4.1.1. The temperature enthalpy graph of the A31 PCM used in the model was determine using differential scanning calorimetry analysis (see Section 4.3.1), while that of Inertek26 was taken from the manufacturer's data sheet [283]. The first change process of PCM is accounted by a user-defined enthalpy temperature as described below (Eqn 4.9) [284].

$$C_p \rho \Delta X \frac{(T_i^{j+1} - T_i^j)}{\Delta t} = k_W \frac{(T_{i+1}^{j+1} - T_i^{j+1})}{\Delta X} + k_E \frac{(T_{i-1}^{j+1} - T_i^{j+1})}{\Delta X} \quad \text{Eqn 4.9}$$

where k_W and k_E (Eqn 4.10 and Eqn 4.11) as thermal conductivities can be defined as:

$$k_W = \frac{(k_{i+1}^{j+1} + k_i^{j+1})}{2} \quad \text{Eqn 4.10}$$

$$k_E = \frac{(k_{i-1}^{j+1} + k_i^{j+1})}{2} \quad \text{Eqn 4.11}$$

where T_i^j is the temperature at node i and time step j , Δt is the time step, ΔX is the

finite difference layer thickness, C_p is the specific heat of the material, and ρ is the density. Note that $k_i = k(T_i^{i+1})$ if the thermal conductivity is variable.

In the CondFD algorithm, all elements are divided or discretized automatically using Eqn 4.12, which depends on a space discretization constant (c), the thermal diffusivity of the material (α), and the time step. Users can leave the default space discretization value of 3 (equivalent to a Fourier number (Fo) of 1/3) or input other values [255].

$$\Delta x = \sqrt{c \cdot \alpha \cdot \Delta t} = \sqrt{\frac{\alpha \cdot \Delta t}{Fo}} \quad \text{Eqn 4.12}$$

Eqn 4.13 was integrated with the Enthalpy-temperature function (HTF), which was given by:

$$h = h(T) \quad \text{Eqn 4.13}$$

where $h(T)$ is the enthalpy node as a function of temperature.

The HTF developed an equivalent specific heat as a function of temperature ($C_p(T)$) at each time step for the PCM contained in the building as it is formulated by Eqn 4.14 [253]:

$$C_p^*(T) = \frac{h_i^j - h_i^{j-1}}{T_i^j - T_i^{j-1}} \quad \text{Eqn 4.14}$$

where $C_p^*(T)$ is the specific heat as a function of temperature.

4.1.2 Location and Climate

Kano State, located in the northern Nigeria [285], is an ideal location for studying the thermal performance of PCM-integrated earthbag building. The study area lies between latitudes 11°.52'N and 12°.07'N and longitudes 8°.24'E and 8°.38'E. It is centrally located in northern Nigeria, about 900 kilometres from the Sahara Desert and 1140 kilometres from the Atlantic Ocean. It covers an area approximately 499 km² [286]. The climate of the study domains are classified by Koppen's climate pattern as Aw (wet and dry tropical continental with a mono-modal rainfall pattern) and BSh (a climate domain that has the characteristics of both the Sahara Desert and tropical wet and dry climate i.e. semi-arid zone, with more of a dry condition) [287]. The region experiences extreme temperature variations throughout the year with hot and dry conditions in the summer and cool and dry conditions in the winter [288]. The summer period in Kano spans approximately three months, starting from March and concluding in May. During this time, the typical daily maximum temperature exceeds 39 °C. April stands out as the hottest month, with an average daily maximum temperature of 43 °C. On the other hand, December and January are the coolest months, featuring an average daily maximum temperature that drops below 12 °C [289]. Hence, the use of appropriate building materials and technologies is critical in creating comfortable living spaces in such environment. In this context, the metrological year (RMY) weather data for this specific location is utilized which was found in EnergyPlus weather data store. The RMY weather data has been edited with field data collected to ensure accuracy. This edited RMY weather data is then employed for simulating a numerical model of a 1-zone building. The development of this numerical model has been completed. Figure 4-6 shows the typical summer outdoor temperature months of Kano state.

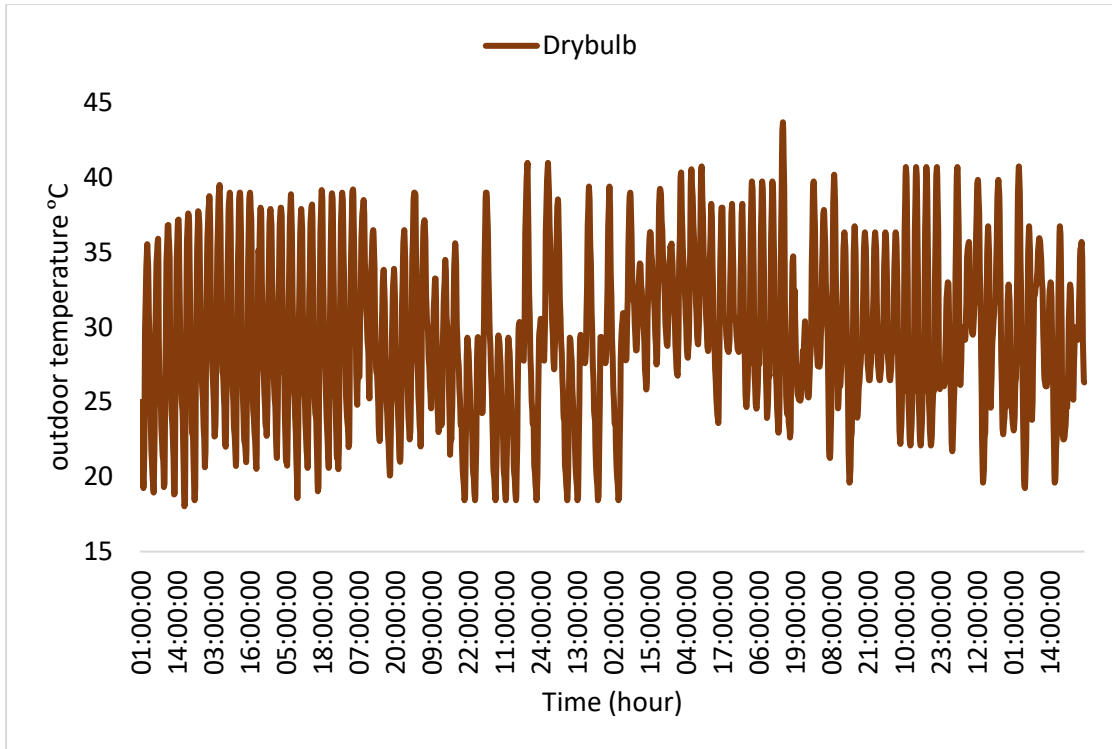


Figure 4-6 Outdoor temperature variation for a typical summer months of Kano state

4.1.3 Model validation metrics

The experiment conducted on PCM-E wall (refer to [Section 4.1.1](#)) was validated against the numerical analysis conducted (see [Section 4.3](#)). The experimental data and the simulation results were compared using different metrics to evaluate the validation process, which includes correlation coefficient (r), fractional bias (FB), normalized mean square error (NMSE), and fraction of predictions within a factor of two (FAC2):

$$r = \frac{n(\sum x_i y_i) - (\sum x_i)(\sum y_i)}{\sqrt{[n \sum x_i^2 - (\sum x_i)^2] - n \sum y_i^2 - (\sum y_i)^2}} \quad \text{Eqn 4.15}$$

$$FB = \frac{[y] - [x]}{([y] + [x])} \quad \text{Eqn 4.16}$$

$$NMSE = \frac{[(x_i - y_i)^2]}{[x][y]} \quad \text{Eqn 4.17}$$

$$FAC2 = \frac{1}{N} \sum_{i=1}^N n_i \quad n_i = 1 \text{ if } 0.5 \leq \frac{x_i}{y_i} \leq 2 \text{ else } n_i = 0 \quad \text{Eqn 4.18}$$

where y_i and x_i are the measured and computed values of a given variable for sample i , respectively. N is the number of data points used in the calibration process. The ideal value of the validation metrics for a complete agreement between two data series is 1 for r and $FAC2$ and 0 for FB and $NMSE$.

4.2 Description of the Case Study PCM-integrated earthbag wall

4.2.1 Climate

The weather condition data utilized for the study, as well as the description of the climate conditions pertaining to the developed model, are explained upon in [Section 4.3.4](#).

4.2.2 Modelling geometry and parameters

The developed case study aims to investigate the effect of PCM-E walls for comparing with experimental results for model validation. The model geometry, as illustrated in [Figure 4-7](#), employed in the simulation is designed to closely resemble the experimental setup (see [Figure 4-4](#)) performed in an environmental chamber. As there is no code for an earthbag building development, literature is consulted to determine the dimensions and the material characteristics as shown in [Table 4-2](#). The model is made as a 1:2 scaled single room, two-story and dual thermal zone, with a size of 800 mm × 400 mm and a height of 800 mm for each room. In the developed geometry, the top wall with a PCM E wall and a reference wall are used as the test walls.

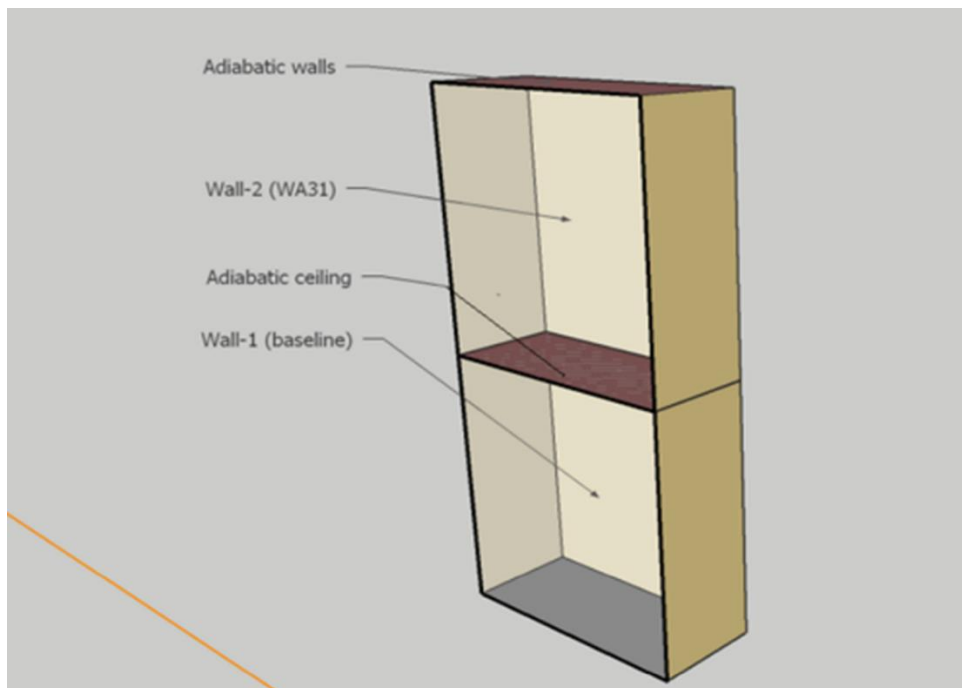
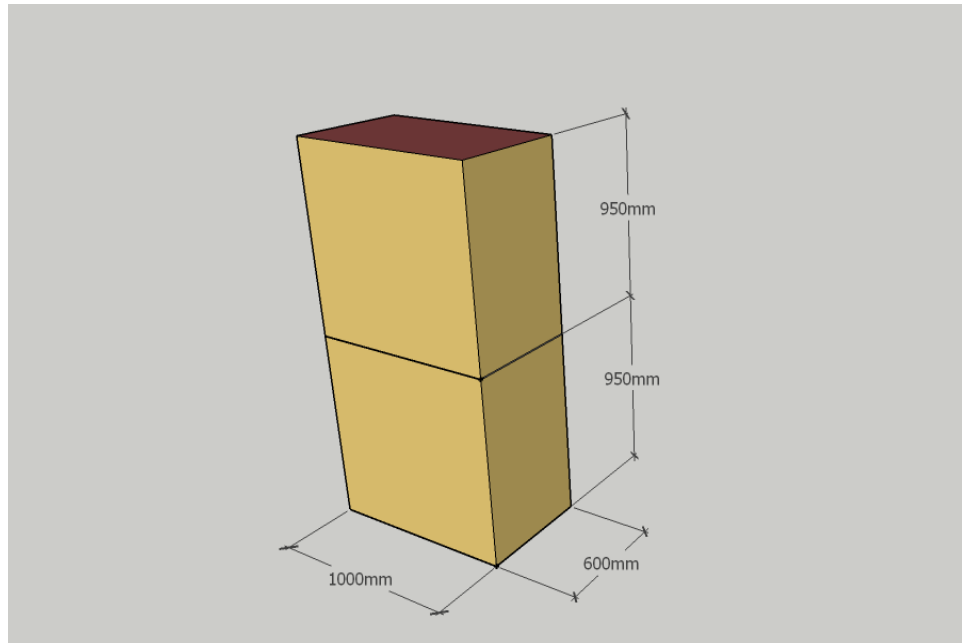


Figure 4-7 Developed SketchUp model geometry

The first floor, the ground floor and all other walls are assumed to be adiabatic walls made from expanded polystyrene insulation (EPS) board with a thickness of 100 mm. The simulation was carried out for the earthbag wall with and without PCM composite and microencapsulated PCM during the summer period. For the validation, this study uses graphical comparison together with recommended evaluation indices as

discussed in Section 4.3.3, and mean error difference between numerical solutions and experimental data. The validation of the model is contingent on meeting specific criteria as outlined in reference [290]. These criteria include achieving a less than 10% validation error between numerical solutions and experimental data and meeting acceptable absolute mean errors. Specifically, an absolute mean error of less than 2°C of inner or outer surface temperature is recommended.

Table 4-2 Numerical model materials properties

System	Thickness <i>m</i>	Conductivity (W/ m. K)	Density (kg/ <i>m</i>³)	Specific heat (J/kg . K)
Earthbag wall	0.25	1.83*	2190	1000
Earthbag wall with A31 composite	-	0.74*	1980*	2100*
Earthbag wall with Inertek26	-	0.43*	1800*	2050*
Floor (expanded polystyrene insulation (EPS) board)	0.075	0.037	2390	1650
Slab (expanded polystyrene insulation (EPS) board)	0.075	0.037	2300	1650

*Calculated from the experiment conducted

Once the EnergyPlus models was validated with experimental data, the developed model was used for a parametric analysis by converting the PCM quantity accumulated within a single wall to a layer and also the supporting material expanded perlite. The important of this is to determine the effect of both storage materials as thermal mass and the insulation materials stands as expanded perlite. The thickness of PCM and Expanded perlite was found to be 0.001m and 0.002m for PCM (A31 and Inertek26) and expanded perlite using PCM equivalent method [291]. The schematic drawing of the process can be seen in Figure 4-8 together with the PCM-E wall arrangement for parametric analysis used in the current study. The PCM enthalpy and DSC curve are experimentally found and presented in this section. The DSC results in this study provide important information about the thermal properties of four different PCMs: A28 and A31 paraffin wax, Inertek26 and Inertek23 powder. The DSC measurements include enthalpy, peak temperature, and onset temperature. The DSC

results are presented in Figure 4-9. The results reveal that A28 paraffin wax has the highest enthalpy among the four PCMs, indicating that it has the highest capacity for thermal energy storage. However, A28 paraffin wax also has the lowest peak and onset temperatures, indicating that it changes phase at lower temperatures than the other PCMs, which may limit its application in regions with higher ambient temperatures.

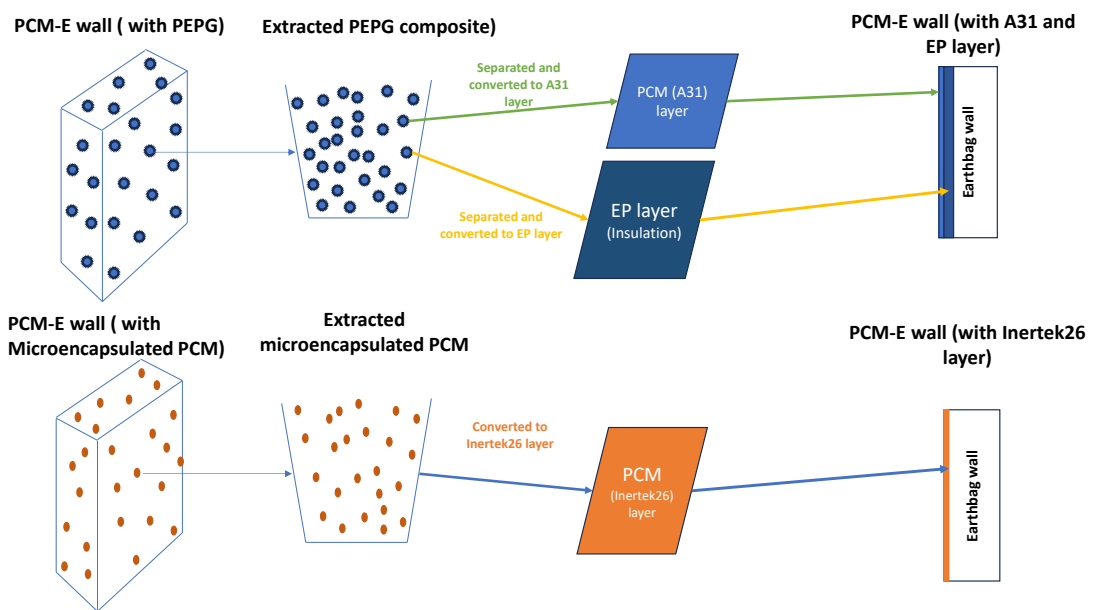


Figure 4-8 Conversion process of PCM composites to layers

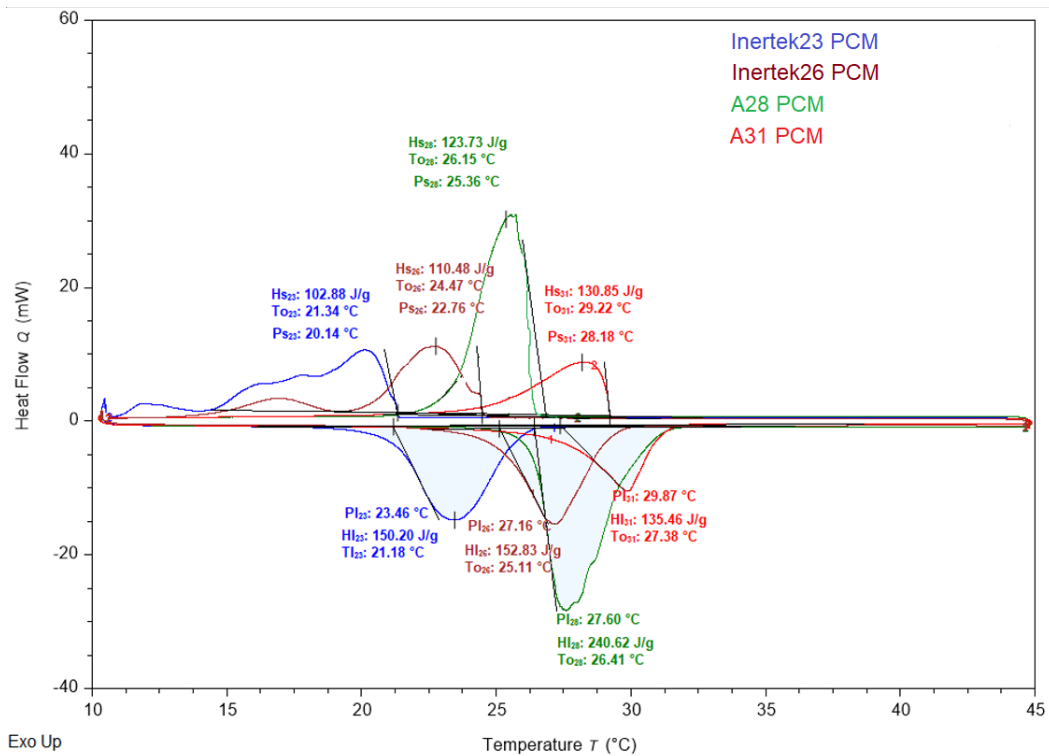


Figure 4-9 Phase transition temperature for A31, A28, Inertek26, and Inertek23 PCM

In contrast, A31 paraffin wax has the highest peak and onset temperatures among the four PCMs, making it suitable for regions with higher ambient temperatures. However, A31 paraffin wax has the lowest enthalpy, meaning it has less thermal energy storage capacity than the other PCMs. The DSC results suggest that the choice of PCM depends on the desired thermal performance and the ambient temperature range. A28 paraffin wax may be preferred for regions with lower ambient temperatures and higher thermal energy storage requirements. A31 paraffin wax may be preferred for regions with higher ambient temperatures and lower thermal energy storage requirements. Inertek26 powder and Inertek23 powder may be considered as alternatives to paraffin wax with similar PCT but different enthalpies. The enthalpy-temperature curve of the PCMs used in the simulation is shown in [Figure 4-10](#).

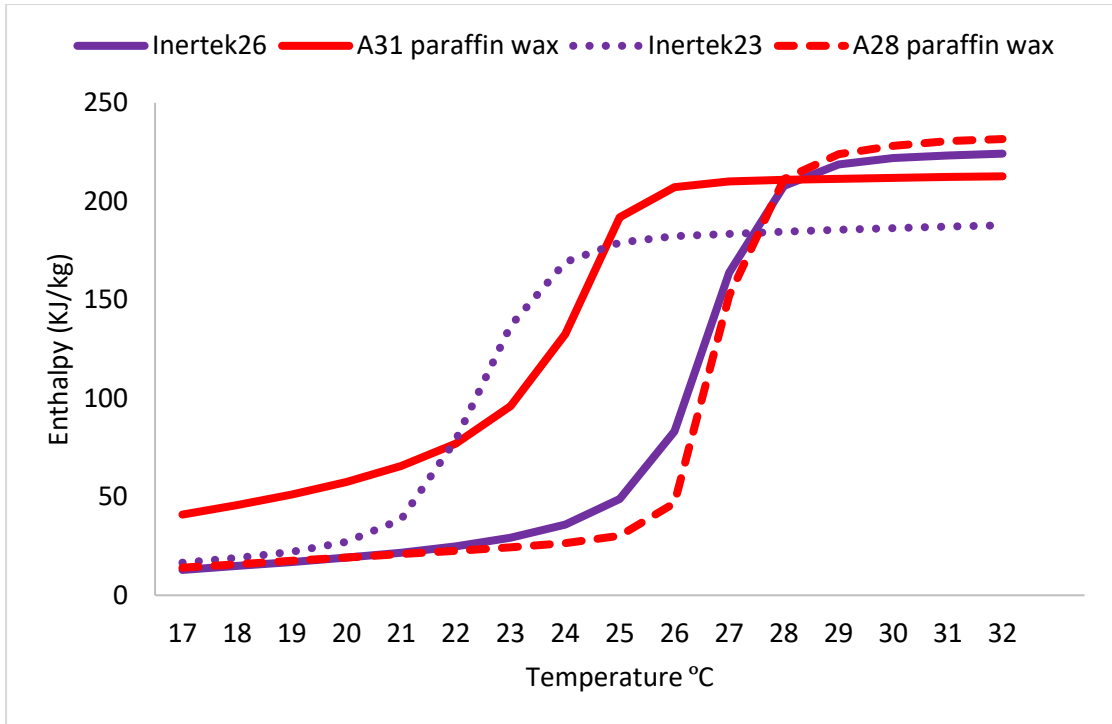


Figure 4-10 Enthalpy temperature curves of Inertek26, 23 and A31, 28 PCM

4.3 Result

4.3.1 Thermal conductivity of earthbag walls

As shown in Figure 4-11, the steady state condition of the wall reached were the difference between the surface temperature of a walls remain constant. The temperature difference between hot and cold side for Wall-1 (baseline), Wall-2 (WA31), and Wall-3 (Wink26) at steady state are 5.0°C, 6.6°C, and 8.6°C, respectively. Hence, the heat flux was found to be 23.3 W/m^2 , 9.5 W/m^2 , and 7.1 W/m^2 which was obtained from the data logger through the heat flux sensors at the steady state period. Therefore the thermal conductivities of earthbag walls with and without PCM are measured in this study with three different samples being tested, including Wall-1 (baseline), Wall-2 (WA31), and Wall-3 (Wink26). Results show that Wall-3 (Wink26) has the lowest thermal conductivity of 0.43 $W/m.K$ compared to Wall-2 (WA31) with the value of 0.74 $W/m.K$, and Wall-1 (baseline) with the values of 1.83 m^2K/W . As expected, the higher the quantity of PCM, the better the thermal performance [292],[293]. The quantity of microencapsulated PCM (Inertek26) in volume is higher

and distributed uniformly than PCM composite in the block. This is likely to be the primary contributing factor to the low thermal conductivity of Wall-3 (Wink26). The presence of PCM in the wall also reduce the heat transfer from the outer wall to the inner wall surface as the lower thermal conductivity of PCM slows down the heat transfer rate. In hot climate regions, this characteristic of PCM is especially beneficial as it can potentially keep the inner surface temperature low [154]. Therefore, the earthbag wall with microencapsulated PCM demonstrates the best thermal conductivity in the experiment.

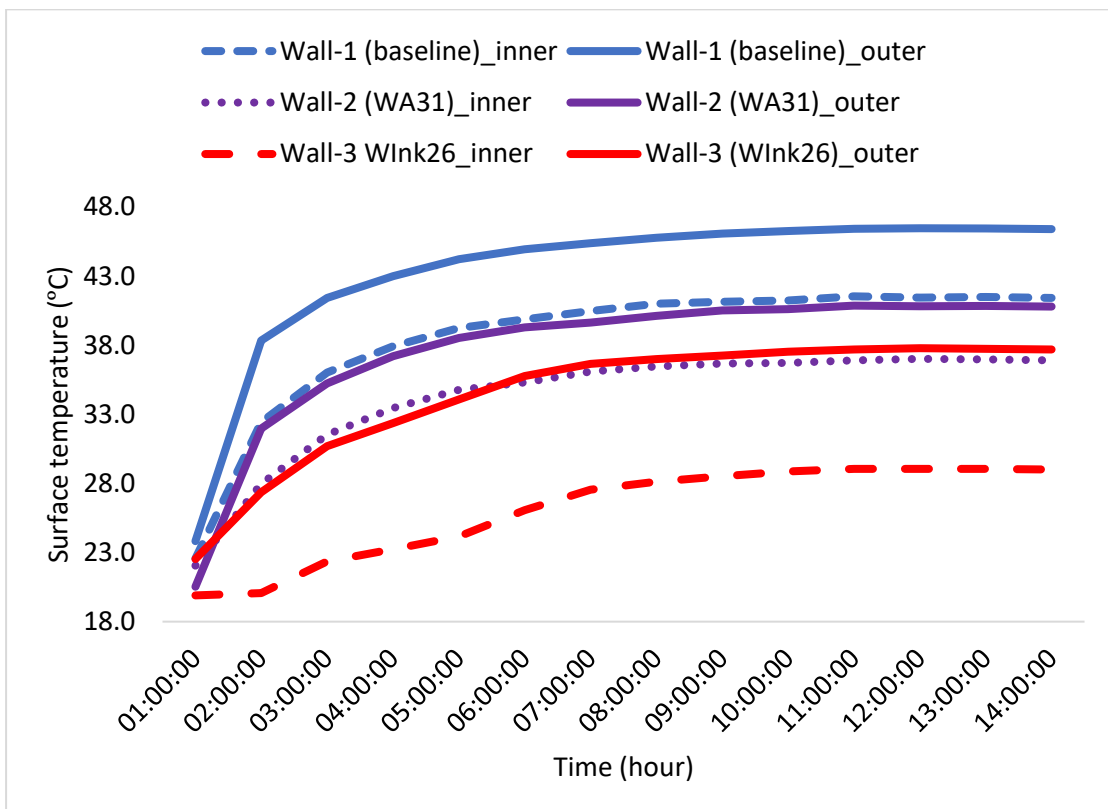


Figure 4-11 Inner and outer surface temperatures of earthbag walls at steady state

4.3.2 Wall surface temperatures

The wall's inner and outer surface temperatures are demonstrated over three days in April in [Figure 4-12](#) and [Figure 4-13](#). It can be seen that Wall-3 (WInk26) has a more stable inner surface temperature than Wall-2 (WA31) and Wall-1 (baseline). This is due to the lower thermal conductivity of Wall-3 (WInk26), resulting in a slower heat transfer to the inner surface temperature. The same pattern can be observed for the outer wall surface while the wall without PCM displays a higher temperature due to its higher thermal conductivity. Considering the melting temperatures of the PCMs used, it can be seen that they are ineffective, as the outdoor temperature during the first day of the experiment is above the melting temperature of the PCM. This causes an instant release of stored heat to the inner surface, resulting in an increase in the inner surface temperature. This can also be observed for the second and third days of the experiment. However, Wall-3 (WInk26) with Inertek26 PCM, whose melting temperature is 26°C, have the most stable inner surface temperature with a temperature variation of not more than 2°C during the day. This results in a decrease in the maximum temperature amplitude compared to Wall-1 (baseline). The average temperature reduction between Wall-2 (WA31) and Wall-3 (WInk26), and the Wall-1 (baseline) is 1.9°C and 2.4°C. [Figure 4-12](#) shows that all internal surface temperature values are higher than the phase transition temperature of the PCMs, rendering them ineffective in charging and discharging. This is likely due to the small quantity of PCM used, as adding a layer does not provide adequate thermal performance. Previous research has shown that if the PCM layer is too thick, it can act as an insulation layer, whereas if it is too thin, solidification may not occur, resulting in inadequate charging or discharging of the PCM [\[294\]](#). Hence, incorporating a greater quantity of PCM is necessary for earthbag blocks to be more effective.

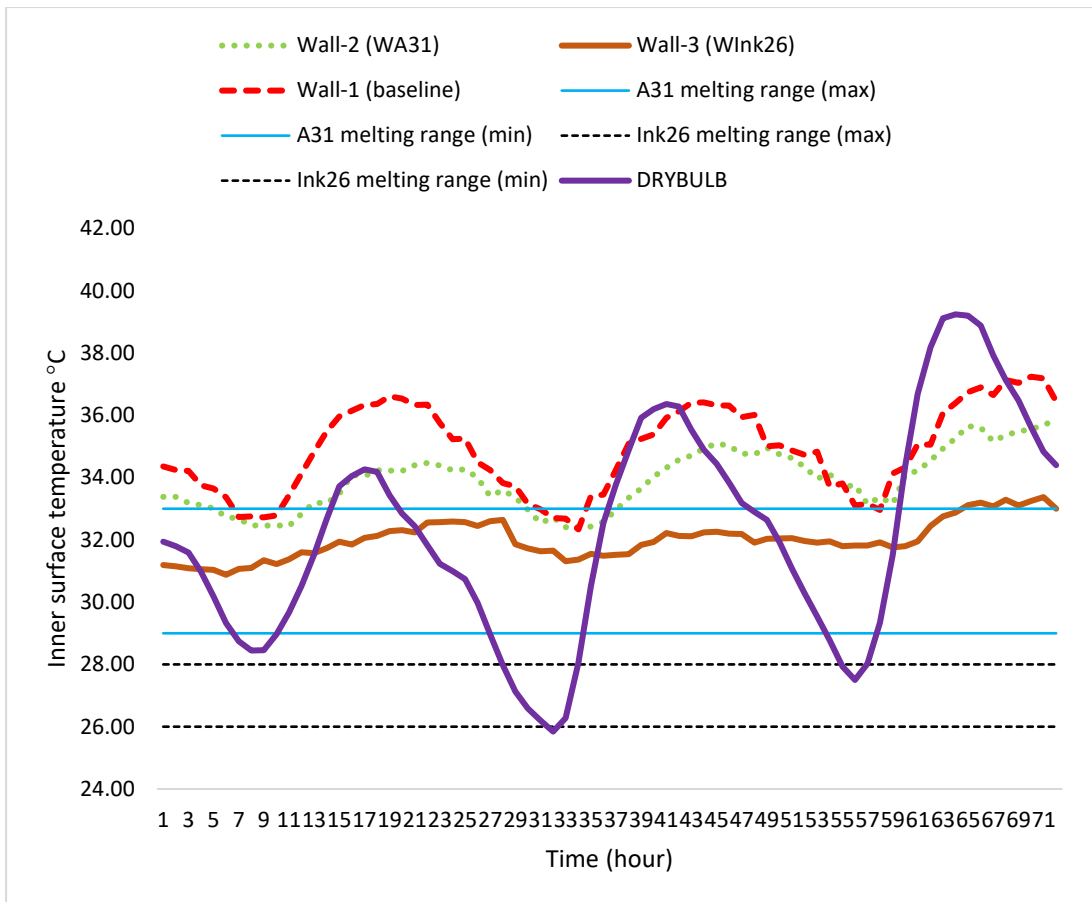


Figure 4-12 Inner surface temperatures of Wall-1 (baseline), Wall-2 (WA31) and Wall-3 (Wink26)

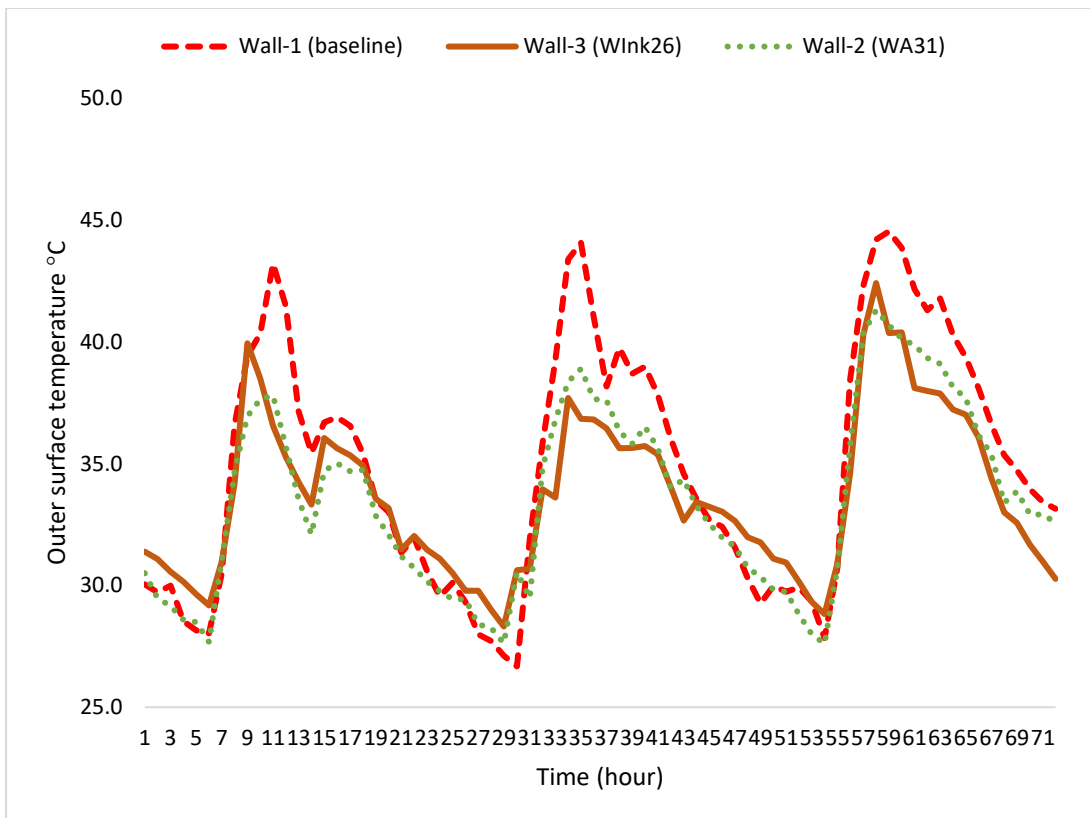


Figure 4-13 Outer surface temperatures of Wall-1 (baseline), Wall-2 (WA31) and Wall-3 (Wink26)

4.3.3 Time lag (TL) and Decrement factor

The graph in Figure 4-14 shows that the time lag of Wall-2 (WA31) and Wall-3 (Wink26) varies throughout the experiment day. It is evident that the integration of PCM leads to an increase in the time lag value, which is more pronounced in the Wall-3 sample (Wink26). In particular, the first and second days of the experiment show time lags of 4hrs and 3hrs, respectively. These values illustrate that PCM composite that includes both PCM and its supporting materials integration can decrease the rate of heat penetration through the wall. However, on the third day, a negative time lag is observed in Wall-2 (WA31), likely due to the high outdoor temperature that causes the PCM within the wall to melt faster than usual, resulting in a high inner surface temperature and a lower time lag. Wall-2 sample (WA31) behaves similarly to the Wall-1 (baseline) on this day.

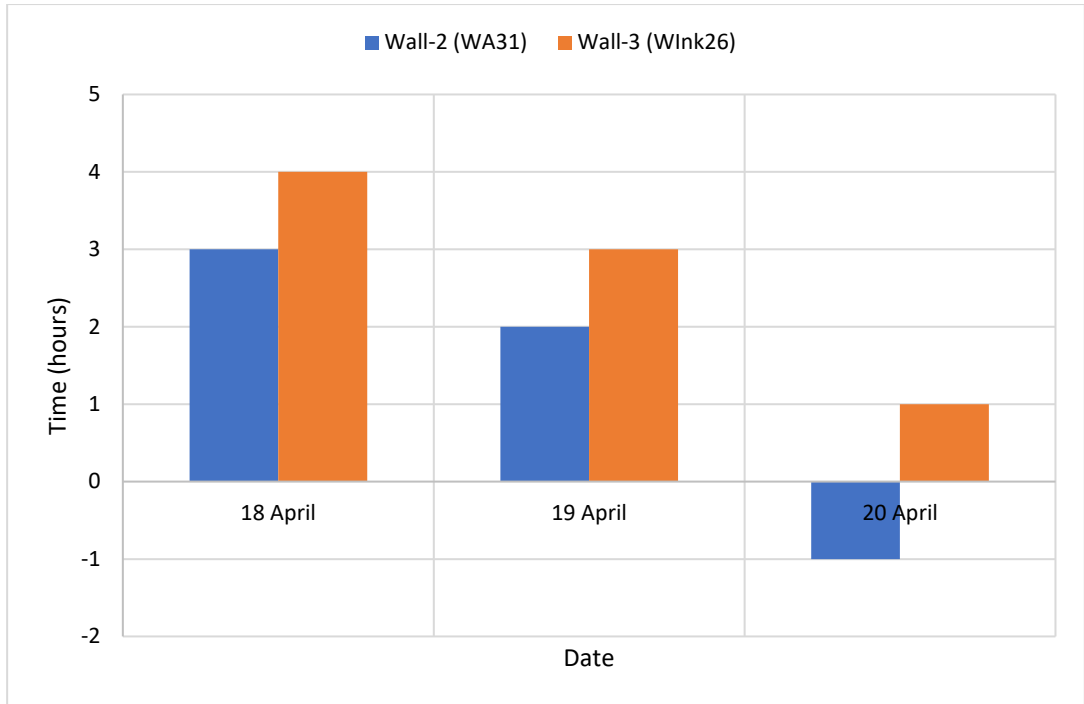


Figure 4-14 Time lags of Wall-2 (WA31) and Wall-3 (WInk26)

Figure 4-15 shows the wall decrement factor for Wall-2 (WA31) and Wall-3 (WInk26) over a three-day experiment. This factor is essential in mitigating the impact of external temperatures on the interior of an earthbag building. Wall-2 (WA31) and Wall-3 (WInk26) have decrement factors of 0.94, 0.96 and 0.95, and 0.89, 0.88 and 0.90, respectively, on the experiment's first, second, and third days. The lowest decrement factor for Wall-3 (WInk26) on all three days indicates a better thermal performance.

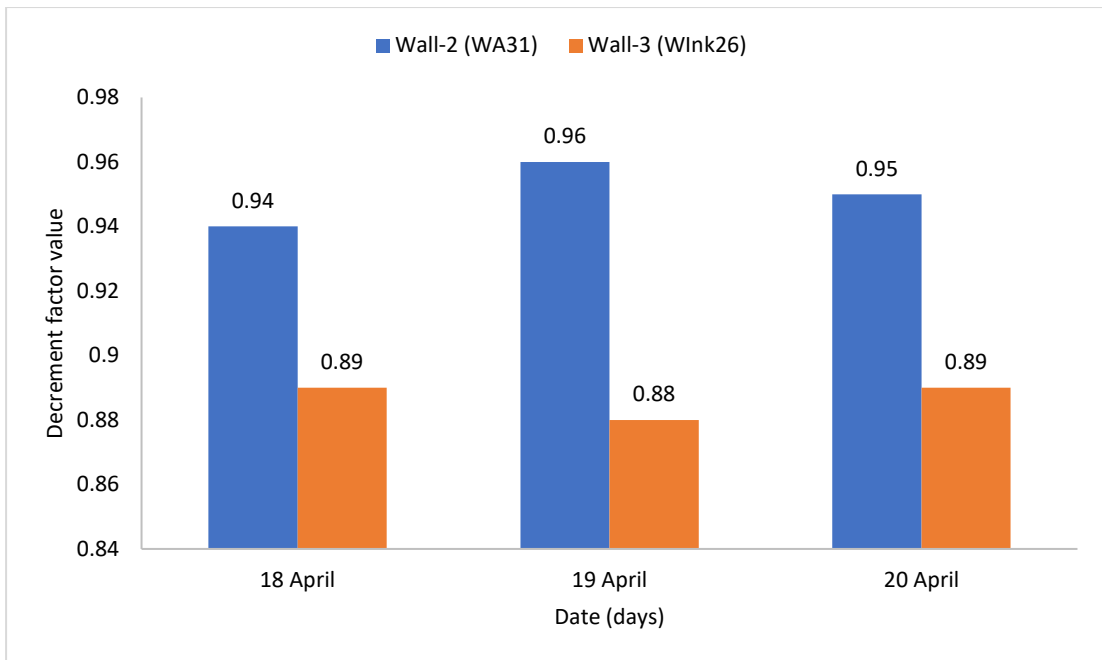


Figure 4-15 Decrement factor of Wall-2 (WA31) and Wall-3 (WInk26)

4.3.4 Heat flux

The heat flux at the inner surface of the earthbag wall is monitored to compare its thermal performance with and without PCM under the same outdoor climate conditions. [Figure 4-16](#) shows that the inner heat fluxes of Wall-3 (WInk26), Wall-2 (WA31), and Wall-1 (baseline) are increasing during sunrise and peaking at different levels. Wall-1 (baseline) reaches its peak surface heat flux at 18:00, Wall-2 (WA31) at 22:00, and Wall-3 (WInk26) at 23:00 during the first day of the experiment. The second and third days of the experiment show a similar pattern with the walls with PCMs, delaying the heat transfer to the inner surface by four hours for Wall-2 (WA31) and five hours for Wall-3 (WInk26), respectively, compared to the Wall-1 (baseline). The maximum heat flux value for the Wall-1 (baseline) is 29.89 W/m^2 , 18.21 W/m^2 for the Wall-2 (WA31), and 10.22 W/m^2 for Wall-3 (WInk26). According to [Table 4-3](#), all walls with PCM have a higher percentage of heat flux reduction than Wall-1 (baseline) with Wall-3 (WInk26) showing the best performance at 63.76% compared to Wall-2 (WA31) at 39.34%. Thus, the average heat flux reduction substantially depends on the PCM type while Inertek26 appears to be the best choice within the thermal comfort range of the region of the experiment.

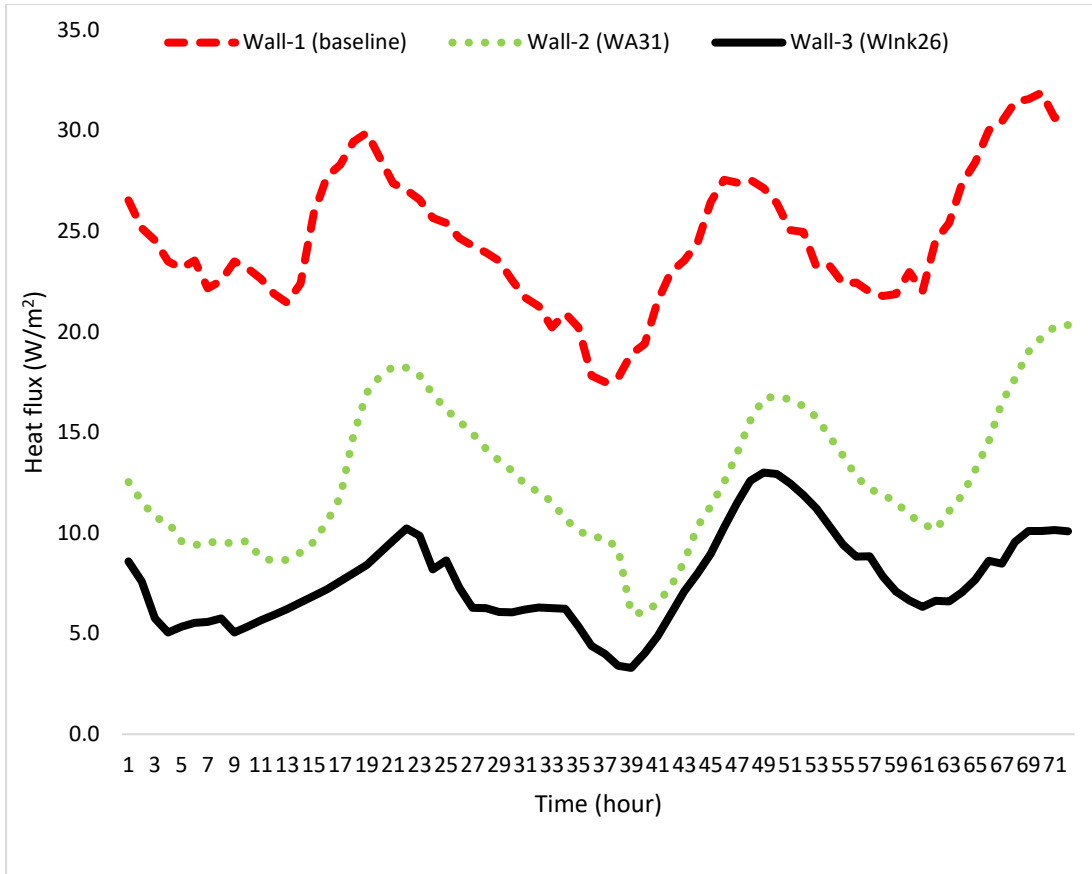


Figure 4-16 Heat flux in the Wall-1 (baseline), Wall-2 (WA31) and Wall-3 (Wink26)

Table 4-3 Average heat flux reduction between reference, WA31, and Wink26 earthbag walls

Date	Wall-1 (baseline) W/m^2	Wall-2 (WA31) W/m^2	Wall-3 (Wink26) W/m^2	% Reduction WA31	% Wink26	Reduction
04/18	29.89	18.27	10.22	40.22	68.09	
04/19	27.55	16.64	13.01	41.09	54.76	
04/20	31.56	20.34	10.65	36.71	68.42	
			% Average	39.34	63.76	

4.3.5 Reduction in heat gain

A reduction in heat gain of the wall integrated with PCM can help to reduce the amount of heat transfer into the building, thus reducing the energy required for cooling or heating of a space. The heat transfer rate of an earthbag wall with and without PCM is depicted in [Figure 4-17](#). The results show that Wall-3 (Wink26) performs the best in terms of heat transfer in comparison to Wall-2 (WA31). This

outcome aligns with many studies such as the one conducted by Saxena et al., 2020 [238] found that PCM integration into buildings had positive effects. Furthermore, due to the larger volume of the microencapsulated PCM, the heat transfer rate from the outer surface to the inner wall surface is lower for Wall-3 (WInk26) than for Wall-2 (WA31). The quantity of heat transfers from the outer surface to the inner surface of Wall-1 (baseline) are 327.33 Wh/m^2 , 156.96 Wh/m^2 , and 196.91 Wh/m^2 associated with the experiment's first, second and third days, respectively. These values are higher than that of Wall-2 (WA31) (81.39 Wh/m^2 , 78.08 Wh/m^2 , and 84.27 Wh/m^2) and Wall-3 (WInk26) (58.96 Wh/m^2 , 49.65 Wh/m^2 , and 38.89 Wh/m^2). The reductions in the heat transfer for Wall-2 (WA31) are 245.94 Wh/m^2 , 78.89 Wh/m^2 , and 73.75 Wh/m^2 and for Wall-3 (WInk26) are 268.37 Wh/m^2 , 107.32 Wh/m^2 , and 112.64 Wh/m^2 , for the first, second and third days, respectively. The percentage reductions in the heat gain for Wall-2 (WA31) are 75.1%, 82.0%, 50.3%, and for Wall-3 (WInk26) are 68.4%, 37.5% and 57.2% associated to the first, second and third days, respectively. It is evident that Wall-3 (WInk26) shows a better performance than Wall-2 (WA31) and Wall-1 (baseline); these findings are consistent with the previous studies when PCM is incorporated into blocks (e.g., [238], [295], [212]).

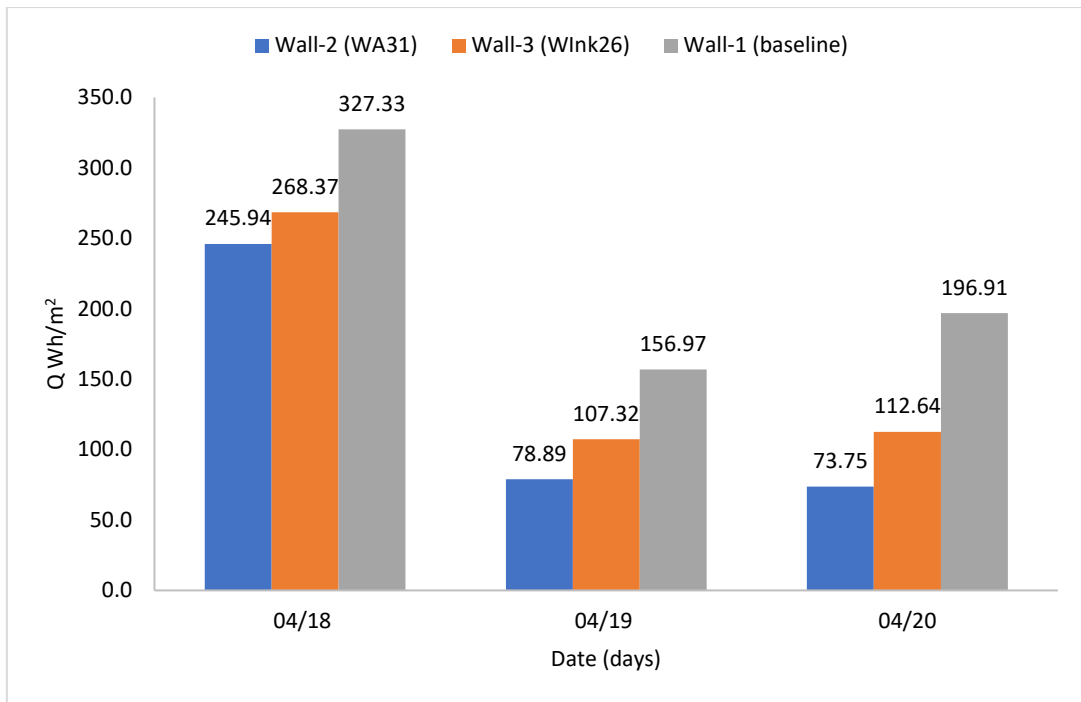


Figure 4-17 Heat transfer reduction comparison between the Wall-1 (baseline), Wall-2 (WA31) and Wall-3 (WInk26)

4.4 Validation of numerical model

The experimental and the EnergyPlus simulation results are compared to validate the PCM-E wall generated model. The assessment of the earthbag wall is based on the reduction of the inner surface wall. After using the validation metrics introduced in [Section 4.3.5](#), the validation results are quite accurate as shown in [Figure 4-18](#). The temperatures measured both experimentally and numerically show a similar pattern and correspond well for all the case studies. The temperature profiles of Wall-1 (baseline), Wall-2 (WA31), and Wall-3 (WInk26) (see [Figure 4-18](#)) in the modelling results are relatively coherent, but there are few experimental measurement fluctuations, which could be due to material, experiment, or human error during the experiment setup. Wall-2 (WA31) has composite PCM that may cause temperature fluctuations due to uneven distribution and differences in its thermal conductivity. On the other hand, Wall-3 (WInk26) uses micro-encapsulated PCM that result in a more uniform distribution and less temperature fluctuation while it also prevents PCM leakage, which can occur with composite materials. The differences in average temperature between the inner wall surface temperature with and without PCM for

the experiment conducted are found to be about 1.90°C and 2.40°C for WA31 and WInk26, respectively, which are fairly close to what are found from the simulation results. The validation and absolute mean error analysis show that the numerical solutions for all three walls are highly accurate and successful as the mean errors are well within the success criterion of less than 10% as presented in [Table 4-4](#). All the maximum temperature differences are also less than 2°C. The Fractional bias (FB), FAC2, NMSE, and r presented in [Table 4-5](#) reveal acceptable ranges of metrics related to the simulation and experimental results when PCM is integrated into the earthbag building. It can be stated that the criteria for both the inner and outer surface temperature of Wall-1 (baseline), Wall-2 (WA31), and Wall-3 (WInk26) are met. The NMSE and FB are nearly 0 in all instances while R ranges from 0.9 to 0.98 for both the inner and outer surface temperature across all cases. Furthermore, the values of FAC2 are all greater than 0.5, but less than 2, indicating a good agreement between the experimental study and numerical models. Overall, it can be concluded that the model tested with Wall-3 (WInk26) performed better than all other case studies. In general, the validation of the results is successful under both earthbag building with and without PCM. The numerical solutions can, therefore, be relied upon for further analysis and simulations. Consequently, it can be assumed that the PCM-E wall model developed in this research could be utilised to predict the thermal comfort of future earthbag buildings in different regions.

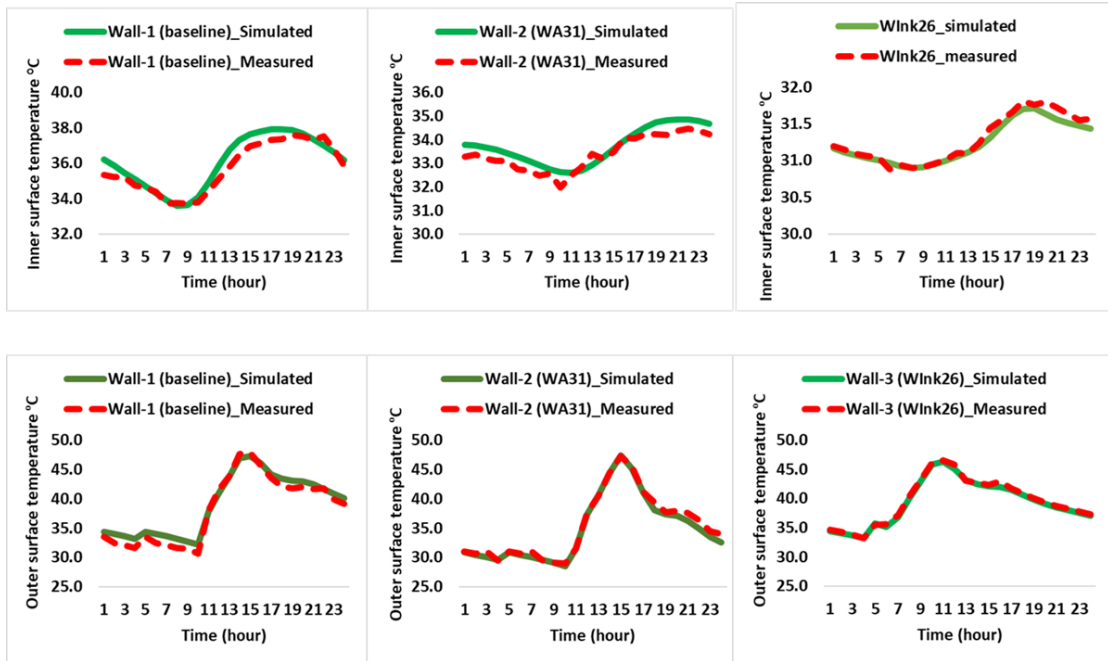


Figure 4-18 Temperature profile of Wall-1 (baseline), Wall-2 (WA31) and Wall-3 (WInk26)

Table 4-4 Discrepancies between numerical and experimental results

Wall	Maximum Inner temp difference (°C)	Maximum outer temp difference (°C)	Inner surface temp Mean Error (%)	Outer surface temp Mean Error (%)
Wall-1 (baseline)	1.0	1.6	0.9	2.3
Wall-2 (WA31)	0.6	1.5	0.7	1.4
Wall-3 (WInk26)	0.1	0.3	0.2	0.7

Table 4-5 Validation metrics

Surface temperature	Fractional bias (FB)	NMSE	r	FAC2
Inner Wall-2 (WA31)	0.0005	0.0011	0.9540	0.9850
Inner Wall-3 (WInk26)	0.0001	0.0001	0.9803	1.4001
Inner Wall-1 (baseline)	0.0030	0.0061	0.9500	0.9404
Outer Wall-2 (WA31)	0.0009	0.0041	0.9000	0.9100
Outer Wall-3 (WInk26)	0.0003	0.0003	0.9670	1.1100
Outer Wall-1 (baseline)	0.0070	0.0081	0.9211	0.9286

4.5 Parametric analysis

The objective of the parametric analysis is to identify the most effective passive design strategies by first determining the optimum PCM transition temperature and then used the optimum PCT to determine optimum combination of PCMs and insulation layers as illustrated in [Figure 4-19](#).

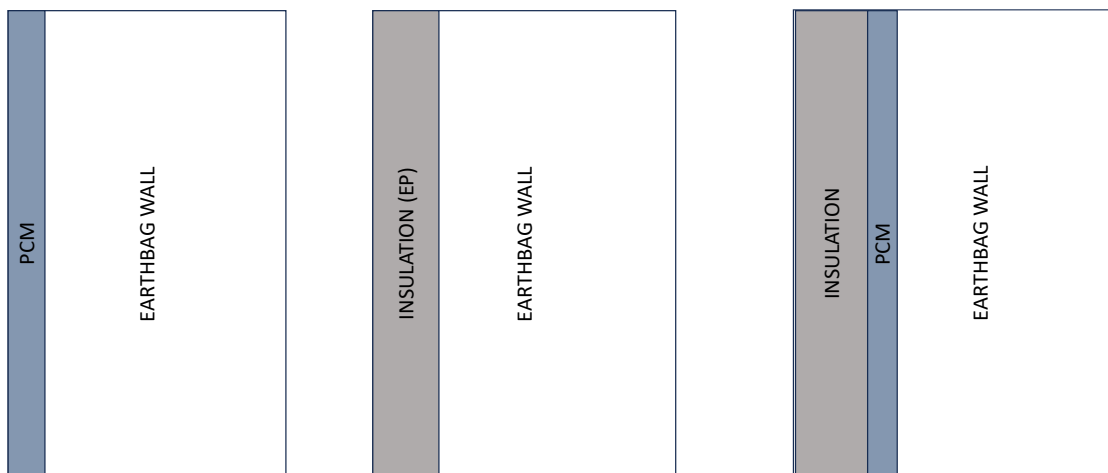


Figure 4-19 Various configurations for parametric analysis

4.5.1 The effect of PCM transition temperature

The transition temperature of the PCM is crucial for determining how much it undergoes a phase change, which affects the thermal performance of walls with PCM. The PCM will not change phase and store thermal energy if the transition temperature is too low or too high. This section introduces various PCMs as layers in an earthbag wall to evaluate the impact of PCM transition temperature. [Figure 4-20](#) shows the inner surface temperature of the earthbag building for different PCMs. The graph shows a significant surface temperature reduction for both PCMs in [Table 4-6](#) compared to the baseline building without PCM. However, the PCM with high transition temperature (PCMA31) has the best temperature reduction, possibly due to outdoor temperature fluctuations. The outdoor temperature can be well below the PCM transition temperature, even during summer nights. PCMA31 acts as an insulation material, preventing outside heat from entering the indoor space of the earthbag. It also stores heat as latent heat and releases it to the indoor space when the outside temperature drops. This can be seen in [Figure 4-20](#) for days 1, 2, and 3 for

PCMA31. For example, on April 19th (day 2), the outside temperature rises from 8:00 am to 5:00 pm (10 hours). The earthbag wall receives excess heat energy, which passes from the outside wall to the inner surface of the earthbag as conductive heat. The earthbag with PCMA31 accumulates this heat as latent heat, which delays the peak of the inner surface temperature. The temperature starts rising at 11:00 am on April 19th and reaches its peak at 1:00 am on April 20th, compared to the earthbag without PCM, which peaks at 9:00 pm. The other PCMs (A28, Inertek26, and Inertek23) also reduce the surface temperature compared to the baseline, but they are above their PCM transition temperature for all days. This makes them release the stored energy quickly and pass it to the indoor space of the earthbag building. Therefore, these PCMs do not work well as PCM. PCMA31 is selected as the optimum PCM for the earthbag building model in Kano state and other locations with similar climatic conditions.

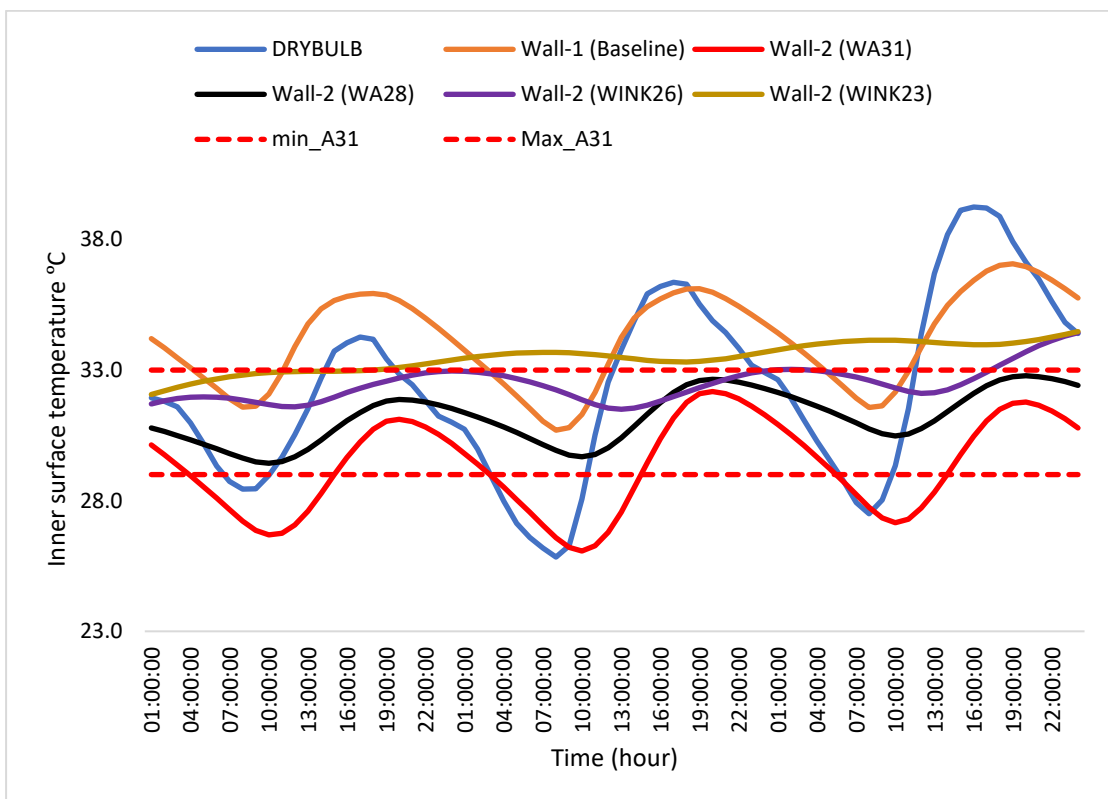


Figure 4-20 Inner surface temperature for PCM A31, A28, Inertek26, and Inertek23

Table 4-6 Inner surface temperature reduction of PCM A31, A28, Inertek26, and Inertek23

DAYS	A31 TEMP°C	A28 TEMP°C	INERTEK26 TEMP°C	INERTEK23 TEMP°C
18TH APRIL	4.8	4.0	3.1	2.3
19TH APRIL	4.0	4.4	3.2	2.0
20TH APRIL	5.3	4.3	3.7	2.5

4.5.2 Comparison between wall with pure PCM, PCM composite and expanded perlite insulation

The first step investigated the possibilities of increasing the thermal inertia of the earthbag wall by using one of the three passive techniques of adding PCM, insulation, or PCM/insulation. [Figure 4-21](#) shows the variation of the inner surface temperature for the studied configurations. Thus, it can be noted that integrating two passive PCM and insulation measures in the same configuration reduces the temperature fluctuations of the indoor surfaces compared to the traditional earthbag. When both PCM and expanded perlite insulation measures are employed in the same configuration, the performance is better than the other configurations, followed by PCM and insulation configurations. The inner peak temperature was reduced by about 2.2 °C, 3.0°C and 3.5 °C when the PCM, insulation, and PCM/insulation was used as passive techniques. The indoor heat flux shows a similar trend to the change in the inner surface temperature. [Figure 4-22](#) shows the percentage reduction in heat flux. It can be noted that the maximum heat flux reduction for the different configurations is 53 % for PCM/insulation configuration, while PCM and insulation have values of 49 % and 42%, respectively. Integrating two measurements simultaneously in the same configuration can decrease the amplitude of the thermal wave and increase the time lag. The aspect shift induced by PCM, insulation, and PCM/insulation is approximately 3.0 h, 2.5 h, and 4.0 h, respectively. The results demonstrate that the integration of PCM and insulation in the same configuration has a significant impact on the dynamic thermal behaviour of the earthbag wall. In conclusion, the PCM and insulation

mounted on the earthbag wall is the most appropriate configuration that prospects the best thermal performance of the earthbag wall subjected to the external climatic conditions of the Nigeria region.

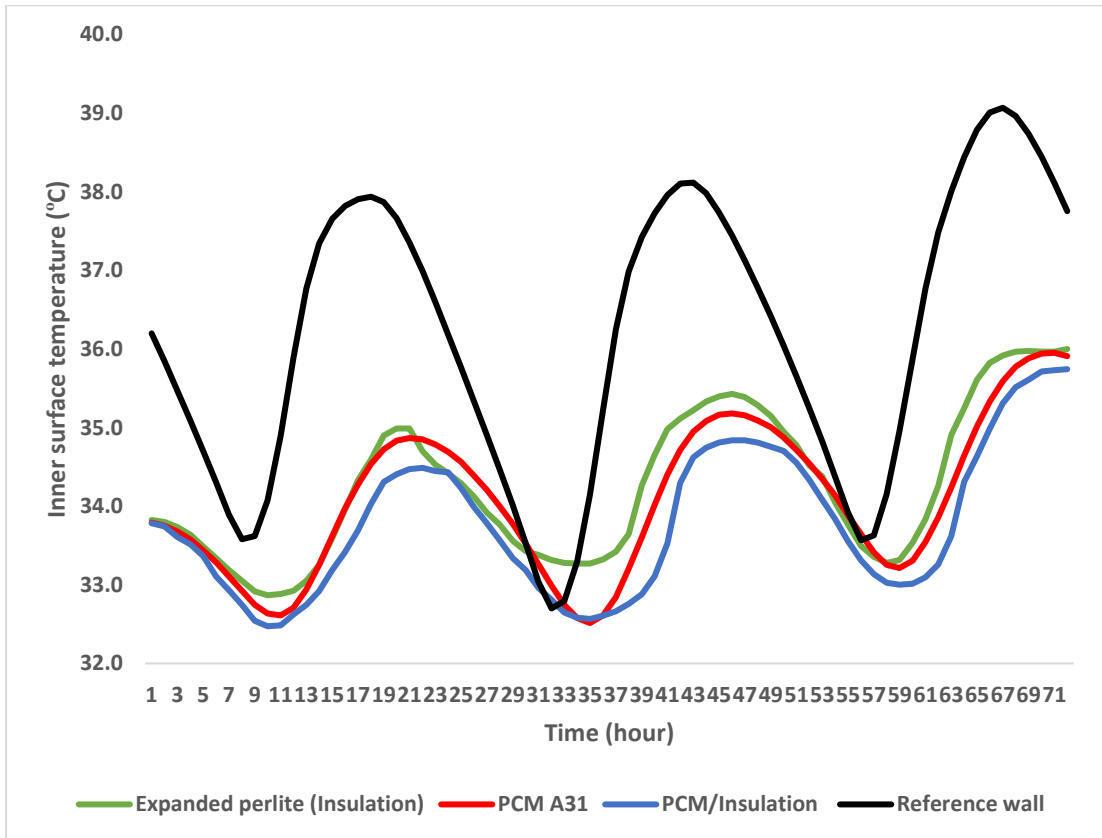


Figure 4-21 Comparison between wall with pure PCM, PCM composite and expanded perlite insulation

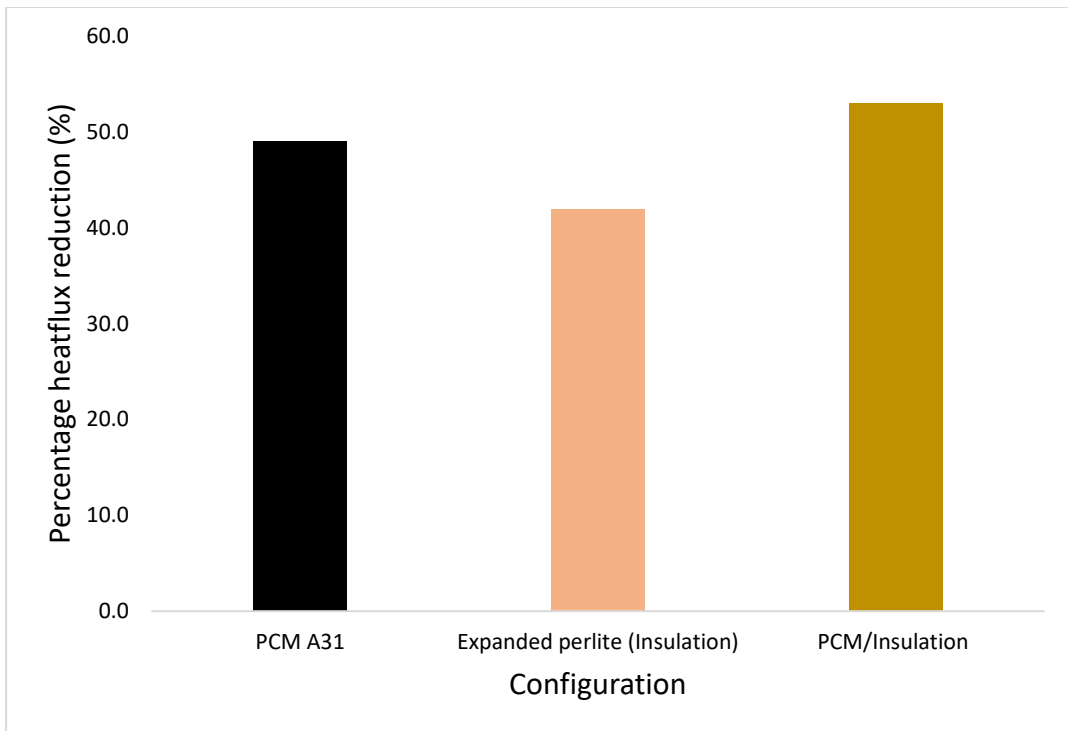


Figure 4-22 Percentage heat flux reduction

4.5.3 Effect of optimum PCM/insulation thickness on earthbag wall surface temperature

As outlined in Section 4.5.2, the most effective pairing is PCM/Insulation. This section examines various combinations of PCM and insulation thickness. Specifically, the following combinations were evaluated: T1 (1cm PCM layer with 2cm insulation), T2 (2cm PCM with 4cm insulation), T3 (3cm PCM with 6cm insulation), and T4 (4cm PCM with 8cm insulation). [Figure 4-23](#) shows the inner surface temperature of an earthbag wall with and without (PCM)/insulation over three days. The reference wall without PCM/insulation shows the highest inner surface temperature, while walls T1-T4 with varying PCM/insulation thicknesses show lower temperatures. The wall with 4cm PCM + 8cm insulation (T4) consistently had the lowest inner surface temperature compared to the other combinations of PCM/insulation. On day 1, 2, and 3, the temperature reduction of T4 compared to the reference wall was 6.9°C, 6.1°C, and 7.0°C respectively. This demonstrates that increasing the thickness of both the PCM layer and insulation layer leads to greater reduction in inner surface temperature. The temperature profile of T4 also showed good charging and discharging cycles over the

three days. The PCM was able to effectively store thermal energy during the day when temperature spiked and release the energy at night when temperature dropped. This is evidenced by the flattened peaks and troughs in T4's temperature profile. The addition of insulation in T4 helped maintain the thermal storage capacity of the PCM by reducing heat transfer to the indoor environment. The insulation layer was able to keep the PCM at a higher temperature during the discharge cycle at night. This allowed the PCM to fully solidify and be ready for the next charge cycle during the day. The time lag of the temperature peak for T4 compared to the reference wall was approximately 5-6 hours over the three days. This demonstrates the thermal mass effect of the PCM/insulation combination in delaying and reducing the peak indoor temperature. In summary, increasing the thickness of both PCM and insulation led to lower inner surface temperatures, larger temperature reductions, effective charging and discharging of the PCM, and time lag in the temperature profile. The PCM/insulation combination in T4 performed the best due to greater thermal mass and reduced heat transfer. These results demonstrate the energy-saving potential of using adequate thicknesses of PCM and insulation in earthbag buildings.

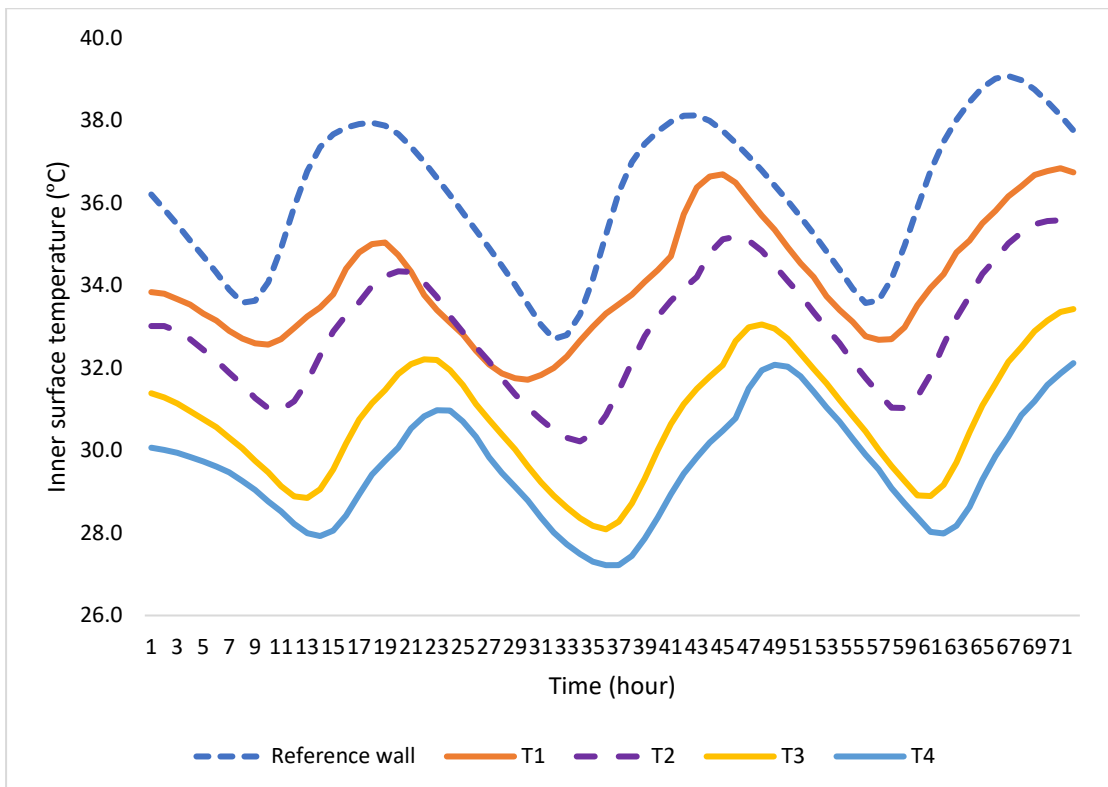


Figure 4-23 Effect of optimum PCM/insulation thickness on earthbag wall surface temperature

4.6 Summary

The main results of this chapter are as follows:

- The thermal conductivity of the earthbag wall was lowest with microencapsulated PCM (Inertek26) compared to PCM composite (A31) and baseline wall without PCM. The microencapsulated PCM was more uniformly distributed and had better thermal performance.
- Earthbag walls with PCM (both A31 and Inertek26) showed lower and more stable inner surface temperatures compared to the baseline wall. The maximum temperature reduction was 2.4°C with Inertek26 PCM.
- Earthbag walls with PCM had increased time lags of 3-4 hours compared to the baseline wall. This delayed the time to reach peak inner surface temperature.
- The decrement factor was lowest for the Inertek26 PCM wall, indicating it had the best thermal damping performance.
- Heat flux through the wall was reduced by 39-64% with the addition of PCM. The microencapsulated Inertek26 PCM showed greater heat flux reduction.
- The heat gain of the wall was reduced by 50-82% by integrating PCM, with the microencapsulated PCM again performing better.
- Validation metrics showed strong agreement between experimental data and simulation results for the PCM-integrated earthbag wall models.
- Parametric analysis showed PCMA31 (higher transition temperature PCM) gave maximum inner surface temperature reduction of 4.8-5.3°C.
- Using both PCM and insulation together reduced inner surface temperature and heat flux more than using either alone.

Increasing PCM and insulation layer thickness further improved performance, with 4cm PCM + 8cm insulation giving best results.

Chapter 5. Numerical Simulation of PCM-Integrated Earthbag Wall in Temporary Housing

In this chapter, a case study of a temporary housing located in Maiduguri, Nigeria, is selected to investigate the performance of PCM-E wall on the thermal comfort performance of temporary housing. The first step is to develop a 3D model using SketchUp modelling software. The developed model is then transferred to the EnergyPlus simulation program for conducting simulations using different configurations of optimum PCM-E wall found in [chapter 4](#). The optimum configuration was selected for each case.

5.1 Determination of thermal performance of PCM-integrated earthbag walls in temporary housing

This section outlined the approach taken to determine the thermal performance of PCM-E wall in temporary housing, specifically in the Nigerian climate. The study aimed to incorporate the optimum PCM-E wall found in [Section 4.5.3](#), into selected IDP house in Nigeria to enhance the thermal performance of the temporary housing. To achieve this, energy, and thermal load simulation engine, such as EnergyPlus, is used to carry out the performance analysis. The study involved a parametric analysis on the impact of PCM-E wall orientation on the performance of PCM-E walls on building envelopes to determine optimal conditions. Various directions were considered for the integration of the wall.

The first step in the methodology involved modelling the geometry of the selected IDP houses in Sketchup ([Figure 5-3](#)). The 3D model from Sketchup was then taken to EnergyPlus engine for the parametric analysis. The analysis was carried out for a summer simulation to account for variations in weather and other external factors. The summer season in Kano state lasted for 2.3 months from March 17 to May 26. Therefore, the analysis was carried out from 1st March to 30th May.

5.1.1 Thermal comfort analysis

PCM can be integrated into earthbag wall construction to improve the thermal performance and indoor comfort of temporary houses. PCMs absorb and release heat as they melt and solidify at a specific temperature, providing thermal mass and damping effects. Several studies have analysed different indicators to evaluate the effectiveness of PCMs in buildings [294], [296], [224], [297] including surface temperature reduction as PCMs can reduce the interior surface temperature of walls by absorbing heat during the daytime and releasing it at night when indoor temperatures drop which flattens out daily temperature swings; peak indoor temperature reduction as by storing excess heat during the hottest parts of the day, PCMs can reduce the maximum indoor air temperature reached which is important for occupant comfort; percentage of hourly comfort increase as the percentage of hours during which indoor temperatures remain within the comfort range (determined to be 23-32°C for Kano state, Nigeria [258]) can be increased with PCMs, time lag as PCMs can delay the time it takes for heat to be transmitted through the wall which is a measure of the thermal damping effect; decrement factor as this evaluates how much PCMs can dampen the amplitude of temperature fluctuations as heat moves through the wall with a higher factor meaning more damping; and heat transfer reduction rate as PCMs can reduce the rate of heat transfer through the wall by absorbing excess heat which also decreases temperature swings. Therefore, PCMs can improve indoor thermal comfort in earthbag buildings by increasing time lag, reducing temperature extremes, and keeping temperatures within comfortable ranges more often with several metrics quantitatively evaluating these benefits. Moreover, For Kano state, the adaptive thermal comfort temperature range is 23.1 - 31.8°C based on the monthly outdoor air temperatures and using the CBE Thermal Comfort Tool adaptive comfort model. The optimal comfort temperature is around 25°C. PCMs can help maintain indoor operative temperatures within this adaptive thermal comfort range more often by reducing temperature extremes and fluctuations. The percentage of time indoor conditions are within the comfort zone is a key metric for evaluating PCM thermal performance. This criterion was used in accessing the thermal performance of earthbag building.

5.2 Description of the case study

5.2.1 Numerical modelling and Methodology

A single-zone numerical model was developed in EnergyPlus representing a detached temporary shelter structure [Figure 5-1](#). The model geometry was defined based on guidelines from the UN Refugee Agency specifying recommended floor areas between 20-40 m² for temporary shelters. A 4m x 4m x 3.5m (length x width x height) geometry was selected within this range for the model.



Figure 5-1 A tent constructed for IDP shelter in Maiduguri (selected case study)

The building was oriented with the long facade facing east, the entrance doorway on the north facade, and windows on the north and south facades. This orientation maximizes passive solar gains through the south facade in the winter. The roof had a 15-degree slope with overhangs sized according to best practices for the climate. The structural system was modelled as a typical earthbag construction with stabilized earth-filled bags stacked in a running bond pattern. The thermal properties of the earthbag walls including density, specific heat, and thermal conductivity were defined based on data from experimental testing of earthbags found and are tabulated in [Table 5-1](#).

The wall assembly consisted of earthbag layers, insulation layer (expanded perlite), and PCM layer. The roof was constructed of corrugated metal decking with fiberglass insulation. The floor was modelled as a concrete slab-on-grade with a thin covering. Details on the materials, layers, and thermal properties of all envelope components can be found in [Table 5-1](#). The windows were modelled as single wooden window with a wood frame, and the door as a solid wood slab. All thermal properties were selected from the EnergyPlus database and literature. The space was first modelled with no ventilation and building energy simulations are carried out in free floating temperature conditions, no ventilation, 0.5 air changes per hour (ACH) due to air infiltrations and later was simulated as naturally ventilated with an air change rate of 4 ACH during the outdoor temperature is below the melting temperature of the PCM used which below 29 until 7am. This ventilation rate was selected to represent operation of operable windows on the north, south, and east facades by occupants. During unoccupied hours from 6pm to 8am, an infiltration rate of 0.5 ACH was set to model air leakage through cracks and small openings in the envelope. The internal heat gains were set to 0 W/m² because no occupancy was designed in this model.

The EnergyPlus model shown in [Figure 5-3](#) was simulated with a 3-minute time step for a full year period to adequately capture annual performance. Weather data was imported from a standard EnergyPlus weather (EPW) file for the closest available weather station location to the site. All heat transfer through the building envelope was modelled using the conduction finite difference (CondFD) solution algorithm. Radiant exchange between indoor surfaces was activated to capture realistic radiant effects.

The PCM was modelled by defining a new material in EnergyPlus with the melt temperature, enthalpy, and thermal properties based on experimental PCM data from literature. The PCM and expanded perlite layer was then incorporated into the wall assembly of the earthbag walls. Different configurations of the PCM-enhanced earthbag wall (PCM-E wall) were simulated by modifying the wall assemblies. The model was simulated in multiple configurations as shown in [Figure 5-2](#).

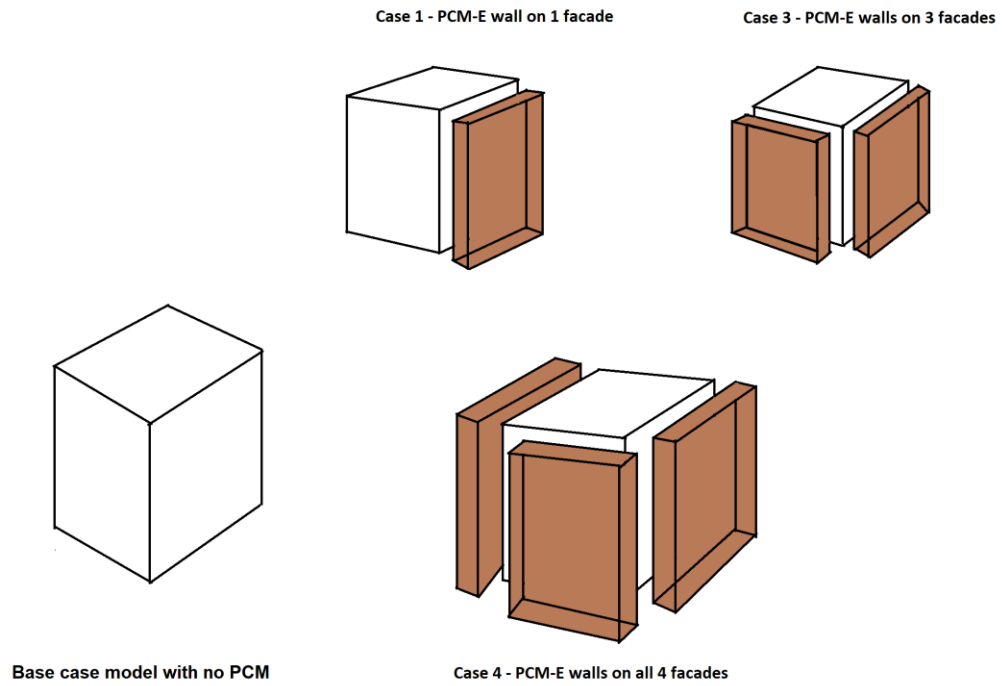


Figure 5-2 PCM-E wall arrangement on earthbag building model

Detailed results were generated including zone temperature, surface heat transfer, PCM heat absorption/release, and thermal comfort metrics. The data was analysed to evaluate the performance of each case compared to the base model and determine the effectiveness of the PCM-E walls.

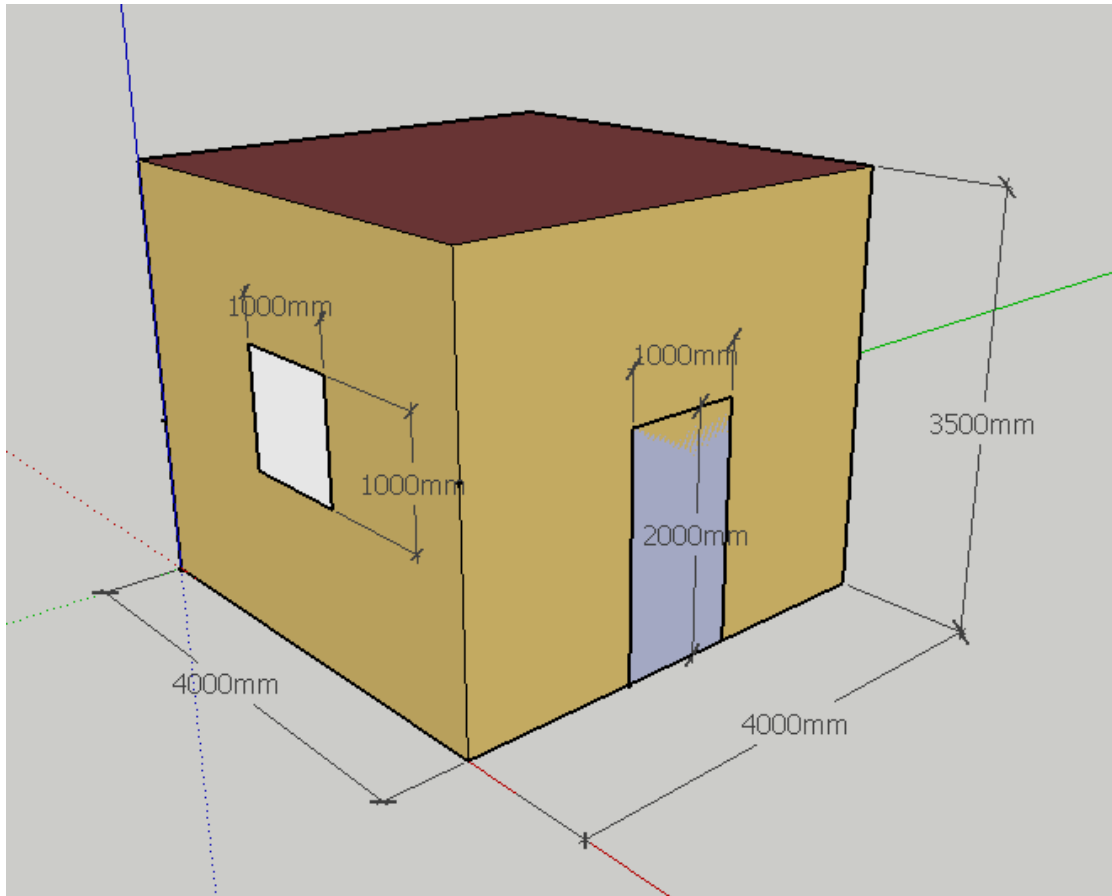


Figure 5-3 Sketchup 3D Earthbag Building Model

Table 5-1 Input parameters for earthbag model geometry

System	Thickness (m)	Conductivity (W/m. K)	Density (kg/m ³)	Specific heat (J/kg. K)	U factor	Glass SHGC
Earthbag wall	0.25	1.83	2190	1000		
Door (wooden door)	0.03	0.14	450	1700		
Cement sand floor	0.07	1.15	1900	950		
Clay tiles	0.1327	0.8	1700	850		
Earth clay	0.07	1.28	1460	880		
Roofing	0.025	1.0	2000	800		
Ceiling joist	0.28	0.14	1500	2300		
Ceiling board	0.0125	0.08	1136	1571		
Window (simple glazing)	0.06				2.7	0.862

5.3 Result

5.3.1 Inner surface temperature reduction

This study examined the thermal performance of PCM-E walls placed in different directions of temporary housing in the hot climate region of Nigeria. The effect of the wall direction was evaluated from April 18 to 20, using various three distinct configurations (case 1, case 2 and case 3) of PCM-E walls to identify the optimal setup for further analysis. [Figure 5-4](#) illustrates the impact of integrating the PCMs on the inner surface temperature of the temporary housing. The results show that, in all cases (case 1, case 2 and case 3), the PCM-E wall reduces the inner surface temperature, with some cases showing a delay in the time of the peak temperature. For example, when the PCM-E wall is placed on the east-facing (case 1) side, the temperature reduction is higher than that in the base case and all other configurations. This was because the wall in this direction received excess solar radiation in the morning, allowing the PCM to melt completely. At night, when the outdoor temperature is low, the wall cools down, causing the PCM to solidify and release stored heat.

According to Ali (2001) [289], buildings in Kano receive the most sunshine hours on their southern facades, followed by their western and eastern facades. Spaces within a building can be positioned based on their function and time of use. Frequently used spaces should be located in the northern part of a building, whereas those used at night can be placed on the coolest side of the building. In this study, the PCM-E wall on the east direction shows a 3.0°C, 3.3°C, and 2.8°C reduction in peak inner surface temperature, respectively, and a 5 h, 5 h, and 3 h time lag compared to the base case without PCM for the first, second, and third day of the simulation analysis. For case 2, the EN-wall shows a higher temperature reduction, with a peak inner surface temperature reduction of 2.3°C, 2.6°C, and 1.8°C, and a time lag of 4 h, 3 h, and 2 h, respectively. For case 3, the ENW-wall is the optimal configuration, with a peak inner surface temperature reduction of 3.6°C, 3.1°C, and 3.1°C, and a time lag of 4 hours for all three days. It can be concluded that the E-, EW-wall-, and ENW-wall configurations exhibit the best peak temperature reductions and time lags.

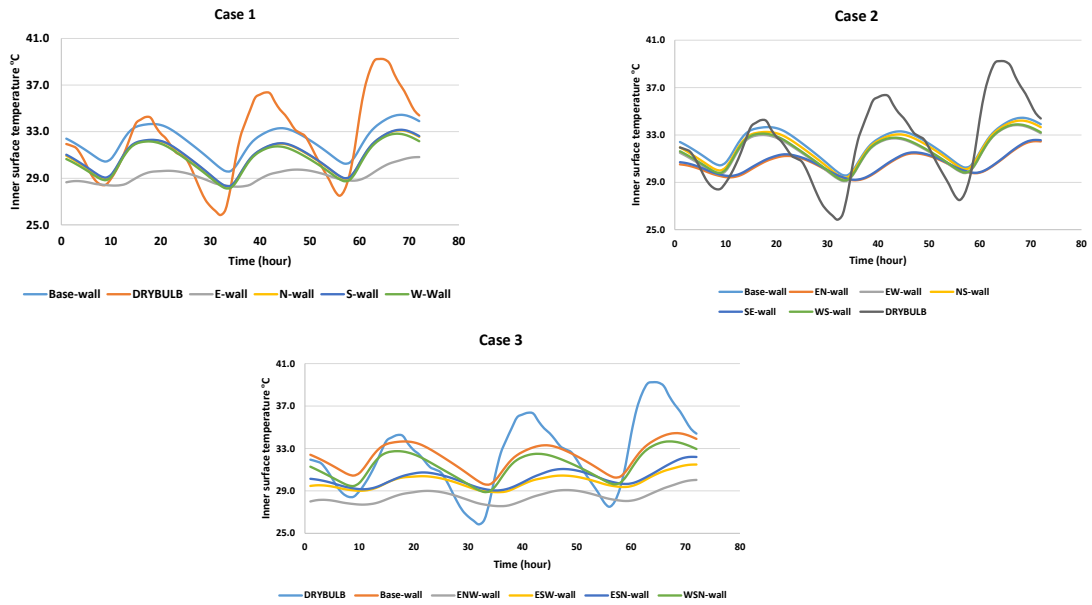


Figure 5-4 Inner surface temperature profile

5.3.2 Effect of night ventilation on Inner surface temperature reduction

The inner surface temperature plot in [Figure 5-5 \(a\)](#) provides insights into the thermal performance of the earthbag wall models with and without night ventilation from April 18th to 20th. Without any ventilation (0 ACH), the base earthbag wall is subject to significant temperature swings, directly correlating with the external temperature profile. The peak daytime temperature reaches almost 38°C, indicating substantial heat gain through the wall. The addition of PCM-E provides some thermal mass benefits, slightly reducing the average and peak indoor temperatures. However, the PCMs are only able to discharge heat for around 14 hours overnight when temperatures drop below 29°C. Introducing night ventilation at 5 ACH [Figure 5-5 \(b\)](#) prevents the inner wall temperature from exceeding 29°C. By flushing out stored heat, the PCMs can now maintain temperatures below their melting point for an additional 2 hours daily, from 14 to 16 hours. This expanded discharging capacity is key, as it allows the PCMs to solidify and be ready to absorb daytime heat gains. Comparing the optimal E-wall to the base wall, night ventilation delivers considerable temperature reduction. The average inner wall temperature decreased by 3.8°C with ventilation versus 3.0°C without. Peak temperatures were also substantially lower for

the ventilated wall. As the baseline comfort threshold is between 23°C - 32°C, these results demonstrate that night ventilation eliminates the need for air conditioning during the 3-day period. The benefits of night ventilation were consistent across all wall variations - W-wall, S-wall, and N-wall. Opening windows when outdoor temperatures drop sufficiently below the PCM melting point enhances the charging and discharging capacity. This in turn attenuates peak indoor temperatures. Overall, the data highlights the importance of night ventilation for improving PCM functionality and thermal comfort in earthbag structures. Further testing could examine the effects over longer time periods and optimize ventilation rates.

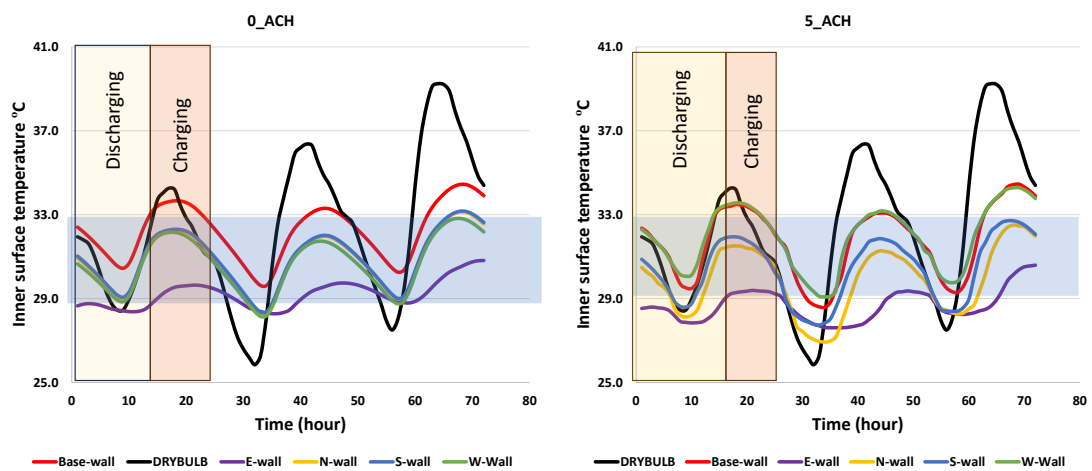


Figure 5-5 Earthbag wall Inner surface temperature (a) without ventilation (0ACH) (b) with Ventilation (5ACH)

5.3.3 Heat flux through the walls

Figure 5-6 depicts the hourly inner-surface heat flux for various PCM-E walls in temporary housing over a three-day simulation. The graph indicates that the heat flux is lower for walls with PCM during the daytime for all selected orientations, owing to the storage of heat energy. This finding aligns with those reported by Sun et al. (2019) [298]. For the east wall, the heat flux reduction is found to be 57.0 W/m², 42.6 W/m², and 44.4 W/m² on the first, second, and third days of the simulation, respectively. The flux reduction for the NE-wall orientation is found to be 51.8 W/m², 40.8 W/m², and 41.2 W/m² on the first, second, and third day, respectively. The flux reduction for the

NEW-wall orientation on the first, second, and third day is found to be 42.3 W/m^2 , 30.7 W/m^2 , and 33.9 W/m^2 , respectively.

The east wall orientation showed the highest flux reduction because it received an optimal amount of radiation. According to Ali (2001) [289], the southern part of a building in Kano receives the highest solar radiation, followed by the eastern and western parts, whereas the northern part receives the lowest. Therefore, using PCM in the southern part of a building in Kano can cause the PCM to completely liquefy and remain in liquid form for too long, rendering it ineffective for charging and discharging cycles.

It can be concluded that the best position to use the PCM-E wall in temporary housing in Kano is to place it in the eastern part of the building. This result is consistent with the findings of Sun et al. (2019) [298] and Li et al., 2021 [299] in a climate similar to that of Kano. As previously mentioned, the east wall showed the second highest flux reduction and delays in heat penetration, which could increase human comfort.

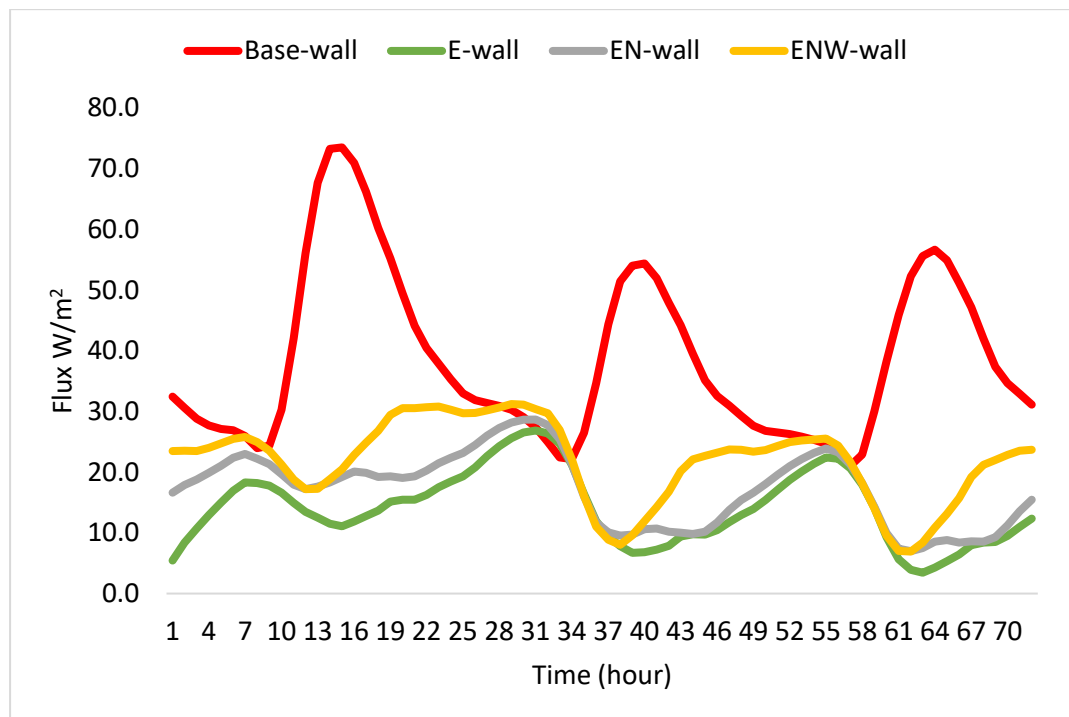


Figure 5-6 Heat flux densities through the walls profile

5.3.4 Peak indoor temperature reduction

The effect of PCM-E walls on indoor temperature in temporary housing is analysed. [Figure 5-7](#) indicates that the ENW-wall orientation with PCM-E results in a significant reduction in the indoor temperature. The effect was significant on some days and slightly significant on others. However, the previous analysis shows that the E-wall performs better than all other walls based on the inner surface temperature and flux reduction, whereas in this analysis, the ENW-wall shows better results based on the indoor temperature indicator. This is because the addition of PCM to all three walls can increase the thermal mass of a building; however, the PCM may only function as an additional layer, as reflected in this scenario. The reduction in indoor temperature is evident on the first, second, and third days for both E-wall, EN-wall-, and ENW-walls, where indoor temperatures are mostly within the thermal comfort range of the Kano state, which is between 23 °C and 32 °C [\[258\]](#). The reductions in the peak indoor air temperatures for E-wall, EN-wall, and ENW-wall are presented in [Table 5-2](#). Furthermore, the diurnal temperature fluctuation was reduced for the temporary housing with the PCM-E wall for the three days, indicating a reduction in the thermal discomfort sensation for the occupants. This verifies the benefit of PCM as a latent heat storage in improving the thermal comfort of a building.

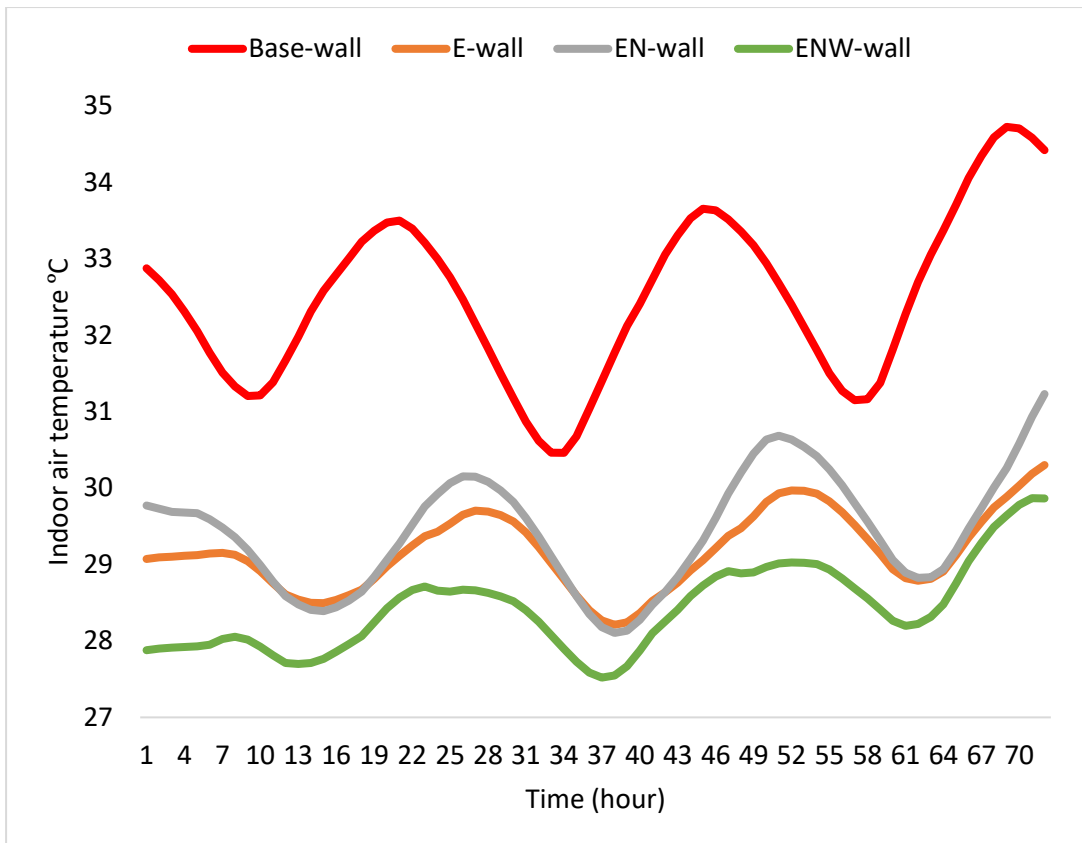


Figure 5-7 Earthbag indoor air temperature profile

Table 5-2 Indoor Temperature reduction for different PCM-E orientation

Days	E-wall (°C)	EN-wall (°C)	ENW-wall (°C)
18 th April	4.1	3.6	4.8
19 th April	4.3	3.5	4.6
20 th April	4.4	3.5	4.8

5.3.5 Effect of night ventilation on peak indoor temperatures reductions

The results in [Figure 5-8](#) demonstrate that ventilation is an effective strategy for reducing indoor air temperatures and improving thermal comfort in earthbag buildings utilizing PCM walls. Across all three experimental cases as in [Figure 5-8](#) PCM in the east wall (E-wall), east and north walls (EN-wall), and east, north and west walls (ENW-wall) - ventilation led to lower peak indoor temperatures and longer time lags for the indoor temperature to reach its peak. Specifically, ventilation reduced the average peak indoor temperature by 0.5-0.3°C compared to the non-ventilated cases. The most significant cooling effect was seen in the E-wall case, where ventilation lowered the peak temperature by 0.5°C from 4.7°C to 4.2°C. Ventilation also increased the time for the indoor temperature to reach its peak by 1-2 hours in the three cases. The E-wall showed the largest delay, with the peak temperature occurring 5 hours after solar noon without ventilation and 6 hours after solar noon with ventilation. These results indicate that PCM-enhanced earthbag buildings can achieve additional indoor temperature reduction and slower evening heat gain when combined with ventilation. The data shows this effect is present regardless of whether PCM walls are installed on one, two or three sides of the building. The consistency of the results across cases suggests that cross-ventilation is the key factor enabling improved temperature regulation. Therefore, the study provides strong evidence that coupling ventilation strategies with PCM-enhanced earthbag building envelopes can provide effective natural temperature regulation in hot climates like Kano, maintaining indoor temperatures within the comfort range. The approach could improve occupant thermal comfort and reduce reliance on energy-intensive mechanical cooling.

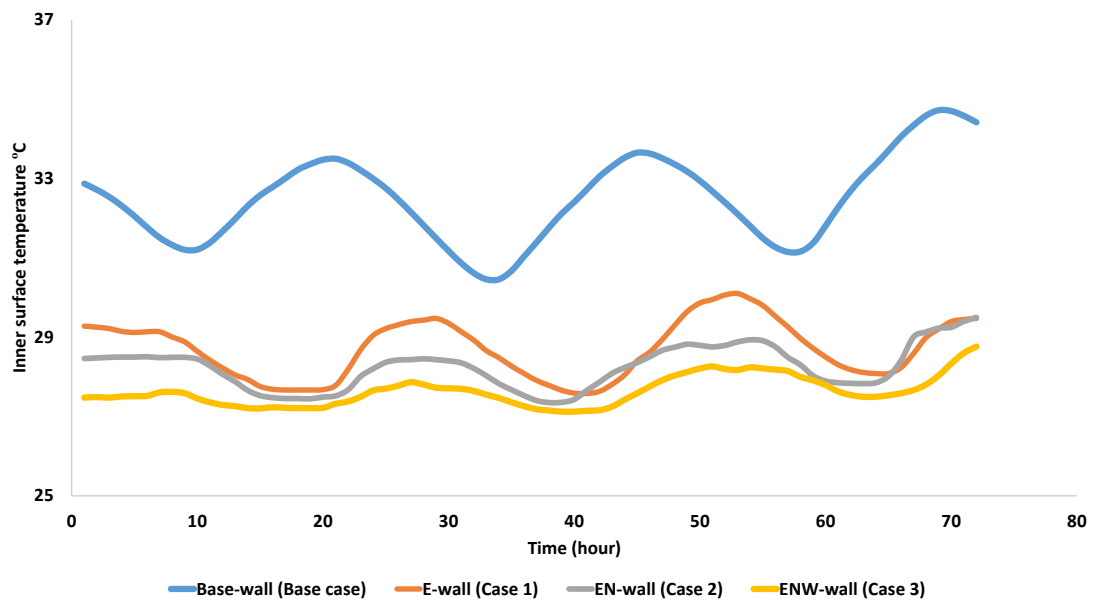


Figure 5-8 Effect of night ventilation on peak indoor temperatures reductions

5.3.6 Effect of ventilation on indoor air temperature for summer period

The effect of incorporating PCM-Insulation in earthbag building walls on indoor thermal comfort is evaluated through simulation models under two ventilation scenarios - without ventilation (0ACH) and with night ventilation (5ACH). Figure 5-9 shows the overall summer indoor air temperature profiles for different wall configurations. In Figure 5-9 (a) (0ACH), the addition of PCM-Insulation in the E-wall, EN-wall, and ENW-wall results in indoor temperatures largely within or slightly above the adaptive comfort range, unlike the base wall without PCM-E. Comparing the PCM-E walls, the ENW-wall provides the best thermal regulation. With 5ACH night ventilation (Figure 5-9 (b)), the indoor temperature profiles of the PCM-Insulation walls shift further into the adaptive comfort range. This indicates night ventilation enhances the thermal regulation effect of the PCM-Insulation by allowing it to discharge excess heat at night. Analysing the percentage of comfort hours and discomfort hours in Figure 5-10. It has shown that without ventilation (Figure 5-10 (a) and 2(b)), the base wall has only 6% comfort hours and 1963 discomfort hours due to lack of thermal regulation. Adding PCM-E significantly improves thermal comfort - the E-wall, EN-wall and ENW-wall have 94%, 84% and 98% comfort hours respectively. Though the ENW-wall gives the best performance, the E-wall also provides substantial comfort improvement over the base wall. With 5ACH ventilation, the discomfort hours

reduce, and comfort hours increase for all walls (Figure 5-10 (a) and (b)). The base wall discomfort hours reduce from 1963h (0ACH) to 1678h (5ACH) and comfort hours increase from 6% (0ACH) to 24% (5ACH). For PCM-E walls, the reduction in discomfort hours is more prominent - E-wall reduces from 140h to 64h; EN-wall 349h to 211h; and ENW-wall 53h to 11h. The comfort hours also increase - E-wall 97.1%, EN-wall 90.4% and ENW-wall 99.5%. Hence, the simulation results demonstrate a significant improvement in indoor thermal comfort with the use of PCM-Insulation in earthbag building walls, which is further enhanced by coupling PCM-E with night ventilation. The ENW-wall configuration provides the best thermal regulation. However, considering factors such as affordability and constructability, the E-wall presents a viable and effective solution for thermally comfortable temporary housing using local earthen construction.

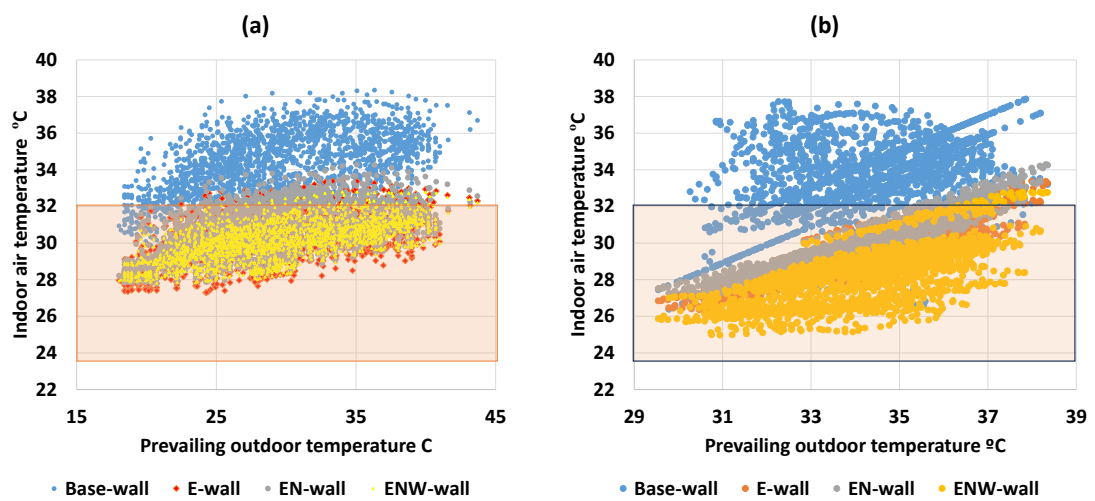


Figure 5-9 Overall summer temperature points over mean outdoor temperature for Earthbag building

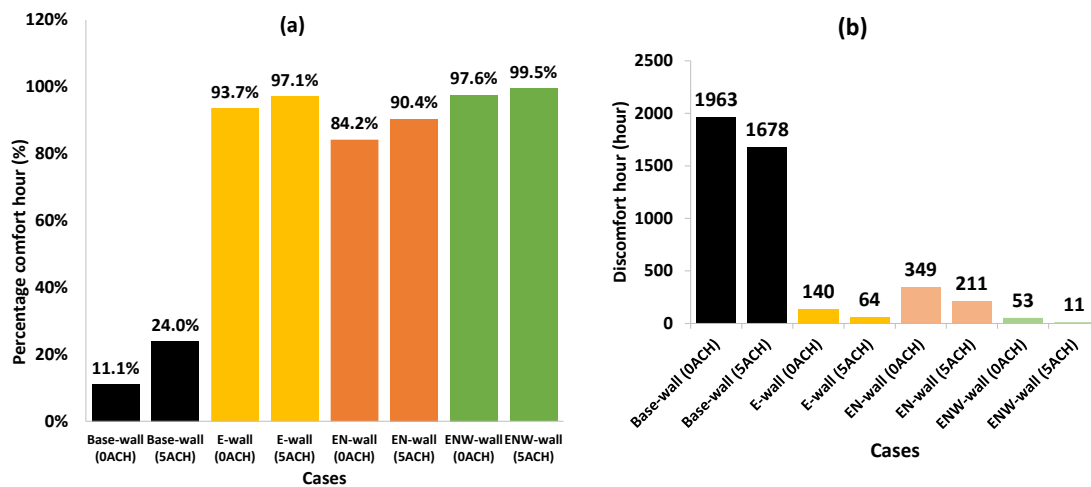


Figure 5-10 Annual Hours of discomfort earthbag base-wall, E-wall, EN-wall, and ENW-wall

5.4 Summary

This chapter provides a detailed thermal performance analysis of PCM-E walls in temporary housing for a thermal comfort assessment. The key findings of this chapter are as follows.

- Simulations of PCM-E walls (PCM-E walls) in different orientations showed the east (E-wall), east-north (EN-wall), and east-north-west (ENW-wall) configurations provided the best inner surface temperature reductions and time lags compared to a base case without PCM.
- The addition of night ventilation further improved the performance of the PCM-E walls by allowing more effective heat discharge at night. With night ventilation, the average inner wall temperature decreased 3.8°C for the optimal E-wall case versus 3.0°C without ventilation.
- Analysis of heat flux densities showed the E-wall orientation resulted in the highest heat flux reduction during the daytime (up to 57 W/m²) due to optimal solar radiation exposure.
- The addition of insulation in the PCM-E walls enhanced the thermal mass effect and improved the walls' ability to dampen temperature fluctuations.

- The insulation effect also reduced conductive heat transfer, allowing the PCM to work more effectively. Insulation expanded the solidification period of the PCM at night.
- The ENW-wall configuration provided the largest reduction in peak indoor air temperature (up to 4.8°C) compared to the base case.
- Simulation of summer indoor temperatures showed the E-wall, EN-wall, and ENW-wall with PCM-E maintained indoor temperatures within or close to the adaptive comfort range. Adding night ventilation further improved thermal regulation.
- The E-wall presents a viable and effective solution considering performance, affordability, and constructability for temporary housing in the studied climate.

Chapter 6. Discussion and Conclusion

6.1 Summary of the research study

This study presents an investigation of the thermal performance and potential use of earthbag buildings, specifically focusing on the integration of PCM for achieving thermal comfort in hot, dry climates. A thorough review of the relevant literature was conducted to gain insights into the thermal comfort levels of earthen and earthbag constructions, as well as the limitations associated with existing techniques used in earthbag buildings. Additionally, this study explores the suitability of earthbag buildings as temporary housing solutions in hot and dry climates. Furthermore, a detailed literature review was conducted to examine the application of PCM in vernacular buildings to enhance their thermal comfort.

A structured methodology was proposed for incorporating PCM into earthbag buildings. This methodology includes the development and characterization of earthbag blocks with integrated PCM, process of constructing earthbag walls using optimum PCM-integrated blocks, testing procedures for evaluating the performance of earthbag walls, experimental validation using the finite difference approach in EnergyPlus (EnergyPlus CondFD), and use of the developed solution scheme in EnergyPlus (EnergyPlus CondFD) to simulate the thermal performance of PCM-E walls for temporary housing.

In this study, preliminary experiments were conducted to identify the optimal soil composition for earthbags, although the existing literature already provides recommendations in this regard. The PCM, specifically paraffin wax (A31), intended for integration within the block, underwent extensive testing to evaluate its effectiveness in enhancing thermal performance and comfort. To address the leakage concerns, the PCM was encapsulated within a porous material to form a PCM composite, which was then subjected to stability tests. The PCM composite was mixed with the best soil composition to produce an earthbag block. Subsequently, the block underwent thorough thermal performance testing under real weather conditions to assess its capability to reduce cooling loads in a hot and dry climate.

The most promising PCM-E block developed in this study was used to construct an earthbag wall, and a series of experiments were conducted within a controlled environmental chamber. Additional PCMs were introduced in the block for more in-depth analysis. A numerical model was developed and validated through an experimental study.

Finally, in this research study, a case study is selected to demonstrate the integration of the PCM-E wall. Through a series of simulations, different PCM-E wall positions based on orientation were evaluated to determine the optimum configuration that achieved the desired thermal comfort for the selected temporary housing in the case study. Comparing the case study with PCM-E wall and the one without PCM-E wall proves that the case study with PCM-E helps reduce the thermal discomfort of temporary housing.

6.2 Conclusions

The main conclusions of this research are:

6.2.1 Development and thermal characteristics of PCM-integrated earthbag block

This research section aims to promote the utilization of PCM technologies in vernacular buildings. The experimental program conducted in this study was aimed at examining the effects of incorporating PCM composites into earthbag building blocks. The primary rationale behind this approach is to mitigate high indoor temperatures by reducing the peak surface temperature of the walls and minimizing the energy consumption required for heating and cooling operations. Based on the experimental study presented in this section, the following conclusions can be drawn.

- The use of PCM in earthbag buildings, as demonstrated in this study, can provide a more efficient and cost-effective method for regulating indoor temperatures, resulting in improved thermal comfort levels when compared to the utilization of mechanical systems to enhance building comfort. This can be attributed to the rising energy costs affecting the global environment.
- The tested system showed the potential to increase the thermal performance of earthbag blocks. In this regard, the optimum composite found from the

experiment was PEPG, whose performance presented favorable results for earthbag block incorporation.

- Based on the results of the latent heat of sample G (147.0 J/g), sample B (83.1 J/g), sample D (83.7 J/g), and sample B (84.9 J/g), it is clear that Sample G has the highest latent heat. Moreover, the melting temperature and latent heat of Sample G were very similar to those of the manufacturer.
- The leakage test, SEM, and DSC experiments showed that the PCM was successfully integrated into the EP pores and was compatible. The TGA results for the manufactured composite PCM indicated a suitable thermal stability.
- The thermal conductivities were improved by the graphite. In the sample developed with PEPG, having a different percentage of PCM, the thermal conductivity is found to be 1.43 $W/m.K$ for the reference sample and 1.33 $W/m.K$, 1.19 $W/m.K$, and 1.09 $W/m.K$ for the tested samples with EG
- The average indoor surface temperature drops generated by Blocks B, C, and D developed with the optimum composite PEPG compared to the reference block, as the values were found to be 1.2, 3.3, and 4.1°C, respectively.
- Block D shows a better thermal performance with a surface temperature reduction of 4.1°C; therefore, the composite combination of PCM, expanded perlite, and expanded graphite was selected to develop a PCM-Ewall.

Overall, the results of this study show the positive impact of PCM on the earthbag block. Consequently, the results were employed for further experimental and numerical simulations of walls incorporating PCMs under longer periods of simulation and experimentation.

6.2.2 Experimental and Numerical Study on the Performance of Earthbag-wall Incorporated with Phase Change Materials

In this study, a test-scale wall prototype placed in a thermally controlled environmental chamber was used to assess the thermal performance of a PCM-E wall. The developed experimental model integrated with the phase-change heat transfer was used to validate the developed simulation model. The model was used to determine the suitable thickness of the earthbag . The main conclusions of this study are summarized as follows.

- The thermal conductivity of the earthbag walls decreased substantially with the addition of PCMs. The wall with microencapsulated PCM (Wall-3) had the lowest thermal conductivity of 0.43 W/mK compared to 0.74 W/mK for the wall with PCM composite (Wall-2) and 1.83 W/mK for the baseline wall without PCM. This demonstrates the excellent insulating properties provided by PCM integration into the earthbags. The microencapsulated PCM was able to lower the thermal conductivity the most due to its even distribution and consistent thermal properties within the earthbag wall matrix. In contrast, the PCM composite led to slightly higher conductivity likely due to uneven distribution and variance in conductivity within the composite material itself.
- Surface temperature measurements showed more stable inner wall temperatures for the PCM-integrated walls, with maximum temperature reductions of 1.9°C for Wall-2 and 2.4°C for Wall-3 compared to the baseline. The microencapsulated PCM in Wall-3 provided superior performance in maintaining a consistent inner wall temperature profile with minimal fluctuations throughout the day. This demonstrates the ability of the properly integrated PCM to increase the thermal mass of the earthbag wall and avoid spike in temperatures. In contrast, the baseline earthbag wall displayed larger temperature swings indicating lower thermal mass and heat storage capacity.
- Heat flux analysis revealed substantially lower heat transfer to the inner wall surface for the PCM walls, with average reductions of 39.34% for Wall-2 and 63.76% for Wall-3 compared to the baseline. This directly translates to lower heat gain and resultant lower indoor temperatures and energy savings for

cooling in actual earthbag buildings. The considerable heat flux reduction verifies the thermal resistance imparted by the PCM layers which slows down and reduces the heat flowing to the inner wall surface.

- The PCM walls demonstrated increased time lag in the range of 3-5 hours in reaching maximum inner wall temperature. This phase change effect where the PCMs absorb heat while melting delays and dampens the peak temperature profile, thereby enhancing thermal comfort. The latent heat absorption provides a buffer against external temperature swings and prevents rapid heat transfer to the interior spaces.
- The optimum PCM transition temperature was determined to be 31°C through testing of four different PCMs in the model. At this melting point, the PCM was able to effectively store and release heat despite fluctuations in outdoor temperature above and below the transition point. PCMs with lower melting temperatures remained in liquid state and failed to provide adequate thermal mass benefits.
- Tests conducted with just insulation (expanded perlite) showed decent reductions in inner wall temperature and heat flux compared to the baseline, although not as much as with PCM integration. This shows the benefits of insulation but highlights they are limited without the latent heat effects of PCMs.
- Increasing the thickness of both the PCM layer and insulation layer led to the best thermal performance, with reductions of 6-7°C in inner wall temperature. The increased thickness allowed for greater heat absorption by the PCM during melting as well as reduced heat transfer rate through the thicker insulation. This optimized configuration provided the maximum thermal mass for the earthbag wall.

The numerical model developed was validated thoroughly against experimental data. The resulting errors were within acceptable limits, and the model accurately captured the thermal performance benefits of PCM integration in earthbag walls. Overall, the use of PCMs has been conclusively proven to enhance the thermal mass of earthbag buildings, reducing temperature fluctuations and improving energy efficiency. The

research provides an optimal PCM configuration and reliable numerical simulation method to promote the use of this passive cooling technique in earthbag construction across hot climates.

6.2.3 Determination of thermal performance of PCM-integrated earthbag walls in temporary housing

In conclusion, this study investigated the thermal performance of PCM-E walls in temporary housing in a hot-climate region of Nigeria. This study aims to evaluate the effect of wall orientation on the inner surface temperature reduction, heat flux density through the walls, and peak indoor temperature reduction. The results show that PCM-E walls can effectively reduce the inner surface temperature, heat flux density, and peak indoor temperature in temporary housing in hot climate regions. Hence, the following conclusions can be drawn.

- PCM-enhanced earthbag walls significantly reduce indoor temperatures and heat flux compared to conventional earthbag walls without PCM. The PCM's latent heat absorption and release ability dampens temperature fluctuations and lowers peak indoor temperatures by storing solar heat during the day and releasing it at night. Optimal PCM melting temperature allows it to solidify at night and absorb more heat the next day. This thermal mass effect is evident in the reduced amplitude of temperature swings.
- Determining the optimal PCM wall configuration depends on the specific evaluation criteria used. Based on peak inner wall surface temperature reduction, the E-wall (PCM integrated only on the east-facing wall) performs best out of the single wall cases, with up to 3.3°C lower maximum temperature compared to the base case wall without PCM. This is attributed to the east wall receiving an intermediate solar radiation level. However, evaluating the overall indoor air temperature reduction, the ENW-wall (PCM integrated on the east, north and west walls) is most effective, decreasing the peak indoor temperature by up to 4.8°C. The combined PCM on three walls likely increases the thermal mass.

- Analysis of the optimal wall direction to place PCM indicates the east side, as it receives a moderate solar radiation level that allows the PCM to fully melt during the day and fully solidify overnight. The east-facing wall shows the highest inner surface temperature and heat flux reduction among single wall cases. The south wall receives excessive radiation that could overheat the PCM beyond its melting point, causing it to remain melted for longer periods and lose effectiveness.
- Night ventilation further improves the thermal regulation performance of PCM walls by flushing out excess solar heat stored during the day, allowing the PCM to re-solidify and be ready to absorb more heat the next day. Ventilation reduces peak indoor temperatures by an additional 0.3-0.5°C over the non-ventilated cases. Ventilation extends the PCM discharging period by 1-2 hours.
- Coupling PCM walls with cross night ventilation eliminates the need for air conditioning, maintaining indoor temperatures within the comfort range of 23-32°C over the simulation period. This demonstrates a very promising passive cooling technique for thermally comfortable low-energy housing in hot climates like Kano.
- The long-term simulation results verify that integrating just the east-facing PCM wall results in significantly improved thermal comfort, with 94% comfort hours over the entire summer period compared to only 6% for the base case wall. This single-wall approach is effective and feasible for affordable temporary housing using local earthen construction.

In summary, this chapter clearly demonstrates through simulations that PCM-enhanced earthbag walls, especially when combined with night ventilation strategies, can provide substantial temperature reduction and indoor thermal comfort improvements for temporary housing in hot climates like Kano, Nigeria. The passive cooling techniques show strong potential to reduce reliance on air conditioning and energy use. Further experimental testing of optimal PCM melting temperature, ventilation rates and configurations can help extend and validate the findings. Overall, the study highlights an effective bioclimatic integration of local earthen materials and

passive cooling to address indoor thermal comfort needs for low-income regions with hot climates.

6.3 Future work

The current research on thermal performance of earthbag building with integrated PCMs has several limitations that future work should address. This initial study was limited to testing PCM-earthbag wall in controlled laboratory conditions, which does not replicate the wide variability of real climate conditions. To better understand real-world performance, future research should examine PCM-earthbag performance through field testing in arid climates with large diurnal temperature variations (e.g., desert areas) as well as humid climates with higher moisture levels (e.g., tropical regions). Testing should assess thermal regulation across seasonal and daily cycles using a significant sample size of earthbag test walls in each climate. Additionally, structural integrity and durability testing should be performed to determine if incorporation of PCMs reduces the stability and robustness of earthbag walls over the long-term compared to standard earthbag designs. Various PCM concentrations and integration methods with the earth material could be analysed. Future work must also evaluate the cost-benefit ratio and social acceptance of PCM-earthbag blocks compared to traditional building materials. Surveys and interviews should assess end-user perspectives on advantages, disadvantages, and willingness to utilize PCM-earthbags, especially in low-income contexts. Addressing these research limitations through rigorous field testing, structural analysis, economic evaluation, and social impact studies will provide a more comprehensive understanding of the real-world viability of earthbag blocks enhanced with PCMs as a sustainable building technology.

Appendix A

In this study, it was determined that the amount of PCM used in each earthbag block was 2.2% of the total volume of the block, as outlined in [Section 4.3.1.2](#). The actual weight of PCM found in each block was 0.39 kg. To calculate the thickness of the PCM layer in the block, the density of the PCM from [Table 3-1](#) was used, along with the dimensions of a single earthbag block shown in [Figure 3-2](#).

By applying the PCM equivalent method, the thickness of the PCM layer was calculated using Eqn.19 below:

$$\textit{Thickness} = \textit{Mass} / (\textit{length} \times \textit{width} \times \textit{density}) \quad \textit{Eqn A6.1}$$

$$\textit{Thickness} = 0.39 \textit{ kg} / (0.1 \textit{ m} \times 0.4 \textit{ m} \times 860 \textit{ kg/m}^3)$$

$$\textit{Thickness} \approx 0.011 \textit{ meters}$$

Publications

Farouq, Mahmoud Murtala, Carlos Jimenez-Bescos, Saffa Riffat, and Parham A. Mirzaei. 2023. "Development and Thermal Characteristic Study of an Integrated Phase Change Material Earthbag Unit for Temporary Housings." *Energy and Buildings* 284: 112852. <https://doi.org/10.1016/j.enbuild.2023.112852>.

Mahmoud, Murtala Farouqa, Parham A. Mirzaei, Carlos Jimenez-Bescos, and Saffa Riffat. "Experimental and Numerical Study on the Performance of Earthbag-Wall Unites Incorporated with Phase Change Materials." *Energy and Buildings*. (Under review)

Rahnama, Samira, Mahmood Khatibi, Alessandro Maccarini, **Mahmoud Murtala Farouq**, Parham A. Mirzaei, Enrico Fabrizio, Maria Ferrara, et al. n.d. "Steps to Smart Design of Thermal Energy Storage Systems for Buildings." *Energy Systems in Buildings*. (Under review)

Bibliography

- [1] R. A. Poschl, "Modelling the thermal comfort performance of tents used in humanitarian relief," Loughborough University, 2016.
- [2] F. Moran, D. Fosas, D. Coley, S. Natarajan, J. Orr, and O. B. Ahmad, "Improving thermal comfort in refugee shelters in desert environments," *Energy Sustain. Dev.*, vol. 61, pp. 28–45, 2021, doi: 10.1016/j.esd.2020.12.008.
- [3] M. Hamdan, F. Abd-Alhamid, and L. Dabbour, "Impact of passive techniques on thermal behavior of emergency shelters," *Ecol. Eng. Environ. Technol.*, vol. 22, no. 3, pp. 112–119, 2021, doi: 10.12912/27197050/135523.
- [4] R. A. Al-Sha'r, "Rethinking shelter design: Zaatari refugee Camp," Mount Holyoke College, 2017.
- [5] M. Dabaieh, "Design and build with straw, earth and reeds for a minus carbon and plus energy building practice," in *IOP Conference Series: Earth and Environmental Science*, 2019, vol. 352, no. 1. doi: 10.1088/1755-1315/352/1/012063.
- [6] D. Fosas, F. Moran, S. Natarajan, J. Orr, and D. Coley, "The importance of thermal

- modelling and prototyping in shelter design,” *Build. Res. Inf.*, vol. 48, no. 4, pp. 379–400, 2020, doi: 10.1080/09613218.2019.1691489.
- [7] S. Domínguez-Amarillo, Á. Rosa-García, J. Fernández-Agüera, and N. Escobar-Castrillón, “Architecture of the scape: Thermal assessment of refugee shelter design in the extremes climates of Jordan, Afghanistan and South Sudan,” *J. Build. Eng.*, vol. 42, no. December 2020, 2021, doi: 10.1016/j.jobee.2021.102396.
- [8] K. I. Praseeda, M. Mani, and B. V. V. Reddy, “Assessing impact of material transition and thermal comfort models on embodied and operational energy in vernacular dwellings (India),” *Energy Procedia*, vol. 54, pp. 342–351, 2014, doi: 10.1016/j.egypro.2014.07.277.
- [9] P. Kabachnik, J. Regulska, and B. Mitchneck, “Where and when is home? The double displacement of Georgian IDPs from Abkhazia,” *J. Refug. Stud.*, vol. 23, no. 3, pp. 315–336, 2010, doi: 10.1093/jrs/feq023.
- [10] W. B. Zanna, “Assessment on Unmet Needs of Internally Displaced Persons in Maiduguri Metropolis , Borno State-Nigeria,” pp. 9–18, 2021.
- [11] M. Lee, L. Shi, A. Zanobetti, and J. D. Schwartz, “Study on the association between ambient temperature and mortality using spatially resolved exposure data,” *Environ. Res.*, vol. 151, pp. 610–617, 2016, doi: 10.1016/j.envres.2016.08.029.
- [12] D. Albadra, M. Vellei, D. Coley, and J. Hart, “Thermal comfort in desert refugee camps: An interdisciplinary approach,” *Build. Environ.*, vol. 124, pp. 460–477, 2017, doi: 10.1016/j.buildenv.2017.08.016.
- [13] Federal Ministry of Power Works and Housing, “Building energy efficiency guideline for Nigeria federal ministry of power, works and housing (housing),” 2016. [Online]. Available: https://energypedia.info/images/c/c7/Building_Energy_Efficiency_Guideline_for_Nigeria_2016.pdf
- [14] J. Liu, X. Chen, S. Cao, and H. Yang, “Overview on hybrid solar photovoltaic-electrical energy storage technologies for power supply to buildings,” *Energy Convers. Manag.*, vol. 187, no. December 2018, pp. 103–121, 2019, doi: 10.1016/j.enconman.2019.02.080.
- [15] S. M. Zanjirchi, S. Shojaei, A. Naser Sadrabadi, and N. Jalilian, “Promotion of solar

- energies usage in Iran: A scenario-based road map," *Renew. Energy*, vol. 150, pp. 278–292, 2020, doi: 10.1016/j.renene.2019.11.104.
- [16] P. A. Østergaard, N. Duic, Y. Noorollahi, H. Mikulcic, and S. Kalogirou, "Sustainable development using renewable energy technology," *Renew. Energy*, vol. 146, pp. 2430–2437, 2020, doi: 10.1016/j.renene.2019.08.094.
- [17] N. M. A. Mutombo and B. P. Numbi, "Assessment of renewable energy potential in Kwazulu-Natal province, South Africa," *Energy Reports*, vol. 5, pp. 874–881, 2019, doi: 10.1016/j.egy.2019.07.003.
- [18] A. Chel and G. Kaushik, "Renewable energy technologies for sustainable development of energy efficient building," *Alexandria Eng. J.*, vol. 57, no. 2, pp. 655–669, 2018, doi: 10.1016/j.aej.2017.02.027.
- [19] Y. Zhou and S. Cao, "Energy flexibility investigation of advanced grid-responsive energy control strategies with the static battery and electric vehicles: A case study of a high-rise office building in Hong Kong," *Energy Convers. Manag.*, vol. 199, no. February, p. 111888, 2019, doi: 10.1016/j.enconman.2019.111888.
- [20] R. Ibrahim, "Energy demand management and integration of sustainable energy sources to determine a 'Best mix approach' to energy generation," *Procedia Manuf.*, vol. 35, pp. 383–388, 2019, doi: 10.1016/j.promfg.2019.05.056.
- [21] P. Denholm, E. Ela, B. Kirby, and M. Milligan, "The role of energy storage with renewable electricity generation," *Energy Storage Issues Appl.*, no. January, pp. 1–58, 2011.
- [22] M. S. Karimi, F. Fazelpour, M. A. Rosen, and M. Shams, "Comparative study of solar-powered underfloor heating system performance in distinctive climates," *Renew. Energy*, vol. 130, pp. 524–535, 2019, doi: 10.1016/j.renene.2018.06.074.
- [23] J. Fernandes, M. Peixoto, R. Mateus, and H. Gervásio, "Life cycle analysis of environmental impacts of earthen materials in the Portuguese context: Rammed earth and compressed earth blocks," *J. Clean. Prod.*, vol. 241, 2019, doi: 10.1016/j.jclepro.2019.118286.
- [24] I. I. Akinwumi, P. O. Awoyera, and O. O. Bello, "Indigenous earth building construction technology in Ota, Nigeria," *Indian J. Tradit. Knowl.*, vol. 14, no. 2, pp. 206–212, 2015.

- [25] S. M. Khoshnava, R. Rostami, R. M. Zin, D. Štreimikienė, A. Mardani, and M. Ismail, "The role of green building materials in reducing environmental and human health impacts," *Int. J. Environ. Res. Public Health*, vol. 17, no. 7, 2020, doi: 10.3390/ijerph17072589.
- [26] O. B. Adegun and Y. M. D. Adedeji, "Review of economic and environmental benefits of earthen materials for housing in Africa," *Front. Archit. Res.*, vol. 6, no. 4, pp. 519–528, 2017, doi: 10.1016/j.foar.2017.08.003.
- [27] H. Niroumand, J. A. Barcelo, C. J. Kibert, and M. Saaly, "Evaluation of Earth Building Tools in Construction (EBTC) in earth architecture and earth buildings," *Renew. Sustain. Energy Rev.*, vol. 70, no. September 2015, pp. 861–866, 2017, doi: 10.1016/j.rser.2016.11.267.
- [28] M. S. Zami and A. Lee, "Economic benefits of contemporary earth construction in low-cost urban housing - State-of-the-art review," *J. Build. Apprais.*, vol. 5, no. 3, pp. 259–271, 2010, doi: 10.1057/jba.2009.32.
- [29] C. Williams, S. Goodhew, R. Griffiths, and L. Watson, "The feasibility of earth block masonry for building sustainable walling in the United Kingdom," *J. Build. Apprais.*, vol. 6, no. 2, pp. 99–108, 2010, doi: 10.1057/jba.2010.15.
- [30] H. Niroumand, J. A. Barceló Álvarez, and M. Saaly, "Investigation of earth building and earth architecture according to interest and involvement levels in various countries," *Renew. Sustain. Energy Rev.*, vol. 57, pp. 1390–1397, 2016, doi: 10.1016/j.rser.2015.12.183.
- [31] O. Geiger and K. Zemskova, "Earthbag Technology-Simple, Safe and Sustainable," *Nepal Eng. Assoc. Tech. J.*, vol. 43, no. 1, pp. 78–90, 2015.
- [32] D. M. dos Santos and J. N. Beirão, "Parametrical design tool and the production of technical data for superadobe domes," *Gestão Tecnol. Proj.*, vol. 14, no. 1, pp. 45–60, 2019, doi: 10.11606/gtp.v14i1.148182.
- [33] A. Castell, S. Vall, A. Carrobé, M. Medrano, I. Martorell, and L. Rincón, "Radiative Cooling to Cover Cooling Demands of an Earthbag Building in a Training Medical Center in Burkina Faso," no. Hunter 2004, pp. 1–6, 2019, doi: 10.18086/eurosun2018.06.03.
- [34] R. Kamal and M. S. Rahman, "A study on feasibility of super adobe technology -an

- energy efficient building system using natural resources in Bangladesh,” in *IOP Conference Series: Earth and Environmental Science*, 2018, vol. 143, no. 1. doi: 10.1088/1755-1315/143/1/012043.
- [35] Q. Al-Yasiri and M. Szabó, “Incorporation of phase change materials into building envelope for thermal comfort and energy saving: A comprehensive analysis,” *J. Build. Eng.*, vol. 36, no. December 2020, 2021, doi: 10.1016/j.jobbe.2020.102122.
- [36] J. S. Sage-Lauck and D. J. Sailor, “Evaluation of phase change materials for improving thermal comfort in a super-insulated residential building,” *Energy Build.*, vol. 79, pp. 32–40, 2014, doi: 10.1016/j.enbuild.2014.04.028.
- [37] F. Kuznik, J. Virgone, and K. Johannes, “In-situ study of thermal comfort enhancement in a renovated building equipped with phase change material wallboard,” *Renew. Energy*, vol. 36, no. 5, pp. 1458–1462, 2011, doi: 10.1016/j.renene.2010.11.008.
- [38] O. Imghoure, N. Belouaggadia, M. Ezzine, R. Lbibb, and Z. Younsi, “Performance evaluation of phase change materials for thermal comfort in a hot climate region,” *Appl. Therm. Eng.*, vol. 186, no. January, p. 116509, 2021, doi: 10.1016/j.applthermaleng.2020.116509.
- [39] D. Snoeck, B. Priem, P. Dubruel, and N. De Belie, “Encapsulated Phase-Change Materials as additives in cementitious materials to promote thermal comfort in concrete constructions,” *Mater. Struct. Constr.*, vol. 49, no. 1–2, pp. 225–239, 2016, doi: 10.1617/s11527-014-0490-5.
- [40] A. Castell, I. Martorell, M. Medrano, G. Pérez, and L. F. Cabeza, “Experimental study of using PCM in brick constructive solutions for passive cooling,” *Energy Build.*, vol. 42, no. 4, pp. 534–540, 2010, doi: 10.1016/j.enbuild.2009.10.022.
- [41] V. V. Tyagi, A. K. Pandey, D. Buddhi, and R. Kothari, “Thermal performance assessment of encapsulated PCM based thermal management system to reduce peak energy demand in buildings,” *Energy Build.*, vol. 117, pp. 44–52, 2016, doi: 10.1016/j.enbuild.2016.01.042.
- [42] F. Ascione, N. Bianco, R. F. De Masi, F. De’Rossi, and G. P. Vanoli, “Energy retrofit of an educational building in the ancient center of Benevento. Feasibility study of energy savings and respect of the historical value,” *Energy Build.*, vol. 95, pp. 172–183, 2015, doi: 10.1016/j.enbuild.2014.10.072.

- [43] G. Evola, L. Marletta, and F. Sicurella, "A methodology for investigating the effectiveness of PCM wallboards for summer thermal comfort in buildings," *Build. Environ.*, vol. 59, pp. 517–527, 2013, doi: 10.1016/j.buildenv.2012.09.021.
- [44] M. Saffari, A. de Gracia, S. Ushak, and L. F. Cabeza, "Passive cooling of buildings with phase change materials using whole-building energy simulation tools: A review," *Renew. Sustain. Energy Rev.*, vol. 80, no. June, pp. 1239–1255, 2017, doi: 10.1016/j.rser.2017.05.139.
- [45] M. Pakand and V. Toufigh, "A multi-criteria study on rammed earth for low carbon buildings using a novel ANP-GA approach," *Energy Build.*, vol. 150, pp. 466–476, 2017, doi: 10.1016/j.enbuild.2017.06.004.
- [46] R. Al Shannaq, "Microencapsulation of phase change materials (PCMs) for thermal energy storage systems," 2015. doi: 10.1533/9781782420965.2.247.
- [47] D. Albadra, D. Coley, and J. Hart, "Toward healthy housing for the displaced," *J. Archit.*, vol. 23, no. 1, pp. 115–136, 2018, doi: 10.1080/13602365.2018.1424227.
- [48] H. Schroeder, "Modern earth building codes, standards and normative development," *Mod. Earth Build. Mater. Eng. Constr. Appl.*, pp. 72–109, 2012, doi: 10.1533/9780857096166.1.72.
- [49] F. Stazi, A. Nacci, F. Tittarelli, E. Pasqualini, and P. Munafò, "An experimental study on earth plasters for earthen building protection: The effects of different admixtures and surface treatments," *J. Cult. Herit.*, vol. 17, pp. 27–41, 2016, doi: 10.1016/j.culher.2015.07.009.
- [50] W. B. Agostino, "Hygro-mechanical characterisation of hypercompacted earth for building construction," 2016.
- [51] D. Johnston, "How to Buy Tickets to the Alhambra in Granada, Spain," 2023. <https://www.roadaffair.com/buy-tickets-to-the-alhambra-in-granada-spain/>
- [52] C. Egenti, J. M. Khatib, and D. Oloke, "Conceptualisation and pilot study of shelled compressed earth block for sustainable housing in Nigeria," *Int. J. Sustain. Built Environ.*, vol. 3, no. 1, pp. 72–86, 2014, doi: 10.1016/j.ijbsbe.2014.05.002.
- [53] A. Fabbri, J.-C. Morel, and D. Gallipoli, "Assessing the performance of earth building materials: a review of recent developments," *RILEM Tech. Lett.*, vol. 3, pp. 46–58, 2018, doi: 10.21809/rilemtechlett.2018.71.

- [54] S. Serrano, C. Barreneche, L. Rincón, D. Boer, and L. F. Cabeza, "Stabilized rammed earth incorporating PCM: Optimization and improvement of thermal properties and Life Cycle Assessment," *Energy Procedia*, vol. 30, pp. 461–470, 2012, doi: 10.1016/j.egypro.2012.11.055.
- [55] I. I. Akinwumi, "Earth building construction processes in Benin city, Nigeria and engineering classification of earth materials used," *Indian J. Tradit. Knowl.*, vol. 13, no. 4, pp. 686–690, 2014.
- [56] M. Cataldo-Born, G. Araya-Letelier, and C. Pabón, "Obstacles and motivations for earthbag social housing in Chile: Energy, environment, economic and codes implications," *Rev. la Constr.*, vol. 15, no. 3, pp. 17–26, 2014, doi: 10.4067/S0718-915X2016000300002.
- [57] R. Rael, *Earth Architecture*. New York: Princeton Architectural Press, 2008.
- [58] A. T. M. Marsh and Y. Kulshreshtha, "The state of earthen housing worldwide: how development affects attitudes and adoption," *Build. Res. Inf.*, vol. 50, no. 5, pp. 485–501, 2021, doi: 10.1080/09613218.2021.1953369.
- [59] T. Ashour, H. Wieland, H. Georg, F. J. Bockisch, and W. Wu, "The influence of natural reinforcement fibres on insulation values of earth plaster for straw bale buildings," *Mater. Des.*, vol. 31, no. 10, pp. 4676–4685, 2010, doi: 10.1016/j.matdes.2010.05.026.
- [60] A. Khaksar, A. Tabadkani, S. M. Mofidi Shemirani, A. Hajirasouli, S. Banihashemi, and S. Attia, "Thermal comfort analysis of earth-sheltered buildings: The case of meymand village, Iran," *Front. Archit. Res.*, no. xxxx, 2022, doi: 10.1016/j.foar.2022.04.008.
- [61] B. V. Venkatarama Reddy, G. Leuzinger, and V. S. Sreeram, "Low embodied energy cement stabilised rammed earth building - A case study," *Energy Build.*, vol. 68, no. PARTA, pp. 541–546, 2014, doi: 10.1016/j.enbuild.2013.09.051.
- [62] E. Hamard, B. Cazacliu, A. Razakamanantsoa, and J. C. Morel, "Cob, a vernacular earth construction process in the context of modern sustainable building," *Build. Environ.*, vol. 106, pp. 103–119, 2016, doi: 10.1016/j.buildenv.2016.06.009.
- [63] N. Chettri, D. Gautam, S. Chikermane, V. Prakash, and K. Vaghela, "Sustainability assessment of Bhutanese vernacular wattle and daub houses," *Innov. Infrastruct.*

Solut., vol. 6, no. 4, 2021, doi: 10.1007/s41062-021-00576-z.

- [64] I. I. Obianyo *et al.*, "Production and utilization of earth-based bricks for sustainable building applications in Nigeria: status, benefits, challenges and way forward," *J. Build. Pathol. Rehabil.*, vol. 6, no. 1, pp. 1–11, 2021, doi: 10.1007/s41024-021-00131-4.
- [65] H. Niroumand, M. F. M. Zain, and S. N. Alhosseini, "The Influence of Nano-clays on Compressive Strength of Earth Bricks as Sustainable Materials," *Procedia - Soc. Behav. Sci.*, vol. 89, pp. 862–865, 2013, doi: 10.1016/j.sbspro.2013.08.945.
- [66] C. Costa, Â. Cerqueira, F. Rocha, and A. Velosa, "The sustainability of adobe construction: past to future," *Int. J. Archit. Herit.*, vol. 13, no. 5, pp. 639–647, 2019, doi: 10.1080/15583058.2018.1459954.
- [67] C. Dico and G. Călăţan, "Construction Sustainability With Adobe Bricks," *Urban. Arhit. Construcţii*, vol. 7, no. 2, pp. 147–157, 2016.
- [68] D. G. Leo Samuel, K. Dharmasastha, S. M. Shiva Nagendra, and M. P. Maiya, "Thermal comfort in traditional buildings composed of local and modern construction materials," *Int. J. Sustain. Built Environ.*, vol. 6, no. 2, pp. 463–475, 2017, doi: 10.1016/j.ijbe.2017.08.001.
- [69] A. S. Dili, M. A. Naseer, and T. Z. Varghese, "Thermal comfort study of Kerala traditional residential buildings based on questionnaire survey among occupants of traditional and modern buildings," *Energy Build.*, vol. 42, no. 11, pp. 2139–2150, 2010, doi: 10.1016/j.enbuild.2010.07.004.
- [70] C. Xu, S. Li, X. Zhang, and S. Shao, "Thermal comfort and thermal adaptive behaviours in traditional dwellings: A case study in Nanjing, China," *Build. Environ.*, vol. 142, no. May, pp. 153–170, 2018, doi: 10.1016/j.buildenv.2018.06.006.
- [71] M. K. Nematchoua, R. Tchinda, and J. A. Orosa, "Thermal comfort and energy consumption in modern versus traditional buildings in Cameroon: A questionnaire-based statistical study," *Appl. Energy*, vol. 114, pp. 687–699, 2014, doi: 10.1016/j.apenergy.2013.10.036.
- [72] M. K. Nematchoua, P. Ricciardi, and C. Buratti, "Adaptive approach of thermal comfort and correlation between experimental data and mathematical model in some schools and traditional buildings of Madagascar under natural ventilation,"

- Sustain. Cities Soc.*, vol. 41, no. October 2017, pp. 666–678, 2018, doi: 10.1016/j.scs.2017.11.029.
- [73] G. Desogus, S. Di Benedetto, and R. Ricciu, “The use of adaptive thermal comfort models to evaluate the summer performance of a Mediterranean earth building,” *Energy Build.*, vol. 104, pp. 350–359, 2015, doi: 10.1016/j.enbuild.2015.07.020.
- [74] M. Palme, J. Guerra, and S. Alfaro, “Thermal performance of traditional and new concept houses in the ancient village of San Pedro de Atacama and surroundings,” *Sustain.*, vol. 6, no. 6, pp. 3321–3337, 2014, doi: 10.3390/su6063321.
- [75] W. Cheikhi, K. Baba, S. M. Lamrani, A. Nounah, M. Khalfaoui, and L. Bahi, “Study of indoor performances of a building using Rammed earth,” *MATEC Web Conf.*, vol. 149, pp. 1–5, 2018, doi: 10.1051/mateconf/201714902089.
- [76] D. Nwalusi, C. Chukwuali, M. U. Nwachukwu, and H. Chike, “Analysis of Thermal Comfort in Traditional Residential Buildings in Nigeria Planning practice View project Housing research View project,” no. May, 2019, doi: 10.5281/zenodo.3234516.
- [77] O. S. Ogunrin, “A parametric analysis of the thermal properties of contemporary materials used for house construction in South-west Nigeria, using thermal modelling and relevant ...,” vol. 2, no. March, 2019, [Online]. Available: <https://livrepository.liverpool.ac.uk/3034534/>
- [78] C. Croft, “Structural resistance of earthbag housing subject to horizontal loading,” The University of Bath, 2011. [Online]. Available: <http://www.earthbagbuilding.com/pdf/croft.pdf>
- [79] S. Canadell, A. Blanco, and S. H. P. Cavalaro, “Comprehensive design method for earthbag and superadobe structures,” *Mater. Des.*, vol. 96, pp. 270–282, 2016, doi: 10.1016/j.matdes.2016.02.028.
- [80] Cal-Earth, “Our founder,” *CalEarth California institute of Earth Architecture*. <https://www.calearth.org/our-founder> (accessed May 18, 2020).
- [81] G. Owen, “Green Retaining Walls,” *Geosynthetics Magazine*, 2010.
- [82] CalEarth, “Our Founder,” *California Insitute of Earth Architecture*, 2021. <https://www.calearth.org/our-founder> (accessed Sep. 20, 2021).
- [83] B. Ross, M. Willis, P. Datin, and R. Scott, “Wind Load Test of Earthbag Wall,” *Buildings*,

- vol. 3, no. 3, pp. 532–544, 2013, doi: 10.3390/buildings3030532.
- [84] D. M. dos Santos and J. N. D. C. Beirão, “Generative tool to support architectural design decision of earthbag building domes,” pp. 538–543, 2017, doi: 10.5151/sigradi2017-083.
- [85] O. Geiger, *Earthbag building guide: VERTICAL WALLS STEP-BY-STEP*. 2011.
- [86] D. M. Santos and J. N. D. C. Beirão, “Data Collection and Constructive Classification of Superadobe Buildings,” *Ciência e Sustentabilidade*, vol. 2, no. 2, p. 208, 2016, doi: 10.33809/2447-4606.222016208-226.
- [87] O. Article, “A Study on Eco Friendly Cost Effective Earthbag House,” vol. 1, no. 5, pp. 1–11, 2013.
- [88] N. Belofsky and K. Zemskova, “Bringing Earthbags to the People – A New, Democratic Approach to Sustainable Building,” *Consilience*, vol. 19, no. 19, pp. 82–102, 2018, [Online]. Available: <http://www.jstor.org/stable/26427714>
- [89] B. Cioruța and M. Coman, “Beyond the Construction, Design and Planning Scenarios of Eco-Buildings,” *Asian J. Adv. Res. Reports*, vol. 2, no. 2, pp. 1–13, 2018, doi: 10.9734/ajarr/2018/v2i229742.
- [90] S. Patti, “Soil for Earthbag part I: Test Soils,” 2011.
- [91] K. Hart, *Essential earthbag construction the complete step-by-step guide*. 2018.
- [92] B. C. Daigle, “Earthbag housing: structural behaviour and applicability in developing countries,” Queen’s University Kingston, 2008.
- [93] B. Daigle, K. Hall, and C. MacDougall, “Earthbag housing: Structural behaviour and applicability in Sri Lanka,” *Proc. Inst. Civ. Eng. Eng. Sustain.*, vol. 164, no. 4, pp. 261–273, 2011, doi: 10.1680/ensu.2011.164.4.261.
- [94] D. K. Kaki Hunter, “Earthbag Building : The Tools , Tricks and Techniques”.
- [95] D. A. Rodriguez, J. Stein, and T. Darby, “Cyclic Testing of Reinforced Earthbag Walls,” 2018, [Online]. Available: https://scholarcommons.scu.edu/ceng_senior/68/
- [96] P. Wojciechowska, *Building with earth: a guide to flexible-form earthbag construction.*, no. March. 2001.
- [97] P. Stouter, O. Geiger, and K. Hart, “Choosing transitional house plans for hazard

- areas," *Earthbag Build.*, 2010, [Online]. Available:
<http://www.earthbagstructures.com/PDFs/ChoosingHousePlans.pdf>
- [98] K. Hunter and D. Kiffmeyer, *Earthbag Building: The Tools, Tricks and Techniques*. 2004.
- [99] B. Cioruța and M. Coman, "Beyond the Construction, Design and Planning Scenarios of Eco-Buildings," *Asian J. Adv. Res. Reports*, no. October, pp. 1–13, 2018, doi: 10.9734/ajarr/2018/v2i229742.
- [100] L. Rincón, A. Carrobé, I. Martorell, and M. Medrano, "Improving thermal comfort of earthen dwellings in sub-Saharan Africa with passive design," *J. Build. Eng.*, vol. 24, no. April, p. 100732, 2019, doi: 10.1016/j.jobbe.2019.100732.
- [101] M. Derek, "How to Build an Earthbag Home for \$11.50 Per Square Foot," 2018. <https://www.treehugger.com/how-build-earthbag-home-square-foot-4858138> (accessed Nov. 12, 2021).
- [102] H. Rose, H. Hassan, J. Amanda, and P. Jeff, "Green Building in Haiti," Haiti, 2010.
- [103] P. Stouter, "SHEAR STRENGTH OF EARTHBAG WALL WITH WEAK COHESIVE FILL," no. August, pp. 1–16, 2011.
- [104] P. STOUTER, "Soil Test for Earthbag," 2010.
- [105] U. Desideri, S. Proietti, P. Sdringola, and E. Vuillermoz, "Feasibility study and design of a low-energy residential unit in Sagarmatha park for environmental impact reduction of high altitude buildings," *Proc. 25th Int. Conf. Effic. Cost, Optim. Simul. Energy Convers. Syst. Process. ECOS 2012*, vol. 7, pp. 173–185, 2012.
- [106] T. H. Schwartz, "The Appropriateness of Earthbag Construction for the Dusun Tribe in Sabah , Malaysia," no. April, 2013.
- [107] P. Ralph, "Plastic limit analysis of earthbag structures," University of Bath, 2009.
- [108] S. Patti and Associates Wycliffe, "FRICTION AND TENSILE STRENGTH OF EARTHBAG COMPONENTS," 2010.
- [109] N. Strong, E. Jensen, and E. Huebner-Schurch, "Analysis of Structural Components During Cyclical Loading of Steel Reinforced Earthbag Construction," SANTA CLARA UNIVERSITY, 2018. [Online]. Available:
https://scholarcommons.scu.edu/cgi/viewcontent.cgi?article=1062&context=ceng_se

nior

- [110] B. Barnes, H. Cao, T. Drab, and J. Pearson, "Design of sustainable relief housing in Ethiopia: An implementation of cradle to cradle design in earthbag construction," *Am. J. Environ. Sci.*, vol. 5, no. 2, pp. 137–144, 2009, doi: 10.3844/ajessp.2009.137.144.
- [111] S. Ahmed *et al.*, "A proposed sandbag housing unit for poor and disadvantaged areas," *Proceedings, Annu. Conf. - Can. Soc. Civ. Eng.*, vol. 2017-May, pp. 35–44, 2017.
- [112] M. Venkateswarulu, K. Suresh, and G. Ashok, "Establishment of Low Cost Homes Using Super Adobe Technology," *IOSR J. Mech. Civ. Eng.*, vol. 16, no. 053, pp. 82–83, 2016, doi: 10.9790/1684-16053018083.
- [113] P. Stouter, "Earthbag Building in the Humid Tropics : Simple Structures," no. June, pp. 1–30, 2011.
- [114] L. Rincón, A. Carrobé, M. Medrano, C. Solé, A. Castell, and I. Martorell, "Analysis of the thermal behavior of an earthbag building in Mediterranean continental climate: Monitoring and simulation," *Energies*, vol. 13, no. 1, 2019, doi: 10.3390/en13010162.
- [115] Z. Zhao, Q. Lu, and X. Jiang, "An Energy Efficient Building System Using Natural Resources - Superadobe System Research," *Procedia Eng.*, vol. 121, pp. 1179–1185, 2015, doi: 10.1016/j.proeng.2015.09.133.
- [116] R. Kamal and M. S. Rahman, "A study on feasibility of super adobe technology -an energy efficient building system using natural resources in Bangladesh," *IOP Conf. Ser. Earth Environ. Sci.*, vol. 143, no. 1, 2018, doi: 10.1088/1755-1315/143/1/012043.
- [117] M. Theodoridou, L. Kyriakou, and I. Ioannou, "PCM-enhanced Lime Plasters for Vernacular and Contemporary Architecture," *Energy Procedia*, vol. 97, pp. 539–545, 2016, doi: 10.1016/j.egypro.2016.10.070.
- [118] A. Eddhahak-Ouni, S. Drissi, J. Colin, J. Neji, and S. Care, "Experimental and multi-scale analysis of the thermal properties of Portland cement concretes embedded with microencapsulated Phase Change Materials (PCMs)," *Appl. Therm. Eng.*, vol. 64, no. 1–2, pp. 32–39, 2014, doi: 10.1016/j.applthermaleng.2013.11.050.
- [119] X. Huang, G. Alva, L. Liu, and G. Fang, "Preparation, characterization and thermal properties of fatty acid eutectics/bentonite/expanded graphite composites as novel form–stable thermal energy storage materials," *Sol. Energy Mater. Sol. Cells*, vol. 166,

- no. March, pp. 157–166, 2017, doi: 10.1016/j.solmat.2017.03.026.
- [120] Y. P. Zhang, K. P. Lin, R. Yang, H. F. Di, and Y. Jiang, “Preparation, thermal performance and application of shape-stabilized PCM in energy efficient buildings,” *Energy Build.*, vol. 38, no. 10, pp. 1262–1269, 2006, doi: 10.1016/j.enbuild.2006.02.009.
- [121] Z. Qunli, Y. Chaohui, L. Yinlong, and D. Hongfa, “Simulation Research on the Thermal Performance of the Cooling Ceiling Embedded with Phase Change Material for Energy Storage,” *Energy Procedia*, vol. 105, pp. 2575–2582, 2017, doi: 10.1016/j.egypro.2017.03.740.
- [122] K. Peippo, P. Kauranen, and P. D. Lund, “A multicomponent PCM wall optimized for passive solar heating,” *Energy Build.*, vol. 17, no. 4, pp. 259–270, 1991, doi: 10.1016/0378-7788(91)90009-R.
- [123] S. Ramakrishnan, K. Pasupathy, and J. Sanjayan, “Synthesis and properties of thermally enhanced aerated geopolymer concrete using form-stable phase change composite,” *J. Build. Eng.*, vol. 40, no. February, p. 102756, 2021, doi: 10.1016/j.jobee.2021.102756.
- [124] S. A. Memon, “Phase change materials integrated in building walls: A state of the art review,” *Renew. Sustain. Energy Rev.*, vol. 31, pp. 870–906, 2014, doi: 10.1016/j.rser.2013.12.042.
- [125] V. V. Tyagi and D. Buddhi, “PCM thermal storage in buildings: A state of art,” *Renew. Sustain. Energy Rev.*, vol. 11, no. 6, pp. 1146–1166, 2007, doi: 10.1016/j.rser.2005.10.002.
- [126] P. Arce Maldonado, “Application of passive thermal energy storage in buildings using PCM and awnings,” *Chem. Eng. Sci.*, vol. 60, no. 6, pp. 1535–1553, 2011, doi: 10.1016/j.ces.2004.10.023.
- [127] K. Menoufi, A. Castell, M. M. Farid, D. Boer, and L. F. Cabeza, “Life Cycle Assessment of experimental cubicles including PCM manufactured from natural resources (esters): A theoretical study,” *Renew. Energy*, vol. 51, pp. 398–403, 2013, doi: 10.1016/j.renene.2012.10.010.
- [128] M. K. Rathod, “Thermal Stability of Phase Change Material,” in *Phase Change Materials and Their Applications*, 2018. doi: 10.5772/intechopen.75923.

- [129] C. Barrenechea, H. Navarro, S. Serrano, L. F. Cabeza, and A. I. Fernández, “New database on phase change materials for thermal energy storage in buildings to help PCM selection,” *Energy Procedia*, vol. 57, pp. 2408–2415, 2014, doi: 10.1016/j.egypro.2014.10.249.
- [130] R. K. Sharma, P. Ganesan, V. V. Tyagi, H. S. C. Metselaar, and S. C. Sandaran, “Developments in organic solid-liquid phase change materials and their applications in thermal energy storage,” *Energy Convers. Manag.*, vol. 95, pp. 193–228, 2015, doi: 10.1016/j.enconman.2015.01.084.
- [131] M. Ozdenefe and J. Dewsbury, “Thermal performance of a typical residential Cyprus building with phase change materials,” *Build. Serv. Eng. Res. Technol.*, vol. 37, no. 1, pp. 85–102, 2016, doi: 10.1177/0143624415603004.
- [132] S. G. Jeong, S. Wi, S. J. Chang, J. Lee, and S. Kim, “An experimental study on applying organic PCMs to gypsum-cement board for improving thermal performance of buildings in different climates,” *Energy Build.*, vol. 190, pp. 183–194, 2019, doi: 10.1016/j.enbuild.2019.02.037.
- [133] L. Fan and J. M. Khodadadi, “Thermal conductivity enhancement of phase change materials for thermal energy storage: A review,” *Renew. Sustain. Energy Rev.*, vol. 15, no. 1, pp. 24–46, 2011, doi: 10.1016/j.rser.2010.08.007.
- [134] Z. A. Qureshi, H. M. Ali, and S. Khushnood, “Recent advances on thermal conductivity enhancement of phase change materials for energy storage system: A review,” *Int. J. Heat Mass Transf.*, vol. 127, pp. 838–856, 2018, doi: 10.1016/j.ijheatmasstransfer.2018.08.049.
- [135] S. Ramakrishnan, X. Wang, and J. Sanjayan, “Thermal enhancement of paraffin/hydrophobic expanded perlite granular phase change composite using graphene nanoplatelets,” *Energy Build.*, vol. 169, pp. 206–215, 2018, doi: 10.1016/j.enbuild.2018.03.053.
- [136] S. Wu, T. Yan, Z. Kuai, and W. Pan, “Thermal conductivity enhancement on phase change materials for thermal energy storage: A review,” *Energy Storage Mater.*, vol. 25, no. April 2019, pp. 251–295, 2020, doi: 10.1016/j.ensm.2019.10.010.
- [137] K. Acurio, A. Chico-Proano, J. Martínez-Gómez, C. F. Ávila, Á. Ávila, and M. Orozco, “Thermal performance enhancement of organic phase change materials using spent

- diatomite from the palm oil bleaching process as support,” *Constr. Build. Mater.*, vol. 192, pp. 633–642, 2018, doi: 10.1016/j.conbuildmat.2018.10.148.
- [138] O. Chung, S. G. Jeong, S. Yu, and S. Kim, “Thermal performance of organic PCMs/micronized silica composite for latent heat thermal energy storage,” *Energy Build.*, vol. 70, pp. 180–185, 2014, doi: 10.1016/j.enbuild.2013.11.055.
- [139] B. Lamrani, K. Johannes, and F. Kuznik, “Phase change materials integrated into building walls: An updated review,” *Renew. Sustain. Energy Rev.*, vol. 140, no. June 2020, p. 110751, 2021, doi: 10.1016/j.rser.2021.110751.
- [140] K. Pielichowska and K. Pielichowski, “Phase change materials for thermal energy storage,” *Prog. Mater. Sci.*, vol. 65, pp. 67–123, 2014, doi: 10.1016/j.pmatsci.2014.03.005.
- [141] P. Dixit *et al.*, “Salt hydrate phase change materials: Current state of art and the road ahead,” *J. Energy Storage*, vol. 51, no. November 2021, p. 104360, 2022, doi: 10.1016/j.est.2022.104360.
- [142] Y. Sheikh, M. Gadalla, M. Umair, E. Mehaisi, and A. Azmeer, “Effect of adding graphene nano-platelets with surfactants on biobased PCM characteristics and its cooling performance,” *ASME Int. Mech. Eng. Congr. Expo. Proc.*, vol. 11, pp. 1–8, 2020, doi: 10.1115/IMECE2020-24373.
- [143] S. Agarwala and K. N. Prabhu, “Review of thermal characterization techniques for salt-based phase change materials,” *J. Energy Storage*, vol. 46, no. November 2021, p. 103865, 2022, doi: 10.1016/j.est.2021.103865.
- [144] S. Sarkar, S. Mestry, and S. T. Mhaske, “Developments in phase change material (PCM) doped energy efficient polyurethane (PU) foam for perishable food cold-storage applications: A review,” *J. Energy Storage*, vol. 50, no. April, p. 104620, 2022, doi: 10.1016/j.est.2022.104620.
- [145] M. F. Junaid *et al.*, “Inorganic phase change materials in thermal energy storage: A review on perspectives and technological advances in building applications,” *Energy Build.*, vol. 252, 2021, doi: 10.1016/j.enbuild.2021.111443.
- [146] B. K. Purohit and V. S. Sistla, “Inorganic salt hydrate for thermal energy storage application: A review,” *Energy Storage*, vol. 3, no. 2, pp. 1–26, 2021, doi: 10.1002/est2.212.

- [147] A. S. Cabeça, “Experimental of the thermal energy storage through the utilization of Phase Change Materials (PCM) in an office room Energy Engineering and Management Examination Committee Experimental of the thermal energy storage through the utilization of Phase Chan,” no. June, pp. 1–10, 2018.
- [148] S. I. Hussain, R. Dinesh, A. A. Roseline, S. Dhivya, and S. Kalaiselvam, “Enhanced thermal performance and study the influence of sub cooling on activated carbon dispersed eutectic PCM for cold storage applications,” *Energy Build.*, vol. 143, pp. 17–24, 2017, doi: 10.1016/j.enbuild.2017.03.011.
- [149] R. Ye, H. Jiang, J. Wang, X. Yang, and X. Shu, “Fabrication and characteristics of eutectic hydrated salts/fumed silica composite as form-stable phase change materials for thermal energy storage,” *Sol. Energy Mater. Sol. Cells*, vol. 238, no. June 2021, p. 111584, 2022, doi: 10.1016/j.solmat.2022.111584.
- [150] P. Singh, R. K. Sharma, A. K. Ansu, R. Goyal, A. Sari, and V. V. Tyagi, “A comprehensive review on development of eutectic organic phase change materials and their composites for low and medium range thermal energy storage applications,” *Sol. Energy Mater. Sol. Cells*, vol. 223, no. January, p. 110955, 2021, doi: 10.1016/j.solmat.2020.110955.
- [151] M. K. Rathod and J. Banerjee, “Thermal stability of phase change materials used in latent heat energy storage systems: A review,” *Renew. Sustain. Energy Rev.*, vol. 18, pp. 246–258, 2013, doi: 10.1016/j.rser.2012.10.022.
- [152] R. D. Beltrán and J. Martínez-Gómez, “Analysis of phase change materials (PCM) for building wallboards based on the effect of environment,” *J. Build. Eng.*, vol. 24, no. December 2017, p. 100726, 2019, doi: 10.1016/j.jobbe.2019.02.018.
- [153] A. F. Regin, S. C. Solanki, and J. S. Saini, “Heat transfer characteristics of thermal energy storage system using PCM capsules: A review,” *Renew. Sustain. Energy Rev.*, vol. 12, no. 9, pp. 2438–2458, 2008, doi: 10.1016/j.rser.2007.06.009.
- [154] K. Faraj, M. Khaled, J. Faraj, F. Hachem, and C. Castelain, “A review on phase change materials for thermal energy storage in buildings: Heating and hybrid applications,” *J. Energy Storage*, vol. 33, no. June 2020, p. 101913, 2021, doi: 10.1016/j.est.2020.101913.
- [155] K. Venkateswarlu and K. Ramakrishna, “Recent advances in phase change materials

- for thermal energy storage-a review," *J. Brazilian Soc. Mech. Sci. Eng.*, vol. 44, no. 1, pp. 1–17, 2022, doi: 10.1007/s40430-021-03308-7.
- [156] L. Dash, "A review on organic phase change materials and their applications," vol. 5, no. 9, pp. 268–284, 2021.
- [157] V. V. Tyagi *et al.*, "A comprehensive review on phase change materials for heat storage applications: Development, characterization, thermal and chemical stability," *Sol. Energy Mater. Sol. Cells*, vol. 234, no. July 2021, p. 111392, 2022, doi: 10.1016/j.solmat.2021.111392.
- [158] N. Kumar, P. Kumar, S. Rathore, R. K. Sharma, and N. Kumar, "Integration of lauric acid / zeolite / graphite as shape stabilized composite phase change material in gypsum for enhanced thermal energy storage in buildings," *Appl. Therm. Eng.*, vol. 224, no. January, p. 120088, 2023, doi: 10.1016/j.applthermaleng.2023.120088.
- [159] S. Hasanabadi, S. M. Sadrameli, H. Soheili, H. Moharrami, and M. M. Heyhat, "A cost-effective form-stable PCM composite with modified paraffin and expanded perlite for thermal energy storage in concrete," *J. Therm. Anal. Calorim.*, vol. 136, no. 3, pp. 1201–1216, 2019, doi: 10.1007/s10973-018-7731-8.
- [160] Y. Liu, E. Xu, M. Xie, X. Gao, Y. Yang, and H. Deng, "Use of calcium silicate-coated paraffin/expanded perlite materials to improve the thermal performance of cement mortar," *Constr. Build. Mater.*, vol. 189, pp. 218–226, 2018, doi: 10.1016/j.conbuildmat.2018.08.213.
- [161] B. Xu, H. Ma, Z. Lu, and Z. Li, "Paraffin/expanded vermiculite composite phase change material as aggregate for developing lightweight thermal energy storage cement-based composites," *Appl. Energy*, vol. 160, pp. 358–367, 2015, doi: 10.1016/j.apenergy.2015.09.069.
- [162] A. Karaipekli and A. Sari, "Capric-myristic acid/expanded perlite composite as form-stable phase change material for latent heat thermal energy storage," *Renew. Energy*, vol. 33, no. 12, pp. 2599–2605, 2008, doi: 10.1016/j.renene.2008.02.024.
- [163] M. Amin, N. Putra, E. A. Kosasih, E. Prawiro, R. A. Luanto, and T. M. I. Mahlia, "Thermal properties of beeswax/graphene phase change material as energy storage for building applications," *Appl. Therm. Eng.*, vol. 112, pp. 273–280, 2017, doi: 10.1016/j.applthermaleng.2016.10.085.

- [164] L. Jiesheng, L. Faping, G. Xiaoqiang, and Z. Rongtang, "Experimental research in the phase change materials based on paraffin and expanded perlite," *Phase Transitions*, vol. 91, no. 6, pp. 631–637, 2018, doi: 10.1080/01411594.2018.1424338.
- [165] B. He, V. Martin, and F. Setterwall, "Phase transition temperature ranges and storage density of paraffin wax phase change materials," *Energy*, vol. 29, no. 11, pp. 1785–1804, 2004, doi: 10.1016/j.energy.2004.03.002.
- [166] J. Yoo, S. J. Chang, S. Wi, and S. Kim, "Spent coffee grounds as supporting materials to produce bio-composite PCM with natural waxes," *Chemosphere*, vol. 235, pp. 626–635, 2019, doi: 10.1016/j.chemosphere.2019.06.195.
- [167] J. M. P. P. da Cunha, "Phase change materials , systems and applications for low and medium temperature thermal energy storage," Loughborough University, 2018.
- [168] L. Boussaba, S. Makhlof, A. Foufa, G. Lefebvre, and L. Royon, "vegetable fat: A low-cost bio-based phase change material for thermal energy storage in buildings," *J. Build. Eng.*, vol. 21, no. October 2018, pp. 222–229, 2019, doi: 10.1016/j.job.2018.10.022.
- [169] X. Zhang *et al.*, "Enhancement of thermal conductivity by the introduction of carbon nanotubes as a filler in paraffin/expanded perlite form-stable phase-change materials," *Energy Build.*, vol. 149, pp. 463–470, 2017, doi: 10.1016/j.enbuild.2017.05.037.
- [170] F. Cheng *et al.*, "Thermal conductivity enhancement of form-stable tetradecanol/expanded perlite composite phase change materials by adding Cu powder and carbon fiber for thermal energy storage," *Appl. Therm. Eng.*, vol. 156, no. 29, pp. 653–659, 2019, doi: 10.1016/j.applthermaleng.2019.03.140.
- [171] X. Zuo, X. Zhao, J. Li, Y. Hu, H. Yang, and D. Chen, "Enhanced thermal conductivity of form-stable composite phase-change materials with graphite hybridizing expanded perlite/paraffin," *Sol. Energy*, vol. 209, no. February, pp. 85–95, 2020, doi: 10.1016/j.solener.2020.08.082.
- [172] R. Li *et al.*, "Enhanced thermal conductivity of composite phase change materials based on carbon modified expanded perlite," *Mater. Chem. Phys.*, vol. 261, no. December 2020, p. 124226, 2021, doi: 10.1016/j.matchemphys.2021.124226.
- [173] Y. Bian, K. Wang, J. Wang, Y. Yu, M. Liu, and Y. Lv, "Preparation and properties of

- capric acid: Stearic acid/hydrophobic expanded perlite-aerogel composite phase change materials," *Renew. Energy*, vol. 179, pp. 1027–1035, 2021, doi: 10.1016/j.renene.2021.07.125.
- [174] D. Sun, L. Wang, and C. Li, "Preparation and thermal properties of paraffin/expanded perlite composite as form-stable phase change material," *Mater. Lett.*, vol. 108, pp. 247–249, 2013, doi: 10.1016/j.matlet.2013.06.105.
- [175] C. Yao, X. Kong, Y. Li, Y. Du, and C. Qi, "Numerical and experimental research of cold storage for a novel expanded perlite-based shape-stabilized phase change material wallboard used in building," *Energy Convers. Manag.*, vol. 155, no. October 2017, pp. 20–31, 2018, doi: 10.1016/j.enconman.2017.10.052.
- [176] P. Dixit, J. R. Vennapusa, S. Parvate, J. Singh, A. Dasari, and S. Chattopadhyay, "Thermal Buffering Performance of a Propyl Palmitate/Expanded Perlite-Based Form-Stable Composite: Experiment and Numerical Modeling in a Building Model," *Energy and Fuels*, vol. 35, no. 3, pp. 2704–2716, 2021, doi: 10.1021/acs.energyfuels.0c03553.
- [177] C. Liu, C. Luo, T. Xu, P. Lv, and Z. Rao, "Experimental study on the thermal performance of capric acid-myristyl alcohol/expanded perlite composite phase change materials for thermal energy storage," *Sol. Energy*, vol. 191, no. September, pp. 585–595, 2019, doi: 10.1016/j.solener.2019.09.049.
- [178] Z. Liu *et al.*, "Paraffin/red mud phase change energy storage composite incorporated gypsum-based and cement-based materials: Microstructures, thermal and mechanical properties," *J. Hazard. Mater.*, vol. 364, no. July 2018, pp. 608–620, 2019, doi: 10.1016/j.jhazmat.2018.10.061.
- [179] T. Gurmen Ozcelik, "Preparation, characterization and thermal properties of paraffin wax - Expanded perlite form-stable composites for latent heat storage," *Medziagotyra*, vol. 23, no. 1, pp. 39–43, 2017, doi: 10.5755/j01.ms.23.1.13661.
- [180] I. Asadi, P. Shafigh, Z. F. Bin Abu Hassan, and N. B. Mahyuddin, "Thermal conductivity of concrete – A review," *J. Build. Eng.*, vol. 20, pp. 81–93, 2018, doi: 10.1016/j.jobe.2018.07.002.
- [181] N. Mekaddem, S. Ben Ali, M. Fois, and A. Hannachi, "Paraffin/expanded perlite/plaster as thermal energy storage composite," *Energy Procedia*, vol. 157, pp. 1118–1129, 2019, doi: 10.1016/j.egypro.2018.11.279.

- [182] P. Cheng *et al.*, “Different dimensional nanoadditives for thermal conductivity enhancement of phase change materials: Fundamentals and applications,” *Nano Energy*, vol. 85, no. February, p. 105948, 2021, doi: 10.1016/j.nanoen.2021.105948.
- [183] A. Sari *et al.*, “Capric-stearic acid mixture impregnated carbonized waste sugar beet pulp as leak-resistive composite phase change material with effective thermal conductivity and thermal energy storage performance,” *Energy*, vol. 247, 2022, doi: 10.1016/j.energy.2022.123501.
- [184] Z. Rao, T. Xu, C. Liu, Z. Zheng, L. Liang, and K. Hong, “Experimental study on thermal properties and thermal performance of eutectic hydrated salts/expanded perlite form-stable phase change materials for passive solar energy utilization,” *Sol. Energy Mater. Sol. Cells*, vol. 188, no. May, pp. 6–17, 2018, doi: 10.1016/j.solmat.2018.08.012.
- [185] S. Ramakrishnan, X. Wang, and J. Sanjayan, “Effects of various carbon additives on the thermal storage performance of form-stable PCM integrated cementitious composites,” *Appl. Therm. Eng.*, vol. 148, no. November 2018, pp. 491–501, 2019, doi: 10.1016/j.applthermaleng.2018.11.025.
- [186] P. K. S. Rathore, S. K. Shukla, and N. K. Gupta, “Synthesis and characterization of the paraffin/expanded perlite loaded with graphene nanoparticles as a thermal energy storage material in buildings,” *J. Sol. Energy Eng. Trans. ASME*, vol. 142, no. 4, pp. 1–8, 2020, doi: 10.1115/1.4046087.
- [187] J. Huang *et al.*, “An innovative phase change composite with high thermal conductivity and sensitive light response rate for thermal energy storage,” *Sol. Energy Mater. Sol. Cells*, vol. 245, no. June, p. 111872, 2022, doi: 10.1016/j.solmat.2022.111872.
- [188] A. Ricklefs, A. M. Thiele, G. Falzone, G. Sant, and L. Pilon, “Thermal conductivity of cementitious composites containing microencapsulated phase change materials,” *Int. J. Heat Mass Transf.*, vol. 104, pp. 71–82, 2017, doi: 10.1016/j.ijheatmasstransfer.2016.08.013.
- [189] H. Chen *et al.*, “Thermal conductivity of polymer-based composites: Fundamentals and applications,” *Prog. Polym. Sci.*, vol. 59, pp. 41–85, 2016, doi: 10.1016/j.progpolymsci.2016.03.001.

- [190] I. I. Hakim, N. Putra, and P. D. Agustin, "Measurement of PCM-concrete composites thermal properties for energy conservation in building material," in *AIP Conference Proceedings*, 2020, vol. 2255, no. September. doi: 10.1063/5.0014120.
- [191] V. D. Cao *et al.*, "Microencapsulated phase change materials for enhancing the thermal performance of Portland cement concrete and geopolymer concrete for passive building applications," *Energy Convers. Manag.*, vol. 133, pp. 56–66, 2017, doi: 10.1016/j.enconman.2016.11.061.
- [192] C. Li, H. Yu, and Y. Song, "Experimental investigation of thermal performance of microencapsulated PCM-contained wallboard by two measurement modes," *Energy Build.*, vol. 184, pp. 34–43, 2019, doi: 10.1016/j.enbuild.2018.11.032.
- [193] P. K. Dehdezi, M. R. Hall, A. R. Dawson, and S. P. Casey, "Thermal, mechanical and microstructural analysis of concrete containing microencapsulated phase change materials," *Int. J. Pavement Eng.*, vol. 14, no. 5, pp. 449–462, 2013, doi: 10.1080/10298436.2012.716837.
- [194] A. Jayalath *et al.*, "Properties of cementitious mortar and concrete containing micro-encapsulated phase change materials," *Constr. Build. Mater.*, vol. 120, pp. 408–417, 2016, doi: 10.1016/j.conbuildmat.2016.05.116.
- [195] P. Rolka, T. Przybylinski, R. Kwidzinski, and M. Lackowski, "Thermal properties of RT22 HC and RT28 HC phase change materials proposed to reduce energy consumption in heating and cooling systems," *Renew. Energy*, vol. 197, no. January, pp. 462–471, 2022, doi: 10.1016/j.renene.2022.07.080.
- [196] M. Campanale and L. Moro, "Thermal Conductivity of Moist Autoclaved Aerated Concrete: Experimental Comparison Between Heat Flow Method (HFM) and Transient Plane Source Technique (TPS)," *Transp. Porous Media*, vol. 113, no. 2, pp. 345–355, 2016, doi: 10.1007/s11242-016-0697-8.
- [197] T. Ruuska, J. Vinha, and H. Kivioja, "Measuring thermal conductivity and specific heat capacity values of inhomogeneous materials with a heat flow meter apparatus," *J. Build. Eng.*, vol. 9, no. November 2015, pp. 135–141, 2017, doi: 10.1016/j.jobe.2016.11.011.
- [198] Y. Abdellatef and M. Kavgic, "Thermal, microstructural and numerical analysis of hempcrete-microencapsulated phase change material composites," *Appl. Therm.*

- Eng.*, vol. 178, no. May, p. 115520, 2020, doi: 10.1016/j.applthermaleng.2020.115520.
- [199] P. Sukontasukkul *et al.*, "Thermal properties of lightweight concrete incorporating high contents of phase change materials," *Constr. Build. Mater.*, vol. 207, pp. 431–439, 2019, doi: 10.1016/j.conbuildmat.2019.02.152.
- [200] M. Ahmad, R. N. S. Al-Dala'ien, S. Beddu, and Z. B. Itam, "Thermo-physical Properties of Graphite Powder and Polyethylene Modified Asphalt Concrete," *Eng. Sci.*, vol. 17, pp. 121–132, 2022, doi: 10.30919/es8d569.
- [201] P. Sukontasukkul *et al.*, "Thermal storage properties of lightweight concrete incorporating phase change materials with different fusion points in hybrid form for high temperature applications," *Heliyon*, vol. 6, no. 9, p. e04863, 2020, doi: 10.1016/j.heliyon.2020.e04863.
- [202] F. Alassaad, K. Touati, D. Levacher, and N. Sebaibi, "Impact of phase change materials on lightened earth hygroscopic, thermal and mechanical properties," *J. Build. Eng.*, vol. 41, no. November 2020, p. 102417, 2021, doi: 10.1016/j.job.2021.102417.
- [203] R. Ye, W. Lin, K. Yuan, X. Fang, and Z. Zhang, "Experimental and numerical investigations on the thermal performance of building plane containing CaCl₂·6H₂O/expanded graphite composite phase change material," *Appl. Energy*, vol. 193, pp. 325–335, 2017, doi: 10.1016/j.apenergy.2017.02.049.
- [204] S. Ramakrishnan, J. Sanjayan, X. Wang, M. Alam, and J. Wilson, "A novel paraffin/expanded perlite composite phase change material for prevention of PCM leakage in cementitious composites," *Appl. Energy*, vol. 157, pp. 85–94, 2015, doi: 10.1016/j.apenergy.2015.08.019.
- [205] M. A. Khalifa, "Application of phase change materials as a solution for building overheating : a case for the UK," 2013.
- [206] X. Wang, H. Yu, L. Li, and M. Zhao, "Research on temperature dependent effective thermal conductivity of composite-phase change materials (PCMs) wall based on steady-state method in a thermal chamber," *Energy Build.*, vol. 126, pp. 408–414, 2016, doi: 10.1016/j.enbuild.2016.05.058.
- [207] C. Guardia, G. Barluenga, and I. Palomar, "PCM cement-lime mortars for enhanced energy efficiency of multilayered building enclosures under different climatic

- conditions,” *Materials (Basel)*, vol. 13, no. 18, 2020, doi: 10.3390/ma13184043.
- [208] M. Prabhakar, M. Saffari, A. de Gracia, and L. F. Cabeza, “Improving the energy efficiency of passive PCM system using controlled natural ventilation,” *Energy Build.*, vol. 228, p. 110483, 2020, doi: 10.1016/j.enbuild.2020.110483.
- [209] H. Jamil, M. Alam, J. Sanjayan, and J. Wilson, “Investigation of PCM as retrofitting option to enhance occupant thermal comfort in a modern residential building,” *Energy Build.*, vol. 133, pp. 217–229, 2016, doi: 10.1016/j.enbuild.2016.09.064.
- [210] T. Xu, Q. Chen, Z. Zhang, X. Gao, and G. Huang, “Investigation on the properties of a new type of concrete blocks incorporated with PEG / SiO₂ composite phase change material,” *Build. Environ.*, vol. 104, pp. 172–177, 2016, doi: 10.1016/j.buildenv.2016.05.003.
- [211] M. Mahdaoui *et al.*, “Building bricks with phase change material (PCM): Thermal performances,” *Constr. Build. Mater.*, vol. 269, p. 121315, 2021, doi: 10.1016/j.conbuildmat.2020.121315.
- [212] A. Hasan, K. A. Al-Sallal, H. Alnoman, Y. Rashid, and S. Abdelbaqi, “Effect of phase change materials (PCMs) integrated into a concrete block on heat gain prevention in a hot climate,” *Sustain.*, vol. 8, no. 10, 2016, doi: 10.3390/su8101009.
- [213] N. B. Azmi and F. S. Khalid, “Thermal analysis of PCM integrated building blocks for passive cooling application Thermal analysis of PCM integrated building blocks for passive cooling application,” in *Materials Science and Engineering*, 2018, p. 376. doi: 10.1088/1757-899X/376/1/012015.
- [214] Y. Qu, J. Chen, L. Liu, T. Xu, H. Wu, and X. Zhou, “Study on properties of phase change foam concrete block mixed with paraffin / fumed silica composite phase change material,” *Renew. Energy*, vol. 150, pp. 1127–1135, 2020, doi: 10.1016/j.renene.2019.10.073.
- [215] Y. Shen *et al.*, “Experimental thermal study of a new PCM-concrete thermal storage block (PCM-CTSB),” *Constr. Build. Mater.*, vol. 293, p. 123540, 2021, doi: 10.1016/j.conbuildmat.2021.123540.
- [216] Q. Al-Yasiri and M. Szabó, “Effect of encapsulation area on the thermal performance of PCM incorporated concrete bricks: A case study under Iraq summer conditions,” *Case Stud. Constr. Mater.*, vol. 15, no. June, 2021, doi: 10.1016/j.cscm.2021.e00686.

- [217] H. Akeiber *et al.*, “A review on phase change material (PCM) for sustainable passive cooling in building envelopes,” *Renew. Sustain. Energy Rev.*, vol. 60, pp. 1470–1497, 2016, doi: 10.1016/j.rser.2016.03.036.
- [218] X. Jin, M. A. Medina, and X. Zhang, “Numerical analysis for the optimal location of a thin PCM layer in frame walls,” *Appl. Therm. Eng.*, vol. 103, pp. 1057–1063, 2016, doi: 10.1016/j.applthermaleng.2016.04.056.
- [219] L. F. Cabeza *et al.*, “Behaviour of a concrete wall containing micro-encapsulated PCM after a decade of its construction,” *Sol. Energy*, vol. 200, no. July 2018, pp. 108–113, 2020, doi: 10.1016/j.solener.2019.12.003.
- [220] B. Srinivasaraonaik, L. P. Singh, S. Sinha, I. Tyagi, and A. Rawat, “Studies on the mechanical properties and thermal behavior of microencapsulated eutectic mixture in gypsum composite board for thermal regulation in the buildings,” *J. Build. Eng.*, vol. 31, no. September 2019, p. 101400, 2020, doi: 10.1016/j.jobbe.2020.101400.
- [221] R. Vicente and T. Silva, “Brick masonry walls with PCM macrocapsules: An experimental approach,” *Appl. Therm. Eng.*, vol. 67, no. 1–2, pp. 24–34, 2014, doi: 10.1016/j.applthermaleng.2014.02.069.
- [222] A. Gounni and M. El Alami, “Experimental study of heat transfer in a reduced scale cavity incorporating phase change material into its vertical walls,” *J. Therm. Sci. Eng. Appl.*, vol. 10, no. 1, 2018, doi: 10.1115/1.4036794.
- [223] K. O. Lee, M. A. Medina, and X. Sun, “Development and verification of an EnergyPlus-based algorithm to predict heat transfer through building walls integrated with phase change materials,” *J. Build. Phys.*, vol. 40, no. 1, pp. 77–95, 2016, doi: 10.1177/1744259115591252.
- [224] Q. Wang, R. Wu, Y. Wu, and C. Y. Zhao, “Parametric analysis of using PCM walls for heating loads reduction,” *Energy Build.*, vol. 172, pp. 328–336, 2018, doi: 10.1016/j.enbuild.2018.05.012.
- [225] Z. X. Li, A. A. A. Al-Rashed, M. Rostamzadeh, R. Kalbasi, A. Shahsavari, and M. Afrand, “Heat transfer reduction in buildings by embedding phase change material in multi-layer walls: Effects of repositioning, thermophysical properties and thickness of PCM,” *Energy Convers. Manag.*, vol. 195, no. April, pp. 43–56, 2019, doi: 10.1016/j.enconman.2019.04.075.

- [226] N. Zhu, N. Hu, P. Hu, F. Lei, and S. Li, "Experiment study on thermal performance of building integrated with double layers shape-stabilized phase change material wallboard," *Energy*, vol. 167, pp. 1164–1180, 2019, doi: 10.1016/j.energy.2018.11.042.
- [227] M. Li, Q. Cao, H. Pan, X. Wang, and Z. Lin, "Effect of melting point on thermodynamics of thin PCM reinforced residential frame walls in different climate zones," *Appl. Therm. Eng.*, vol. 188, no. January, p. 116615, 2021, doi: 10.1016/j.applthermaleng.2021.116615.
- [228] M. Salihi *et al.*, "Evaluation of global energy performance of building walls integrating PCM: Numerical study in semi-arid climate in Morocco," *Case Stud. Constr. Mater.*, vol. 16, no. October 2021, p. e00979, 2022, doi: 10.1016/j.cscm.2022.e00979.
- [229] C. Sandra, C. André, J. Aguiar, and M. Francisco, "Compacted Earth Blocks Additivated with Phase Change Material," *Sci. Electron. Libr. Online*, vol. 2, p. 27, 2022.
- [230] S. Serrano, C. Barreneche, L. Rincón, D. Boer, and L. F. Cabeza, "Optimization of three new compositions of stabilized rammed earth incorporating PCM: Thermal properties characterization and LCA," *Constr. Build. Mater.*, vol. 47, pp. 872–878, 2013, doi: 10.1016/j.conbuildmat.2013.05.018.
- [231] Y. M'hamdi, K. Baba, M. Tajayouti, and A. Nounah, "Energy, environmental, and economic analysis of different buildings envelope integrated with phase change materials in different climates," *Sol. Energy*, vol. 243, no. July, pp. 91–102, 2022, doi: 10.1016/j.solener.2022.07.031.
- [232] A. Gounni and H. Louahlia, "Dynamic behavior and economic analysis of sustainable building integrating cob and phase change materials," *Constr. Build. Mater.*, vol. 262, p. 120795, 2020, doi: 10.1016/j.conbuildmat.2020.120795.
- [233] V. Toufigh and S. Samadianfard, "Experimental and numerical investigation of thermal enhancement methods on rammed-earth materials," *Sol. Energy*, vol. 244, no. August 2021, pp. 474–483, 2022, doi: 10.1016/j.solener.2022.08.049.
- [234] Z. Ben Zaid, A. Tilioua, I. Lamaamar, O. Ansari, H. Souli, and M. A. Hamdi Alaoui, "An experimental study of the efficacy of integrating a phase change material into a clay-straw wall in the Drâa-Tafilalet Region (Errachidia Province), Morocco," *J. Build. Eng.*, vol. 32, no. January, 2020, doi: 10.1016/j.job.2020.101670.

- [235] V. Toufigh and E. Kianfar, "The effects of stabilizers on the thermal and the mechanical properties of rammed earth at various humidities and their environmental impacts," *Constr. Build. Mater.*, vol. 200, pp. 616–629, 2019, doi: 10.1016/j.conbuildmat.2018.12.050.
- [236] P. Bannister, T. P. A. C., and S. M., "The Design and Control of a Building With Structurally Incorporated Phase Change Material," in *International Conference on Improving Energy Efficiency in Commercial Buildings: IE ECB Focus 2008*, 2008, vol. 2, no. April 2008, p. 372. doi: 10.2790/21625.
- [237] A. Batagarawa, "Assessing the thermal performance of phase change materials in composite hot humid / hot dry climates: An examination of office buildings in Abuja-Nigeria," 2013.
- [238] R. Saxena, D. Rakshit, and S. C. Kaushik, "Experimental assessment of Phase Change Material (PCM) embedded bricks for passive conditioning in buildings," *Renew. Energy*, vol. 149, pp. 587–599, 2020, doi: 10.1016/j.renene.2019.12.081.
- [239] M. Sovetova, S. A. Memon, and J. Kim, "Thermal performance and energy efficiency of building integrated with PCMs in hot desert climate region," *Sol. Energy*, vol. 189, no. April, pp. 357–371, 2019, doi: 10.1016/j.solener.2019.07.067.
- [240] Y. Shukla, R. Rawal, N. Agrawal, and K. Biswas, "Influence of Phase Change Material on Thermal Comfort Conditions Inside Buildings in Hot and Dry Climate of India," *Plea*, no. February 2017, 2005.
- [241] N. A. Tari, M. Nozaripour, and K. Parrish, "Using bio PCM as sensible heat storage in a hot arid climate: A case study," *ASHRAE Trans.*, vol. 126, no. Energy 2013, pp. 357–365, 2020.
- [242] H. J. Akeiber, M. A. Wahid, H. M. Hussen, and A. T. Mohammad, "A newly composed paraffin encapsulated prototype roof structure for efficient thermal management in hot climate," *Energy*, vol. 104, pp. 99–106, 2016, doi: 10.1016/j.energy.2016.03.131.
- [243] A. Waqas and S. Kumar, "Thermal performance of latent heat storage for free cooling of buildings in a dry and hot climate: An experimental study," *Energy Build.*, vol. 43, no. 10, pp. 2621–2630, 2011, doi: 10.1016/j.enbuild.2011.06.015.
- [244] M. Özdenefe, U. Atikol, and M. Rezaei, "Trombe wall size-determination based on economic and thermal comfort viability," *Sol. Energy*, vol. 174, no. September, pp.

359–372, 2018, doi: 10.1016/j.solener.2018.09.033.

- [245] M. Ozdenefe and J. Dewsbury, “Dynamic Thermal Simulation of A PCM Lined Building with Energy Plus,” *Recent Res. Environ. Geol. Sci. Dyn.*, pp. 359–364, 2010.
- [246] J. Mun and M. Krarti, “Implementation of a new CTF method stability algorithm into EnergyPlus,” *Build. Simul.*, vol. 8, no. 6, pp. 613–620, 2015, doi: 10.1007/s12273-015-0237-4.
- [247] C. O. Pedersen, “Advanced zone simulation in energyplus: Incorporation of variable properties and phase change material (PCM) capability,” *IBPSA 2007 - Int. Build. Perform. Simul. Assoc. 2007*, pp. 1341–1345, 2007.
- [248] Y. B. Seong and J. H. Lim, “Energy saving potentials of phase change materials applied to lightweight building envelopes,” *Energies*, vol. 6, no. 10, pp. 5219–5230, 2013, doi: 10.3390/en6105219.
- [249] V. R. Voller and L. Shadabi, “Enthalpy methods for tracking a phase change boundary in two dimensions,” *Int. Commun. Heat Mass Transf.*, vol. 11, no. 3, pp. 239–249, 1984, doi: 10.1016/0735-1933(84)90040-X.
- [250] Y. Zhang, K. Du, M. A. Medina, and J. He, “An experimental method for validating transient heat transfer mathematical models used for phase change materials (PCMs) calculations,” *Phase Transitions*, vol. 87, no. 6, pp. 541–558, 2014, doi: 10.1080/01411594.2014.885522.
- [251] M. Maeda, *Heat conduction*, vol. 16, no. 9. 1972. doi: 10.1201/b22157.
- [252] A. Al-Janabi and M. Kavgic, “Application and sensitivity analysis of the phase change material hysteresis method in EnergyPlus: A case study,” *Appl. Therm. Eng.*, vol. 162, no. May, p. 114222, 2019, doi: 10.1016/j.applthermaleng.2019.114222.
- [253] Y. Sang, J. R. Zhao, J. Sun, B. Chen, and S. Liu, “Experimental investigation and EnergyPlus-based model prediction of thermal behavior of building containing phase change material,” *J. Build. Eng.*, vol. 12, no. March, pp. 259–266, 2017, doi: 10.1016/j.job.2017.06.011.
- [254] A. Zastawna-Rumin, T. Kisilewicz, and U. Berardi, “Novel simulation algorithm for modeling the hysteresis of phase change materials,” *Energies*, vol. 13, no. 5, 2020, doi: 10.3390/en13051200.

- [255] P. C. Tabares-Velasco, C. Christensen, and M. Bianchi, "Verification and validation of EnergyPlus phase change material model for opaque wall assemblies," *Build. Environ.*, vol. 54, no. July, pp. 186–196, 2012, doi: 10.1016/j.buildenv.2012.02.019.
- [256] D. M. dos Santos and J. N. D. C. Beirão, "Generative tool to support architectural design decision of earthbag building domes," 2017, no. November, pp. 538–543. doi: 10.5151/sigradi2017-083.
- [257] Y. Rashid, "Thermal and Structural Characterization of Macro-Encapsulated Phase Change Material Integrated Into Concrete Cubes," United Arab Emirates University, 2018. [Online]. Available: https://scholarworks.uaeu.ac.ae/all_theseshttps://scholarworks.uaeu.ac.ae/all_theses/731
- [258] S. Ali, B. Martinson, and S. Al-Maiyah, "Evaluating neutral , preferred , and comfort range temperatures and computing adaptive equation for Kano region computing adaptive equation for Kano region," 2020.
- [259] S. Ramakrishnan, X. Wang, J. Sanjayan, E. Petinakis, and J. Wilson, "Development of thermal energy storage cementitious composites (TESC) containing a novel paraffin/hydrophobic expanded perlite composite phase change material," *Sol. Energy*, vol. 158, no. October 2016, pp. 626–635, 2017, doi: 10.1016/j.solener.2017.09.064.
- [260] Z. Wang, H. Su, S. Zhao, and N. Zhao, "Influence of phase change material on mechanical and thermal properties of clay geopolymer mortar," *Constr. Build. Mater.*, vol. 120, pp. 329–334, 2016, doi: 10.1016/j.conbuildmat.2016.05.091.
- [261] GEG, "How to Build an Earthquake-Resistant Home: An Earthbag Construction Manual," *Good Earth Global*, 2018.
- [262] B. Ma, S. Adhikari, Y. Chang, J. Ren, J. Liu, and Z. You, "Preparation of composite shape-stabilized phase change materials for highway pavements," *Constr. Build. Mater.*, vol. 42, pp. 114–121, 2013, doi: 10.1016/j.conbuildmat.2012.12.027.
- [263] B. Xu and Z. Li, "Paraffin/diatomite composite phase change material incorporated cement-based composite for thermal energy storage," *Appl. Energy*, vol. 105, pp. 229–237, 2013, doi: 10.1016/j.apenergy.2013.01.005.
- [264] X. Sun, K. O. Lee, M. A. Medina, Y. Chu, and C. Li, "Melting temperature and enthalpy

- variations of phase change materials (PCMs): a differential scanning calorimetry (DSC) analysis," *Phase Transitions*, vol. 91, no. 6, pp. 667–680, 2018, doi: 10.1080/01411594.2018.1469019.
- [265] G. Sang *et al.*, "Thermo-mechanical properties of compaction molded cement-based composite containing a high mass fraction of phase change material for thermal energy storage," *Compos. Part A Appl. Sci. Manuf.*, vol. 128, no. October 2019, p. 105657, 2020, doi: 10.1016/j.compositesa.2019.105657.
- [266] J. Singh, J. R. Vennapusa, and S. Chattopadhyay, "Protein-polysaccharide based microencapsulated phase change material composites for thermal energy storage," *Carbohydr. Polym.*, vol. 229, no. October 2019, p. 115531, 2020, doi: 10.1016/j.carbpol.2019.115531.
- [267] M. Velasco-Carrasco, Z. Chen, J. L. Aguilar-Santana, and S. Riffat, "Experimental evaluation of thermal energy storage (TES) with phase change materials (PCM) for ceiling tile applications," *Futur. Cities Environ.*, vol. 6, no. 1, pp. 1–11, 2020, doi: 10.5334/FCE.101.
- [268] B. Inventions, "Drive innovation and creative pursuit of superior performance," 2017. <https://www.bd-inventions.com/product/100-series-heat-flow-meter/> (accessed Nov. 02, 2022).
- [269] G. Giannotas, V. Kamperidou, M. Stefanidou, P. Kampragkou, and A. Liapis, "Utilization of tree-bark in cement pastes," *J. Build. Eng.*, vol. 57, no. July, p. 104913, 2022, doi: 10.1016/j.jobbe.2022.104913.
- [270] U. W. Robert, S. E. Etuk, G. P. Umoren, and O. E. Agbasi, "Assessment of Thermal and Mechanical Properties of Composite Board Produced from Coconut (*Cocos nucifera*) Husks, Waste Newspapers, and Cassava Starch," *Int. J. Thermophys.*, vol. 40, no. 9, pp. 1–12, 2019, doi: 10.1007/s10765-019-2547-8.
- [271] X. Li, H. Chen, L. Liu, Z. Lu, J. G. Sanjayan, and W. H. Duan, "Development of granular expanded perlite/paraffin phase change material composites and prevention of leakage," *Sol. Energy*, vol. 137, pp. 179–188, 2016, doi: 10.1016/j.solener.2016.08.012.
- [272] L. Feng, J. Wu, W. Sun, and W. Cai, "Effects of Pore Structure and Pore Size of Expanded Graphite on the Properties of Paraffin Wax/Expanded Graphite Composite

- Phase Change Materials,” *Energies*, vol. 15, no. 12, 2022, doi: 10.3390/en15124201.
- [273] A. Karaipekli, A. Biçer, A. Sarı, and V. V. Tyagi, “Thermal characteristics of expanded perlite/paraffin composite phase change material with enhanced thermal conductivity using carbon nanotubes,” *Energy Convers. Manag.*, vol. 134, pp. 373–381, 2017, doi: 10.1016/j.enconman.2016.12.053.
- [274] C. Kutlu *et al.*, “Incorporation of controllable supercooled phase change material heat storage with a solar assisted heat pump: Testing of crystallization triggering and heating demand-based modelling study,” *J. Energy Storage*, vol. 55, no. PD, p. 105744, 2022, doi: 10.1016/j.est.2022.105744.
- [275] R. Sharma, J. G. Jang, and J. W. Hu, “Phase-Change Materials in Concrete: Opportunities and Challenges for Sustainable Construction and Building Materials,” *Materials (Basel)*, vol. 15, no. 1, 2022, doi: 10.3390/ma15010335.
- [276] U. Berardi and S. Soudian, “Experimental investigation of latent heat thermal energy storage using PCMs with different melting temperatures for building retrofit,” *Energy Build.*, vol. 185, pp. 180–195, 2019, doi: 10.1016/j.enbuild.2018.12.016.
- [277] A. Tokuç, T. Başaran, and S. C. Yesügey, “An experimental and numerical investigation on the use of phase change materials in building elements: The case of a flat roof in Istanbul,” *Energy Build.*, vol. 102, pp. 91–104, 2015, doi: 10.1016/j.enbuild.2015.04.039.
- [278] T. Sensors, “HFP01 Heat flux plate / heat flux sensor,” 2014. [Online]. Available: https://www.hukseflux.com/uploads/product-documents/HFP01_v2114.pdf
- [279] Q. Al-Yasiri and M. Szabó, “Thermal performance of concrete bricks based phase change material encapsulated by various aluminium containers: An experimental study under Iraqi hot climate conditions,” *J. Energy Storage*, vol. 40, no. May, 2021, doi: 10.1016/j.est.2021.102710.
- [280] S. Shaik, K. K. Gorantla, and A. B. T. P. Setty, “Investigation of Building Walls Exposed to Periodic Heat Transfer Conditions for Green and Energy Efficient Building Construction,” *Procedia Technol.*, vol. 23, pp. 496–503, 2016, doi: 10.1016/j.protcy.2016.03.055.
- [281] K. A. Quagraine, E. W. Ramde, Y. A. K. Fiagbe, and D. A. Quansah, “Evaluation of time lag and decrement factor of walls in a hot humid tropical climate,” *Therm. Sci. Eng.*

- Prog.*, vol. 20, no. October, p. 100758, 2020, doi: 10.1016/j.tsep.2020.100758.
- [282] N. Soares, A. R. Gaspar, P. Santos, and J. J. Costa, "Multi-dimensional optimization of the incorporation of PCM-drywalls in lightweight steel-framed residential buildings in different climates," *Energy Build.*, vol. 70, pp. 411–421, 2014, doi: 10.1016/j.enbuild.2013.11.072.
- [283] MCI Technologies and Winco Technologies, "INERTEK Microcapsules," France, 2012. [Online]. Available: <https://www.winco-tech.com/en/produit/inertek-2/>
- [284] P. C. Tabares-Velasco, C. Christensen, and M. Bianchi, "Verification and validation of EnergyPlus phase change material model for opaque wall assemblies," *Build. Environ.*, vol. 54, pp. 186–196, 2012, doi: 10.1016/j.buildenv.2012.02.019.
- [285] A. Abdulkadir, M. T. Usman, and A. H. Shaba, "An integrated approach to delineation of the eco-climatic zones in Northern Nigeria," *J. Ecol. Nat. Environ.*, vol. 7, no. 9, pp. 247–255, 2015, doi: 10.5897/jene2015.0532.
- [286] K. State, M. A. Matazu, and A. F. Ali, "Geo-spatial Mapping of Plastic Waste Recycling Plants in Kano Metropolis , Geo-spatial Mapping of Plastic Waste Recycling Plants in Kano Metropolis , Kano State , Nigeria," no. June, 2023, doi: 10.4314/dujopas.v9i2a.27.
- [287] D. O. Edokpa, P. N. Ede, B. E. Diagi, and S. I. Ajiere, "Rainfall and Temperature Variations in a Dry Tropical Environment of Nigeria," *J. Atmos. Sci. Res.*, vol. 6, no. 2, pp. 50–57, 2023, doi: 10.30564/jasr.v6i2.5527.
- [288] O. K. Akande, "Passive design strategies for residential buildings in a hot dry climate in Nigeria," *WIT Trans. Ecol. Environ.*, vol. 128, pp. 61–71, 2010, doi: 10.2495/ARC100061.
- [289] S. M. Ali, "Measured and Perceived Conditions of Indoor Environmental Qualities (IEQ) of University Learning Environments in Semi-arid Tropics : a Field Study in Kano-Nigeria," no. June, pp. 74–75, 2018.
- [290] S. Guichard, F. Miranville, D. Bigot, B. Malet-Damour, T. Libelle, and H. Boyer, "Empirical validation of a thermal model of a complex roof including phase change materials," *Energies*, vol. 9, no. 1, 2016, doi: 10.3390/en9010009.
- [291] H. Cui, S. A. Memon, and R. Liu, "Development, mechanical properties and numerical simulation of macro encapsulated thermal energy storage concrete," *Energy Build.*,

- vol. 96, pp. 162–174, 2015, doi: 10.1016/j.enbuild.2015.03.014.
- [292] L. Erlbeck *et al.*, “Adjustment of thermal behavior by changing the shape of PCM inclusions in concrete blocks,” *Energy Convers. Manag.*, vol. 158, no. October 2017, pp. 256–265, 2018, doi: 10.1016/j.enconman.2017.12.073.
- [293] A. V. Sá, M. Azenha, H. De Sousa, and A. Samagaio, “Thermal enhancement of plastering mortars with Phase Change Materials: Experimental and numerical approach,” *Energy Build.*, vol. 49, pp. 16–27, 2012, doi: 10.1016/j.enbuild.2012.02.031.
- [294] J. Yu, K. Leng, F. Wang, H. Ye, and Y. Luo, “Simulation study on dynamic thermal performance of a new ventilated roof with form-stable pcm in Southern China,” *Sustain.*, vol. 12, no. 22, pp. 1–21, 2020, doi: 10.3390/su12229315.
- [295] Y. Rashid, F. Alnaimat, and B. Mathew, “Energy performance assessment of waste materials for buildings in extreme cold and hot conditions,” *Energies*, vol. 11, no. 11, 2018, doi: 10.3390/en11113131.
- [296] F. Fiorito, “Phase-change materials for indoor comfort improvement in lightweight buildings. A parametric analysis for Australian climates,” *Energy Procedia*, vol. 57, no. 0, pp. 2014–2022, 2014, doi: 10.1016/j.egypro.2014.10.066.
- [297] R. Ye, W. Lin, X. Fang, and Z. Zhang, “A numerical study of building integrated with CaCl₂·6H₂O/expanded graphite composite phase change material,” *Appl. Therm. Eng.*, vol. 126, pp. 480–488, 2017, doi: 10.1016/j.applthermaleng.2017.07.191.
- [298] X. Sun, M. A. Medina, and Y. Zhang, “Potential thermal enhancement of lightweight building walls derived from using Phase Change Materials (PCMs),” *Front. Energy Res.*, vol. 7, no. February, pp. 1–10, 2019, doi: 10.3389/fenrg.2019.00013.
- [299] Q. Li *et al.*, “Thermoeconomic analysis of a wall incorporating phase change material in a rural residence located in northeast China,” *Sustain. Energy Technol. Assessments*, vol. 44, no. January, 2021, doi: 10.1016/j.seta.2021.101091.